



Provided by the author(s) and University of Galway in accordance with publisher policies. Please cite the published version when available.

Title	A numerical modelling investigation of jellyfish transport and swimming behavior in Killary Harbour using a coastal hydrodynamic model
Author(s)	Sayeed, Md Ashkar Bin
Publication Date	2024-01-24
Publisher	NUI Galway
Item record	http://hdl.handle.net/10379/18033

Downloaded 2024-05-02T11:43:21Z

Some rights reserved. For more information, please see the item record link above.





OLLSCOIL NA
GAILLIMHE
UNIVERSITY
OF GALWAY

**A NUMERICAL MODELLING INVESTIGATION OF
JELLYFISH TRANSPORT AND SWIMMING BEHAVIOUR
IN KILLARY HARBOUR USING A COASTAL HYDRODYNAMIC MODEL**

by

Md Ashkar Bin Sayeed

Supervisor: Dr Stephen Nash

Co-Supervisor: Prof Michael Hartnett

A dissertation submitted to the University of Galway as fulfilment of the
requirements for the Degree of Doctor of Philosophy

Discipline of Civil Engineering

School of Engineering

College of Science and Engineering

February 2023

DECLARATION

I declare that this dissertation, in whole or in part, has not been submitted to any University as an exercise for a degree. I further declare that, except where reference is given, the work is entirely my own.

Signed:



Md Ashkar Bin Sayeed

Feb 2023

ABSTRACT

The occurrence of jellyfish in coastal areas, particularly in large numbers or swarms, can pose a significant threat to tourism and aquaculture. They can sting swimmers and bathers, become entangled in fishing nets, and harm and/or kill farmed fish. There have been many records of fish kills and large associated economic losses reported globally. Despite their threat, there is still quite a limited understanding of the mechanisms of jellyfish transport and swarming. While jellyfish primarily drift passively on the ocean's currents, they also have the ability to swim with and against currents. However, their swimming behaviours are poorly understood, and the effects of their swimming on their total transport are relatively unknown. In this research, a jellyfish transport model was developed and used to investigate jellyfish transport in Killary Harbour, a fjord on the west coast of Ireland. Killary was chosen as a case study site as it has experienced damage and mass kills of farmed fish by jellyfish in recent years.

A 3D baroclinic hydrodynamic model of Killary Harbour was developed using the Environmental Fluid Dynamics Code (EFDC) and was coupled with a Lagrangian particle-tracking module to simulate the transport of jellyfish. The particle-tracking model was developed to produce three different jellyfish transport models incorporating different transport mechanisms (1) passive drifting only, (2) passive drifting and diel vertical migration and (3) passive drifting, diel vertical migration, and horizontal swimming. Jellyfish transport predictions were compared with recorded movements of tagged jellies within the fjord. Tagged jelly movements were detected by 8 GPS receivers placed along the banks of the fjord. The percentage of the available number of modelled particles within each detector's range was determined temporally and compared with the GPS observations.

The jellyfish modelled as passively drifting particles agreed relatively well with the observed jellyfish positions in the short term, but longer term, results were mixed. The diel vertical migration (DVM) model offers a new approach to investigating jellyfish DVM behaviour in coastal waters through the use of a constant migration-limiting threshold depth and synchronised movement with passive drift. Although this resulted in some improvements in performance over the passive drift model, the results were varied. Finally, in the horizontal swimming model, swimming behaviours were incorporated through a set of swim rules that govern horizontal swimming rates and times, while vertical swimming is implemented according to the DVM strategy. The main factors influencing jellyfish transport in this model were found to be swim speed and swim direction. The motility of jellyfish, combined with tidal and wind-driven currents, in the model can indeed cause particles to be transported in a similar manner to the observed jellyfish. However, the results also suggest that individual variations in jellyfish, such as size and development, may play a role in their transport. Overall, these investigations provide valuable insights into understanding jellyfish transport mechanisms and their relative contributions to their total transport.

ACKNOWLEDGEMENT

I am extremely grateful to have successfully completed my PhD despite facing immense challenges during the course of my research. Over the past 5.5 years, I have faced many challenges, including a massive heart attack, but I have been fortunate to have received constant support from many individuals.

Firstly, I am extremely grateful to the Almighty for blessing me with the strength, perseverance, and determination to overcome the obstacles that came my way during my PhD journey. His grace helped me stay focused and determined to achieve my goals. Without His blessings, none of this would have been possible, and I am eternally grateful for that.

I would like to express my sincere gratitude to the doctors and nurses who provided me exceptional care during my illness, especially cardiologist Dr Barton and heart failure nurse Mary. Without their constant care and support, it would not have been possible for me to continue with my research.

I am humbled and indebted to my research supervisors for their unwavering support and guidance throughout this journey. I also express my sincere appreciation to my main supervisor, Dr Stephen Nash, for his guidance, support, and encouragement throughout my research. His expertise, valuable inputs, invaluable feedback, and insights were instrumental in shaping my thesis.

I express my sincere appreciation to all those who have supported and encouraged me during my PhD journey. I would like to thank specially, Fearghal O'Donncha, who helped me a lot in solving model code related issues. I would like to thank Tom Doyle's team for their jellyfish observation data.

I owe a debt of gratitude to my wife Monica and my daughter Farishta for their unconditional love, support, and encouragement throughout this journey. They have been my pillars of strength, and their constant motivation kept me going through the toughest of times.

My parents, who are a thousand miles away, have been patiently waiting for this moment, and I would like to dedicate my thesis to them, my wife, and my daughter for being supportive and encouraging and for their patience and understanding during my PhD journey.

I would also like to extend my gratitude to the retired faculty of Physics, Professor Thomas Glynn, who provided me with constant inspiration and support throughout my thesis writing period.

Finally, I would like to acknowledge the Irish Research Council's financial support, which enabled me to undertake this research. I am deeply grateful for their assistance and for providing me with the opportunity to pursue my academic goals.

Once again, I offer my heartfelt gratitude to all those who have contributed to my success, and I pray that the Almighty continues to bless us all. Thank you all for being a part of my journey, and for contributing to my success.

TABLE OF CONTENTS

DECLARATION	ii
ABSTRACT	iii
ACKNOWLEDGEMENT.....	iv
TABLE OF CONTENTS	vi
LIST OF FIGURES	xiii
CHAPTER 1: INTRODUCTION	1
1.1. Jellyfish and Their Impacts	1
1.2. Jellyfish Transport, Bloom Formation, and their Modelling	4
1.3. Aims and Objectives	6
1.4. Thesis Outline.....	8
CHAPTER 2: LITERATURE REVIEW.....	10
2.1. Introduction	10
2.2. Jellyfish: What are they?	11
2.3. Jellyfish behaviours and modelling approaches.....	14
2.4. Jellyfish Occurrence and Consequences in Coastal Seas.....	18
2.5. Jellyfish Forecasting: the State of the Art	22
2.5.1. Hydrodynamic Factors in Jellyfish Transportation	25
2.5.2. Salinity and Temperature Dynamics in Jellyfish Transport Modelling.....	28
2.5.3. Modelling of Jellyfish Swimming.....	29
2.5.4. Transport of Invasive Jellyfish.....	30
2.6. Conclusions	34
CHAPTER 3: MODEL THEORY.....	38

Table of Contents

3.1. Introduction	38
3.2. Model History and Description	38
3.3. Governing Equations	40
3.3.1. Boundary Conditions	44
3.3.2. Vertical Mixing and Turbulence Models	46
3.3.3. Mode-splitting.....	47
3.4. Drifter Module.....	50
3.5. Conclusion.....	53
CHAPTER 4: HYDRODYNAMIC MODELLING OF KILLARY HARBOUR.....	54
4.1. Introduction	54
4.2. Study Site	56
4.3. Model Description.....	58
4.4. Model Configuration and Development	59
4.4.1. Grids and Bathymetry	59
4.4.2. ADCP Data.....	61
4.4.3. Boundary Conditions and Other Input Data	61
4.4.4. Model Parameters, State Variables, and Constants.....	63
4.5. Model Calibration and Validation	65
4.5.1. Observed Hydrodynamics.....	66
4.5.2. Modelled Hydrodynamics	66
4.6. Sensitivity Analysis	70
4.7. Results and Discussion.....	72
4.7.1. Model Stability	72
4.7.2. Sensitivity to Model Properties and Parameters	73
4.7.2.1. Model Physics	74

Table of Contents

4.7.2.1.1. Baroclinity	74
4.7.2.1.2. Barotropy	76
4.7.2.1.3. Difference Between The Scenarios	77
4.7.2.2. Initial and Sea Boundary Conditions.....	79
4.7.2.3. Wind	84
4.7.2.3.1. Wind Speed Scenarios	84
4.7.2.3.2. Differences Among the Wind Scenarios.....	86
4.7.2.4. River Discharge	89
4.7.2.4.1. Discharge Scenarios.....	89
4.7.2.4.2. Differences Among The Discharge Scenarios	92
4.7.2.5. Density-driven Vertical Circulations	98
4.8. Conclusions	100
CHAPTER 5: PASSIVE-DRIFT MODELLING OF JELLYFISH.....	102
5.1. Introduction	102
5.2. Study Site	105
5.3. Methodology.....	105
5.3.1. Monitoring of Jellyfish Transport in Killary Harbour.....	105
5.3.2. Setup of the Particle-track Model	109
5.3.3. Code Modifications	111
5.3.4. Model Scenarios - Sensitivity of LPT Module.....	113
5.3.5. Analysis of Model Results	116
5.3.5.1. Particle Centroid and RMSE	116
5.3.5.2. Transport Diffusivity	117
5.3.5.3. Transport Agreement and Ranking	117
5.4. Results and Discussion.....	120

Table of Contents

5.4.1. Results – Jellyfish Monitoring	120
5.4.2. Results – LPT Model Sensitivity.....	129
5.4.2.1. LPT Model Setup	131
5.4.2.1.1. Numerical Scheme	131
5.4.2.1.2. Transport Processes: Horizontal Diffusion	132
5.4.2.1.3. Transport Processes: Vertical Transport	134
5.4.2.2. Specification of Particle Releases	135
5.4.2.2.1. Depth of Release	135
5.4.2.2.2. Depth Sourcing.....	136
5.4.2.2.3. Number of Particles Released.....	137
5.4.2.2.4. Particle Release Location	138
5.4.2.3. Hydrodynamic Forcings.....	140
5.4.2.3.1. Wind.....	140
5.4.2.3.2. River Discharge.....	141
5.4.3. Results – Comparison of Modelled and Observed Movements.....	143
5.5. Summary and Conclusions.....	151
CHAPTER 6: DIEL VERTICAL MIGRATION MODELLING OF JELLYFISH....	153
6.1. Introduction	153
6.2. Study Site	156
6.3. Methodology.....	156
6.3.1. DVM Model Development	157
6.3.1.1. Simple Conceptual Model	157
6.3.1.2. Model Processes and Rules.....	158
6.3.1.3 DVM Model Algorithm.....	163
6.3.1.4. Implementation and Governing Equations.....	165

Table of Contents

6.3.2 Model Details	168
6.3.2.1. Input data	169
6.3.3. Scenario Modelling	170
6.3.3.1. Assessing Model Sensitivity	171
6.3.3.2 Assessing Model Performance	172
6.4. Results	172
6.4.1. Testing the DVM Code	172
6.4.2. Sensitivity of DVM Model to Jellyfish Properties	174
6.4.2.1 Jellyfish Motility Rate (JMR)	175
6.4.2.2 Diel migration depth threshold (DMT)	177
6.4.3. Sensitivity to Particle Release Depth	179
6.4.4. Assessment of DVM Accuracy Versus Passive Drift	181
6.4.4.1. Jellyfish J-18495	181
6.4.4.2. Jellyfish J-18500	190
6.4.4.3. Jellyfish J-1162	195
6.4.5. Multicriteria Analysis (MCA) of Model Performance	200
6.5. Conclusions	202
CHAPTER 7: SWIM MODELLING OF JELLYFISH	204
7.1. Introduction	204
7.2. Methodology.....	207
7.2.1. Analysis of Observed Transport of Jellyfish	209
7.2.2. Swim Model Development.....	217
7.2.2.1. Swim Model Concept	218
7.2.2.2. Swim Rule Development and Implementation	219
7.2.3. Swim Model Details.....	230

Table of Contents

7.2.3.1. Entities, State Variables, and Scale	231
7.2.3.2. Input Data	231
7.2.4. Scenario Modelling	232
7.2.4.1. Assessing Model Sensitivity and Effects of Swim Rules	232
7.2.4.2. Assessment of Model Performance.....	236
7.3. Results	236
7.3.1. Testing the Performance of the Swim Code and Comparison with the Passive Drift Model.....	236
7.3.2. Sensitivity of Swim Model to Particle Release Depth	239
7.3.3. Sensitivity of Model to Swim Parameters.....	240
7.3.3.1. Effect of Relationship Between Swimming and Stage of Tide ...	241
7.3.3.2. Swim Speed	242
7.3.3.3. Swimming at Slack Tide	249
7.3.3.4. Drift Neutralisation	249
7.3.3.5. Flood Tide Swimming	250
7.3.3.6. Minimum Swim Speed	251
7.3.4. Comparison of Model Performance Across Swim Rules	253
7.3.4.1 Spatiotemporal Analysis of Transport	253
7.3.4.2. Agreement with Observations	261
7.3.4.3 Multicriteria Analysis	280
7.3.5. Behavioural Integration: Comparison across the Jellyfish Models ..	284
7.3.5.1. J-1162 Swim Scenarios	284
7.3.5.2. J-18500 Swim Scenarios.....	291
7.3.6. Swimming Versus Passive Drift.....	295
7.4. Summary and Conclusions	296

Table of Contents

CHAPTER 8: SUMMARY, CONCLUSIONS, AND RECOMMENDATIONS ...	299
8.1. Summary of the Research	299
8.2. Key Conclusions of the Research.....	301
8.2.1. Hydrodynamic Modelling of Killary Harbour	301
8.2.2. Passive-drift Modelling of Jellyfish	302
8.2.3. DVM Modelling of Jellyfish	303
8.2.4. Swim Modelling of Jellyfish.....	304
8.3. Recommendations for future work.....	305
REFERENCES	307

LIST OF FIGURES

Fig 1.1 A collage of pictures showing (a) a jellyfish bloom, (b) jellyfish sting on humans (photo courtesy: Google), (c) mortality and skin pathology of farmed Atlantic salmon caused by exposure to jellyfish (Mitchell et al., 2021).	1
Fig 1.2 A collage featuring a series of pictures that depict a jellyfish with floating tentacles and slight deformations applied to the bell, showcasing two contraction steps on the left and two expansion steps on the right.....	6
Fig 2.1 An assortment of jellyfish varieties - (a) <i>Staurocladia</i> sp., (b) <i>Nemopilema nomurai</i> , (c) <i>Aurelia aurita</i> , (d) <i>Cyanea capillata</i> , (e) <i>Physalia physalis</i> , and (f) <i>Chironex fleckeri</i>	14
Fig 3.1 The sigma coordinate system. z^* = Cartesian coordinate in the vertical, and z = the sigma coordinate. The illustration was adapted from Ji (2008), who reserves the copyright of it.	41
Fig 3.2 Boundary conditions. Illustration adapted from Ji (2008).	44
Fig 4.1 Map of Killary Fjord, Ireland. [(A) relative location of Ireland; (B) the west coast of Ireland; (C) Killary Fjord. Referenced and rendered using R mapping packages).....	58
Fig 4.2 Killary harbour bathymetry (The legend on the top-right showing the colour scale represents the water depths in metres; map axes are represented as easting and northing in km along the x-and y-axis, respectively.)	60
Fig 4.3 Wind comparison over Aug 2015 between recorded (Belmullet) and model (ECMWF) data for their (a) speed and (b) direction.....	63
Fig 4.4 Current speed and direction at the ADCP bins (A) 17 and (B) 11.....	66
Fig 4.5 Comparison between modelled and observed surface elevation.....	67
Fig 4.6 Killary hydrodynamics of EFDC model (black) and ADCP observation (grey) showing comparisons of the respective (a,c,e) current speeds and (b,d,f) current	

List of Figures

directions. Speed and direction are displayed along the y-axis and are measured in m/s and deg units, respectively.	70
<i>Fig 4.7</i> Surface elevation convergence over a simulation period (x-axis) in different timesteps.	73
<i>Fig 4.8</i> Maps showing the (A~H) salinity and (I~P) temperature stratifications as per the BC-All model scenario. The stratifications are investigated in the (A~D & I~L) neap and (E~H & M~P) spring tides at the (A & E) low, (B & F) mid-flood, (C & G) high, and (D & H) mid-ebb tidal levels. (The x-axis represents the spatial points of investigation along the east-west at every 2 km, and the y-axis represents the water depths in metres. The legends on the top represent the salinity scale in psu shown on the left and the temperature scale in °C on the right.).....	75
<i>Fig 4.9</i> Maps showing the (A~D) surface and (E~H) depth-averaged currents in the BC-All model scenario. The currents are sampled in the spring tide at the (A & E) low, (B & F) mid-flood, (C & G) high, and (D & H) mid-ebb tidal levels.	76
<i>Fig 4.10</i> Maps showing the (A~D) surface and (E~H) depth-averaged currents in the BT-TW model scenario. The currents are sampled in the spring tide at the (A & E) low, (B & F) mid-flood, (C & G) high, and (D & H) mid-ebb tidal levels.	77
<i>Fig 4.11</i> Maps showing differences in the (A~D) surface and (E~H) depth-averaged currents between the BC-All and BT-TW model scenarios. The currents are sampled in the spring tide at the (A & E) low, (B & F) mid-flood, (C & G) high, and (D & H) mid-ebb tidal levels.....	79
<i>Fig 4.12</i> Maps showing the (A~H) salinity and (I~P) temperature stratifications as per the BC-All-tv model scenario. The stratifications are investigated in the (A~D & I~L) neap and (E~H & M~P) spring tides at the (A & E) low, (B & F) mid-flood, (C & G) high, and (D & H) mid-ebb tidal levels. (The x-axis represents the spatial points of investigation along the east-west at every 2 km, and the y-axis represents the water depths in metres. The legends on the top represent the salinity scale in psu shown on the left and the temperature scale in °C on the right.).....	81

List of Figures

- Fig 4.13* Maps showing the (A~D) surface and (E~H) depth-averaged currents in the BC-All-tv model scenario. The currents are sampled in the spring tide at the (A & E) low, (B & F) mid-flood, (C & G) high, and (D & H) mid-ebb tidal levels.82
- Fig 4.14* Maps showing differences in the (A~B) salinity and (C~D) temperature stratifications in the BC-All scenario with respect to the BC-All-tv scenario. The differences are investigated in the (A & C) neap and (B & D) spring tides at the mid-flood tidal level. (The x-axis represents the spatial points of investigation along the east-west at every 2 km, and the y-axis represents the water depths in metres. The legends on the top represent the scale of difference in the salinity (psu) shown on the left and the temperature (°C) on the right.)83
- Fig 4.15* Maps showing differences in the (A) surface and (B) depth-averaged currents between the BC-All and BC-All-tv model scenarios. The currents are sampled in the spring tide at the mid-flood tidal level.....83
- Fig 4.16* Maps showing the (A~B) salinity and (C~D) temperature stratifications as per the BC-NW model scenario. The stratifications are investigated in the (A & C) neap and (B & D) spring tides at the mid-ebb tidal level. (The x-axis represents the spatial points of investigation along the east-west at every 2 km, and the y-axis represents the water depths in metres. The legends on the top represent the salinity scale in psu shown on the left and the temperature scale in °C on the right.)85
- Fig 4.17* Maps showing differences in the (A~B) salinity and (C~D) temperature stratifications in the WX scenario with respect to the W0 or W8 scenarios. The differences are investigated in the (A & C) neap and (B & D) spring tides at the mid-ebb tidal level. (The x-axis represents the spatial points of investigation along the east-west at every 2 km, and the y-axis represents the water depths in metres. The legends on the top represent the scale of difference in the salinity (psu) shown on the left and the temperature (°C) on the right.)87
- Fig 4.18* Maps showing differences in the (A~B & E~F) salinity and (C~D & G~H) temperature stratifications in (A~D) the W0 scenario with respect to the W4 or W8 scenarios and in (E~H) the W4 scenario with respect to the W8 scenario. The differences are investigated in the (A~D & I~L) neap and (E~H & M~P) spring tides

List of Figures

at the mid-ebb tidal levels. (The x-axis represents the spatial points of investigation along the east-west at every 2 km, and the y-axis represents the water depths in metres. The legends on the top represent the scale of difference in the salinity (psu) shown on the left and the temperature (°C) on the right.)	87
<i>Fig 4.19</i> Maps showing differences in the (A) surface and (B) depth-averaged currents between the WX and the W0 or W8 model scenarios. The currents are sampled in the spring tide at the mid-flood tidal level.....	88
<i>Fig 4.20</i> Maps showing differences in the (A & C) surface and (B & D) depth-averaged currents (A~D) between the W0 and the W4 or W8 scenarios and (E~H) between the W4 and the W8 scenario. The currents are sampled in the spring tide at the mid-flood tidal level.....	88
<i>Fig 4.21</i> Maps showing (A~B & E~F) salinity and (C~D & G~H) temperature stratifications as per (A~D) R3 and (E~H) R33 model scenarios. The stratifications are investigated in the (A, C, E, & G) neap and (B, D, F, & H) spring tides at the mid-ebb tidal level. (The x-axis represents the spatial points of investigation along the east-west at every 2 km, and the y-axis represents the water depths in metres. The legends on the top represent the salinity scale in psu shown on the left and the temperature scale in °C on the right.).....	90
<i>Fig 4.22</i> Maps showing the (A~D) surface and (E~H) depth-averaged currents in the R0 or R3 model scenario. The currents are sampled in the spring tide at the (A & E) low, (B & F) mid-flood, (C & G) high, and (D & H) mid-ebb tidal levels.	91
<i>Fig 4.23</i> Maps showing the (A~D) surface and (E~H) depth-averaged currents in the R33 model scenario. The currents are sampled in the spring tide at the (A & E) low, (B & F) mid-flood, (C & G) high, and (D & H) mid-ebb tidal levels.	92
<i>Fig 4.24</i> Maps showing differences in the salinity (two left-most columns) and temperature (two right-most columns) stratifications in (A~H) the RX scenario with respect to the (A~D) R0 and (E~H) R33 scenarios, in (I~P) the R0 scenario with respect to the (A~D) R3 and (E~H) R33 scenarios, and in (Q~T) the R3 scenario with respect to the R33 scenario. The differences are investigated in the neap and spring tides at the mid-ebb tidal level, and the respective figures are organised in the 1 st &	

List of Figures

3 rd and the 2 nd & 4 th columns, respectively. (The x-axis represents the spatial points of investigation along the east-west at every 2 km, and the y-axis represents the water depths in metres. The legends on the top represent the scale of difference in the salinity (psu) shown on the left and the temperature (°C) on the right.).....	94
<i>Fig 4.25</i> Maps showing differences in (A~D) surface and (E~H) depth-averaged currents in the discharge scenario pairs RX-R0 or R0-R33 or RR3-R33. The currents are sampled in the spring tide at (A & E) low, (B & F) mid-flood, (C & G) high, and (D & H) mid-ebb tidal levels.	96
<i>Fig 4.26</i> Maps showing differences in (A~D) surface and (E~H) depth-averaged currents between the R0 and R3 model scenarios. The currents are sampled in the spring tide at (A & E) low, (B & F) mid-flood, (C & G) high, and (D & H) mid-ebb tidal levels.....	97
<i>Fig 4.27</i> Map showing the difference in (A~D) surface and (E~H) depth-averaged currents between RX and R33 model scenarios. The currents are sampled in the spring tide at (A & E) low, (B & F) mid-flood, (C & G) high, and (D & H) mid-ebb tidal levels.....	98
<i>Fig 4.28</i> Map showing the difference in (A~D) surface and (E~H) depth-averaged currents between baroclinic and barotropic model scenarios. The currents are sampled in the spring tide at (A & E) low, (B & F) mid-flood, (C & G) high, and (D & H) mid-ebb tidal levels.	99
<i>Fig 5.1</i> Map showing 500 m radius detection zones for 8 geostationary receivers deployed to monitor the jellyfish transportation in Killary.	106
<i>Fig 5.2</i> Conditions of (1) wind and (2) tide at the release events of the jellyfish (A) J-18495, (B) J-1160, (C) J-1162, (D) J-18499, and (E) J-18500 tracked in the Killary harbour. The top indicates the north as a reference for the wind direction.	107
<i>Fig 5.3</i> Sequential detections of J-18495 according to tide (inset) across 8 detectors along Killary harbour.....	123

List of Figures

Fig 5.4 Times and locations of jellyfish detections in Killary Harbour for 5 jellyfish and the corresponding tide levels. [Legends are in order of simulation period of the respective jellyfish.]	124
Fig 5.5 Illustration of current vector plots for two consecutive ebb tide events, depicting current directions at 17:00 hr on August 25, 2015 (top) and 05:00 hr on August 26, 2015 (bottom).	129
Fig 5.6 Particle transport at various RWM conditions.	131
Fig 5.7 Spatiotemporal trajectories of particle centroid and RMSE of trajectory-pairs along the (A) east-west, (B) north-south, and (C) vertical directions illustrated upon three LPT numerical scheme scenarios as per J-18495 model. The RMSE is calculated for the short-term (st) and long-term (lt) periods of the simulation, which are separated by the golden vertical dash being st on its left and lt on its right side.	132
Fig 5.8 Particle density plots upon simulations at D_H (A) sourced within the model, (B) $0.007 \text{ m}^2/\text{s}$, (C) $0.00007 \text{ m}^2/\text{s}$, and (D) combined. A~C indicate the time-specific KDE at 91.5 hr after releasing the particles, and D indicates the time-varying KDE over the model domain.	133
Fig 5.9 Map of distribution of the particles released at the surface with and without vertical movements.	134
Fig 5.10 Spatiotemporal trajectories of particle centroid and RMSE of trajectory-pairs along the (A) east-west, (B) north-south, and (C) vertical directions illustrated upon four different particle releasing depth scenarios as per J-18495 model....	136
Fig 5.11 Map of distribution of the particles simulated without any vertical movement comparing depth sourcing induced transport variability between (A) surface and (B) mid-depth releasing scenarios.	137
Fig 5.12 Spatiotemporal trajectories of particle centroid and RMSE of trajectory-pairs along the (A) east-west, (B) north-south, and (C) vertical directions illustrated upon three particle releasing number scenarios as per J-18495 model. The RMSE is calculated for the short-term (st) and long-term (lt) periods of the simulation, which	

List of Figures

are separated by the golden vertical dash being st on its left and lt on its right side.	138
Fig 5.13 Map showing the distributions of modelled particles released at the exact release location (red) and three other locations at different distances from the shore. Inset plot shows particle locations at the time of release.	140
Fig 5.14 Variation of Kernel density estimation of the model particles with and without wind for J-18495.	141
Fig 5.15 A comparison of the net transport of particles between with and without river discharge (Q) scenarios combined with the depth of release.	142
Fig 5.16 Depiction of current differences between conditions with and without river discharge illustrated for mid-ebb (top) and low-tide (bottom), highlighting higher current speed in the mid-channel where potential particle entrapment may occur.	143
Fig 5.17 Qualitative spatiotemporal transport agreement between the particles and the model jellyfish (A) J-18495, (B) J-1160, (C) J-1162, (D) J-18499, and (E) J-18500.	145
Fig 5.18 Observed transport of jellyfish (J-18495) detections based on (A) tidal stage and (B) detection zone, and snapshot agreement of modelled particles with the correct detection zone at (C) 3 hrs and (D) 128 hrs after particle release.	146
Fig 5.19 SCA determined percentage agreements of the modelled particle locations with observed locations of jellyfish for five jellyfish models for surface and mid-depth releases.	148
Fig 5.20 MCA-based quantitative spatiotemporal transport agreement of the particles as per the jellyfish model (A) J-18495, (B) J-1160, (C) J-1162, (D) J-18499, and (E) J-18500 to the respective jellyfish.	150
<i>Fig 6.1</i> A simple graphical conception of jellyfish DVM model.	158
<i>Fig 6.2</i> Schematic representation of DVM conditions and rules. The open end of the trajectory arrow indicates the source, and the pointed end indicates the destination of the transport. The vertical transport strategies are represented by Number IDs	

List of Figures

(blue), and their abbreviated terms (green) are defined in the following paragraph.	160
<i>Fig 6.3</i> DVM model algorithm implemented in EFDC.....	164
<i>Fig 6.4</i> A diagram shows the model particles released from the surface (purple ring) and mid-depth (orange ring) water undergoing DVM with depth thresholds at 5.0 m (top) and 7.5 m (bottom). (Note: every 8 and 20 hr ticks are representative of day-night cycles and used for illustrative purposes only; real-time cycles were originally coded.).....	174
<i>Fig 6.5</i> Centroid trajectories and RMSE of JMR scenarios in the (A) east-west, (B) north-south, and (C) vertical directions.	177
<i>Fig 6.6</i> Snapshot of distributions of the passive drift and DVM particles at 109 hr after their release.....	177
<i>Fig 6.7</i> Centroid trajectories and RMSE of DMT scenarios in the (A) east-west, (B) north-south, and (C) vertical directions.	179
<i>Fig 6.8</i> Centroid trajectories and RMSE of release depth scenarios in the (A) east-west, (B) north-south, and (C) vertical directions.....	181
<i>Fig 6.9</i> Snapshots of particle locations 120 and 133 hr after their release for (A & C) DVM Scenario 4 and (B & D) passive drift scenario. The black circle marks the S1 detector range. The centroids of the particles released at different depths are marked by coloured diamonds (some are overlapping).....	183
<i>Fig 6.10</i> Comparing agreements as per J-18495 among the transport scenarios in terms of (A) percentage and (B) centroid distance for (1) surface and (2) mid-depth released particles over the short-term (S) and long-term (L) simulation periods. Real estimations are represented by the dashed lines and calculated means by the solid lines. [Notes: Specifications for the model scenarios are in Table 6.3. Centroid distances are from the periphery of the respective detectors.].....	189
<i>Fig 6.11</i> Spatiotemporal detections of the surface-released particles as per J-18495 model jellyfish detections in (A) passive drift, (B) DVM with 2.5 m threshold (Scenario 4), (c) DVM with 5.0 m threshold (Scenario 3) scenarios.	190

List of Figures

<i>Fig 6.12</i> Comparing agreements as per J-18500 between the DVM and the passive drift transport scenarios in terms of (A) percentage and (B) centroid distance for (1) surface and (2) mid-depth released particles over the short-term (S) and long-term (L) simulation periods. Real estimations are represented by the dashed lines and calculated means by the solid lines. [Notes: Specifications for the model scenarios are in Table 6.4. Centroid distances are from the periphery of the respective detectors.].....	193
<i>Fig 6.13</i> Snapshot of J-18500 modelled particle locations 52 hr after their release in Scenario 4 (DVM) and Scenario 6 (passive drift). The black circle marks the respective detector (S4) range. Coloured diamonds mark the centroids of the particles released at different depths.	194
<i>Fig 6.14</i> Spatiotemporal detections of the surface-released particles as per J-18500 model jellyfish detections in (A) passive drift, (B) DVM with 2.5 m threshold (Scenario 4) scenarios.....	195
<i>Fig 6.15</i> Comparing agreements as per J-1162 among the transport scenarios in terms of (A) percentage and (B) centroid distance for (1) surface and (2) mid-depth released particles over the simulation period. Real estimations are represented by the dashed lines and calculated means by the solid lines. [Notes: Specifications for the model scenarios are in Table 6.5. Centroid distances are from the periphery of the respective detectors.].....	198
<i>Fig 6.16</i> Snapshot of J-1162 modelled particle locations 19 and 21 hr after their release in Scenario 4 (DVM). Respective colour circles mark the respective detectors (S5 and S6) ranges.....	199
<i>Fig 6.17</i> Spatiotemporal detections of the surface-released particles as per J-1162 model jellyfish detections in (A) passive drift, (B) DVM with 2.5 m threshold (Scenario 4) scenarios.....	199
<i>Fig 6.18</i> MCA of Scenario-4 (DVM at 2.5 m threshold depth and 0.02 m/s motility rate) simulated for (A) J-18495, (B) J-1162, and (C) J-18500 models.	201

List of Figures

<i>Fig 7.1</i> Times and locations of jellyfish detections in Killary Harbour for 5 jellyfish and the corresponding tide levels. Detections are colour-coded by tag number. (Note: It is replicated here from Fig 5.3 in Chapter 5.).....	209
<i>Fig 7.2</i> Graphic showing all theoretical transport processes of the jellyfish. The red asterisks indicate the starting point of a movement, and the blue the destination. The dashed arrows indicate the movement directions.	211
<i>Fig 7.3</i> A summary of the different types of inter-zone travel observed in Killary. Each type of inter-zone travel is assigned a number from 1-8, which is used in subsequent analyses, while 0 is used to indicate intrazone travel. The eight detectors' zones are listed in order of location from east to west along the harbour. The arrow indicates the direction of transport, and the arrow length determines the specific shift. ...	212
<i>Fig 7.4</i> Observed jellyfish movements overlaid on water level graphs and visualised in terms of residency in particular detection zones (blue lines) or inter-zone travel (other coloured lines). The colour of the line indicates the type of governing transport process as per the legend, and the number of each line indicates the type of inter-zone travel based on Fig 7.3. Transports are shown for jellyfish: (a) J-1160, (b) J-1162, (c) J-18499, (d) J-18500, and (e) J-18495 (divided into e1 and e2 due to longer observation record). The orange circle indicates the releasing time of each jellyfish.	214
<i>Fig 7.5</i> Graphic showing scenarios of tidal transport of jellyfish; point pairs A-B and P-Q indicating the start-end of the tide and the jellyfish transport, respectively.	216
<i>Fig 7.6</i> Snapshots of particle distributions captured from (a-d) multiple swimming scenarios and (e) a drift-only scenario, along with (f) representative comparative traces of their travel paths.	238
<i>Fig 7.7</i> RMSEs (in meter, m) between pairs of particle centroids estimated across the (A) east-west, (B) north-south, and (C) water column depths upon releasing the particles at different water depths viz, surface, first quarter, mid-depth, and third-quarter.....	240

List of Figures

<i>Fig 7.8</i> Spatiotemporal trajectories of particle centroid and RMSE of trajectory-pairs along the (A) east-west, (B) north-south, and (C) vertical directions illustrated upon passive drift and swim scenarios 1, 2, and 3(1) as per J-18495 model.	242
<i>Fig 7.9</i> Spatiotemporal trajectories of particle centroid and RMSE of trajectory-pairs along the (A) east-west, (B) north-south, and (C) vertical directions illustrated upon passive drift and swim scenario 3 as per J-18495 model.....	244
<i>Fig 7.10</i> Spatiotemporal trajectories of particle centroid and RMSE of trajectory-pairs along the (A) east-west, (B) north-south, and (C) vertical directions illustrated upon passive drift and swim scenarios 7 and 8 as per J-18495 model.....	245
<i>Fig 7.11</i> Spatiotemporal trajectories of particle centroid and RMSE of trajectory-pairs along the (A) east-west, (B) north-south, and (C) vertical directions illustrated upon passive drift and swim scenarios 7 and 10 as per J-18495 model.	247
<i>Fig 7.12</i> Spatiotemporal trajectories of particle centroid and RMSE of trajectory-pairs along the (A) east-west, (B) north-south, and (C) vertical directions illustrated upon passive drift and swim scenarios 8 and 10 as per J-18495 model.	247
<i>Fig 7.13</i> Spatiotemporal trajectories of particle centroid and RMSE of trajectory-pairs along the (A) east-west, (B) north-south, and (C) vertical directions illustrated upon passive drift and swim scenario 12 as per J-18495 model.	248
<i>Fig 7.14</i> Spatiotemporal trajectories of particle centroid and RMSE of trajectory-pairs along the (A) east-west, (B) north-south, and (C) vertical directions illustrated upon passive drift and swim scenarios 4 and 5 as per J-18495 model.....	249
<i>Fig 7.15</i> Spatiotemporal trajectories of particle centroid and RMSE of trajectory-pairs along the (A) east-west, (B) north-south, and (C) vertical directions illustrated upon passive drift and swim scenarios 7 and 11 as per J-18495 model.	250
<i>Fig 7.16</i> Spatiotemporal trajectories of particle centroid and RMSE of trajectory-pairs along the (A) east-west, (B) north-south, and (C) vertical directions illustrated upon passive drift and swim scenarios 6 and 7 as per J-18495 model.....	251

List of Figures

<i>Fig 7.17</i> Spatiotemporal trajectories of particle centroid and RMSE of trajectory-pairs along the (A) east-west, (B) north-south, and (C) vertical directions illustrated upon passive drift and swim scenarios 8 and 9 as per J-18495 model.....	252
<i>Fig 7.18</i> Spatiotemporal detections of surface-released particles from J-18495 scenarios.....	258
<i>Fig 7.19</i> Spatiotemporal detections of mid-depth-released particles for J-18495 scenarios.....	260
<i>Fig 7.20</i> Comparing agreements as per J-18495 among the swim scenarios in terms of (A) percentage and (B) centroid distance for (1) surface and (2) mid-depth releasing particles over the short-term (S) and long-term (L) simulation periods. Real estimations are represented by the dashed lines and calculated means by the solid lines. [Notes: Specifications for the model scenarios are in Table 7.3. Centroid distances are from the periphery of the respective detectors.].....	275
<i>Fig 7.21</i> Comparing agreements as per J-18495 among the swim scenarios in terms of (A) percentage and (B) centroid distance for (1) surface and (2) mid-depth releasing particles over the short-term (S) and long-term (L) simulation periods. Real estimations are represented by the dashed lines and calculated means by the solid lines. [Notes: Specifications for the model scenarios are in Table 7.3. Centroid distances are from the periphery of the respective detectors.].....	276
<i>Fig 7.22</i> Comparing agreements as per J-18495 among the swim scenarios in terms of (A) percentage and (B) centroid distance for (1) surface and (2) mid-depth releasing particles over the short-term (S) and long-term (L) simulation periods. Real estimations are represented by the dashed lines and calculated means by the solid lines. [Notes: Specifications for the model scenarios are in Table 7.3. Centroid distances are from the periphery of the respective detectors.].....	277
<i>Fig 7.23</i> Comparing agreements as per J-18495 among the swim scenarios in terms of (A) percentage and (B) centroid distance for (1) surface and (2) mid-depth releasing particles over the short-term (S) and long-term (L) simulation periods. Real estimations are represented by the dashed lines and calculated means by the solid	

List of Figures

lines. [Notes: Specifications for the model scenarios are in Table 7.3. Centroid distances are from the periphery of the respective detectors.].....	278
<i>Fig 7.24</i> Comparing agreements as per J-18495 among the swim scenarios in terms of (A) percentage and (B) centroid distance for (1) surface and (2) mid-depth releasing particles over the short-term (S) and long-term (L) simulation periods. Real estimations are represented by the dashed lines and calculated means by the solid lines. [Notes: Specifications for the model scenarios are in Table 7.3. Centroid distances are from the periphery of the respective detectors.].....	279
<i>Fig 7.25</i> Graphical representations of MCA of active swim scenarios (A~S) and passive drift scenario (T) for J-18495 jellyfish model.....	282
<i>Fig 7.26</i> Comparing long-term MCA scores for J-18495 for (A) Scenario-10(1, 2), (B) Scenario-12(1, 2, 3) and (C) their bests along with scenarios 5 and 11 modelled. Real estimations are represented by the dashed lines and calculated means by the solid lines. [For the scenario specifications, please see Table 7.3.]	284
<i>Fig 7.27</i> Modelled spatiotemporal detections of J-1162 for (A) surface and (B) mid-depth released particles and (C) observed spatiotemporal detections.	285
<i>Fig 7.28</i> Spatiotemporal detections of (A~C) surface and (D~F) mid-depth released particles of J-1162 jellyfish model across scenarios.	286
<i>Fig 7.29</i> Comparison of the modelled swim scenarios of the J-1162 jellyfish model in terms of (A) percentage agreement and (B) centroid distance shown by the particles released at (1) surface and (2) mid-depth water.....	290
<i>Fig 7.30</i> Snapshot of particle locations (A) 15-16 hr and (B) 19-21 hr after their release in all depths in Scenario-12(7)......	291
<i>Fig 7.31</i> Modelled and observed spatiotemporal detections of the J-18500 jellyfish model [(A) surface and (B) mid-depth releasing particles and (C) observation]..	292
<i>Fig 7.32</i> Comparison of the modelled swim scenarios of the J-18500 jellyfish model in terms of (A) percentage agreement and (B) centroid distance shown by the particles released at (1) surface and (2) mid-depth water.....	294

List of Figures

<i>Fig 7.33</i> Snapshot of particle locations of the J-18500 jellyfish model at two different travel instances of (A) 15 hr and (B) 52 hr after their release in different depths as per Scenario-12(4).	295
<i>Fig 7.34</i> Comparing MCA scores of (A) J-18495, (B) J-1162, and (C) J-18500 jellyfish models between the best swim and passive drift scenarios at short- and long-term simulations. Real estimations are represented by the dashed lines and calculated temporal means by the solid lines.....	296

List of Tables

Table 4.1 Model parameters, state variables and constants.....	63
Table 4.2 Comparing the equivalence of EFDC layers to ADCP bins.	68
<i>Table 4.3 Sensitivity investigation plan.....</i>	<i>71</i>
<i>Table 4.4 Sensitivity effect analysis matrix.....</i>	<i>72</i>
Table 4.5 Summary of the model sensitivity study to the wind.	84
Table 4.6 Summary of the model sensitivity study to the river discharge.....	89
Table 5.1 Information on jellyfish release for observation in Killary	106
Table 5.2 Sample of raw data file which contained sequential records of all pings from all 8 receivers for all jellyfish.	108
Table 5.3 Operational and functional settings for the particle-track sub-model.	110
Table 5.4 Details of LPT module sensitivity study.	114
Table 5.5 Multicriteria analysis (MCA) for quantifying transport agreements.	119
Table 5.6 Transport events determined for J-18495 - (a) residence and (b) movement.....	121
<i>Table 6.1 A summary of DVM conditions and respective rules.....</i>	<i>161</i>
<i>Table 6.2 Sensitivity study plan for the DVM model.</i>	<i>171</i>
<i>Table 6.3a A comparison of model performance metrics for surface particle releases for J-18495.</i>	<i>187</i>
<i>Table 6.4 A comparison of model performance metrics of surface and mid-depth particle releases for J-18500.....</i>	<i>191</i>
<i>Table 6.5 A comparison of model performance metrics for surface and mid-depth particle releases for J-1162.</i>	<i>197</i>
<i>Table 7.1 Summary of the swim rules.</i>	<i>229</i>
<i>Table 7.2 List of model scenarios run for assessment of model sensitivity and accuracy.....</i>	<i>233</i>

List of Tables

<i>Table 7.3a</i> Quantitative transport agreement of surface released particles in different scenarios.	264
<i>Table 7.4</i> Customized swim scenarios for the J-1162 jellyfish model.	285
<i>Table 7.5</i> A comparison of quantitative transport agreement of surface and mid-depth releasing particles (as per J-1162) among different swim scenarios	288
<i>Table 7.6</i> Quantitative transport agreement of surface and mid-depth releasing particles (as per J-18500) in Scenario-12(4).	293

CHAPTER 1:INTRODUCTION

1.1. Jellyfish and Their Impacts

Jellyfish are planktonic gelatinous invertebrates with more than 200 different species. They frequently occur along coastlines and can be found anywhere in the water column from the surface to the deep sea. Apart from their role in ecosystem functioning, they have become notable to researchers, and the public, for their negative impacts on maritime activities such as fisheries, tourism, and recreation. In recent times, they have gained much negative public attention due to beach closures and damage/mass kills of marine-farmed fish arising from the sudden occurrence of jellyfish swarms or 'blooms' (Fig 1.1) and are often considered a nuisance species in marine and coastal ecosystems or as indicators of ecosystem alteration (Doyle et al., 2014). Their tendency to form large blooms has made them renowned (Pitt & Lucas, 2014). Jellyfish numbers are thought to be increasing worldwide (Brotz et al., 2012; Mills, 2001), which would partly explain the recent increases in their notoriety.

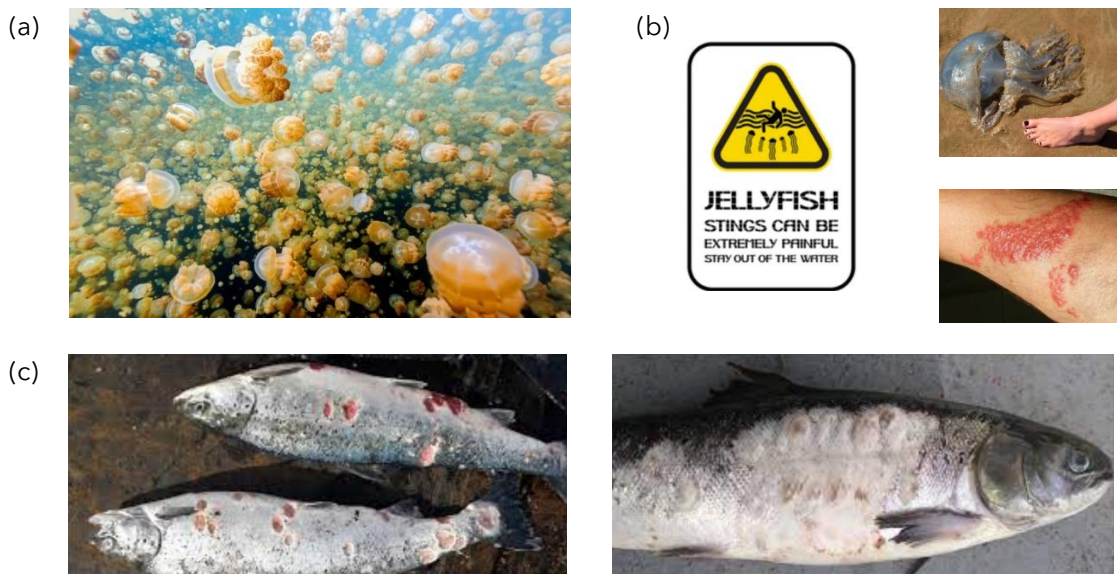


Fig 1.1 A collage of pictures showing (a) a jellyfish bloom, (b) jellyfish sting on humans (photo courtesy: Google), (c) mortality and skin pathology of farmed Atlantic salmon caused by exposure to jellyfish (Mitchell et al., 2021).

Chapter 1: Introduction

Jellyfish aggregation events like swarm formation, seasonal bloom, and beach strandings in coastal waters have resulted in the deterioration of water quality, alterations within the food chain, hindrance in seawater uptake by power plants, and declines in tourism (Baliarsingh et al., 2020). The stinging incidents by jellyfish on beachgoers have had a significant impact on marine-based tourism and coastal recreation (Gómez & Gutiérrez-Hernández, 2020; Ruiz-Frau, 2022), which has led to more frequent beach closures, decreased attendance at seaside resorts, and a reduction in water-based activities such as swimming and surfing.

Fish kill events or gill disorders in marine-farmed fish due to jellyfish sting toxins are a global problem (Purcell et al., 2007; Rodger et al., 2011). Jellyfish outbreaks can have a significant negative influence on the activities of fishing and aquaculture through damage to fish stocks (Boero, 2013; Richardson et al., 2009). Large blooms can pose a direct threat to the sustainability of fishing for finfish and other stocks (Lynam et al., 2006). They interfere with the operation of nets, thus reducing the fish catch and restricting the fishers' activities, sometimes forcing them to move to another fishing area. These problems may result in an increase in working time and consequent economic losses (Nagata et al., 2009). Indirectly, large numbers of jellyfish can also affect fishing by competing for food with fish species of commercial value (Boero, 2013) and/or by preying on the eggs, larvae, and juveniles of those species.

Jellyfish occurrence in Irish waters is a significant natural phenomenon, with various species making regular appearances along the country's coastal regions. While these gelatinous creatures play essential roles in marine ecosystems, their presence can also pose potential hazards. Ireland experiences seasonal influxes of jellyfish, particularly during the warmer months when favourable conditions support their blooms. The hazard they pose primarily stems from their ability to deliver painful stings, often causing discomfort and mild to moderate reactions in humans. Though most jellyfish stings are not life-threatening, some species found in Irish waters, such as lion's mane jellyfish (*Cyanea capillata*), can deliver more severe stings, requiring medical attention in certain cases.

Chapter 1: Introduction

In the summer of 2017, there was a notable increase in lion's mane jellyfish sightings along the west coast of Ireland (Surve, 2018). This influx prompted warnings to beachgoers and swimmers to be cautious and aware of the potential risks associated with encountering these jellyfish. Portuguese Man O' War jellyfish (*Physalia physalis*) can also be found in Irish waters. In 2016, there were reports of sightings of this jellyfish on beaches in counties Kerry and Clare (McSorley, 2016). These organisms have long tentacles that can deliver painful stings, and authorities issued warnings to the public about their presence. Moon jellyfish (*Aurelia aurita*) are common in Irish waters and are usually harmless to humans. However, in 2014, there were reports of large numbers of moon jellyfish washed up on beaches in Co. Donegal (Maguire, 2017). While not directly hazardous to people, their presence can indicate favourable conditions for jellyfish blooms, which might lead to an increase in other, more harmful species. In the summer of 2007, there was a significant increase in the abundance of mauve stinger jellyfish (*Pelagia noctiluca*) off the coast of Ireland (O'Sullivan, 2017). These jellyfish can form large swarms and have been known to impact tourism and aquaculture activities in affected areas. Compass jellyfish (*Chrysaora hysoscella*) are commonly found in Irish waters during the summer months. There were reports of numerous compass jellyfish sightings in Dublin Bay (Thomas K. Doyle et al., 2007). While their stings are generally not severe, their presence in popular swimming areas can still pose a hazard to beachgoers. In 2012, there were reports of a large number of blue jellyfish (*Cyanea lamarckii*) washing up on beaches in Co. Waterford (Hogan, 2012). In 2018, there were reports of large numbers of by-the-wind sailors jellyfish (*Velella velella*) washing up on beaches along the west coast of Ireland (McLaughlin, 2021). While they are not dangerous to humans, their presence can indicate the presence of oceanic currents that may also transport other jellyfish species. Additionally, these jellyfish can impact local fisheries and aquaculture operations by damaging fishing gear or clogging nets.

The study site selected for this research, Killary Harbour, located on the west coast of Ireland, is home to salmon and mussel farming and has experienced the harmful

impacts of jellyfish (a quantitative account of this impact will follow in the Literature Review chapter). This was one of the reasons for its selection as a case study.

1.2. Jellyfish Transport, Bloom Formation, and their Modelling

Jellyfish transport is a crucial aspect of bloom formation, as it determines how jellyfish move through the water and where they end up. Jellyfish use a variety of mechanisms to transport themselves, including passive drifting, active swimming, and vertical migration. Passive drifting occurs when jellyfish allow themselves to be carried by ocean currents, while active swimming involves using muscular contractions to move through the water. Vertical migration is a behaviour in which jellyfish move up and down in the water column, typically to follow food sources or avoid predators. The factors that influence jellyfish transport are numerous and complex. Physical factors such as ocean currents, water temperature, and salinity can all affect jellyfish movement, as can biological factors such as food availability, predation risk and light sensitivity. Jellyfish also exhibit a range of behaviours that can influence their transport, including phototaxis (movement towards light), geotaxis (movement towards gravity), and rheotaxis (movement towards water flow).

Jellyfish blooms occur when large numbers of jellyfish congregate in one area. Once jellyfish have been transported to a specific location, they may begin to form a bloom. The mechanisms behind jellyfish bloom formation are complex and must be fully understood. Several factors have been proposed as contributors to jellyfish bloom formation. These include oceanographic factors such as temperature, salinity, and nutrient availability, as well as biological factors such as predation pressure and reproductive success; biophysical and mechanical forcing factors have received relatively less attention in the investigation. Further research is needed to fully understand the mechanisms behind jellyfish transport and bloom formation and develop effective management strategies to mitigate their impacts.

Efforts to predict and manage jellyfish blooms require a priority focus on investigating strategies to identify the factors that contribute to their formation and understanding their respective contributions. These strategies include developing

Chapter 1: Introduction

technologies to detect and predict jellyfish transport mechanisms. Jellyfish blooms often cause significant ecological and economic damage. Understanding the mechanisms behind jellyfish transport and bloom formation is essential for predicting and managing these events, which ultimately helps to mitigate their ecological and economic impacts.

The most common process-based modelling approach used to simulate jellyfish transport to date has been the use of a hydrodynamic model coupled with a Lagrangian particle tracking model where the jellyfish are simulated as passive drifters (e.g. David et al., 2015; Moon et al., 2010). However, it has been shown that coupling behavioural and biological models with hydrodynamics can be advantageous in this regard (e.g. Fossette et al., 2015; Rahi et al., 2020). Depending on the purpose of transport and the nature of energy utilisation for the associated displacement, jellyfish move in the water either by the fluid force or swimming motility or a combination of both. Sea currents are thought to be primarily responsible for the movements of jellyfish, and inter-annual and/or seasonal variations in currents can determine the extent and timing of their blooms. Such information is considered valuable for modelling jellyfish spread and distribution. Local hydrological and weather characteristics regarding riverine discharge, monsoon precipitation, wind patterns, tidal currents, salinity and temperature, and the seasonal/annual variations of these conditions can also trigger blooms (Wei et al., 2015).

Although jellyfish generally drift on the currents, they are not always passive drifters. They can actively swim for navigation by pulsating their bell body (Fig 1.2). Jellyfish motility behaviour is exhibited on purpose. Some bio-physical factors and/or bio-behavioural features, which are thought to be highly influential for jellyfish swimming motility, are light-sensitive diel vertical migration (DVM), movement for food/nutrition/prey/mating, optimising and/or maintaining safe/preferred shelters, avoiding pollution and/or stress, hiding from predators, and tendency towards preferential physicochemical properties of water (e.g., salinity, temperature, density etc.). These are not mutually exclusive; they often occur in combination and are found to exhibit relative significance over each other on a case-by-case basis. The

literature suggests that jellyfish motility can help them achieve better survival, avoid stranding, and withstand tidal currents, thereby favouring swarms. To date, DVM has been the preferred motility behaviour to include in hydrodynamic models.

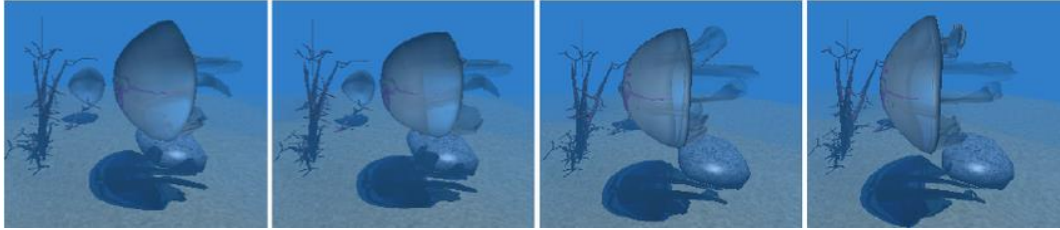


Fig 1.2 A collage featuring a series of pictures that depict a jellyfish with floating tentacles and slight deformations applied to the bell, showcasing two contraction steps on the left and two expansion steps on the right.

1.3. Aims and Objectives

For the current research, it was hypothesised that the active swimming motility of jellyfish contributes to their net transportation, and its inclusion could improve transport prediction modelling. The combination of active (behavioural) and passive (floating or drifting) movements of jellyfish through coupling these respective strategies in jellyfish transport modelling could help to investigate their transport and dynamics more precisely. The primary aim of this research was therefore the development of a novel coastal biophysical model to simulate the transport and fate of jellyfish, which included passive drifting, diel migration, and horizontal swimming. This was achieved by completing the following objectives:

- 1) Review the jellyfish transport and modelling literature to understand the primary mechanisms of jellyfish transport the modelling strategies used to date.
- 2) Develop and validate a 3D baroclinic hydrodynamic model of the Killary Harbour study area to simulate circulation in the harbour.

Chapter 1: Introduction

- 3) Use Lagrangian particle tracking (LPT) to model jellyfish as free-swimming drifters subject to advection and diffusion only.
- 4) Develop the LPT approach to incorporate the diel vertical migration (DVM) behaviour of the jellyfish so as to incorporate the contribution of their diel transport behaviour within their net transportation.
- 5) Further, develop the LPT approach to incorporate horizontal swimming motility in their transport modelling.
- 6) Using the jellyfish transport models developed in objectives 3-5 to investigate the contributions and relative importance of the various transport processes on net jellyfish transportation.

The hydrodynamic model used for the research was the Environmental Fluid Dynamics Code (EFDC). EFDC can be run in a 2D or 3D model and contains an LPT sub-module. A field study conducted by researchers at University College Cork collected transport records for a number of jellyfish tagged and released within Killary. These data were used for comparison with model predictions.

The spatial and temporal scales of a model can vary depending on the specific purpose of investigation and the availability of measured data for validation. For instance, a hydrodynamic model may encompass a spatial range spanning from a small local waterbody to a larger regional area. Similarly, the temporal scale can range from a day, week, month, to even years or centuries. In the particular case of this hydrobiological model used to investigate jellyfish transport mechanisms in the Killary Harbour estuary, the chosen spatial scale was focused on the estuarine level. This decision aligns with the typical operations of aquaculture activities in the area. The temporal scale of the model was intentionally chosen to align with the available measured data on jellyfish transport in Killary so that the model could be effectively used to investigate the role of different transport mechanisms operating at the inter-tidal scale. By matching the spatial and temporal scales in this way, the model was better equipped to address the specific jellyfish dynamics and phenomena

involved, leading to more meaningful and reliable results for understanding jellyfish transport mechanisms in the estuary.

In addition to tracking jellyfish in marine waters, the particle tracking approach has the potential for various applications, such as tracking other marine organisms (e.g. Pearce et al., 2011) like fish or lobsters. These species share similar motility patterns and may undergo diel migration, making the particle tracking method applicable to their modelling as well. The versatility of this biophysical modelling approach extends beyond just jellyfish tracking in the seas. It can be effectively utilized and useful for a wider range of similar studies in digital planet, sustainability research, bioengineering, etc. By leveraging the particle tracking approach, researchers and scientists can gain valuable insights into the movement and behaviour of various species and particles in complex environments. This valuable tool can open up new possibilities for understanding ecological dynamics, optimizing resource management, and designing innovative solutions in diverse domains.

1.4. Thesis Outline

The layout and content of this thesis are as follows:

Chapter 2 presents a literature review of jellyfish transport modelling. Key findings from previous studies made to investigate jellyfish occurrence and distribution are presented. State of the art in jellyfish transport modelling investigations are highlighted. The research gaps that were not addressed or remained unanswered in the published literature are also explored.

Chapter 3 presents the theories for the EFDC hydrodynamic model and its LPT drifter module. Descriptions of the equations are presented with their mathematical justifications. The numerical discretisation for hydrodynamic and transport solution schemes is presented.

Chapter 4 describes the hydrodynamic model of Killary Harbour. The model setup is presented, and the validation process is described. The chapter also presents an investigation of the sensitivity of the hydrodynamic circulation in Killary to the various forcing functions, including wind, river flow and density.

Chapter 1: Introduction

Chapter 5 presents the development and application of the passive drift model for jellyfish transportation in Killary. Technical and operational details of EFDC's Drifter module and its modification and integration within the model are also described. Model assessment and evaluation, scenario simulations, and model sensitivity analyses are presented in detail. The chapter presents comparisons of modelled transport with observed transports of jellyfish. The observational dataset is also presented and analysed.

Chapter 6 provides the details of the novel DVM model development. The light-induced behavioural transport rules used in the modelling are described. The synchronised coupling of the DVM model within the passive drift and hydrodynamic models are also described. Simulations, analyses, and comparisons are presented.

Chapter 7 presents the development of a novel swim model for jellyfish. Possible swimming behaviours of jellyfish were deduced from a comprehensive analysis of their observed transport in Killary. The swim rules included in the model are described. Rule implementation, transport processes synchronisation, and submodel integration are also described. Model sensitivity to swim properties and parameters, particle distributions and insights on transport patterns due to swim, and agreement of the modelled transports to the observation are analysed, visualised, and discussed.

Finally, Chapter 8 presents a short summary of the research, the key conclusions and recommendations for possible future progression of the research.

CHAPTER 2: LITERATURE REVIEW

2.1. Introduction

Over the last few decades, there has been a concern that the jellyfish population has had dramatic spatial increases and temporal shifts in distributions. Trends exhibit that this concern will likely become more frequent in future. Studies show that jellyfish numbers have increased for years (Brotz et al., 2012; Lynam et al., 2006; Qu et al., 2015). Events like climate change, eutrophication, overfishing, species invasion, etc. are thought to be causing this increase of jellyfish in the world's oceans (e.g. Mills, 2001).

The adverse consequences of increased jellyfish numbers, which are also occurring in greater numbers, include ecosystem alterations and damage to the fisheries and tourism industries (Condon et al., 2012, 2013). The deterioration of the coastal ocean ecosystem is supported by the evidence that there are increasing incidences of jellyfish blooms (Jackson et al., 2001). While global assessments of this fact are abundant, evidence and a composite understanding of its comprehensive mechanisms are still lacking. Despite the increased occurrence of bloom events, jellyfish are relatively less scientifically investigated and monitored than other marine species (Baliarsingh et al., 2020). Efforts have remained fragmented in scope missing synthesised information across marine ecosystems (Condon et al., 2012, 2013). Hence, the question of how and why jellyfish populations are rising globally or even on a regional and local scale remains unanswered as does the question of how and why jellyfish blooms occur, and so this creates an opportunity for jellyfish transport research. Through the advent of computer modelling techniques, it is possible to analyse the potential transport mechanisms of jellyfish and the conditions that trigger jellyfish swarming to work toward an effective prediction and monitoring strategy. Numerical models with a Lagrangian particle-tracking approach are useful here as they have the potential to simulate the movements of jellyfish (e.g. Kimmerer et al., 2014; Qiu et al., 2010; Wei et al., 2015).

Chapter 2: Literature Review

This chapter highlights the previous studies efforted to investigate jellyfish occurrence with regard to their transports. The chapter is structured as follows: Section 2.2 provides an overview of jellyfish characteristics, while Section 2.3 delves into their behaviours; Section 2.4 reviews the occurrence and consequences of jellyfish in coastal seas; Section 2.5 provides an overview of the latest developments in jellyfish prediction, including advancements in modelling techniques in line with incorporating the hydrodynamic factors, salinity and temperature dynamics, and jellyfish swimming behaviour in the modelling; and finally, Section 2.6 presents the conclusions drawn from the review of jellyfish and their transportation.

2.2. Jellyfish: What are they?

Jellyfish are mesmerizing, graceful, and enigmatic creatures which have long captivated the human imagination. Scientists and marine biologists have made significant efforts to understand the life cycle and behaviours of these otherworldly creatures. The physical and biological characteristics of jellyfish showcase the remarkable adaptability of marine life and the delicate balance of ecosystems. These ethereal marine invertebrates belong to the phylum Cnidaria and are members of the class Scyphozoa. With a history spanning over 500 million years, jellyfish have evolved into diverse and fascinating organisms. This section aims to delve into the intricate physical and biological aspects of jellyfish, shedding light on their appearance and the wonders of their uniqueness.

One of the most distinctive features of jellyfish is their gelatinous, umbrella-shaped body, known as the bell. This bell is composed of a transparent, jelly-like substance called mesoglea, which gives the jellyfish its characteristic texture and flexibility. The mesoglea acts as a buoyancy aid, allowing jellyfish to float effortlessly in the water column. Jellyfish exhibit radial symmetry, which means their body is organized around a central point. This arrangement allows them to detect and respond to stimuli from all directions equally. Their symmetry is evident in the numerous tentacles that dangle from the bell's edge. Hanging from the bell, jellyfish possess long, trailing tentacles equipped with specialized cells called nematocysts. Nematocysts are harpoon-like structures containing venom that jellyfish use to

Chapter 2: Literature Review

capture and immobilize their prey. When touched, these nematocysts rapidly discharge and deliver a paralyzing sting.

Jellyfish exhibit a remarkable diversity in size, shape, and form, which is a testament to their adaptation to various marine environments. They come in a wide range of sizes, from tiny or minuscule to giants of the sea. Some jellyfish, like the Irukandji jellyfish, the *Staurocladia* spp. or *Sarsia* spp., are tiny, measuring only a few millimetres in bell diameter. These species often go unnoticed due to their diminutive size. On the other end of the spectrum, jellyfish can grow exceptionally large. The colossal Nomura's jellyfish (*Nemopilema nomurai*) is one of the largest known jellyfish species, with bells that can reach up to two meters in diameter and tentacles extending over 30 meters. The medusa form of jellyfish is the most familiar one, characterized by the bell-shaped, umbrella-like body. However, even within this category, there are several variations like dome-shaped medusae, saucer-shaped medusae, elongated medusae among others. Some jellyfish have a more rounded, dome-like bell, which gives them a distinctive appearance. An example of this shape is the Moon jellyfish (*Aurelia aurita*), a common species found in coastal waters around the world. Saucer-shaped medusae jellyfish have a flat, saucer-like bell with a pronounced rim. The Upside-down jellyfish (*Cassiopea* spp.) is an excellent example of this shape. They often lie on the seafloor with their bell facing upwards, exposing their photosynthetic symbiotic algae to the sunlight. Elongated medusae jellyfish have an elongated bell shape, which allows them to move through the water with greater efficiency. The Lion's Mane jellyfish (*Cyanea capillata*) is a prominent example of an elongated medusa, and its long, flowing tentacles can extend up to several meters.

The tentacles of jellyfish can vary significantly in terms of structure and length. Some species, like the Portuguese Man o' War (*Physalia physalis*), have long, trailing tentacles equipped with powerful stinging cells. These tentacles can extend several meters, allowing them to capture prey and defend against predators. Other jellyfish have shorter and more delicate tentacles with a frilly appearance. These tentacles are often used for filter-feeding on plankton and small particles from the water.

Chapter 2: Literature Review

Jellyfish coloration varies greatly, with some species exhibiting vibrant hues and others appearing more subdued. They can display a stunning array of patterns and colours on their bell, adding to their aesthetic allure. Certain species possess bioluminescent capabilities, producing flashes of light or glowing patterns. This phenomenon is especially striking in deep-sea species, where bioluminescence is used for attracting prey or confusing predators. Some jellyfish have striped or spotted patterns on their bells, providing camouflage or visual cues for mating and communication. The Box jellyfish (*Chironex fleckeri*) exhibits striking patterns on its bell. Many jellyfish are nearly transparent, making them almost invisible in the water. This transparency allows them to blend seamlessly into their surroundings, making it easier to surprise prey and evade predators.

The jellyfish life cycle begins with a tiny, tubular polyp that attaches itself to the ocean floor or other surfaces. The polyp undergoes asexual reproduction, forming colonies and producing buds. The asexually produced buds eventually develop into the free-swimming medusa, which represents the typical jellyfish form that we recognize. The medusa stage is when jellyfish reach their peak mobility and can be seen gracefully gliding through the water. During the medusa stage, jellyfish engage in sexual reproduction. Males release sperm into the water, which are captured by females' tentacles and transferred to specialized structures for fertilization. Fertilized eggs develop into larvae called planulae, which eventually settle on the seafloor and grow into polyps, completing the life cycle.

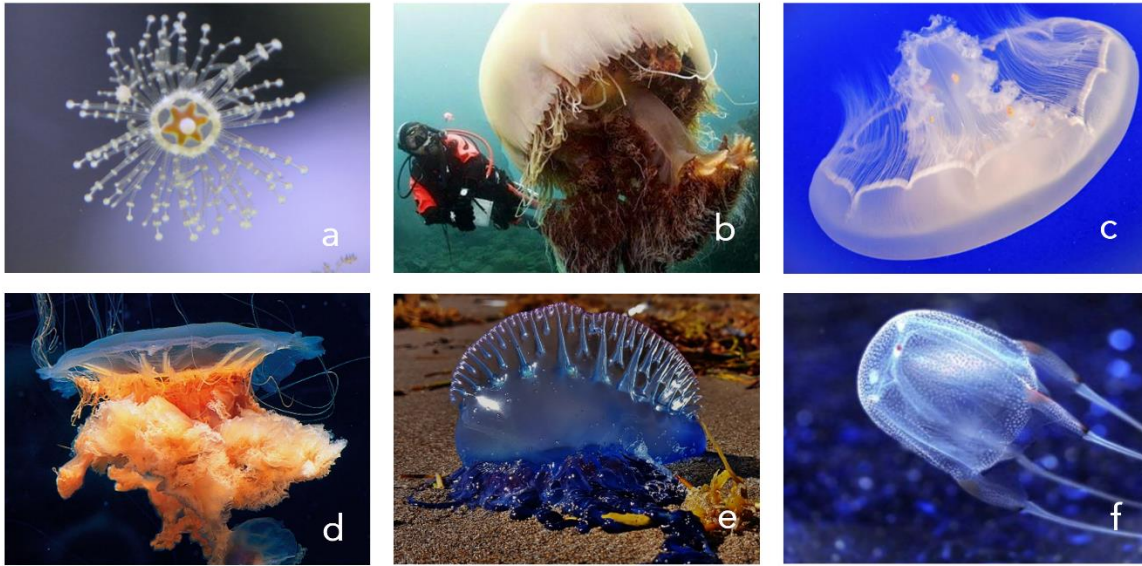


Fig 2.1 An assortment of jellyfish varieties - (a) *Staurocladia* sp., (b) *Nemopilema nomurai*, (c) *Aurelia aurita*, (d) *Cyanea capillata*, (e) *Physalia physalis*, and (f) *Chironex fleckeri*.

2.3. Jellyfish behaviours and modelling approaches

Jellyfish swarms or blooms are mesmerizing natural phenomena where large numbers of jellyfish congregate in specific areas of the ocean. Transportation plays a crucial role in the formation of these swarms, acting as a driving factor that brings jellyfish together. These blooms can have significant ecological impacts, disrupting marine ecosystems and affecting fish populations. The reasons behind these population explosions are complex and often related to hydro-environmental factors. Several key transportation mechanisms contribute to the formation of jellyfish swarms. Ocean currents play a significant role in transporting jellyfish across vast distances. Jellyfish are predominantly passive drifters, meaning they have limited control over their movement and rely on the direction and speed of ocean currents. When favourable currents carry jellyfish larvae or adult individuals to specific regions, they can accumulate and form swarms in those areas. By riding ocean currents, they can spread due to their passive dispersal capabilities, be transported to distant locations, colonizing new habitats, or encountering food sources along the way. This process also aids in the dispersion of jellyfish larvae

Chapter 2: Literature Review

during their early life stages. Ocean currents may also concentrate food resources, leading to higher jellyfish abundance. Surface winds can influence jellyfish transportation by creating wind-driven drift, causing them to accumulate in particular areas. Wind can also influence the direction and speed of ocean currents, indirectly impacting jellyfish movement and aggregation. Tidal movements, driven by gravitational forces of the moon and the sun, can create water movements that influence jellyfish transportation. During certain tidal cycles, water flow patterns may concentrate jellyfish into estuaries, bays, or near the coast, leading to the formation of swarms in these regions. Jellyfish movements are also influenced by oceanic processes like upwelling and downwelling, which can impact their transportation and lead to their clustering in specific areas. This phenomenon plays a crucial role in the formation of jellyfish swarms.

Another important transport mechanism of jellyfish is their seasonal migrations. Some jellyfish species undertake seasonal migrations in response to changing environmental conditions, such as temperature and food availability. During these migrations, jellyfish may move en masse to different regions, leading to the formation of large swarms. For example, certain species may migrate to warmer waters for breeding or to follow their prey. Jellyfish exhibit diurnal (daytime) and nocturnal (nighttime) vertical migrations in response to changing light levels. This behavioural response of jellyfish is known as phototaxis, where they are attracted to, or repelled by, light. In response to light cues, jellyfish adjust their direction, often ascending toward the water's surface during the day to bask in sunlight and descending into deeper waters at night. During the day, they tend to stay in deeper waters to avoid predation, while at night, they ascend closer to the surface to feed on plankton and other small organisms. Another navigational strategy employed by jellyfish is geotaxis, which involves their response to gravity. They use specialized balance receptors, called statocysts, to detect changes in their orientation. This ability helps them maintain their desired depth in the water column. Jellyfish also exhibit a behaviour known as rheotaxis, where they reorient their body axis and swim with respect to the flow velocity field of a current. This mechanical stimulation by the moving water serves as a guiding factor in their transportation. By turning to

Chapter 2: Literature Review

face into an oncoming current, jellyfish can effectively hold their position, preventing them from being swept downstream. This behavioural tendency allows jellyfish to align themselves with the current flow, reducing the energy expenditure during their passive drifting. By doing so, they can travel considerable distances with minimal effort. Rheotaxis is a crucial adaptation that enables jellyfish to navigate through ocean currents efficiently, contributing to their ability to form swarms and occupy specific areas in marine waters. Jellyfish have also been observed to exhibit aggregation responses, where the presence of other jellyfish can attract additional individuals to a particular location. This behaviour is thought to be influenced by chemical cues released by jellyfish or triggered by the visual presence of conspecifics. As more jellyfish accumulate, the aggregation effect intensifies, resulting in the formation of a swarm.

Jellyfish showcase remarkable adaptations in their navigation skills, achieved through their distinctive pulsations and graceful undulations, enabling them to master the art of dancing with the currents. Central to their locomotion is the bell, the umbrella-shaped body that propels them through the water. Through rhythmic contractions and expansions of the bell, jellyfish generate water flow to propel themselves forward. These pulsations create a gentle and rhythmic movement, allowing them to navigate with efficiency. This elegant method of propulsion enables jellyfish to gracefully glide through marine waters, a testament to their ability to harmoniously interact with their environment. However, jellyfish are not strong swimmers and primarily rely on passive drift to move through the water. Their gelatinous bodies provide buoyancy, allowing them to float effortlessly with ocean currents. By adjusting their bell contractions and body posture, jellyfish can regulate their depth and direction, albeit to a limited extent.

Jellyfish, despite their seemingly delicate and passive nature, possess remarkable locomotion, motility, navigation, movement, and transportation capabilities that have allowed them to thrive in marine waters for millions of years. Through their pulsations and bell contractions, they gracefully traverse the oceans, relying on currents and buoyancy to cover vast distances. With simple navigation mechanisms like phototaxis, geotaxis, and rheotaxis, they adjust their movement to optimize their

Chapter 2: Literature Review

survival in ever-changing environments. It's essential to note that while transportation factors play a role in swarm formation, the specific drivers can vary depending on the jellyfish species, the geographic region, and the prevailing environmental conditions. Additionally, other factors, such as reproduction, predation, and food availability, can also interact with transportation mechanisms to contribute to the formation and dynamics of jellyfish swarms. Understanding the intricacies of swarm formation is essential for studying the ecological impacts and potential consequences of these aggregations on marine ecosystems and human activities.

The transport and dispersal of jellyfish in marine waters have long fascinated scientists and researchers, owing to its implications on ecological dynamics, aquaculture, and tourism. As jellyfish populations continue to flourish and impact marine ecosystems, understanding their movement patterns becomes crucial for effective management strategies. In recent years, numerical modelling approaches have emerged as powerful tools to help predict jellyfish transport, offering valuable insights into their spatial distribution and behaviour. By harnessing the potential of numerical modelling, scientists and users of the ocean can make informed decisions for the sustainable coexistence of human activities and the enigmatic world of jellyfish in our oceans.

The ability to model jellyfish locomotory behaviour allows for the representation of movement patterns independent of passive drifting that are crucial for understanding their transport dynamics within these confined and dynamic environments. Many jellyfish species possess the ability to control their buoyancy, allowing them to move vertically within the water column. For example, during flood tides, jellyfish might adjust their swimming behaviour to ascend in the water column, while during ebb tides, they might swim downward to optimize their transport within the estuary or fjord. Swimming motility models can simulate this behaviour, which is especially important in environments where density gradients are pronounced, such as in estuaries with varying salinity levels. Locomotory behaviour and swimming motility enable jellyfish to respond realistically to environmental forcing, such as changes in current speed, direction, and temperature. Tidal cycles in estuaries and

fjords result in significant variations in water speed and direction. By incorporating swimming motility, models can capture how jellyfish respond to these tidal changes. Understanding how jellyfish locomotion and swimming motility influence their transport within confined water bodies has broader ecosystem implications. Jellyfish play critical roles as both predators and prey, and their movements can have cascading effects on local food webs and nutrient cycling. Accurate modelling of their behaviour contributes to a more comprehensive assessment of these ecological dynamics. In estuaries and fjords where human activities like fishing and aquaculture are common, knowledge of jellyfish transport, influenced by their locomotory behaviour, is vital for resource management and mitigating potential conflicts or impacts on these activities. Thus, incorporating locomotory behaviour and swimming motility into jellyfish transport models is essential for capturing the subtle responses of these organisms to their dynamic, localized environments. It allows researchers to gain insights into how jellyfish navigate complex currents, respond to tidal variations, and adapt to changing environmental conditions within estuaries and fjords. This understanding is not only valuable for scientific research but also for practical applications related to ecosystem management and conservation in these unique and ecologically significant habitats.

2.4. Jellyfish Occurrence and Consequences in Coastal Seas

Jellyfish occurrences in marine and coastal waters, whether individually, in small groups, as swarms or blooms, or as beach strandings, have been reported all over the world (e.g., Baliarsingh et al. (2020) reported jellyfish blooms in Indian coastal waters; Boero (2013) in the Mediterranean, Rutkowski et al. (2018) in Brazil etc.). A variety of natural factors (e.g., hydroclimatic) and human activities (e.g., translocation, habitat modification etc.) have been identified as influences on jellyfish distribution and occurrence in a particular place.

The jellyfish population constitutes a large variety of species recognised group-wise and called by their common names. According to the review by Purcell et al. (2007), approximately 190 species of scyphomedusae (Arai 1997), 20 species of cubomedusae (Mianzan & Cornelius 1999), 840 species of hydromedusae (Boullion

Chapter 2: Literature Review

& Boero 2000), 200 species of siphonophores (Pugh 1999) and 150 species of ctenophores (Mianzan 1999) have been identified so far. Due to having such a vast collection of jellyfish variety, the potential for further problems with their unwanted occurrence is very significant.

Studies of jellyfish investigations in the literature are primarily fragmented and sporadic on spatial and temporal scales. These studies were inspired by their historical occurrence, bloom events, and consequences in the respective areas. There is a long history of evidence of jellyfish bloom occurrence globally. For instance, the presence of jellyfish blooms in the Mediterranean has been known for a long time, the first account being reported dating back to 1775, with some 55 records of *Pelagia noctiluca* blooms being identified in the literature in the period 1775–1987 (Goy et al., 1989). Periodic episodes of the presence of jellyfish in swarms were also reported in other European waters.

Jellyfish can have a negative influence when they occur in large numbers (Richardson et al. 2009; Boero 2013), usually called blooms, can be deleterious to coastal fisheries, mariculture, tourism industries, and even swimmers and boaters (Tiller et al., 2014). Large blooms of jellyfish can threaten the sustainability of these operations, including fishing activities (Lynam et al., 2006). Purcell et al. (2007) highlighted the direct consequences of jellyfish blooms, such as breaking fishing operations, damaging aquaculture installations, competing with commercial mariculture species for food, and clogging tidal turbines. Jellyfish mainly damage aquaculture by causing fish kills and gill disorders due to their stings, but also indirectly through fouling of cages or net pens (Purcell et al., 2013). They even interfere in fishing operations by forcing the potential catch to leave a usual fishing area and restricting the fishers' regular activities, thereby reducing the fish catch (Nagata et al. 2009). Their occurrence might also be associated with production impacts as they compete with fish for food (Boero, 2013) and/or prey on fish larvae (Rutkowski et al., 2018). Jellyfish consequences with respect to fish farming in terms of stinging the farmed fishes and/or entangling with the farming structures are evident in many published literature, for example, Baxter, Rodger et al. (2011); Baxter et al. (2011); Bosch-Belmar et al. (2016, 2017); Doyle et al. (2008); Halsband

et al. (2018); Marcos-López et al. (2016); Purcell et al. (2007, 2013); Rodger et al. (2011); Småge et al. (2017); Towers (2014).

Numerous fish-kill events or gill disorders due to jellyfish sting toxins in marine-farmed fish, especially salmonids in northwest Europe, have been reported (Rodger et al., 2011; Purcell et al., 2007). Aquaculture operations in other regions, such as Asia, North America, and Australia, have also been affected (Rodger et al., 2011). The economic consequences of jellyfish blooms, in general, might thus be significant; for example, an annual loss of USD 68–205 million and USD 10 million was previously estimated for Korea (Kim et al., 2012) and the Gulf of Mexico (Graham et al., 2003), respectively. The fishing operation data in southern Brazil during the period 2010–2014 evidenced the occurrence of jellyfish as a bycatch in that area (according to the review and survey by Rutkowski et al., 2018). The coastal regions of the Indian Ocean also experienced jellyfish occurrence and its consequences. For instance, a temporary closure of Madras Atomic Power Station (MAPS) was reported in 1995–1996 due to the ingress of large numbers of jellyfish in the plant cooling system, which resulted in high revenue loss (~5.5 million Indian Rupees/day) (Masilamoni et al., 2000). In a survey of the plant, made later during 2013–2014 (Kumar et al., 2017), jellyfish contributed ~95% of the total biomass trapped by the seawater screening. In Ireland, in 2017, swarms of jellyfish wiped out about 80 percent of the salmon stock from several farms in Killary Harbour and some 10,000 fish from adjacent waters along the west coast (O’Sullivan, 2017).

The increase of jellyfish occurrence on a seasonal or annual scale is mainly motivated by their transports from one place to another, which are attributed to the dynamics of current circulations and jellyfish motility behaviour. Jellyfish swarms or blooms are actualised through their transportation either by their drifting action on the prevailing tidal flows or their own independent movement. Scientific studies have been made worldwide to investigate jellyfish's transport-led occurrence. However, an understanding of their transport mechanisms is still limited. Despite the increase in reports of jellyfish blooms in many coastal regions worldwide, substantiating the cause-effect relationship of jellyfish occurrence remains challenging. One of the main difficulties lies in the fact that there are limited long-

Chapter 2: Literature Review

term findings in the literature, which would otherwise enable researchers to validate the increase of jellyfish in quantity in the ecosystem (Rutkowski et al., 2018). Moreover, the complex and dynamic nature of marine ecosystems makes it difficult to tease apart the many factors that contribute to jellyfish abundances, such as changing water temperatures, overfishing of natural predators, and nutrient pollution. Addressing these knowledge gaps is crucial for predicting and mitigating the impacts of jellyfish blooms on marine ecosystems and human activities.

Jellyfish transportation may be driven merely by the fluid flow or in combination with their motility (Chapman et al., 2011). Adult jellyfish in the marine ecosystem are often considered weak swimmers with limited control over horizontal movement. According to some studies, they are primarily guided by advection, which means they are at the mercy of ocean currents, tides, and winds (Watson, 2006; Whitaker et al., 2014). As a result, they have long been thought of as passive drifters. However, many recent studies have shown that, in addition to their passive drifting action, the motility of jellyfish can also contribute to and supplement their movements (e.g. Chapman et al., 2011; Depra, 2015; Fossette et al., 2015; Gemmell et al., 2013; Hays et al., 2008; Moriarty et al., 2012; Neil & Askew, 2018; Rathi, 2014). This motility is achieved through the contraction of their bell-shaped bodies, which expels water and propels them forward. The ability to actively move through the water has important implications for their survival and distribution, as it allows them to seek out food and avoid predators. Understanding the mechanics of jellyfish movement is therefore crucial for predicting their behaviour and impact on marine ecosystems.

Fossette et al. (2015) investigated and modelled the current-oriented swimming of jellyfish. According to them, depending on the ability and intention of jellyfish to overpower their passive drifting on tidal flows, they can propel themselves considerable distances by responding or orienting themselves counter to the currents. Propulsive movements of jellyfish in response to currents have been found to facilitate the maintenance of jellyfish swarms (confirmed by Fossette et al., 2015; also mentioned in Gill, 2015).

Further to their horizontal propulsion, vertical motility is also possible. The light sensitivity of jellyfish (Garm & Ekström, 2010; Martin, 2002; Nilsson et al., 2005) can

result in vertical swimming behaviour along with horizontal movements. This property and the respective movement behaviour of jellyfish may be vital in the prediction/forecasting of jellyfish transport. Such light-sensitivity-induced (behavioural) transportation of jellyfish can be included within coastal hydrodynamic models using the Lagrangian particle tracking (LPT) approach (Berline et al., 2013; Chung & Craig, 2009).

2.5. Jellyfish Forecasting: the State of the Art

A relatively small number of studies have attempted to model jellyfish transport and/or forecast jellyfish occurrence/bloom formation. Empirical models have been used which have tried to match jellyfish observations to oceanographic or meteorological conditions, but process-based models have also been used to good effect. The process-based modelling approach most commonly favoured involves coupling a Lagrangian particle tracking model with a hydrodynamic ocean model or its output.

Examples of studies using LPT modelling for jellyfish prediction include David et al. (2015), Dawson et al. (2005), Fossette et al. (2015), Johnson et al. (2001, 2005), Lee et al. (2013), Moon et al. (2010), Rahi et al. (2020), Wei et al. (2015). In such studies, particles released in LPT as passive drifters are assumed to represent the agent population to be modelled for their transportation and their movement through the model domain is tracked over time. However, model outcomes are highly dependent on the particle release information inputted in the model, such as the number, frequency, interval, time, location, depth, and duration of the particle releases (Simons et al., 2013).

The accuracy and performance of the transport models reviewed depend on many external and internal factors, which can broadly be categorised under (1) the development of the hydrodynamic model and (2) the integration of the LPT sub-model within the developed hydrodynamic model. There are many examples of the development of such a modelling framework with its corresponding configuration details in the literature. All these share some common ways of development;

however, they vary to some degree in their methods depending upon the nature of the modelling, selection of the numerical tool, and the sourcing of the forcings for input.

Jellyfish models mostly use some established numerical modelling tools to simulate hydrodynamic circulations, such as the Regional Ocean Modelling System - ROMS (e.g., Moon et al., 2010), Princeton Ocean Model - POM (e.g., Wei et al., 2015), General Estuarine Transport Model - GETM (e.g., David et al., 2015), Parallel Ocean Climate Model - PCP/POP (e.g., Dawson et al., 2005), Gulf of Mexico circulation model - GOM (e.g., Johnson et al., 2001, 2005), Proudman Oceanographic Laboratory Coastal Ocean Modelling System - POLCOMS (e.g., Lee et al., 2013), CH3D Hydrodynamic Model (e.g., Li et al., 2002), and Ocean General Circulation Model - OGCM (e.g., Jaspers et al., 2018).

Moon et al. (2010) describe the development of a numerical model based on ROMS (Shchepetkin and McWilliams, 2005), which was used to investigate jellyfish distribution in the East Asian Marginal Seas (EAMS). ROMS features a sigma-coordinate terrain-following vertical coordinate system allowing a high resolution in the upper ocean while maintaining the bathymetry, which benefits handling the steep topography of the coastal oceans. The model is designed to solve the hydrostatic primitive equations for momentum using a split-explicit time-stepping scheme, which allows the barotropic and baroclinic modes to advance separately in time, the former being faster and the latter being slower. The advection scheme in the model is run on a third-order solution and biased to the upstream, which is to minimise dispersive errors and excessive dissipation rates for gaining smoothness, thereby ensuring a better resolution on a given grid. The model covered a $1/8^\circ$ horizontal resolution domain with 30 vertical layerings.

The model forcing data were sourced from various databases and input into the model. The bathymetry data were retrieved from the ETOPO5 earth topography database of the US Naval Oceanographic Office, the temperature and salinity data from the World Ocean Atlas 2001 (Stephens et al., 2002), and the climatological forcing data (wind stress, thermal flux) from the Comprehensive Ocean-Atmosphere Data Set (COADS). The freshwater river discharge at a range of $1\text{-}5 \times 10^4 \text{ m}^3\text{s}^{-1}$ were

introduced in the model. Vertical mixing at the boundary layer of the ocean surface and interior was adopted on the nonlocal K-profile parameterisation scheme of Large et al. (1994) to unify varieties of unresolved processes involved, thereby helping to enhance the mixing at turbulent or unstable water columns. To generate an appropriate initial state for the model that represents the current conditions of the system being modelled, the model was spun up with the open boundary climatology for 17 model years, followed by one additional year for 2005 with the sea-surface wind (QuikSCAT). An LPT scheme activated on a fourth-order Runge-Kutta numerical solution was integrated at each model timestep within the three-dimensional current velocity fields from ROMS (computational details are described by Banas et al., 2009). Fifty particles per day were released constantly for a period of 3 months from 3m depth to the surface at two different locations (suggested by Yoon et al., 2008).

Wei et al. (2015) describe the development of a jellyfish model in the Yellow and East China Seas (YECS) based on POM (A.F. Blumberg & Mellor, 1987). POM was configured horizontally after Guo (2002) with a triple nested structure with coarse-to-fine model grid ratios of 2:1 once and 3:1 (based on RMSE and suggested by Spall & Holland, 1991). Such nesting ensured a higher resolution of the model by decreasing the grid size from $1/2^\circ$ (NEST1) to $1/18^\circ$ (NEST3). All three nested submodels were solved vertically at 21 sigma layers each. The model variables for the higher-resolution submodels were obtained from their immediate lower-resolution antecedent through spatial bilinear interpolation.

Particles resembling virtual jellyfish were repeatedly released in the model, and their release was controlled by the water temperature. According to Kawahara et al. (2006), 13°C is the critical temperature for triggering the release. The process was meant to replicate the induction of scyphistoma strobilation by temperature dynamics and the readiness for their transport, which enabled the study to investigate the influence of water temperature in jellyfish dynamics. Initially, ten particles (considered each a super-particle representing it to be a collection of jellyfish with the same behaviour) were released along the west shore of the Yellow sea, and their gatherings at the tidal fronts (observed sites of their occurrence) were

tracked throughout the simulation (May to Sep 2008 and 2009), which enabled the study to investigate the seasonal and inter-annual variation of their numbers transported to the east of the release. The vertical distribution of the released particles in the water column was modelled through an observation-based probability distribution function, which was resorted to letting them migrate vertically and spend to a particular depth layer (sea surface, sub-surface, or near-thermocline) on a random basis depending upon the time of the day and the depth of their occurrence.

2.5.1. Hydrodynamic Factors in Jellyfish Transportation

Any anthropogenic or natural introduction of a non-indigenous or unwanted species into a marine environment of particular interest (e.g. the transport of marine jellyfish into coastal fish farming areas) can be a potential threat to alter the native ecosystem (Kideys, 2002; Xian et al., 2005) and damage any economic activities there (Simberloff, 2000). Such introductions of jellyfish have mostly remained unpredictable in general (Heger & Trepl, 2003) as the biogeographic and hydrographic causes of their transport have been poorly known (Cowen et al., 2000).

Dawson et al. (2005) simulated the dispersion of moon jellyfish (*Aurelia* sp.) over multi-century time scales by a life-history incorporated global Lagrangian biophysical ocean model to investigate the nature, extent, and limit of their transport. The model was based on a steady-state seasonal circulation pattern without an interannual variability forcing a stable climate and driven by monthly advection and random-walk fields derived from a 20-year integration (1979–1998) of the Parallel Ocean Climate Model.

Cumulative occurrence distribution (COD) was calculated in terms of drifting particles destined in a grid cell per time step, which represents a potential spatiotemporal range of residence, settlement, and colonisation in any given lifespan of the jelly (reasonably approximated a year). After exhaustion of each lifespan, the process was repeated for the subsequent cycle following a new release of the particles in the model, which corresponded to the immediately previous COD

Chapter 2: Literature Review

values. The repetitions continued until the jelly distributions reached an approximate steady state within a century of the model simulation, thereby limiting the geographic extent over which they could advect or migrate. The particle dispersion results were found to be insensitive to the steady-state assumption and various levels of diffusion. However, the sensitivity analyses were made on a regional or macro scale, which does not reveal if the dispersion was sensitive to diffusion at a coastal or local scale. Such information may be worthy of consideration in predicting the potentiality of jellyfish swarm formation, which is included in the current jellyfish transport modelling investigation and analysis.

Due to the steady-state assumption of circulation, the influence of seasonal and annual variation in flows on the distribution of jellyfish was not known from the above-stated investigation by Dawson et al. (2005). This was, however, known from an earlier modelling study that investigated the distribution patterns of jellyfish life cycle components in current flows by Johnson et al. (2001). The mode of transportation of jellyfish, whether active swim due to motility or passive drift by ocean currents or a combination of both processes, varies with their life cycle stages. Swarms are primarily formed by transporting the free-swimming life forms of jellyfish.

With an aim to investigate the relationship and dependence of jellyfish life history dynamics to drift-causing ocean currents, particularly the role of circulations in the successful cycling from sessile polyp to mature jellyfish and subsequent return, Johnson et al. (2001) modelled how repetitive patterns of current flows aid settling for recruitment, residence, dispersal, and inter-annual density variation of stinging jellyfish (*Chrysaora quinquecirrha*), a prominent scyphomedusa (adult jellyfish) in the northern Gulf of Mexico (GOM).

The GOM currents were simulated using the Princeton Ocean Model (Blumberg & Mellor, 1983) based GOM circulation model for four model years with the same annual forcings cycled annually. The GOM model was primarily developed by Choi & Kantha (1997) and later used by Johnson & Perry (1999) to model blue crab larval transportation. The modelled currents were applied to a simple advection scheme of an LPT model for developing trajectories of jellyfish metamorphosis (polyp to

Chapter 2: Literature Review

maturity) in time and distance scales. The source and sink of jellyfish dispersal were determined through backward and forward integration in the model, respectively, for a usual growth period (90 days, according to Cargo & King (1990)). Seasonal change of circulation processes was found to favour the shoreward distribution of this species of oceanic origin, and the loop currents and spin-off eddies that alter shelf circulation were found to favour the inter-annual variations in their distribution. The model results concluded that the bloom dynamics of this jellyfish in GOM were more related to circulation patterns than their productivity enhancement.

There is also other evidence of the seasonal and annual influence of the local/regional circulations on jellyfish transport distribution. For instance, Wei et al. (2015) mentioned such an influence in the distribution of the giant Nomura jellyfish in the Yellow Sea, where their drifts with currents over the summer formed a large biomass by gathering in winter. Their model results suggest an inter-annual variation in the giant Nomura jellyfish rallies found between two consecutive years of 2008 and 2009, which supports the fact found by Cheng et al. (2004) that the jellyfish biomass and concentration areas might be different from year to year. According to both, inter-annual variation of the physical environment is essential for jellyfish growth (e.g., optimal water temperature) and behaviour (e.g., currents for their dispersal). These findings provide empirical evidence, which helps plan the current jellyfish transport investigation through hydrodynamics-based numerical modelling.

Jellyfish swarms that form blooms near areas of human and economic activity are considered a threat, and the jellyfish are often labelled as nuisance organisms. Despite this, researchers worldwide continue to debate whether blooms of these organisms in the ocean and coastal seas are caused by local or regional processes. Lee et al. (2013) studied identifying geographical connectivity through oceanographic modelling, which was thought to partly answer the question. They used Lagrangian dispersion modelling of *Rhizostoma octopus* jellyfish to explore the spatial connectivity network in the Irish Sea and northeastern (NE) Atlantic waters.

The modelling considered the network evolved by the drifts of the free-swimming forms of jellyfish (ephyrae and medusae) in their strobilation to maturity period covering 6 months during the spring and the summer. Ocean circulations were simulated for this period using the Proudman Oceanographic Laboratory Coastal Ocean Modelling System (POLCOMS) (Holt & James, 2001) and subsequently exported offline to an advection-diffusion-enabled Lagrangian particle tracking (LPT) model for simulating jellyfish dispersal. Potential travel sites for the jellyfish were determined based on historical bloom spots (remotely determined by aerial surveys) and centre-to-centre distances among the spots. A total number of particles dispersed within a capture distance of 40 km of the centre of each potential travel site were counted, which represents jellyfish movement-dependent oceanographic connectivity between locations and provides estimates of relative dispersal connectivity strength.

This investigation identified three types of locations based on the composition of transported jellyfish populations (genetically determined) in their swarm, which in turn indicated the extent of jellyfish transport - 1) swarm composed of geographically isolated transporting population, 2) swarm composed of migratory population, and 3) non-swarm occurrence dominated by immigrant jellyfish. Although the approach used in this study provided an introductory guide in modelling jellyfish drifting over oceanic circulations, the particle trajectory determination might suffer from accuracy as the LPT model was integrated offline within the flow field in this study. The current numerical modelling uses online integration of LPT to secure better accuracy in jellyfish transport prediction.

2.5.2. Salinity and Temperature Dynamics in Jellyfish Transport Modelling

Among many abiotic factors regarded as the driving force in modelling biomechanical processes of a marine population, salinity and temperature are two crucial physicochemical properties of the marine water environment, which influence the hydrodynamics by causing gradients in the water and thereby influencing the biological activity dynamics therein. According to Li et al. (2002), process interactions in coastal waters induced by the salinity and temperature can

be modelled as jellyfish activity regulating properties in modelling their movement, distribution, and occurrence. Their views support that a water environment characterised by seasonal as well as inter-annual variation and a strong gradient of salinity and temperature that regulates biological activities and species distributions can promote jellyfish invasions and outbreaks. According to them, the Chesapeake Bay and similar other coastal environments are examples of such, which provide an ideal habitat for the periodic infestation of stinging jellyfish.

From this viewpoint, they developed a model to predict the occurrence and probable distributions of stinging jellyfish in the Chesapeake Bay areas. The model used a near-real-time version of a well-validated CH3D hydrodynamic model modified for the Chesapeake Bay (Johnson et al., 1991, 1993; Wang and Johnson, 2000) and was based on simulated salinity and temperature. Various oceanic boundary forcing parameters of this nowcast system were based on real-time data acquisition except the salinity and temperature, which were climatological. The modelled parameters were finally used in an empirical relationship model (based on historical observations) by an algorithm or a logit function determining the probability distribution of the jellyfish as a function of salinity and temperature. While the model by Li et al. (2002) tried to establish a direct functional relationship of jellyfish with salinity and temperature to link to jellyfish distribution, the current modelling study considers the hydrodynamic influence of salinity and temperature to investigate jellyfish transport and distribution in the coastal water of Killary.

2.5.3. Modelling of Jellyfish Swimming

Although jellyfish are thought to mostly drift on the ocean currents, they also have swimming ability, which may contribute to / help facilitate the formation of blooms (confirmed by Fossette et al., 2015; also mentioned in Gill (2015)). Yet, until the early part of this century, modelling of jellyfish transportation had been limited to simulations based on their flow-governed movements disregarding their active propulsive behaviour.

Matanoski & Hood (2006) were among the first to incorporate swimming behaviour into jellyfish transport models when they aimed to develop a three-dimensional

model of the swimming transport of jellyfish medusa (an adult free form of its kind). In the swim model, they used an individual-based modelling (IBM) approach, which considers individual variations in physiological and behavioural traits of the organism within the population to be modelled, with correlated random walk movements of the jellyfish. The use of the IBM approach was based on the principle that jellyfish swimming ability might vary among individuals and might also be influenced by the local environment.

Jellyfish swimming behaviour was observed within a mesocosm setup (an outdoor controlled facility or laboratory condition replicating a natural system) where swimming of a total of 19 medusae of stinging jellyfish was observed in the presence or absence of prey assemblage to investigate the individual responses in swimming. The model was set in a domain identical to the observation tank. Model runs were parameterised with appropriate correlation terms to associate locomotive behaviours with swimming vectors to capture periodic changes in motility (e.g., controlling the strength of bell pulsation by probabilistic conditional function).

Depending on prey availability, the predator jellyfish were found to change prey-oriented looping trajectory motion to gravity swimming at linear trajectories with cyclic changes in speeds. Swimming trajectories within the domain were surmised by summing position vectors in three dimensions independently retrieved from the corresponding propulsive (jellyfish bell pulsations) velocity vectors at each time step in the model. The results were presented to demonstrate an individual-level statistical comparison of jellyfish movement between the modelled and the observed data set. The study recommended the modelling framework as a generalised motility model for all other jellyfish and similar planktonic species. The model was designed to incorporate biotic-to-biotic interactions, such as prey-oriented motility, but did not include any biotic-to-abiotic interactions, such as light- or current-oriented motility, to simulate the swimming transport of jellyfish.

2.5.4. Transport of Invasive Jellyfish

Jellyfish invasion in coastal and marine environments is a common phenomenon, and a share of a jellyfish bloom composed of invasive individuals is not likely to be

uncommon. Such invasions cause ecosystem threats and disturbances (Molnar et al., 2008). Transport, seasonal occurrence, and residence of these jellyfish have been reported in different parts of the world's oceans. For example, the transportation of invasive comb jelly *Mnemiopsis leidyi* in the North Sea was investigated through modelling by David et al. (2015). They investigated the distribution and transport pathways of the comb jelly in the North Sea to understand the occurrence, residence, and unexpected overwintering of this species. For this, they coupled two modelling strategies - (1) a statistical quantile regression model (QR) based on 20 environmental variables used to identify the potential habitats where the invasive comb jelly could survive the North Sea cold winters, and (2) an advection-only Lagrangian particle tracking model (ICHTHYOP - an Individual-Based Model capable of simulating individual variations; Lett et al., 2008) anchored within a General Estuarine Transport hydrodynamic model (GETM) used to explore jellyfish dispersals to the favourable habitats where sustainable populations could have been established.

The QR habitat model prediction showed a satisfactory relationship ($r^2=0.63$) to the environmental variables tested and was found to be significant at the 90th quantile. The temperature in the winter was found to be crucial to the transport and distribution of the comb jelly in the North Sea, which had a quadratic polynomial negative relationship (parabolic) with the jellyfish abundance. Thus, the coastal and estuarine areas influenced by river discharge indicated the most potential high-density jellyfish occurrence area distinguished by their temperature-influenced transport.

All the biotic factors showed a positive linear relationship with their abundance, which indicated their motility transport. Based on this model prediction, the North Sea was divided into 14 homogeneous abundance zones, and then the zones were statistically classified to distinguish the high-potential overwintering habitats. From 12 simulations over a year, the dispersal model could segregate the highest cumulated particle density (ten times the release density) zone contributed by drifting from neighbouring and distant areas. The density of the open-water individuals transported from the population residing along the coast was found to

be dependent on the flux of the jellyfish offspring from the coastal areas. Finally, based on the habitat and dispersal model agreements, the zones were clustered according to the distance of particle transportation. Of the particles released, those in spring had the most extended dispersal, while those in winter had the shortest. A favourable environment leading the transported invasive comb jelly to overwinter and swarm at a high density indicated the likelihood of a potential bloom. However, the jellyfish transport mechanisms were not explored much in this study.

The transport system in marine invasion ecology suggests that individuals are mainly translocated by ballast water, which is considered a primary vector for transporting invasive organisms over long distances (Seebens et al., 2016). This might happen in the case of jellyfish transportation as well. Ocean currents contributing to the post-invasion secondary transport, spread, range occupancy, and recolonisation of these organisms have rarely been accounted for in most marine invasion studies; however, this can be a significant driver, as mentioned by Jaspers et al. (2018) who investigated the potential role of ocean currents in post-invasive transportation or secondary spread dynamics of the non-native comb jelly across western Eurasia on a continental scale.

Transport of the jellyfish was modelled upon the circulation data of the area calculated from the outputs of the ocean general circulation model (OGCM) of the Copernicus Marine Environment Monitoring Service (CMEMS, <http://marine.copernicus.eu>). The potential modelling errors due to physical simplifications, numerical limitations, and the nonlinear character of the ocean were managed by using a Kalman filter approach while assimilating the model inputs, which led to a realistic representation of the ocean.

To infer the invasion corridors and the source-sink dynamics (transport pathways) of the comb jelly in the area, the invasion history and spatiotemporal distribution of the jellyfish were reconstructed using the model validated upon 12,400 geo-referenced observations throughout the area for the period from 1980 to 2016. Current stabilities were calculated after Lehmann & Hinrichsen (2000) to measure the variability of the general circulation patterns and matched thereby with the spread dynamics of the comb jelly for exploring the current-based connectivity

Chapter 2: Literature Review

between regions of their occurrence. High current stabilities demonstrated steady circulation patterns indicating a solid link between adjacent areas benefiting jellyfish spread and vice-versa. Highly interconnected areas hosting invasive species are crucial for secondary spread dynamics on a continental scale.

The distinction between current-induced invasive (advective) and dispersive (diffusive) transports of jellyfish is obvious and has been demonstrated through investigations. Johnson et al. (2001) modelled the lifecycle-led dispersal of stinging jellyfish in GOM relating to the ocean currents, which demonstrated the influences of the currents on their dispersals (described earlier). Such influences might lead to a potential bloom of the jellyfish on a later occasion.

However, there are reports of jellyfish blooms in GOM caused not by the current-induced diffusive transport but by some other ecosystem processes. For instance, Johnson et al. (2005) studied a bloom of white-spotted jellyfish (*Phyllorhiza punctata*) in GOM and found them exotic and the event a bio-invasion as opposed to a current-induced diffusive transport. According to them, the sudden appearance events of swarms of this jellyfish were likely because of periodic introductions of expatriate medusae from a Caribbean source with or without the establishment of this population in the northern GOM.

They experimented with this hypothesis by retroactively analysing the modelled hydrodynamics, satellite imagery, and altimetry. The intrusion of warm tropical loop currents (LC) and eddy spin-off events was analysed using thermal contrast from satellite-captured high-resolution radiometric thermograms with contrast enhancement (gamma-correction). In the case of low-contrast unproductive satellite outputs, the real-time dynamics of the highly nonlinear LC were explored with adequate resolution from the numerical model configured by integrating satellite altimetry (TOPEX/Poseidon and ERS) and phase-locking to the current loops. The model was phased properly with the assimilated altimetry data since LC intrusion and eddy spin-off events being nonlinear could not be readily modelled for real-time reconstruction.

Possible jelly transport pathways into and around the GOM were traced using both the archived model results and the new simulation. The simulation was based on the 3D Princeton Ocean Model (POM) (Blumberg & Mellor 1983) with $1/12^\circ$ horizontal (about 8 to 9 km) and 21 sigma-coordinate levelled vertical resolution and the time steps being 400 sec for the baroclinic and 10 sec for the barotropic split-mode solutions.

Using the model in hindcast mode, possible sources of the jellyfish and their transport mechanisms (probability of intruding LC, eddy spin-off, and cross-slope flux) were traced and evaluated either by back-tracing from known endpoints or by forward-tracing from potential origins in a linear fashion. Distance and direction of their travel were determined according to the modelled current speed and direction at regular time intervals (0.1 day since endpoint solutions converged down to time steps of 0.01 day). Even after having the vertical swimming ability, the jellyfish tended to remain in the upper ocean; hence their advective transport is mostly driven by the near-surface currents and modelled accordingly. Their particle-tracking results suggest that the invasion and mass redistribution of the jellyfish were due to the advective currents from the Caribbean in an intruding loop current and subsequent flux through eddies.

2.6. Conclusions

Computer models that are able to simulate the movements of jellyfish can play an important role in understanding how we can prevent them from adversely affecting economic activities. Different modelling approaches have been used to simulate the transport of jellyfish. In addition to the hydrodynamic forcing causing their passive drifting motion, a successful transport modelling of jellyfish should also take into account their hydrobiological aspects chosen upon their relative significance as a causative factor of motility, e.g., light-sensitive locomotory behaviour and/or individual swimming behaviour of jellyfish in this case. Such modelling works are very limited in the literature compared to more survey-based studies. To the Author's knowledge, there have been no studies where passive drifting, diel

Chapter 2: Literature Review

migration, and horizontal swimming have all been included in a coastal circulation jellyfish transport model; the proposed research is novel in this respect.

An existing oceanographic model, the 'Environmental Fluid Dynamics Code' (EFDC), which can simulate coastal hydrodynamics, was selected for the current research and developed in a way so that it can simulate jellyfish movements on local tidal flows and as per organismal behaviours either separately or simultaneously. EFDC is a three-dimensional coastal hydrodynamic model of industry standards having a modified drifter module integrated within the model to allow it to simulate particle transport online with the current flows. Among different modelling approaches previously used to simulate with drifters, EFDC has been appraised to be a versatile surface water hydrodynamic modelling system (Wu & Xu, 2011). Apart from current flows and transport process investigations, the model tool has been extensively applied in many other hydro-environmental studies, including analytical solutions (e.g., Hur & Park, 2009), laboratory experiments (e.g. James et al., 2010), and marine energy investigations (e.g. James et al., 2011), and validated at numerous sites worldwide over the last three decades (a list of references is available in EPA (2022), and reviews are available in Ai et al. (2014) and Hayter (2014)). It is used by universities, research organisations, governmental agencies, and consulting firms (Hamrick, 2007b; Hamrick, 2007a). The scope of this study is limited to EFDC's hydrodynamic module only. The model has been tested by application to Killary Harbour, Ireland, where both fish farms and jellyfish are present. Further details of the EFDC model have been presented in Chapter 3. Measured records of hydrodynamic currents conducted by deploying ADCP and jellyfish movement observation monitored by tracking electronically tagged individuals in Killary Harbour are used to compare with the model results for model validation.

Three-dimensional, time-dependent, fine-resolution modelling techniques with density and salinity capabilities are crucial when modelling jellyfish transport using Lagrangian Particle Tracking (LPT). Incorporating these modelling techniques is essential for capturing the complexity of the flows which drive jellyfish transport. These capabilities enhance the realism of simulations, enable the study of fine-scale

Chapter 2: Literature Review

behaviours, and provide a more comprehensive understanding of how environmental and behavioural factors influence jellyfish distribution and movement. Jellyfish exhibit complex vertical and horizontal movements that are potentially influenced by factors like buoyancy, salinity gradients, and variation of current speed and directions spatially and with depth. Three-dimensional modelling allows for the investigation of these effects, resulting in more realistic simulations. Jellyfish movement can vary over time, especially in response to tides and currents. Time-dependent modelling accounts for these dynamic changes, providing insights into daily and seasonal patterns.

In the realm of jellyfish transport modelling, researchers employ various techniques to gain insights into their behaviours and dispersal patterns. One methodology that has gained considerable prominence is Lagrangian Particle Tracking (LPT). This numerical modelling approach serves as a powerful tool for simulating the movement and dispersion of discrete particles within a fluid medium. LPT involves meticulously tracking the trajectories of individual particles representing these organisms within a water body and it can be specifically tailored to the context of jellyfish and analogous aquatic organisms. The utility of LPT in elucidating their distribution, transport, and behaviour patterns in response to a multitude of environmental factors cannot be overstated.

LPT boasts several distinct advantages that make it particularly suitable for examining the intricacies of jellyfish dynamics. Firstly, it affords the capacity to model individual organisms, thereby achieving an unparalleled level of resolution and precision. This characteristic proves invaluable when dissecting the subtle behaviours of organisms such as jellyfish, especially at finer scales. LPT uses environmental data such as currents, winds, temperature, and salinity to drive the transport of particles. By coupling it with a hydrodynamic model which reproduces the actual conditions faced by aquatic organisms, it significantly enhances the reliability of model predictions, contributing to more accurate and informed analyses. LPT also allows complex behavioural traits exhibited by jellyfish, including swimming patterns, buoyancy control, and diel vertical migration to be attributed to the individual particles. This feature enhances the authenticity and realism of

Chapter 2: Literature Review

simulations, allowing researchers to delve deeper into the intricate behaviours of these organisms. LPT also facilitates the modelling of multi-species interactions, offering researchers a unique vantage point for exploring predator-prey dynamics and competition for resources within aquatic ecosystems. Nevertheless, LPT does come with its share of challenges, including computational demands, parameterization, validation, and predictive limitations. Yet, these challenges do not overshadow the immense potential of LPT to advance understanding of jellyfish transport behaviour and their intricate interactions within marine ecosystems. Continued research and innovation in LPT techniques hold the promise of unearthing new insights into the behaviours and distributions of these vital components of aquatic environments.

CHAPTER 3: MODEL THEORY

3.1. Introduction

The Environmental Fluid Dynamics Code (EFDC) has been used in this study as the numerical modelling tool to model jellyfish transport in Killary Harbour. While the primary determinant for its selection was an existing experience of the model in the Marine Modelling Group at NUI Galway and an existing EFDC hydrodynamic model of Killary Harbour, the model's fitness for purpose was also considered based on the following set of features: level of standard, wide availability, user validation, user community, technical support system, cost of use, source code accessibility, flexibility to modify source code, simplicity, comprehensiveness, and effectiveness. On top of these, the characteristics of the Killary system to be modelled and the purpose of the modelling were also considered.

EFDC is a multifunctional general-purpose modelling package for simulating fluid flows, mass transport through the fluid medium, water quality, and biogeochemical processes in surface water systems. The model is based on equations which describe the conservation of mass, momentum, and energy in a fluid. It is a three-dimensional numerical modelling system, which solves the momentum and continuity equations for a variable-density, turbulent fluid. To represent the physical characteristics of a waterbody, EFDC uses a grid system that is either curvilinear or orthogonal horizontally and sigma-stretched or terrain-following vertically. Dynamically-coupled scalar transport equations for temperature, salinity, dye tracer, and sediment can also be computed simultaneously in EFDC.

3.2. Model History and Description

The EFDC model was initially developed at the Virginia Institute of Marine Science and later supported by the US Environmental Protection Agency (EPA) (Hamrick, 1996). It has been developed for simulating water flows, transport of pollutants, nutrient cycling, and ecological responses. To date, it has been applied to more than 100 modelling studies of various water bodies, including lakes, rivers, reservoirs,

Chapter 3: Model Theory

wetlands, marine, estuaries, and coastal regions, meaning it has been classified as one of the most widely used and technically defensible hydrodynamic models in the world (EPA, 2022). Since its development, it has been used extensively by individual scientists, universities, research organisations, governmental agencies, and consulting firms (Ji, 2017) in a wide range of coastal and freshwater modelling applications, including environmental impact assessment (EIA) (Hamrick, 1992), currents and salinity transport (Moustafa & Hamrick, 1994), hydrodynamic analysis (Hur & Park, 2009; Liu et al., 2007), water quality (Li et al., 2009), sediment transport (James et al., 2010; Pak et al., 2016), larval transport (Kim et al., 2010), fish egg transport (Heer et al., 2020), nutrient transport (Torres-Bejarano et al., 2023), eutrophication modelling (Luo & Li, 2018), algal bloom prediction (Wu & Xu, 2011), and hydrodynamic impacts of aquaculture installations (O'Donncha et al., 2017). Despite its many different applications, to the Authors' knowledge, this is the first time the EFDC model has been used in jellyfish transport modelling.

The EFDC model is an advanced, time-dependent, comprehensive water model. It includes modules for simulating advection, diffusion, and turbulence in the fluid. It also includes modules for simulating the transport of dissolved and suspended substances, as well as the biological processes that occur in the water. For these simulations, the model consists of four independent modules: (1) hydrodynamics, (2) water quality and eutrophication, (3) sediment transport, and (4) toxicant transport and fate submodels. The primary model can link these modules internally. Its hydrodynamic submodel, which is of interest here in this study, comprises six transport modules: dynamics, dye, temperature, salinity, near-field plume, and drifter. The EFDC model is implemented in the FORTRAN programming language and can run on serial and parallel computing platforms. It uses a time-stepping algorithm to advance the solution in time and a non-linear iterative solver to converge the solution at each timestep. It also has options for accounting for wetting and drying in shallow areas by a mass conservation scheme and various features to account for specific environments such as estuaries, lakes, rivers, and coastal zones. Its physics and computational aspects take after the widely used Blumberg-Mellor model (Blumberg & Mellor, 1987) and the US Army Corps of Engineers' Chesapeake

Bay model (Johnson et al., 1993). It uses a finite difference method to approximate differential equations on a structured grid (staggered or C grid), which is defined by a set of nodes and elements that are interconnected by edges and faces. Horizontal flows are simulated using equations of motion with no-flow boundary conditions at lateral walls. A hydrostatic assumption with free surface and dynamic bathymetry is used when simulating density-dependent vertical flows, which are established by satisfying mass conservation at each cell with a specified flow boundary condition at the top and the bottom. Small-scale, non-hydrostatic processes like internal waves and mixing are represented with appropriate parameterisation. A second-order turbulence closure scheme developed by Mellor & Yamada (1982) and modified by Galperin et al. (1988) is formulated within the model to solve the turbulent-averaged variable-density equations of motion to provide vertical viscosity and diffusivity in the model. The model physics also features the convection-resolving property, which is to be solved on Boussinesq approximation.

3.3. Governing Equations

The hydrodynamic framework of the EFDC model and many aspects of its computational scheme are equivalent to the widely used Princeton Ocean Model (Blumberg and Mellor, 1987) (Hamrick and Wu, 1997). The equations that form the basis for the model are based on the Reynolds-averaged Navier-Stokes equations of motion. The model solutions adopt a transformation and an approximation for the turbulent and variable density equations. The model governing equations are solved on a spatial coordinate system where the sigma vertical coordinate replaces the traditional fixed elevation vertical coordinate. This allows for a more refined grid resolution in the surface and bottom layers, where many of the hydrodynamic processes take place. It also allows for a more accurate representation of the bathymetric irregularities that lead to errors and inaccuracies in the simulation results. To provide a uniform resolution in the vertical direction and a free surface permitting long wave motion, a time variable mapping or stretching transformation is desirable, which is given by Phillips (1957):

Chapter 3: Model Theory

$$z = \frac{z^* + h}{h + \eta} \quad (3.1)$$

where z = the dimensionless stretched vertical coordinate (sigma coordinate), z^* = the physical vertical or Cartesian coordinate, h = the water depth below the undisturbed or mean water level (MWL) or equilibrium water, and η = the water surface elevation or the free surface displacement relative to the MWL or equilibrium. The sigma coordinate system gives:

$$z = 0 \quad \text{at bottom topography} \quad z^* = -h$$

$$z = 1 \quad \text{at free surface} \quad z^* = \eta$$

Fig 3.1 shows an illustrative representation of the sigma coordinate system. According to the figure, the sigma coordinate system allows a smooth representation of the bathymetry and the same order of accuracy in shallow and deep waters. Blumberg and Mellor (1987), and Hamrick (1986) can be consulted for details of the transformation.

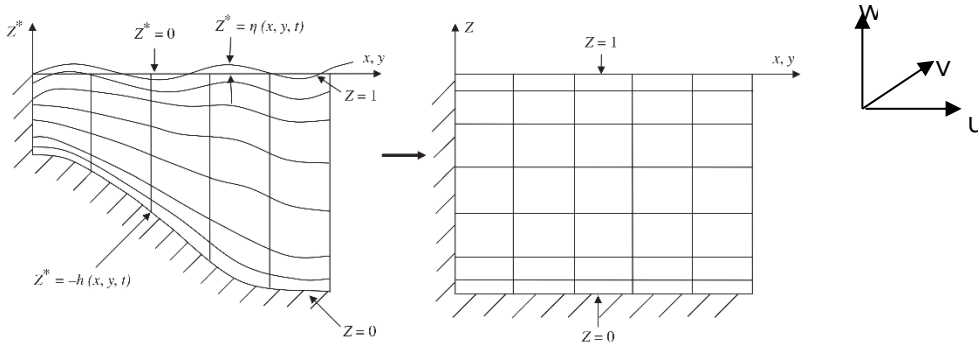


Fig 3.1 The sigma coordinate system. z^* = Cartesian coordinate in the vertical, and z = the sigma coordinate. The illustration was adapted from Ji (2008), who reserves the copyright of it.

For the solution of a variable-density fluid in the model, the equations adopt the Boussinesq approximation, which states that the density differences are sufficiently small to be neglected except where they appear to be a function of g (acceleration due to gravity). The mentioned transformation and approximation result in the model governing equations in the following form:

Continuity equation

Chapter 3: Model Theory

$$\frac{\partial \eta}{\partial t} + \frac{\partial Hu}{\partial x} + \frac{\partial Hv}{\partial y} + \frac{\partial w}{\partial z} = Q_H \quad (3.2)$$

where x, y, z are the three dimensions of the coordinate system and u, v, w are the respective components of the motion, H is the total water depth, and Q is the source/sink term.

Depth-integrated continuity equation

$$\frac{\partial \eta}{\partial t} + \frac{\partial \left(H \int_0^1 u dz \right)}{\partial x} + \frac{\partial \left(H \int_0^1 v dz \right)}{\partial y} \quad (3.3)$$

x-direction momentum equation

$$\begin{aligned} \frac{\partial Hu}{\partial t} + \frac{\partial (Huu)}{\partial x} + \frac{\partial (Hvu)}{\partial y} + \frac{\partial wu}{\partial z} - fHv \\ = -H \frac{\partial (p + g\eta)}{\partial x} + Hgb \frac{\partial h}{\partial x} - Hgbz \frac{\partial H}{\partial x} + \frac{\partial \left(\frac{\nu_v}{H} \frac{\partial u}{\partial z} \right)}{\partial z} + Q_u \end{aligned} \quad (3.4)$$

where f is the Coriolis parameter, p is the excess hydrostatic pressure, b is the buoyancy, and ν_v is the vertical turbulent or eddy viscosity.

y-direction momentum equation

$$\frac{\partial Hv}{\partial t} + \frac{\partial (Huu)}{\partial x} + \frac{\partial (Hvu)}{\partial y} + \frac{\partial wu}{\partial z} + fHu = -H \frac{\partial (p + g\eta)}{\partial y} + Hgb \frac{\partial h}{\partial y} - Hgbz \frac{\partial H}{\partial y} + \frac{\partial \left(\frac{\nu_v}{H} \frac{\partial v}{\partial z} \right)}{\partial z} + Q_v \quad (3.5)$$

Hydrostatic equation

$$\frac{\partial p}{\partial z} = -gH \frac{\rho - \rho_0}{\rho_0} = -gHb \quad (3.6)$$

$$\rho = \rho(p, S, T) \quad (3.7)$$

Chapter 3: Model Theory

where ρ is the density, ρ_0 is the reference density, S is the salinity, and T is the temperature.

The hydrodynamic module also contains a pair of transport equations describing the evolution of temperature (T) and salinity (S). The mass balance equation for three-dimensional advection-diffusion transport can be expressed as:

$$\frac{\partial H\phi}{\partial t} + \frac{\partial Hu\phi}{\partial x} + \frac{\partial Hv\phi}{\partial y} + \frac{\partial w\phi}{\partial z} = \frac{\partial \left(\frac{\nu_b}{H} \frac{\partial \phi}{\partial z} \right)}{\partial z} + Q_\phi \quad (3.8)$$

where ϕ represents the concentration of water quality variables (e.g. salinity or temperature), and ν_b is the vertical turbulent or eddy diffusivity.

The momentum source-sink terms Q_u and Q_v and the water quality source-sink term Q_ϕ are included in equations (3.4), (3.5), and (3.8) to model subgrid-scale processes such as horizontal diffusion and mixing. These terms represent motions induced by small-scale processes and not directly resolved by the model grid. They are parameterised using the terms of diffusion coefficients and can be expressed as:

$$Q_u = \frac{\partial}{\partial x} \left(2A_H \frac{\partial u}{\partial x} \right) + \frac{\partial}{\partial y} \left(A_H \left[\frac{\partial u}{\partial y} + \frac{\partial v}{\partial x} \right] \right) \quad (3.9)$$

$$Q_v = \frac{\partial}{\partial x} \left(A_H \left[\frac{\partial u}{\partial y} + \frac{\partial v}{\partial x} \right] \right) + \frac{\partial}{\partial y} \left(2A_H \frac{\partial u}{\partial x} \right) \quad (3.10)$$

$$Q_\phi = \frac{\partial}{\partial x} \left(A_\phi \frac{\partial \phi}{\partial x} \right) + \frac{\partial}{\partial y} \left(A_\phi \frac{\partial \phi}{\partial y} \right) \quad (3.11)$$

In the solution, the horizontal diffusivity coefficients, A_H and A_ϕ , are used to represent subgrid-scale mixing and determined by the respective scheme that Smagorinsky (1963) suggested. These are often specified as a minimum value necessary to smooth out cell-to-cell spatial oscillations. The values are chosen such that they do not produce excessive smoothing of real features. Values as low as 10 m²/s have been successfully used in various modelling studies (Blumberg and Mellor, 1987). The minimum value for the horizontal diffusivity is again justified in a physical sense by the resultant effect of advection coupled with vertical mixing (Aiguo, 2003).

3.3.1. Boundary Conditions

The model equations require the provision of boundary conditions for the system to drive the simulation. Fig 3.2 shows a flowchart of the types of boundary conditions present in a three-dimensional hydrodynamic model, which include both horizontal and vertical boundary conditions.

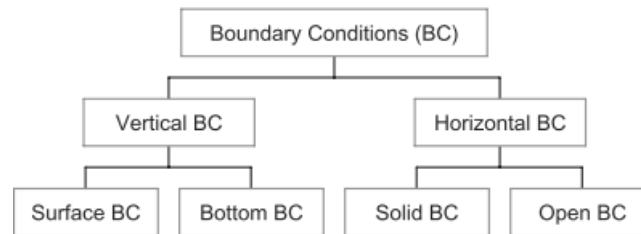


Fig 3.2 Boundary conditions. Illustration adapted from Ji (2008).

Vertical boundary conditions

In hydrodynamic models, the vertical boundary conditions specify how the fluid properties and flows behave at the top and bottom boundaries of the modelled region. These can include conditions such as the type of flow (open or closed), the density and pressure of the fluid, and the velocity of the fluid at the boundaries. Some common types of vertical boundary conditions used in hydrodynamic models include free-surface conditions, where the velocity and pressure of the fluid at the surface are specified, and no-slip conditions, where the velocity of the fluid at the bottom boundary is assumed to be zero. Theoretical aspects of vertical boundary conditions include the mathematical equations and models used to describe the behaviour of the fluid at the boundaries, as well as the underlying assumptions and physical principles that govern the behaviour of the fluid.

The vertical velocity conditions at the surface and bottom boundaries being zero can be elucidated by the following symbolic expression:

$$w(0) = w(1) = 0 \quad (3.12)$$

Chapter 3: Model Theory

Vertical boundary conditions for the momentum equations are presented in terms of surface ($z=1$) and bottom ($z=0$) kinematic shear stress (τ). Expressions for bottom bed and surface wind shear stresses, as per Ji (2017), are:

$$\frac{v_v}{H} \frac{\partial}{\partial z} (u, v)_{z=0} = (\tau_{xz}, \tau_{yz})_{z=0} = c_b \sqrt{u_{bl}^2 + v_{bl}^2} (u_{bl}, v_{bl}) \quad (3.13)$$

$$\frac{v_v}{H} \frac{\partial}{\partial z} (u, v)_{z=1} = (\tau_{xz}, \tau_{yz})_{z=1} = c_w \sqrt{U_w^2 + V_w^2} (U_w, V_w) \quad (3.14)$$

where u_{bl} and v_{bl} refers to velocities computed at mid-height of the bottom layer, U_w and V_w are wind velocity components at 10 m above the water surface, c_b is the bottom drag coefficient, and c_w is wind stress coefficient.

The bottom drag coefficient in a sigma coordinate model is usually computed using (Mellor, 2004):

$$c_b = \frac{K^2}{\left(\ln \left(\Delta z_b / 2z_0 \right) \right)^2} \quad (3.15)$$

where $K = 0.4$ is the von Karman constant, Δz_b is the dimensionless thickness of the bottom layer, $z_0 = z_0^*/H$ is the dimensionless roughness height, and z_0^* is the bottom roughness height.

The wind stress coefficient can be expressed as:

$$c_w = 1.2 \times 10^{-6} \left(0.8 + 0.065 \sqrt{U_w^2 + V_w^2} \right) \quad (3.16)$$

Horizontal boundary conditions

In hydrodynamic models, the horizontal boundary conditions specify how fluid properties and flows behave at the open and closed side boundaries of the modelled region. The open boundary describes interactions between the modelled domain and the open oceans, and the closed boundary condition describes the influences of shorelines on the interior domain of the model. The model boundary can include conditions such as periodicity, no flow, normal flow, and climatological forcing variables. Each boundary condition assumes different conditions for fluid

flow at the boundary and impacts the simulation results differently. The boundary conditions are chosen based on the specific problem being modelled and the available data. The open boundary is delimited by specifying the water surface elevations for barotropic flow as well as other variables like water salinity and temperature for baroclinic flow. For the coastal open boundary, the surface elevations are specified as tidal variations prescribed by the tidal components as follows (Shen, 2002):

$$\eta = \sum_{n=1}^N H_n \cos\left(\frac{2\pi t}{T_n} + \xi_n\right) \quad (3.17)$$

where H_n , T_n , and ξ_n are the mean amplitude, period, and phase angle of the tidal component (n), respectively.

The closed (solid) boundary conditions are characterised by no-slip and free-slip conditions, the former featuring flow prohibition through and along the boundary and the latter featuring flow permission along the boundary and prohibition through it. The EFDC model features a partial-slip flow condition at the solid boundaries referring to normal velocities diminishing to zero and non-normal velocities reflected by the boundary walls without any loss of energy (Tuckey et al., 2006).

3.3.2. Vertical Mixing and Turbulence Models

Vertical mixing and turbulence models are important components of EFDC to predict how water and suspended or dissolved particles mix and distribute in the vertical dimension. The vertical mixing models in EFDC can be based on turbulence closure schemes, such as k-epsilon or Reynolds stress, or on physically-based mixing parameterisation, such as shear-driven mixing. The turbulence models account for turbulence production, transfer, and dissipation in the water column, affecting the vertical mixing and distribution of water properties. These models are crucial for accurate predictions of water temperature, salinity, oxygen, nutrients, and other variables that are impacted by the vertical mixing processes. However, choosing the right mixing and turbulence model is problem-specific and depends on the

available data, the physical processes being studied, and the computational resources.

To provide the vertical turbulent viscosity (ν_v) and diffusivity (ν_b), a second-order turbulence closure model developed by Mellor and Yamada (1982) and modified by Galperin et al. (1988) and Blumberg et al. (1992) is adopted. The model relates the turbulence terms (ν_v and ν_b) to vertical turbulence intensity (q), turbulence length scale (l), and the Richardson number (R_q) by:

$$\nu_v = \phi_v q l = 0.4 \frac{(1 + 8R_q)ql}{(1 + 36R_q)(1 + 6R_q)} \quad (3.18)$$

$$\nu_b = \phi_b q l = 0.4 \frac{0.5ql}{(1 + 36R_q)} \quad (3.19)$$

$$R_q = -\frac{gH(\partial b/\partial \rho)}{q^2} \frac{l^2}{H^2} \quad (3.20)$$

where ϕ_v and ϕ_b refer to the stability functions (Galperin et al., 1988) accounting for reduced and enhanced vertical mixing in stable and unstable stratified environments, respectively. The Richardson number (R_q) in Eq-3.20 is a turbulence indicator and an index of stability. It quantifies the vertical stratification by the ratio of the buoyancy force to the vertical velocity shear. It provides quantitative information on the stabilising effect of buoyancy and the destabilising effect of velocity shear. It indicates the tendency of the water column to either insist or resist the mixing creating a weak or strong stratification respectively (Ji, 2017).

3.3.3. Mode-splitting

The mode splitting technique in EFDC separates the model governing equations into an external and internal mode with a provision that they are solved at the same model timestep. The numerical scheme of the model represents a time integration solution with such an internal-external mode splitting procedure to separate internal shear (baroclinic mode) from the external free-surface gravity wave (barotropic mode). The computational efficiency and accuracy of the solution in split mode are achieved based on the locations on the model grid cell selected for

calculating the model variables. The velocity components are defined on the cell boundary or face of the model grid, and the concentration variables and turbulence parameters are computed at the cell centre in a vertically staggered manner (Hamrick and Wu, 1997), thereby minimising the spatial averaging of the variables to calculate their dynamics (Ji, 2017) making the procedure effective for high-resolution models.

External mode solution

The external mode solution is semi-implicit, associated with barotropic long wave motion, and is completed by measuring the depth-averaged velocities. The mode is solved by vertically integrating the governing equations and then explicitly in a short time step to satisfy the gravity wave. Its computational algorithm is formulated based on modifying the model variables and reorganising the equations, which gives the forms (Hamrick, 1992, 2007) of the momentum and continuity equations as:

$$\begin{aligned} \frac{\partial H\bar{u}}{\partial t} + \sum_{k=1}^K \left\{ \frac{\partial(H\Delta_k u_k u_k)}{\partial x} + \frac{\partial(H\Delta_k u_k v_k)}{\partial y} - f\Delta_k H v_k \right\} \\ = -H \frac{\partial p_s}{\partial x} - Hg \frac{\partial \eta}{\partial x} + Hg \left(\bar{b} \frac{\partial h}{\partial x} - \bar{B} \frac{\partial H}{\partial x} - 0.5H \frac{\partial \bar{\beta}}{\partial x} \right) + (\tau_{xz})_K - (\tau_{xz})_0 + \bar{Q}_u \end{aligned} \quad (3.21)$$

$$\frac{\partial \eta}{\partial t} + \frac{\partial H\bar{u}}{\partial x} + \frac{\partial H\bar{v}}{\partial y} = 0 \quad (3.22)$$

where:

$$\bar{B} = (\sum_{k=1}^K \Delta_k \beta_k + 0.5\Delta_k(z_k + z_{k-1})b_k)$$

$$\bar{\beta} = (\sum_{k=1}^K \Delta_k \beta_k); \quad \text{with: } \beta_k = \sum_{j=k}^K \Delta_j b_j - 0.5\Delta_k b_k$$

Δ_k = vertical layer thickness and the overbar denotes depth averaging.

Equations (3.23) and (3.24) equate the depth-integrated (external) volumetric transport dynamics to the pressure gradients associated with the terms such as free surface slope, atmospheric pressure, buoyancy, advective acceleration, Coriolis and curvature accelerations, free surface and bottom tangential stresses, and general

source-sink terms. The spatial derivatives in the equations are represented by second-order central difference approximation resulting in the conservation of volume, mass, momentum, and energy (found in Hamrick, 2007). The central difference formulations along the x and y coordinates have the forms as

$$\frac{\partial(\phi(x, y))}{\partial x} = \frac{\phi(x + 0.5, y) - \phi(x - 0.5, y)}{\Delta x} \quad (3.23)$$

$$\frac{\partial(\phi(x, y))}{\partial y} = \frac{\phi(x, y + 0.5) - \phi(x, y - 0.5)}{\Delta y} \quad (3.24)$$

Internal mode solution

The internal mode solution is implicit with respect to vertical diffusion and is associated with the vertical shear of the horizontal velocity (baroclinic components). The depth-averaged velocities solved in the external mode are used to compute the layer-integrated velocities in the internal mode helping the implicit solution of the equations in time. The free surface elevation resulting from the external mode is used to solve the stability of the internal mode against the effect of gravity waves. This allows the equations to be processed for a longer timestep independently from the external mode. The scheme uses fractional steps of the solution, which involve a combination of an implicit step for the vertical shear terms and an explicit discretisation for all other terms. Additionally, the turbulence and transport equations are solved using a fractional step scheme with implicit vertical diffusion and explicit advection and horizontal diffusion.

The discretisation of the internal mode equations proceeds by:

- 1) integrating the momentum equation with respect to z over a cell layer,
- 2) dividing the resulting equation by the cell layer thickness (Δ_k),
- 3) subtracting the equation for cell layer k from cell layer $k + 1$, and
- 4) dividing the result by the average thickness of the two cell layers.

Thus, the x-direction momentum equation in the internal mode solution takes the following form.

$$\begin{aligned}
 & \frac{\partial \left(H \Delta_{k+1,k}^{-1} (u_{k+1} - u_k) \right)}{\partial t} + \frac{\partial \left(H \Delta_{k+1,k}^{-1} (u_{k+1} u_{k+1,k} - u_k u_k) \right)}{\partial x} + \frac{\partial \left(H \Delta_{k+1,k}^{-1} (v_{k+1} u_{k+1,k} - v_k u_k) \right)}{\partial y} \\
 & + \Delta_{k+1,k}^{-1} (\Delta_{k+1}^{-1} ((wu)_{k+1} - (wu)_k) - \Delta_k^{-1} ((wu)_k - (wu)_{k-1})) \\
 & - \Delta_{k+1,k}^{-1} (fHv_{k+1} - fHv_k) \\
 & = H \Delta_{k+1,k}^{-1} g(b_{k+1} - b_k) \left(\frac{\partial h}{\partial x} - z_k \frac{\partial H}{\partial x} - 0.5 H^2 \Delta_{k+1,k}^{-1} g \left(\Delta_{k+1} \frac{\partial b_{k+1}}{\partial x} + \Delta_k \frac{\partial b_k}{\partial x} \right) \right) \\
 & + \Delta_{k+1,k}^{-1} (\Delta_{k+1}^{-1} ((\tau_{xz})_{k+1} - (\tau_{xz})_k) - \Delta_k^{-1} ((\tau_{xz})_k - (\tau_{xz})_{k-1})) \\
 & + \Delta_{k+1,k}^{-1} ((Q_u)_{k+1} - (Q_u)_k)
 \end{aligned} \tag{3.25}$$

where $\Delta_{k+1,k} = 0.5(\Delta_{k+1} + \Delta_k)$

An equivalent process is applied to the solution of the y-direction momentum equation.

3.4. Drifter Module

The Drifter module in the EFDC model is used to simulate the movement of drifters, such as buoyant particles, in a fluid environment. It has been developed as an effective tool for solving numerous problems in fluid dynamics related to predicting the trajectory of objects travelling in rivers, lakes, and marine systems. It can also be used to model the movement of aquatic organisms, such as fish or zooplankton, and their interactions with the surrounding fluid environment. The theoretical and computational aspects of the EFDC Drifter module are based on a Lagrangian particle tracking (LPT) scheme coded as a separate subroutine and integrated within the model. The module calculates the velocity and direction of the drifters based on the flow field simulated by the EFDC hydrodynamic model, allowing for the prediction of the movements of particles in the water. The module allows the simulation of floating and neutrally buoyant drifter and particle trajectories from a specified time and space release points.

The Drifter module uses equations of motion to simulate the movement of drifters in a fluid environment. When considering the movement of drifters, they take into account the velocity and direction of the fluid, along with any external forces, such as winds, that might influence their motion. The governing equations used in the Drifter module typically include the advection equation, which describes the

transport of the drifters due to the flow of the fluid, and the Stokes' drag equation, which accounts for the drag force experienced by the drifters due to their interaction with the fluid. The randomness and diffusion due to turbulence are also included in the model to simulate the dispersion of particles and the behaviour of drifter trajectories. Particles are subjected to a random walk process to simulate turbulent diffusion. The inclusion of turbulent diffusive mixing in this way serves the purpose of compensating for the additional mixing that would result from turbulent eddies present in the flow below the scale of the model resolution, i.e. sub-grid turbulent eddies. These eddies cause additional mixing in the real world and the random walk process is a way of including this in the simulation. A diffusion coefficient is used to specify the strength of this mixing. Horizontal and vertical random walk diffusion are treated separately with different diffusion coefficients, due to the substantial differences in the scales at which these diffusion processes occur. The process equations used in the Drifter module can be further developed or modified by a user to better represent the physical system being studied.

The original drifter module of EFDC was modified by Chung & Craig (2009). The mathematical model of the modified version of the EFDC Drifter module is based upon the advection-diffusion equation in a three-dimensional curvilinear orthogonal coordinate system.

The governing equations of Lagrangian transport of particles include horizontal and vertical advection and diffusion. The horizontal (dx , dy) and vertical (dz) distances travelled by particles during a model timestep (dt) are computed as follows:

$$dx = \left(u + \frac{\partial A_H}{\partial x} \right) dt + (2p - 1)\sqrt{2A_H dt} \quad (3.26)$$

$$dy = \left(v + \frac{\partial A_H}{\partial y} \right) dt + (2p - 1)\sqrt{2A_H dt} \quad (3.27)$$

$$dz = \left(w + \frac{\partial A_b}{\partial z} \right) dt + (2p - 1)\sqrt{2A_b dt} \quad (3.28)$$

where the first term on the right-hand side computes advective and diffusive transport, and the second term computes random walk diffusion. In the second term, p is a random number ranging from -1 to $+1$ with a mean 0 (upon transformation using $2p - 1$) used to diffuse particles about the advected position.

Chapter 3: Model Theory

The random walk approach (diffusion) in Eqs (3.27) - (3.29) is followed after Dunsbergen & Stalling (1993). The equations incorporated within the EFDC model can be used to solve the advective and diffusive transports independently to allow user control over the activation of the processes with the directions.

The transport equations may be solved using three numerical methods.

- 1) First-order Explicit Euler Method
- 2) Second-order Predictor-corrector or Improved Euler Method
- 3) Fourth-order Runge-Kutta Method

The discretisation for the equations according to these methods is as follows:

Explicit Euler

$$x_{n+1} = x_n + u(t_n, x_n, y_n, z_n)\Delta t \quad (3.29)$$

$$y_{n+1} = y_n + v(t_n, x_n, y_n, z_n)\Delta t \quad (3.30)$$

$$z_{n+1} = z_n + w(t_n, x_n, y_n, z_n)\Delta t \quad (3.31)$$

Predictor-corrector

$$x_{n+1} = x_n + \frac{1}{2} [u(t_n, x_n, y_n, z_n) + u(t_{n+1}, x_{n+1}^p, y_{n+1}^p, z_{n+1}^p)]\Delta t \quad (3.32)$$

$$y_{n+1} = y_n + \frac{1}{2} [v(t_n, x_n, y_n, z_n) + v(t_{n+1}, x_{n+1}^p, y_{n+1}^p, z_{n+1}^p)]\Delta t \quad (3.33)$$

$$z_{n+1} = z_n + \frac{1}{2} [w(t_n, x_n, y_n, z_n) + w(t_{n+1}, x_{n+1}^p, y_{n+1}^p, z_{n+1}^p)]\Delta t \quad (3.34)$$

where $(x_{n+1}^p, y_{n+1}^p, z_{n+1}^p)$ are calculated by equations (3.30)-(3.32).

Runge-Kutta

$$x_{n+1} = x_n + \frac{1}{6} (\Delta x_1 + 2\Delta x_2 + 2\Delta x_3 + \Delta x_4) \quad (3.35)$$

$$y_{n+1} = y_n + \frac{1}{6} (\Delta y_1 + 2\Delta y_2 + 2\Delta y_3 + \Delta y_4) \quad (3.36)$$

$$z_{n+1} = z_n + \frac{1}{6} (\Delta z_1 + 2\Delta z_2 + 2\Delta z_3 + \Delta z_4) \quad (3.37)$$

where

$$\Delta x_1 = u(t_n, x_n, y_n, z_n) \Delta t \quad (3.38)$$

$$\Delta y_1 = v(t_n, x_n, y_n, z_n) \Delta t \quad (3.39)$$

$$\Delta z_1 = w(t_n, x_n, y_n, z_n) \Delta t$$

$$\Delta x_2 = u \left(t_n + \frac{1}{2} \Delta t, x_n + \frac{1}{2} \Delta x_1, y_n + \frac{1}{2} \Delta y_1, z_n + \frac{1}{2} \Delta z_1 \right) \Delta t \quad (3.40)$$

$$\Delta y_2 = v \left(t_n + \frac{1}{2} \Delta t, x_n + \frac{1}{2} \Delta x_1, y_n + \frac{1}{2} \Delta y_1, z_n + \frac{1}{2} \Delta z_1 \right) \Delta t \quad (3.41)$$

$$\Delta z_2 = w \left(t_n + \frac{1}{2} \Delta t, x_n + \frac{1}{2} \Delta x_1, y_n + \frac{1}{2} \Delta y_1, z_n + \frac{1}{2} \Delta z_1 \right) \Delta t \quad (3.42)$$

$$(3.43)$$

$$(3.44)$$

$$\Delta x_3 = u \left(t_n + \frac{1}{2} \Delta t, x_n + \frac{1}{2} \Delta x_2, y_n + \frac{1}{2} \Delta y_2, z_n + \frac{1}{2} \Delta z_2 \right) \Delta t \quad (3.45)$$

$$\Delta y_3 = v \left(t_n + \frac{1}{2} \Delta t, x_n + \frac{1}{2} \Delta x_2, y_n + \frac{1}{2} \Delta y_2, z_n + \frac{1}{2} \Delta z_2 \right) \Delta t \quad (3.46)$$

$$\Delta z_3 = w \left(t_n + \frac{1}{2} \Delta t, x_n + \frac{1}{2} \Delta x_2, y_n + \frac{1}{2} \Delta y_2, z_n + \frac{1}{2} \Delta z_2 \right) \Delta t \quad (3.47)$$

$$\Delta x_4 = u(t_n + \Delta t, x_n + \Delta x_3, y_n + \Delta y_3, z_n + \Delta z_3) \Delta t \quad (3.48)$$

$$\Delta y_4 = v(t_n + \Delta t, x_n + \Delta x_3, y_n + \Delta y_3, z_n + \Delta z_3) \Delta t \quad (3.49)$$

$$\Delta z_4 = w(t_n + \Delta t, x_n + \Delta x_3, y_n + \Delta y_3, z_n + \Delta z_3) \Delta t$$

3.5. Conclusion

The EFDC model was deemed fit-for-purpose for modelling jellyfish transport within Killary Harbour, particularly as it already contained a drifter module which had been used in previous studies to successfully model larval transport. It is a 3D model and can be run in a baroclinic model, so it had the potential to accurately simulate the temperature- and density-driven circulation, which is known to exist within Killary Harbour. A 3D barotropic model had been previously developed by researchers in the Marine Modelling Group at NUI Galway, and this had been adapted to run on parallel processors. Given the existing model, the user experience in the research group and the model's suitable capabilities, it was selected for use in the research.

CHAPTER 4: HYDRODYNAMIC MODELLING OF KILLARY HARBOUR

4.1. Introduction

Killary Harbour, an Irish fjord, has been an active research site for many years due to its attractive geographic features and the Atlantic climate. An extensive hydrographic survey of the Killary Harbour was conducted in the 1970s and 1980s, which included a survey of the hydrodynamic circulation of the system by Keegan & Mercer (1986). Since then, research on Killary requiring its hydrodynamic data to complement the investigations has been chiefly conducted based on that surveyed hydrodynamic data in the literature. Attempt to predict Killary hydrodynamics using numerical modelling technique has been very rare. Here, the study aimed to develop a hydrodynamic model capable of accurately modelling circulation in Killary and use it to investigate the different drivers of circulation in the harbour; the reason was to generate a set of hydrodynamic data to investigate the transport of jellyfish in the harbour.

Killary Harbour is a site of significant economic activity in aquaculture, with a focus on mussel and salmon farming. However, the harbour has been known to experience impacts from jellyfish occurrence, likely due to their transport from the Atlantic. In 2017, swarms of jelly wiped out about 80 percent of the salmon stock from several farms in Killary and some 10,000 fish from adjacent waters along the western Irish coast (O'Sullivan, 2017). Thus, the mass transport of jellyfish in Killary is a threat to the system's economic activities. If the jellyfish transport in coastal waters can be predicted and an early warning system of this can be developed from the prediction, then such a threat can be minimised, which is also true for the Killary. Worldwide, researchers have tried to investigate jellyfish transport through predictions such as Jaspers et al. (2018), Johnson et al. (2005), Wei et al. (2015) etc., to name some. Each serves its specific purpose and is unique in its investigative method and limitations. But, for all, this prediction requires a knowledge of the jellyfish transport mechanism in water. Since the jellyfish are primarily passive drifters, which makes them move on the ocean current flows, the foremost part of

the investigation would be the prediction of the current flows of the system where the jellyfish are residents or potential migrants. From this viewpoint in Killary, the harbour hydrodynamics is modelled for its prediction. Hydrodynamic flows of waterbodies are influenced by a variety of factors, including geography and climate. As such, it is expected that Killary, being a unique fjord system, would exhibit its own distinct flow behaviour. The flow behaviour is analysed here for uniqueness to provide a better understanding of the process mechanisms to integrate into future jellyfish model development in the harbour.

The successful ecological and resource management operations in Killary require the harbour's hydrography to be known in detail (Roden et al., 1987) and predictable on demand. Systematic documentation or publications of modelling works of the harbour are still scarce in the literature. It is essential to have a systematic and well-documented hydrodynamic model of Killary due to its economic and ecological significance. The need for reliable hydrodynamic models of waterbodies has been recognised for many years. While there have been previous attempts to develop such models (e.g. O'Donncha, 2012; UISCE, 2010), they have not been widely available or systematically described in scientific articles. This knowledge gap motivated the current study to develop a hydrodynamic model that is both verifiable and reproducible. The survey by Keegan & Mercer (1986) shows the current measurement at limited locations in Killary, only near the mouth; the currents inside the harbour were unknown from this record. This limitation can be dealt with through the modelling approach, which would have a scope of investigating much broader aspects of the Killary hydrodynamics through multiple scenario investigations.

The primary objective of this study was to develop a three-dimensional baroclinic hydrodynamic model of Killary using EFDC (Environmental Fluid Dynamics Code). EFDC is an extensively applied model (reviewed by Ai et al. (2014) and Hayter (2014)), which can handle stratified conditions of an estuarine system through the solution of salinity and temperature in the model (Wool et al., 2003). For a successful and meaningful prediction of Killary coastal hydrodynamics, an appropriate mathematical abstraction of the complex physical reality of its hydrodynamic

processes was developed using this model. The model was calibrated using measurements of current speed and direction from an ADCP. The influences of the wind, river discharge, salinity, and temperature on the current flows and the density stratification were also investigated. However, the jellyfish transport model development in Killary based on this modelled hydrodynamics, which was one of the motivations of this study, was planned to carry out separately in subsequent research.

Here, the chapter highlights (1) the Killary Harbour as the research site, (2) the description of the EFDC model, (3) the development of the Killary model, (4) the processing and analyses of the ADCP recorded data, (5) the calibration and validation of the developed hydrodynamic model, (6) the model sensitivity, and (7) the modelled current flows and stratification in Killary. The chapter is structured as follows. Section 2 provides the study site, Section 3 provides the model description, Section-4 provides the model development, Section-5 provides the model calibration and validation, Section 6 provides the sensitivity analysis, Section 7 provides the results of various model scenarios, and Section 8 provides the conclusions.

4.2. Study Site

Killary Harbour is a fjord that intrudes the northeastern shore of the Atlantic on the west coast of Ireland (Fig 4.1). The valley was formed by glacial erosion and subsequently flooded by rising sea levels. It is an indented fissure that runs in a south-easterly direction between flanked hills and is thus sheltered from wind and wave action. Starting from 442 km E 5942.8 km N, it is approximately 13 km long and 0.7 km wide (Keegan & Mercer, 1966), with a total area of 9 km². It has an average depth of about 20 m, extending to 45 m in the centre and at the mouth. The site encompasses a diverse range of hydro-morphology featuring shallow coastal bathymetry, steep seafloor topography, complex estuarine flows, headland, sandbanks, shoals, reefs, and protected areas. The northeastern rivers Errif and Bundorragha (marked in Fig 4.2) discharge most freshwater into the system (average input at 6 m³/s), and streams account for the remainder (Nunes et al., 2011).

Chapter 4: Hydrodynamic Modelling

Killary's water column structure has been characterised as partially mixed or semi-stratified by the influence of local weather and hydrography, mainly due to the high winds and freshwater runoff, respectively (Keegan & Mercer, 1986). Its circulation was classified as a double-layer estuarine with a net outflow near the surface and inflow below (Keegan & Mercer, 1986). The average strongest surface currents (0.5 m/s) usually occur at the mouth of the inlet with a semi-diurnal tidal range of 3.7 m (AQUAFAC, 2013; Nunes et al., 2011).

The Killary Harbour is a place of significance for recreation, sightseeing, mussel raft and fish cage economies, and ecology. The harbour has been reported to be experiencing the impacts of these activities by jellyfish occurrence from the Atlantic. Atlantic salmon and rope mussels have been grown in Killary for the last 50 years or more (The Fish Site, 2012) as a major economic venture here. Licensed annual production of salmon aquaculture in the harbour is reported to be increased from 450 t in 1986 to 2200 t by 2006 (Shephard & Gargan, 2017), which gives an idea of its growth in the area. Anchored floating cages are deployed in the harbour water to contain and culture the salmon, and the cages are arranged in grids. For mussel culture in the harbour, long lines supported by a series of small floats are used to attach the mussels. The lines are joined by a cable and anchored at the bottom on both ends. Droppers are suspended from the lines to collect mussel seeds. The sea-induced hydrodynamics in Killary is thought to influence the transportation of jellyfish inside the harbour, which becomes a potential impact-causing agent within the harbour. Furthermore, the fish-cage and mussel-line structures have an influence on the hydrodynamics. The position of the farms and the extent of their infrastructures within the harbour make the system an excellent experimental site to study the possible influences of its hydrodynamics on jellyfish transportation in or around the farms or largely within the harbour.

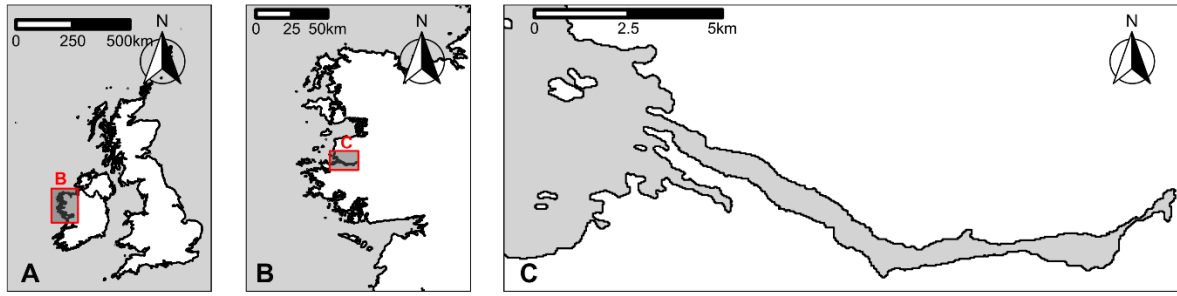


Fig 4.1 Map of Killary Fjord, Ireland. [(A) relative location of Ireland; (B) the west coast of Ireland; (C) Killary Fjord. Referenced and rendered using R mapping packages).

4.3. Model Description

The three-dimensional finite-difference coastal model, EFDC, was used to simulate the hydrodynamic circulation of Killary fjord. An outline of the model is presented here, and the reader is referred to (Hamrick, 1992, 1996) for a more detailed description. EFDC was initially developed at the Virginia Institute of Marine Science (Hamrick, 1992) and subsequently supported by the US Environmental Protection Agency (EPA) and the National Oceanic and Atmospheric Administration's (NOAA) Sea Grant Program (EPA, 2022). EFDC is a multifunctional numerical tool for water modelling with dynamically coupled (integrated) frameworks of hydrodynamics, water quality and eutrophication, sediment transport, and toxicant fate submodels. It is mainly used to simulate physical and biogeochemical transport processes of rivers, stratified estuaries, lakes, marshes, and coastal seas (e.g., fish egg transport by Heer et al. (2020), sediment transport by Pak et al. (2016) etc.).

EFDC is based on continuity, momentum, salt-balance, and heat-balance equations. Its hydrodynamic module solves the Reynolds-averaged Navier-Stokes equations for an incompressible and variable density fluid (Hamrick, 2007a, 2007b) on a staggered C-grid (ARAKAWA & LAMB, 1977). It uses a cartesian or curvilinear coordinate system, orthogonal in the horizontal and sigma-stretched or terrain-following in the vertical, to represent the physical characteristics of the waterbody under investigation. Its state-of-the-art schemes allow for drying and wetting in shallow areas (Z. G. Ji et al., 2001) and include an efficient internal/external mode-splitting of numerical solutions to distinguish the internal shear (or depth-explicit

baroclinity) from the external free-surface gravity wave (or depth-implicit barotropy) (mentioned in James et al., 2016). Model governing equations in full are presented previously in Chapter 3 (Model Theory).

4.4. Model Configuration and Development

The present model is a further development of the EFDC application in Killary Harbour by Donncha (2012). While a lot of the configuration of the model was adapted from the previous model, the following four major enhancements were made: 1) the domain was extended westward to include more of the sea, thereby making the model domain larger, 2) baroclinity was included with dynamic temperature and salinity, 3) the model was forced with dynamic freshwater discharges, and 4) the model was set up to using EFDC's new parallel computing method developed by (O'Donncha et al., 2014). Parallelization uses domain partitioning with MPI synchronisation for efficient execution (O'Donncha et al., 2017).

4.4.1. Grids and Bathymetry

The model domain extends approximately 20 km East-West (435400 m to 455816 m Easting) and 16 km North-South (5938550 m to 5944886 m Northing) within UTM zone 29. It is horizontally partitioned using a regular-sized cartesian grid with a spatial resolution of 64×64 m². Grid generation was carried out as per the EFDC User Manual (Hamrick, 1996). In the vertical direction, the model is resolved on a terrain-following sigma grid with 20 layers, each covering 5% of the water column. The model includes high resolution in the vertical to accurately parameterise vertical shear gradients resulting from varied density waters. The meshing yields $320 \times 100 \times 20$ (x, y, z) computational cells. A fixed temporal resolution of 0.25 s timestep was used to ensure model stability and accuracy upon optimisation trials and analyses.

Chapter 4: Hydrodynamic Modelling

The bathymetry was developed by depth interpolation using data sourced from INFOMAR (a joint programme between the Geological Survey Ireland and the Marine Institute for mapping various features of Ireland's seabed). The Admiralty Chart - 2706 was also digitised and incorporated where the INFOMAR datasets were insufficient. Data compilation, digitisation, and slope assessment were done with ArcGIS (ESRI, 2018) in the development of the final bathymetry. Fig 4.2 shows the bathymetry contour plot of the Killary Harbour.

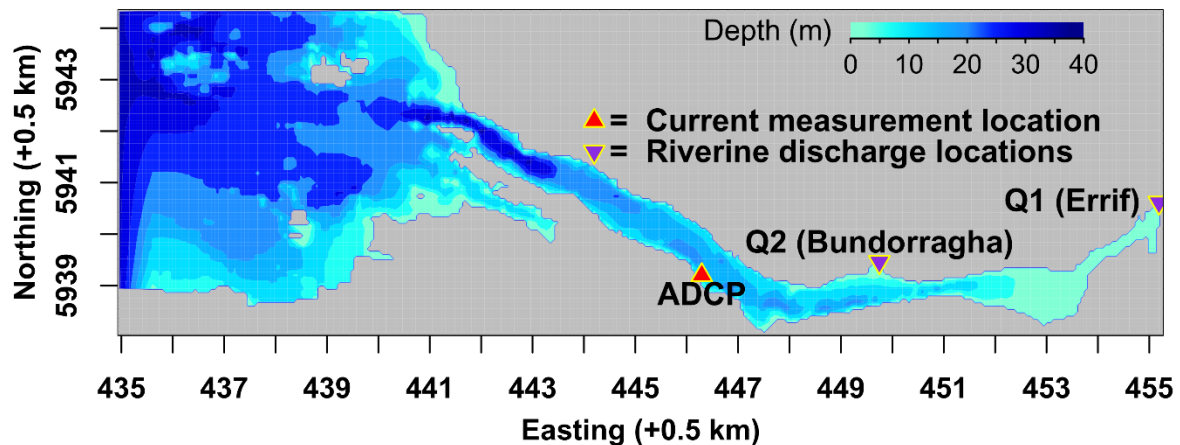


Fig 4.2 Killary harbour bathymetry (The legend on the top-right showing the colour scale represents the water depths in metres; map axes are represented as easting and northing in km along the x-and y-axis, respectively.)

The spatial resolutions of the model, both in the longitudinal and vertical directions, were carefully chosen to achieve a high level of accuracy in the simulation outputs, particularly in modelling the currents within the estuary. The horizontal grid spacing was decided at 65 m² as it was considered small enough to achieve a satisfactory level of accuracy but not overly small so as to make runtimes prohibitively long. A important determinant was ensuring that flows through the narrowest part of the estuary could be satisfactorily modelled which requires a minimum of 6-8 grid cells. The choice to utilize 20 layers for the vertical resolution was based on providing adequate resolution of the variations of velocity with depth so that the effects of diel migratory behaviour could be adequately captured.

4.4.2. ADCP Data

Current speeds and directions were measured using a bed-mounted ADCP deployed from Aug to Oct 2015 at 446.7 km E and 5939.7 km N (Fig 4.2). The vertical profile of the ADCP data contains 17 bins up to the surface. The current velocity measurement area of the ADCP was based on Eq (4.1) and Eq (4.2) (Mohn & White, 2016).

$$D = d_t - (d_s + d_b + d_m) \quad (4.1)$$

$$d_s = 1 - \cos(\text{beam angle}) \times d_t \quad (4.2)$$

where D is the vertical profile distance of the ADCP data, d_t is the total depth at the point of measurement (14 m), d_s is the sidelobe interference distance from the surface (1.875 m, calculated from Eq (4.2) on a 30° beam angle), d_b is the blanking distance over the ADCP (0.4 m), d_m is the mount or transducer head distance from the bottom (3.225 m).

The total distance of the vertical profile at 1.875 m sub-surface is thus calculated to be 8.5 m, where each bin comprises 0.5 m in thickness. Since the numbers of EFDC-layer (total 20) and ADCP-bin (total 17) are not equal, an equivalence was determined based on the depth to find a corresponding match and allow necessary comparisons of the outputs. Quality control was undertaken before comparison to improve the recorded data precision. The ADCP current speed data was passed through the Butterworth lowpass filter for noise filtering and smoothing. Frequency filter cut-off was explored by converting the original signals from the time domain to a representative frequency domain using the FFT (Fast Fourier Transform) analysis.

4.4.3. Boundary Conditions and Other Input Data

Killary's western open sea boundary used the standard specification of water surface elevations, using combinations of harmonic constituents and time series. In the absence of any high-resolution tidal data sources close to the study area, tidal heights were collected from 'tidetimes.org.uk' for Aug-Oct 2015, and harmonic

Chapter 4: Hydrodynamic Modelling

analysis with 33 tide constituents was carried out using T_TIDE (Pawlowicz et al., 2002), a tide prediction toolbox in Matlab.

The initial and open boundary conditions for salinity and temperature followed two scenarios: one in which the concentrations were treated as variables and another in which they were held constant. Spatially dynamic and time-series data for the variable concentration scenario were obtained from the Connemara Model, provided by the Marine Institute of Ireland.

Riverine discharges (Q in m^3/s) from the rivers Errif ($Q1$) and Bundorragha ($Q2$) (marked in Fig 4.2) were used as the freshwater inflow in the model. The time series of Q was calculated based on a rating curve and water level at the Aasleagh Bridge hydrometric station (source: Hydro-Data of the Office of Public Works at www.waterlevel.ie). River temperature time series were also collected and used as model input. Thus, to simulate the baroclinity within the system, the model was programmed to actively transport concentrations and discharge. Land-water interfaces in the lateral, terminal, and bottom boundaries featured a no-slip no-leakage condition with zero fluid velocity relative to a stationary wall or side. Meteorological data were used as atmospheric input in the model to define the surface boundary of the system. For this, data at 0.125 deg and 3 hr resolution for variables 6-11 in Table 4.1 were downloaded from the ERA-Interim model (a reanalysis of the global atmosphere by ECMWF) and used to simulate wind-induced surface currents. Wind data compared with that of the nearest weather station (at Belmullet, 67 km northwest of Killary; available at www.met.ie) confirms its acceptability as input in the model by showing a similar trend in speed and direction (Fig 4.3).

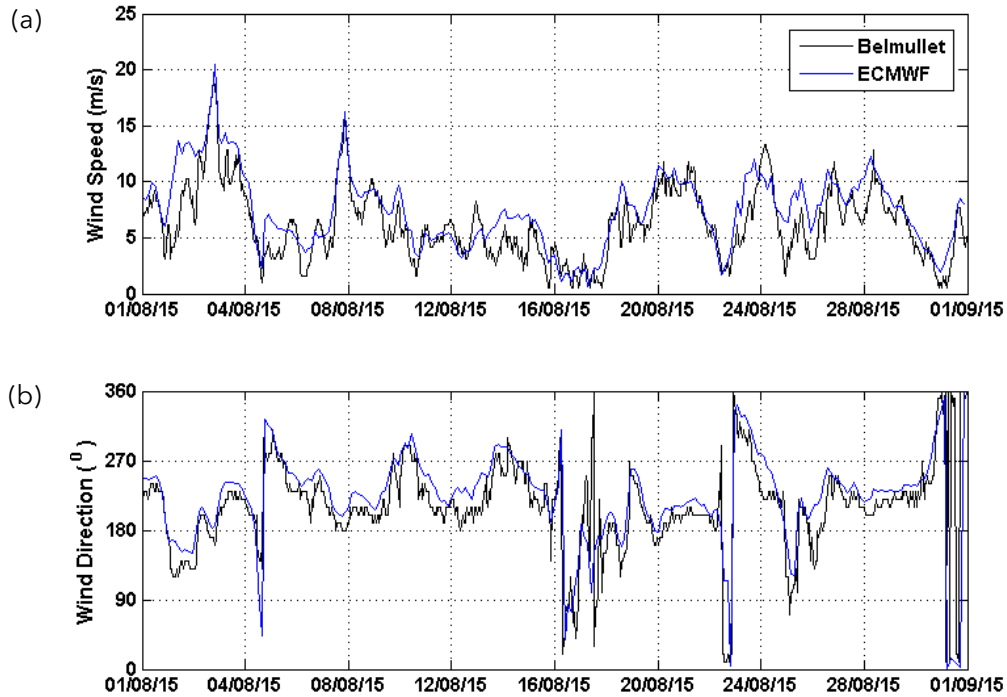


Fig 4.3 Wind comparison over Aug 2015 between recorded (Belmullet) and model (ECMWF) data for their (a) speed and (b) direction.

4.4.4. Model Parameters, State Variables, and Constants

Table 4.1 below states the set-up specifications used for the Killary model.

Table 4.1 Model parameters, state variables and constants.

Sl.	Name	Unit	Value
<i>Parameters</i>			
01	Cells in I direction (longitudinal)	-	320
02	Cells in J direction (lateral)	-	100
03	Layers in K direction (vertical)	-	20
04	Active or water cells	-	10746
05	Cartesian grid spacing	m	64
06	Layer thickness	%	5

Chapter 4: Hydrodynamic Modelling

07	Model timestep	sec	0.25
08	Reference time	sec	86400
09	Simulation period	ref. time (day)	24
10	Simulation starting time	date	18/08/2015 00:00 hr
11	Domain decomposition and parallel execution	processor	6
<i>Variables</i>			
01	Surface elevation at the open boundary	m	Time-series
02	Salinity at the open boundary	psu	Time-series
03	Temperature at the open boundary	°C	Time-series
04	Initial spatial salinity	psu	Dynamic
05	Initial spatial temperature	°C	Dynamic
04	River discharge	m ³ /s	Time-series
05	River temperature	°C	Time-series
06	Wind (speed and direction)	m/s and deg	Time-series
07	Atmospheric pressure	millibar	Time-series
08	Atmospheric temperature	°C	Time-series
09	Relative humidity	%	Time-series
10	Rainfall	mm/hr	Time-series
11	Cloud	fraction	Time-series
<i>Constants</i>			
01	Wind drag coefficient	-	0.0015

Chapter 4: Hydrodynamic Modelling

02	Hydrodynamic roughness height	m	0.02
03	Horizontal momentum diffusivity	m ² /s	1E-6
04	Eddy viscosity	m ² /s	1E-4
05	Eddy diffusivity	m ² /s	1E-7
06	Coriolis coefficient	sec ⁻¹	0.0001167
07	Dry cell depth	m	0.30
08	Wet cell depth	m	0.35
09	River salinity	psu	00
10	Initial and sea-boundary salinity (if constant)	psu	35
11	Initial and sea-boundary temperature (if constant)	°C	15

4.5. Model Calibration and Validation

The values that proved optimal for this model are already presented in Table 4.1 above. The model performance was assessed by comparing the surface elevations and flows resulting in the model against those observed at Killary for the same period. For calibration, the model was run from 18 Aug to 11 Sep 2015 to sufficiently cover both spring and neap tidal cycles and capture the entire variation in tidal currents. Model results were extracted after 48 hrs of the simulation to allow time for model spin-up. Calibration was performed by tuning the temporal resolution at four timesteps of 2.00, 1.00, 0.50, and 0.25 s. Wind stress and bottom roughness coefficients and turbulence parameters were fine-tuned based on agreements with the observed data. Surface shear stress was modulated by the wind drag coefficient. The actual bottom condition was simulated by varying the hydrodynamic roughness height. Turbulent diffusion parameters such as horizontal momentum diffusivity, eddy viscosity, and eddy diffusivity were adjusted to dampen the velocity gradients.

Turbulence closure parameters were not adjusted; instead, empirically derived coefficients for those were prescribed.

4.5.1. Observed Hydrodynamics

The observed current speeds and directions at particular ADCP bins were analysed and are presented in Fig 4.4. The figure shows a model scale of ADCP bin measurement used in the Killary and the respective current speeds and directions at bins 17 and 11, marked on the figure by A and B, respectively. According to the figure, near-surface ADCP bins contain a lot of noise due to tide level variation and are therefore ignored for the calibration and validation analysis. Bin 11, which is at less than 5 m water depth and provides relatively regular and smooth data, was mainly chosen to serve calibration and validation purposes.

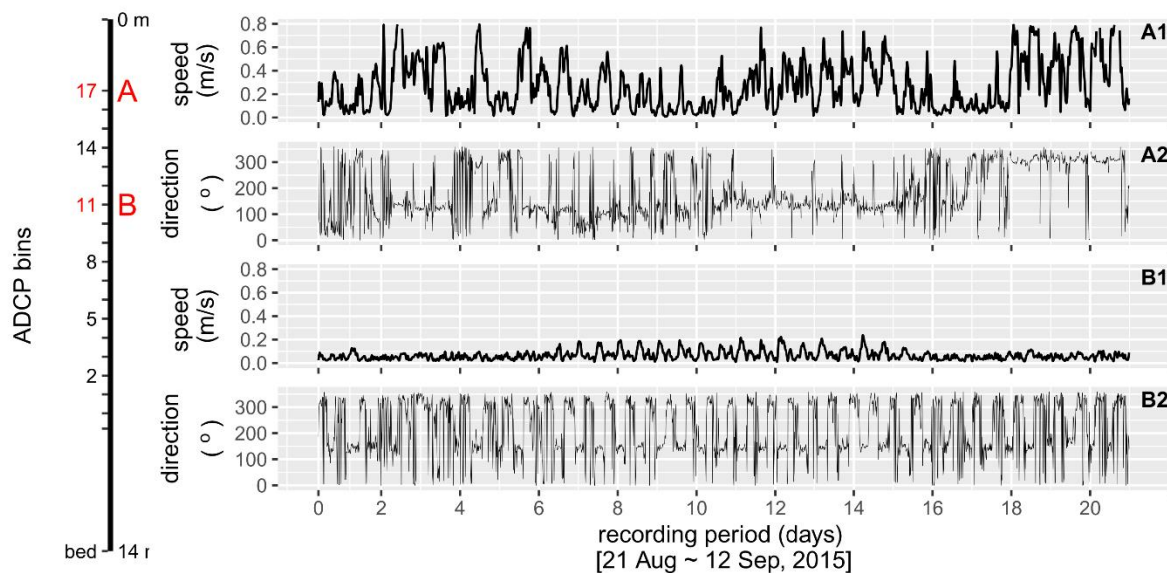


Fig 4.4 Current speed and direction at the ADCP bins (A) 17 and (B) 11.

4.5.2. Modelled Hydrodynamics

The modelled surface elevation and currents were compared with the observed hydrodynamic data and are presented in Fig 4.5 and Fig 4.6, respectively. Fig 4.5 shows the comparison of the surface elevation between the model and the observation. According to the figure, there is a good agreement between them.

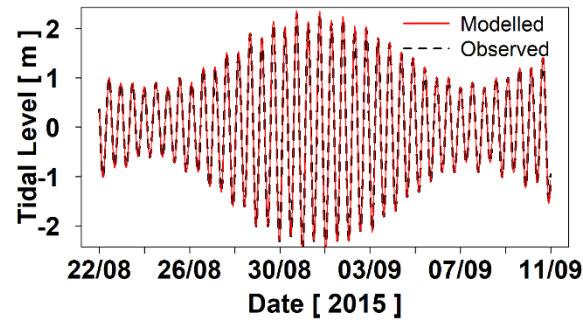


Fig 4.5 Comparison between modelled and observed surface elevation.

The flow comparison required a pre-processing of the modelled and measured data as the data structures were layered and unequal, making them incomparable. A strategy was resorted to bringing them on comparable platforms and filtering the matched layers. Table 4.2 shows the model layers and ADCP bins across the water depth. According to the table, Bin 11, which was selected for calibration (Fig 4.4), looks equivalent to Layer-13 in terms of the depth (at around 4.9 m down to the surface), thereby identified as vertically representative for the comparison.

Table 4.2 Comparing the equivalence of EFDC layers to ADCP bins.

EFDC		ADCP		Mutual equivalence
Layers	Depth (m)	Bins	Depth (m)	
20	0.0	d_s^*	0.0	
19	0.7			
18	1.4			
17	2.1	17	1.875	
16	2.8	16	2.375	
15	3.5	15	2.875	
14	4.2	14	3.375	
13	4.9	13	3.875	
12	5.6	12	4.375	
11	6.3	11	4.875	
10	7.0	10	5.375	
9	7.7	9	5.875	
8	8.4	8	6.375	
7	9.1	7	6.875	
6	9.8	6	7.375	
5	10.5	5	7.875	
4	11.2	4	8.375	
3	11.9	3	8.875	

2	12.6	2	9.375	
1	13.3	1	9.875	
		d_b^*	10.375	
		d_m^*	10.775	
Bed	14.0	Bed	14.0	
*Please consult the description of Eqs. (4.1) and (4.2) for full form.				L represents EFDC layers, and B represents ADCP bins

Fig 4.6 shows the comparison of the current speeds and directions between the EFDC model and the ADCP observation. Besides the reference comparison made between the 13-11 layer-bin pair, two other comparisons were made and shown in the figure, one at the surface at the 18-17 pair and another below the reference at the 8-4 pair. According to the figure, their level of agreement is relatively better at the subsurface water depths (≥ 4.9 m) than at the surface or near-surface one. The model's current directions, which is one of the important checks of model performance in terms of prediction efficiency and confidence, are reasonably synchronous with the ADCP at the subsurface layers. RMSE provides a better estimate and understanding of this agreement in quantitative terms. For calculating RMSE, the modelled current speeds at every 15 min timestep were filtered to match the temporal resolution of the ADCP data. The calculation reveals a larger value of 0.3281 m/s near the surface (estimated for the 18-17 pair), and the values are smaller at the subsurface layers, 0.0439 m/s and 0.0442 m/s (estimated for the 13-11 and 8-4 pairs respectively). The lower RMSE supporting the visual estimation of the model prediction and accuracy is shown in Fig 4.6. Thus, the developed Killary hydrodynamic model is calibrated and validated upon this agreement of the subsurface currents.

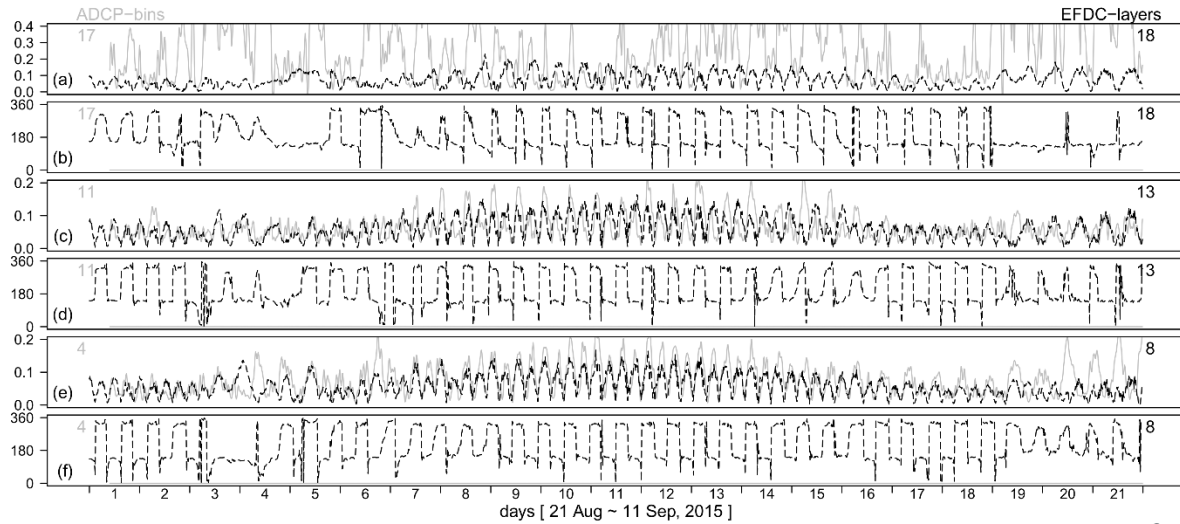


Fig 4.6 Killary hydrodynamics of EFDC model (black) and ADCP observation (grey) showing comparisons of the respective (a,c,e) current speeds and (b,d,f) current directions. Speed and direction are displayed along the y-axis and are measured in m/s and deg units, respectively.

4.6. Sensitivity Analysis

Model sensitivity to the processes such as tide, wind, salinity, temperature, and river discharge was investigated across their configurations. The scenarios comprising these process configurations were simulated and compared. The effects of baroclinity, sea boundary, wind, river discharge, and salinity-temperature stratification on the tidal current flows were investigated through those simulations. The plan of simulation is presented in Table 4.3, which shows the name and ID of the simulations executed and the processes included in the respective simulations. The plan of sensitivity effect analysis is presented in Table 4.4, which shows a matrix of comparisons.

Chapter 4: Hydrodynamic Modelling

Table 4.3 Sensitivity investigation plan.

Num	ID	Simulation	Process included			
			Tide	Wind	Salinity- Tem- perature	River Dis- charge
1	BT- TW	Barotropic with tide and wind	<input checked="" type="checkbox"/>	<input checked="" type="checkbox"/> *	<input checked="" type="checkbox"/>	<input checked="" type="checkbox"/>
2	BC- All	Baroclinic with time-varying wind and river discharge and with time-constant salinity-temperature	<input checked="" type="checkbox"/>	<input checked="" type="checkbox"/> *	<input checked="" type="checkbox"/> **	<input checked="" type="checkbox"/> *
3	BC- All-tv	Baroclinic with time-varying processes	<input checked="" type="checkbox"/>	<input checked="" type="checkbox"/> *	<input checked="" type="checkbox"/> *	<input checked="" type="checkbox"/> *
4	BC- NW	Baroclinic with no wind	<input checked="" type="checkbox"/>	<input checked="" type="checkbox"/>	<input checked="" type="checkbox"/> **	<input checked="" type="checkbox"/> *
5	BC- W4	Baroclinic With Constant Wind (4 m/s)	<input checked="" type="checkbox"/>	<input checked="" type="checkbox"/> **	<input checked="" type="checkbox"/> **	<input checked="" type="checkbox"/> *
6	BC- W8	Baroclinic With Constant Wind (8 m/s)	<input checked="" type="checkbox"/>	<input checked="" type="checkbox"/> **	<input checked="" type="checkbox"/> **	<input checked="" type="checkbox"/> *
7	BC- NR	Baroclinic with no river	<input checked="" type="checkbox"/>	<input checked="" type="checkbox"/> *	<input checked="" type="checkbox"/> **	<input checked="" type="checkbox"/>
8	BC- R3	Baroclinic with Constant Low Flow (3 m ³ /s)	<input checked="" type="checkbox"/>	<input checked="" type="checkbox"/> *	<input checked="" type="checkbox"/> **	<input checked="" type="checkbox"/> **
9	BC- R33	Baroclinic with Constant high flow (33 m ³ /s)	<input checked="" type="checkbox"/>	<input checked="" type="checkbox"/> *	<input checked="" type="checkbox"/> **	<input checked="" type="checkbox"/> **
* time-varying. **time-constant.						

Table 4.4 Sensitivity effect analysis matrix

<p>The matrix shows the model sensitivity effects analysed upon the comparisons. The numbers across the rows and columns represent the ID of the simulations investigated as per Table 4.3. A row-column pair indicates the scenario comparison made, and the respective cell tag at the row-column intersection indicates the influence investigated. The model sensitivity effects are represented by BCL for baroclinic, SBC for sea-boundary conditions, WND for wind, and RIV for river discharge.</p>									
ID Num	1	2	3	4	5	6	7	8	9
1	-	BCL	-	-	-	-	-	-	-
2	BCL	-	SBC	WND	WND	WND	RIV	RIV	RIV
3	-	SBC	-	-	-	-	-	-	RIV
4	-	WND	-	-	WND	WND	-	-	-
5	-	WND	-	WND	-	WND	-	-	-
6	-	WND	-	WND	WND	-	-	-	-
7	-	RIV	-	-	-	-	-	RIV	RIV
8	-	RIV	-	-	-	-	RIV	-	RIV
9	-	RIV	-	-	-	-	RIV	RIV	-

4.7. Results and Discussion

4.7.1. Model Stability

The model stability was found sensitive to temporal resolution. The convergence of the model surface elevation was achieved at the smaller timesteps among the four iterations tested at 2, 1, 0.5, and 0.25 s. This convergence was confirmed by Fig 4.7, which showed that the residuals of the equations were reduced to near-zero values as the time step size was decreased. As per Courant et al., (1928), the maximum Courant number computed for the model ($C_{max}=0.008$) also satisfies the Courant-

Friedrich-Lewy condition ($C_{max} < 1.0$) of the numerical solutions. The smallest timestep 0.25 s showed a significant improvement in model performance (smoothness of surface elevations), thus, was selected as the appropriate temporal resolution to be used in the Killary model. The higher time resolution selected thereby was computationally costly. This cost was partly tackled by parallelisation on six processors of the computer. The parallelisation adopts an efficient domain decomposition approach that theoretically permits deployment on a large cluster of machines and thus runs a high-resolution model more quickly (O'Donncha et al., 2014). The strategy, along with the 0.25 s timestep, took six times longer to simulate the model than that with the 2 s timestep. However, the convergence was very important for the model stability and precision as failing to achieve that at any instance would have generated a numerically erroneous initial condition for the next timestep, which eventually would have propagated until the simulation reached the final.

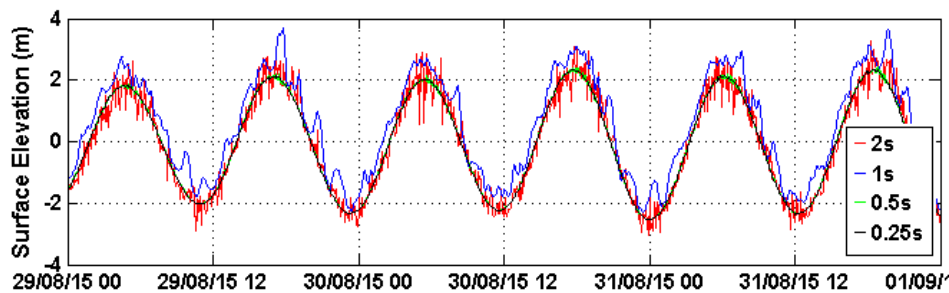


Fig 4.7 Surface elevation convergence over a simulation period (x-axis) in different timesteps.

4.7.2. Sensitivity to Model Properties and Parameters

As the first three-dimensional baroclinic hydrodynamic model of Killary Harbour, which incorporates baroclinic features and extends the seaward domain, this study investigates the influence of various properties and parameters on the simulation of current flows. Due to the uniqueness of the model, it is crucial to understand the effects of different factors on the accuracy of the simulations. So, the sensitivity of the developed baroclinic model was tested to some important properties and parameters such as model physics, initial and sea boundary conditions, wind, and

river discharge. The model sensitivities are described below, along with the respective illustrations. The sensitivities are shown at the low, mid-flood, high, and mid-ebb tidal levels. There will be two types of illustrations at four different tidal levels: (1) maps showing vectors and contours of the modelled current speed and direction of the surface and depth-averaged flows organised, and (2) maps showing stratifications of the modelled salinity and temperature during the neap and spring tide stages. In the figures, the panels are organised such that different depth flows and tidal stages are shown across the columns, and different tidal levels are shown across the rows. Where there is no difference in stratification or currents between the scenarios being investigated, only a single representative difference plot has been illustrated at a particular tidal instance for demonstration purposes.

4.7.2.1. Model Physics

4.7.2.1.1. Baroclinity

As baroclinity is a significant attribute of estuarine systems, it has been included in the developed model with the aim of maximising its quality. The outputs of the baroclinic simulations demonstrating salinity and temperature stratifications are illustrated in Fig 4.8. The figure shows the stratifications in various tidal stages and levels generated by the model. According to the figure, during neap tides, the salinity stratification is limited within the harbour (Figures A-D), whereas during spring tides, it is stronger and extends from the harbour towards the sea (Figures E-H). This pattern occurs at all tidal levels. With respect to temperature, which varies between 11-15 °C, the stratifications within the harbour are dominated by colder waters (Figures I-P). This lower temperature in the harbour may be due to the mixing of cold river water, which has an average temperature of 12.8 ± 1.8 °C in the river and 14.34 ± 0.7 °C in the estuary, into the harbour. Along the harbour, a horizontal stratification extends from the head through the mouth to the sea, characterised by colder water followed by warmer water. This stratification is more pronounced during spring tides than during neap tides. The vertical stratification occurring within the harbour can be characterised by colder water lying over the warmer water with subtle variations among the tidal levels and tends to reduce towards the sea.

Chapter 4: Hydrodynamic Modelling

Thus, these salinity and temperature stratifications confirm a density variation inside the harbour, which consequently would cause hydrodynamic turbulence and influence the passive transportation of the drifters in the harbour.

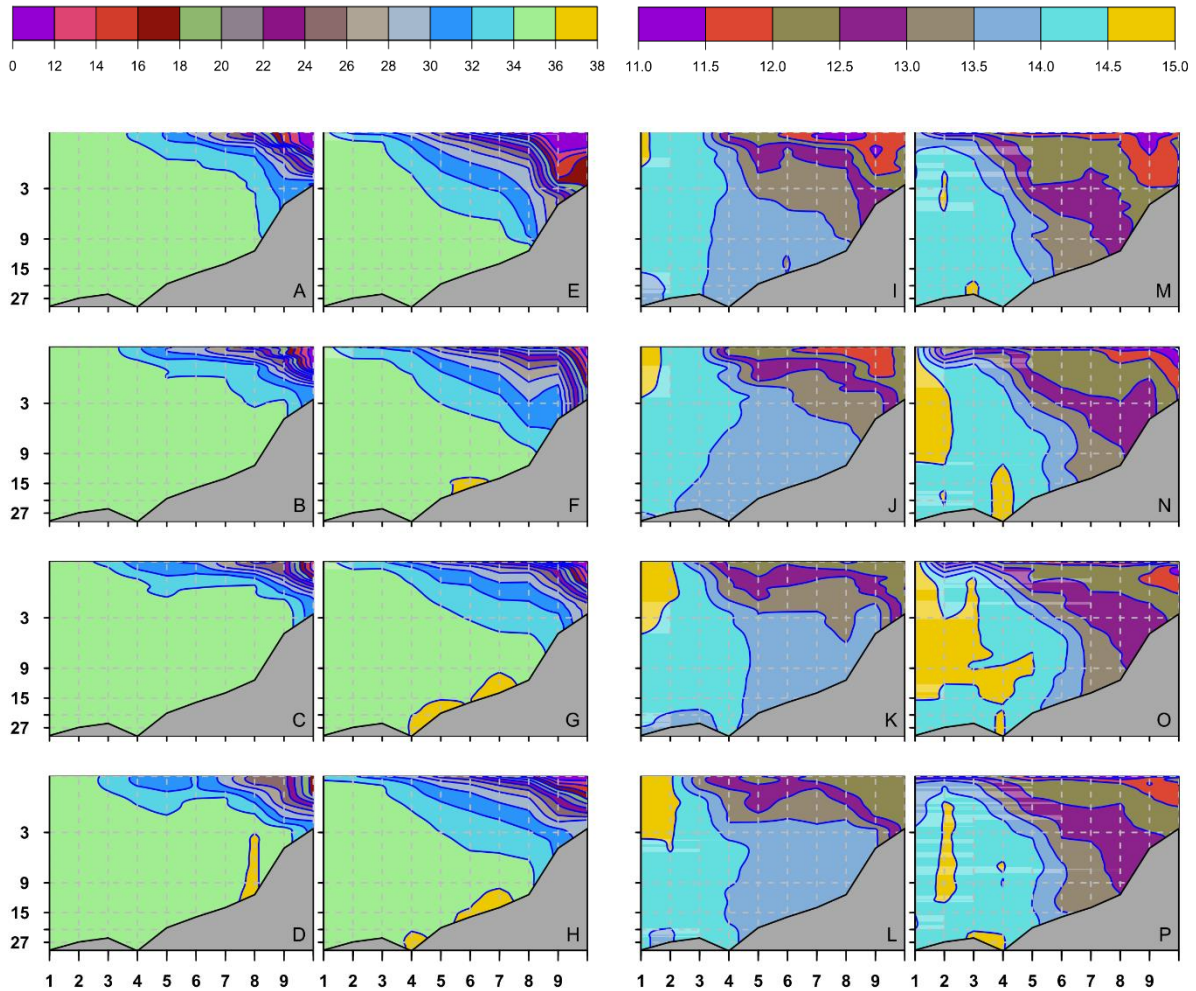


Fig 4.8 Maps showing the (A~H) salinity and (I~P) temperature stratifications as per the BC-All model scenario. The stratifications are investigated in the (A~D & I~L) neap and (E~H & M~P) spring tides at the (A & E) low, (B & F) mid-flood, (C & G) high, and (D & H) mid-ebb tidal levels. (The x-axis represents the spatial points of investigation along the east-west at every 2 km, and the y-axis represents the water depths in metres. The legends on the top represent the salinity scale in psu shown on the left and the temperature scale in °C on the right.)

The outputs of the baroclinic simulations demonstrating modelled currents are illustrated in Fig 4.9. Since little or no remarkable variation in the stratification has been observed among the tidal levels during neap tides, the currents have been analysed only during spring tides and are presented in the figure. The figure shows current velocity variations generated by the model in terms of tide and depth.

According to the figure, the currents are lower at the slack water during the high and low tides (Fig A and C) and higher halfway at the tides during mid-flood and mid-ebb (Fig B and D), as would be expected; the surface velocities are higher than the depth-averaged velocities.

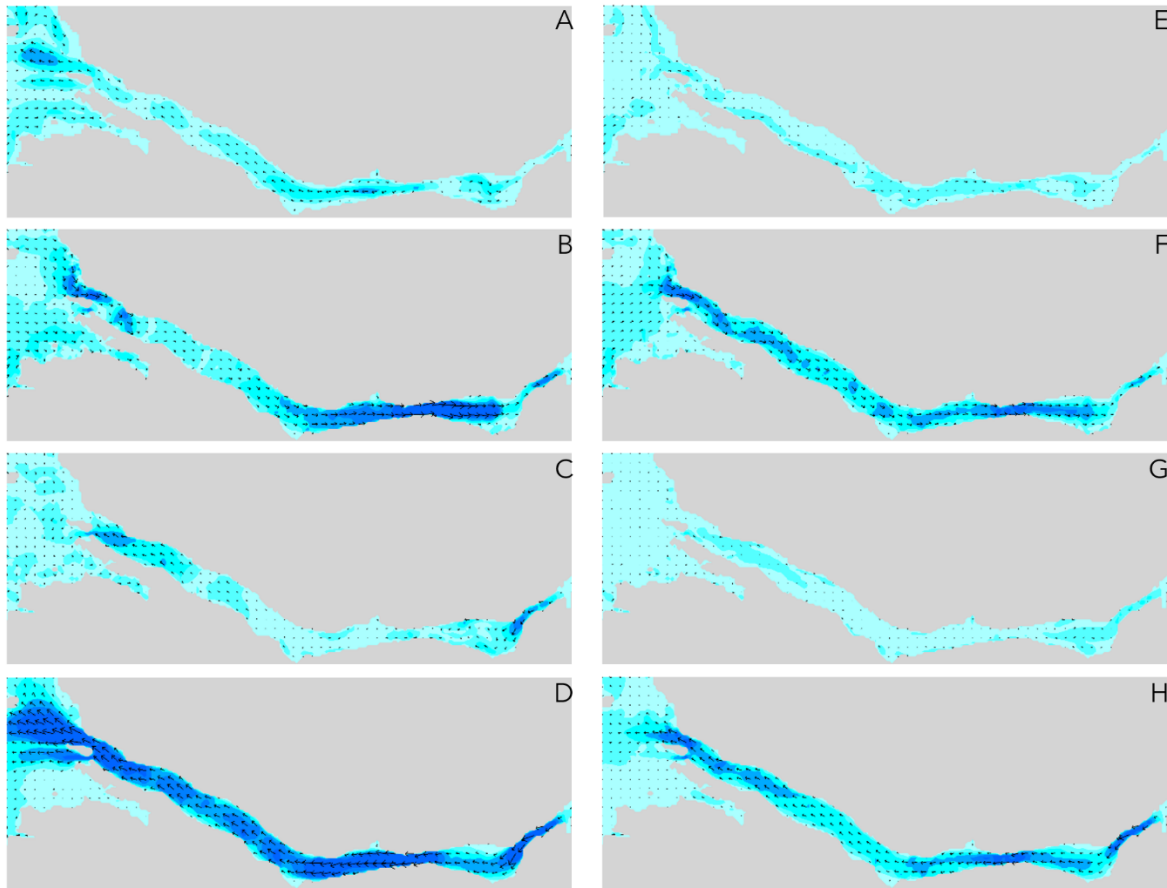


Fig 4.9 Maps showing the (A~D) surface and (E~H) depth-averaged currents in the BC-All model scenario. The currents are sampled in the spring tide at the (A & E) low, (B & F) mid-flood, (C & G) high, and (D & H) mid-ebb tidal levels.

4.7.2.1.2. Barotropy

The barotropic scenario of Killary would be worthy of investigation to understand the sensitivity of the barotropic-baroclinic physics of the estuary in the model. For this, the barotropic currents were also investigated, and the simulation outputs were illustrated in Fig 4.10. The variations in the current velocities, as shown in the figure, are like that seen in the baroclinic scenario. A relative variation between the

scenarios is apparent mostly during the mid-flood and mid-ebb stages, but this cannot be effectively explored from the figures. So, a difference plot is illustrated and presented in the following section to properly investigate the model's sensitivity to its physics.

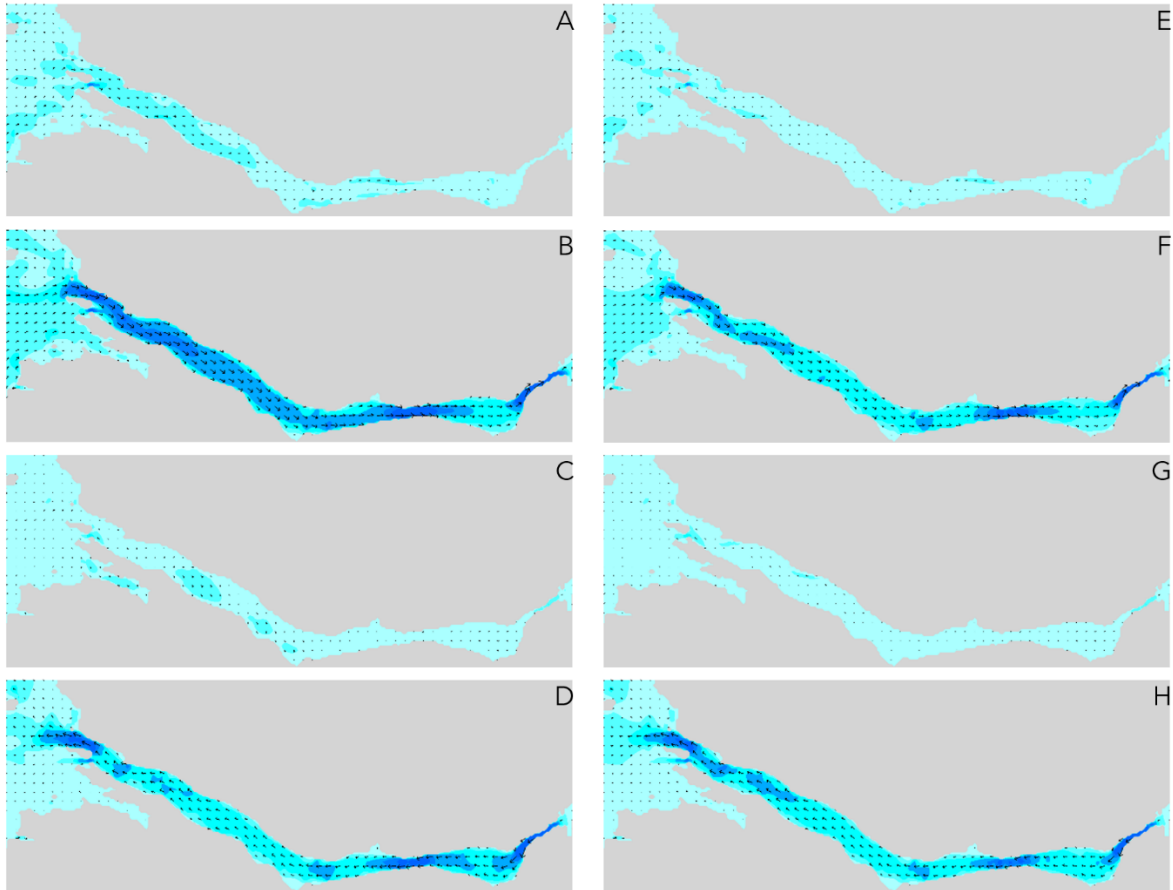


Fig 4.10 Maps showing the (A~D) surface and (E~H) depth-averaged currents in the BT-TW model scenario. The currents are sampled in the spring tide at the (A & E) low, (B & F) mid-flood, (C & G) high, and (D & H) mid-ebb tidal levels.

4.7.2.1.3. Difference Between The Scenarios

The baroclinic property of an estuary can have a significant impact on the circulation patterns of its waters. To investigate this influence in Killary, we compared the model results for a baroclinic scenario with those for a barotropic condition of the estuary. The differences in water currents between these two scenarios are presented in Fig 4.11. The figure shows the baroclinic current flow variation relative to the barotropic

condition. According to the figure, flow variations are primarily prominent in the surface water around the head and mouth of the estuary; however, although not that much, the variation is still evident in the depth-averaged flows as well. This variation in flows clearly indicates the sensitivity of the model physics, which was captured well in the model developed. As expected, the baroclinic scenario resulted in complex patterns of circulation, with the denser, saltier water sinking to the bottom and pushing the lighter, fresher water upwards. The results created vertical shear and horizontal convergence and divergence of water masses, leading to a vertical gradient in water density and pressure, which in turn drove the water flow. This mechanism led to increased mixing and turbulence in the estuary, which had important implications for the ecology of the system, leading to a more dynamic and diverse ecosystem. In the hydrodynamic model of Killary, the baroclinic set-up that was used to simulate the effects of vertical density gradients on the water flow created a hydrodynamic condition characterised by stratification, which increased the current velocity in the estuary. The model results showed that the baroclinic set-up resulted in more complex and dynamic circulation patterns, as compared to the barotropic set-up. These results have important implications for the management of estuarine systems and highlight the need for accurate hydrodynamic models to guide decision-making.

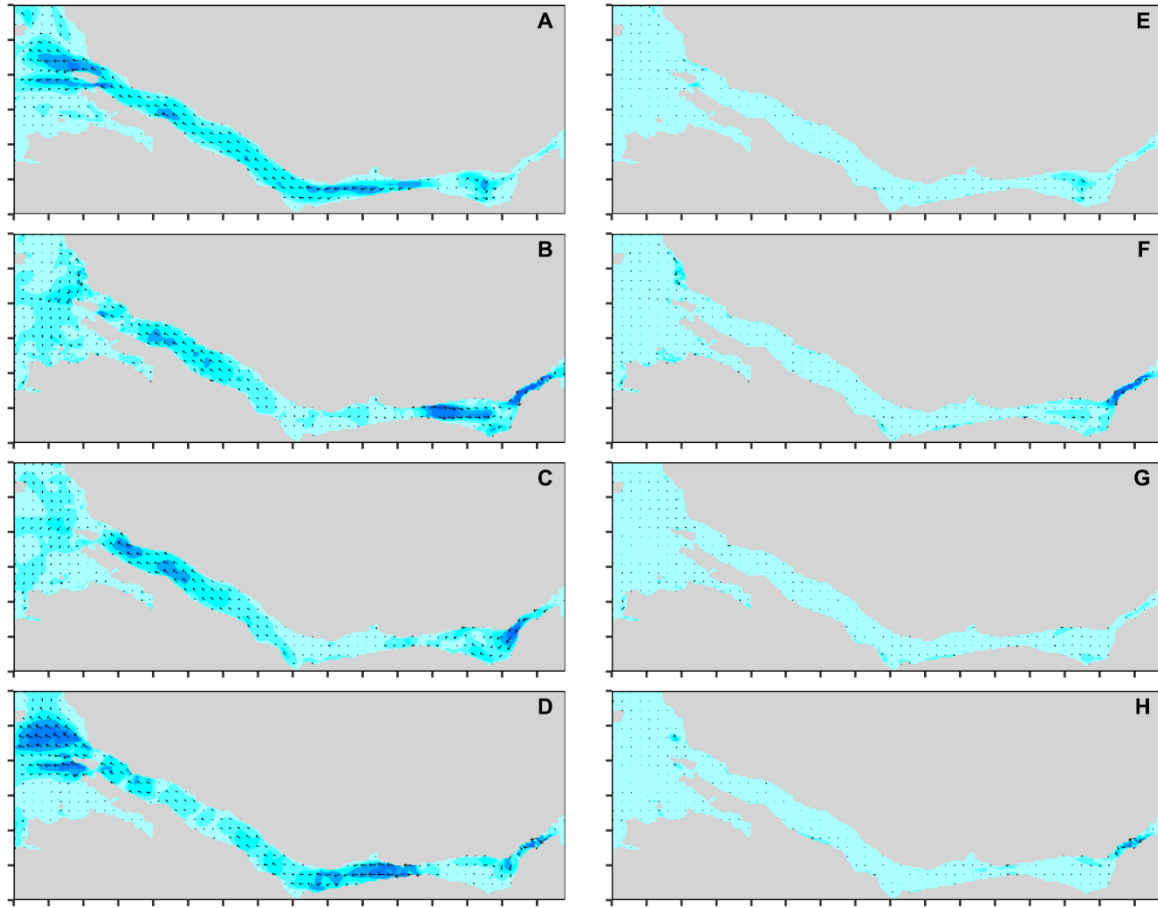


Fig 4.11 Maps showing differences in the (A~D) surface and (E~H) depth-averaged currents between the BC-All and BT-TW model scenarios. The currents are sampled in the spring tide at the (A & E) low, (B & F) mid-flood, (C & G) high, and (D & H) mid-ebb tidal levels.

4.7.2.2. Initial and Sea Boundary Conditions

To investigate the sensitivity of the Killary hydrodynamic model to variations in initial and boundary conditions, the model was simulated in multiple scenarios with different salinity and temperature specifications as initial and sea boundary conditions. The model inputs were either constant or variable over time, and the resulting outputs were analysed and compared. The model results with the constant inputs were previously analysed and described in Fig 4.8 and Fig 4.9, which showed that the model was sensitive to changes in the input parameters, with higher salinity and temperature resulting in stronger currents and deeper mixed layers. These

changes highlight the importance of the need for sensitivity analysis to identify key drivers of system behaviour.

The stratifications and current flows in the modelled scenario forced with time-varying and spatially-varying salinity and temperature are now analysed and described in Fig 4.12 and Fig 4.13, respectively. According to the figures, the stratification and currents in the variable input scenario closely resemble those in the constant input scenario. However, their differences were investigated and are illustrated in Fig 4.14 (stratifications) and Fig 4.15 (currents). Figure 4.14 shows that the spatiotemporal variations in salinity input to the model have very little influence on the stratification, probably due to the small difference in salinity values between the constant (35 psu) and varying (35.03425 ± 0.1 psu with a range of 34.26~35.30 psu) input scenarios. On the other hand, the temperature input does show a slight difference in stratification between the input scenarios. The constant temperature was at 15 °C, and the variable temperature was at 14.34 ± 0.7 °C with a range 12.39~15.93 °C. The model forced with constant initial and sea boundary temperature input shows a temperature reduction of ≤ 1 °C along the harbour compared to the varying input scenario, while remaining similar to the comparative scenario with mostly no variation from the mouth up to the sea boundary and across various tidal levels. Figure 4.15 indicates that spatiotemporally constant salinity and temperature inputs did not have any significantly different influence on the modelled currents from their varying inputs. Based on this comparative investigation, it appears that the initial and sea boundary conditions of salinity and temperature do not appear to be sensitive to their input specifications in terms of constancy or variability in short-term simulation. However, accurate and realistic boundary conditions might be critical for estuarine modelling in the long term. These findings highlight the importance of careful parameterisation and sensitivity analysis in hydrodynamic modelling and provide valuable insights into the complex dynamics of the Killary estuary.

Chapter 4: Hydrodynamic Modelling

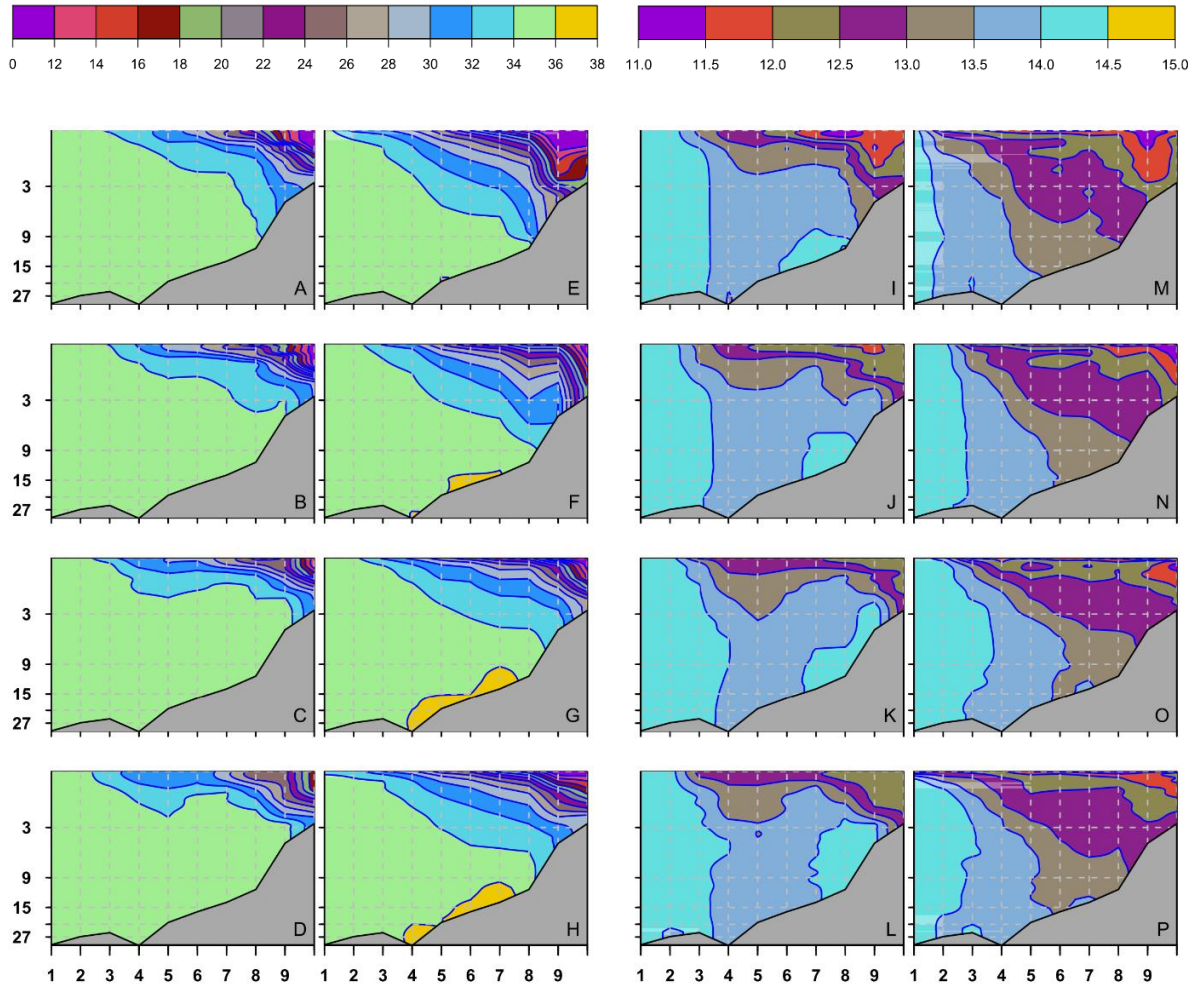


Fig 4.12 Maps showing the (A~H) salinity and (I~P) temperature stratifications as per the BC-All-tv model scenario. The stratifications are investigated in the (A~D & I~L) neap and (E~H & M~P) spring tides at the (A & E) low, (B & F) mid-flood, (C & G) high, and (D & H) mid-ebb tidal levels. (The x-axis represents the spatial points of investigation along the east-west at every 2 km, and the y-axis represents the water depths in metres. The legends on the top represent the salinity scale in psu shown on the left and the temperature scale in °C on the right.)

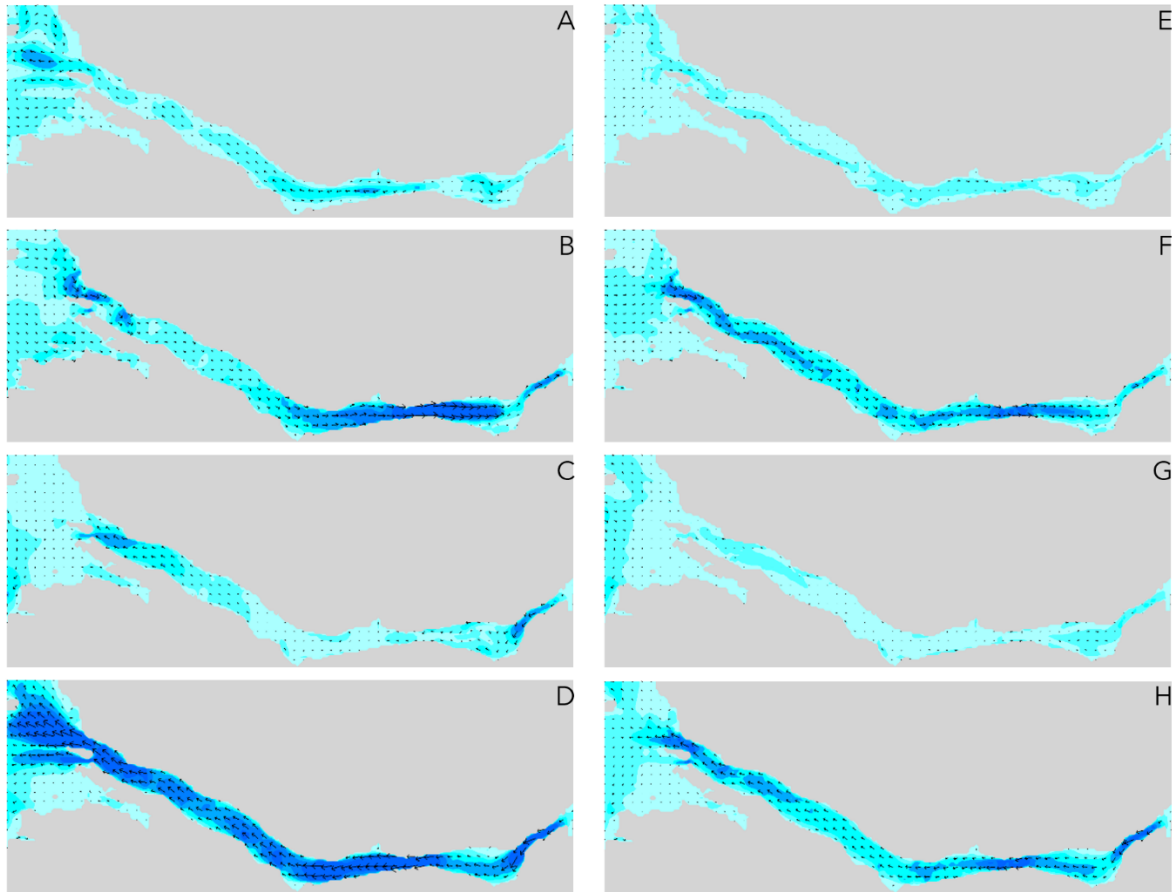


Fig 4.13 Maps showing the (A~D) surface and (E~H) depth-averaged currents in the BC-All-tv model scenario. The currents are sampled in the spring tide at the (A & E) low, (B & F) mid-flood, (C & G) high, and (D & H) mid-ebb tidal levels.

Chapter 4: Hydrodynamic Modelling

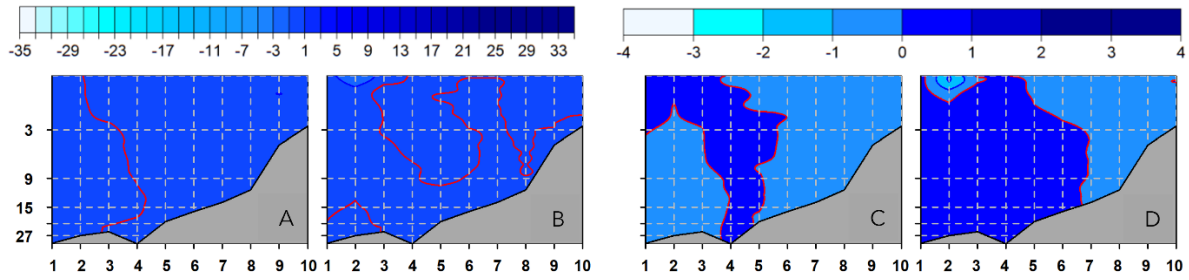


Fig 4.14 Maps showing differences in the (A~B) salinity and (C~D) temperature stratifications in the BC-All scenario with respect to the BC-All-tv scenario. The differences are investigated in the (A & C) neap and (B & D) spring tides at the mid-flood tidal level. (The x-axis represents the spatial points of investigation along the east-west at every 2 km, and the y-axis represents the water depths in metres. The legends on the top represent the scale of difference in the salinity (psu) shown on the left and the temperature (°C) on the right.)

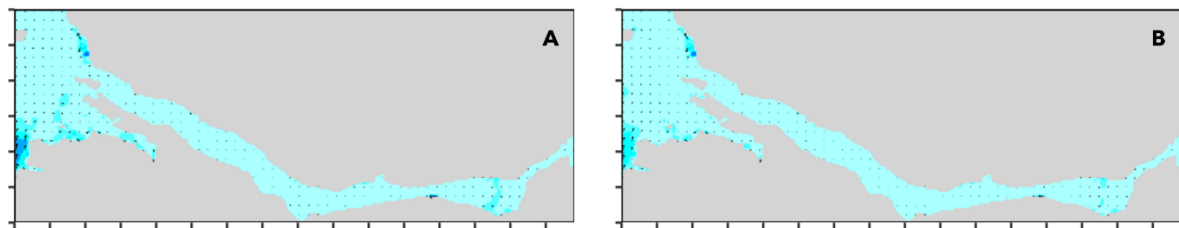


Fig 4.15 Maps showing differences in the (A) surface and (B) depth-averaged currents between the BC-All and BC-All-tv model scenarios. The currents are sampled in the spring tide at the mid-flood tidal level.

It is important to note that some limitations of the salinity and temperature analysis. As the simulations were run for a relatively short period of time (due to the matching the simulation times to the period of recorded observations of jellyfish movement), equilibrium conditions may not have been achieved. When modelling baroclinic flows, it can take a substantial amount of time for the temperature and salinity fields to reach a state of quasi-equilibrium; this contrasts with the relatively short period of time required for barotropic models to reach steady state. Short simulation periods may not allow the system to progress towards a stable equilibrium. This stems from the fact that baroclinic models account for variations in temperature and salinity, leading to the development of density gradients. These gradients create stratification, which significantly influences the vertical distribution of currents and

requires time to evolve and stabilize (Bernsen et al., 2008). Conversely, barotropic models assume a constant density throughout the water column, simplifying the simulation and requiring shorter durations to capture the dominant flow patterns driven primarily by external forces like tides and winds. In addition to the above, estuaries and coastal regions often undergo seasonal fluctuations in temperature and salinity due to factors like temperature variations, rainfall, and tidal influences. It is therefore recommended that a longer simulation period should be used to ensure steady state has been achieved and to capture seasonal variations and their impacts on the system. Depending on the specific dynamics of the estuary, the system may require time to respond to external forcing factors such as tides, wind, and freshwater inflow. Longer simulation periods provide a more comprehensive exploration of these responses.

4.7.2.3. Wind

4.7.2.3.1. Wind Speed Scenarios

Four wind scenarios were simulated in order to investigate their influence on stratifications and currents and analysed through five paired comparisons illustrated in various figures. Table 4.5 summarises the key results of the analyses in terms of sensitivity.

Table 4.5 Summary of the model sensitivity study to the wind.

Scenario ID	Comparative analysis	Sensitivity to W		
		Salinity	Temperature	Currents
WX = with time-varying wind; W0 = without wind (0 m/s); W4* = with time-constant wind at 4 m/s; W8* = with time-constant wind at 8 m/s.	WX vs. W0	Y	Y	Y
	W0 vs. W4	Y**	N	N
	W0 vs. W8	Y**	N	N
	W4 vs. W8	N	N	N
	WX vs. W8	Y	Y	Y
*South-westerly wind. **Limited (only during the neap tide).				

Chapter 4: Hydrodynamic Modelling

The analyses of the reference wind scenario, which is with the time-varying wind (WX), have been shown previously in Fig 4.8 (stratifications) and Fig 4.9 (currents). The modelled currents across the wind scenarios are visually the same or similar; therefore, their presentations are skipped here in this section. Fig 4.16 presents the analysis of stratifications in various tidal stages and levels for three scenarios: no wind (W0) and constant winds at 4 m/s (W4) and 8 m/s (W8). According to the analyses, the stratifications do not appear to vary visually across these wind scenarios in any of the tidal stages or tidal levels. Due to having similar results of all these analyses, only a representative illustration of the analyses is presented here in Fig 4.16 for demonstration. The salinity stratifications do not show any diurnal influence across various tidal levels but vary across the spring and neap tides indicating the lunar influence. The stratifications occurring during the spring tide are stronger than the neap tide. The scenarios with the time-constant wind at either 0, 4, or 8 m/s speed show warmer water than the time-varying wind scenario. Thus, wind shows an influence on the temperature stratification in Killary. However, it appears to be a bit critical to precisely interpret the extent and influence of the stratifications from these preliminary visual inspections of the individual illustrations. So, a quantitative difference plot is illustrated and presented in the following section to properly investigate the sensitivity of the model to the wind.

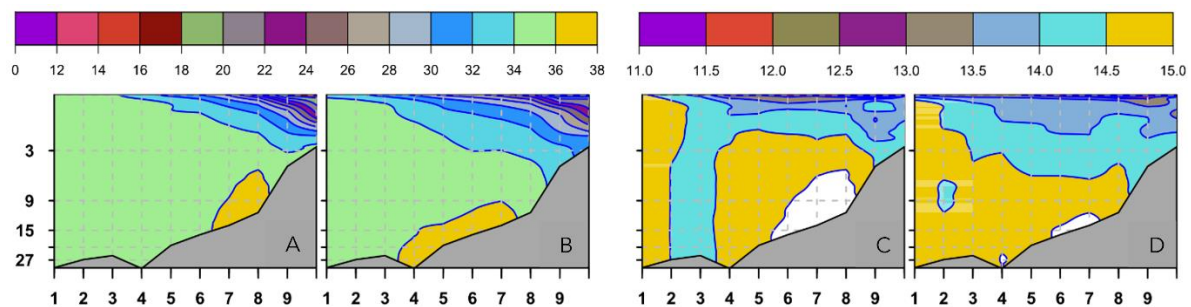


Fig 4.16 Maps showing the (A~B) salinity and (C~D) temperature stratifications as per the BC-NW model scenario. The stratifications are investigated in the (A & C) neap and (B & D) spring tides at the mid-ebb tidal level. (The x-axis represents the spatial points of investigation along the east-west at every 2 km, and the y-axis represents the water depths in metres. The legends on the top represent the salinity scale in psu shown on the left and the temperature scale in °C on the right.)

4.7.2.3.2. Differences Among the Wind Scenarios

To examine the impact of wind on the stratification and currents in Killary, the wind scenarios were compared in pairs according to the analysis plan outlined in Table 4.5. The respective plots of difference in stratification are presented in Fig 4.17 and Fig 4.18. Where the same or similar results are observed at various tidal levels, only a representative illustration of the analyses is presented in the figures for demonstration. According to Fig 4.17, which displays the relative differences between scenarios with the time-varying wind (WX) and those without wind (W0) or with the time-constant wind (e.g. W8), the upper harbour areas exhibit lower salinity and temperature in WX compared to W0 or W8, whereas no significant differences were observed in deeper waters or oceanic areas between the wind scenarios. Fig 4.18 shows the relative differences among three time-constant wind scenarios viz., W0, W4, and W8, where the wind blew at 0, 4, and 8 m/s speed, respectively. According to the figure, the salinity and the temperature are slightly higher in the upper harbour areas during the neap tide in the zero-speed wind scenario W0 (no wind) than in the higher-speed wind scenarios W4 or W8; the deeper waters and the oceanic areas do not show any difference between the wind scenario pairs. The W4 vs. W8 scenario pair also shows no difference at all. These mainly indicate that the time-varying wind had an obvious influence on the stratification. Wind contributed to the mixing of the river discharge into the harbour, thereby resulting in the reduction of the salinity and temperature where the rivers joined the harbour near its head. This effect was higher while the tidal influence was lower (i.e., neap tide) and lower while the tidal influence was higher (i.e., spring tide). The impact of time-constant wind on creating differences in stratification appears to be less significant than that of time-varying wind, as the variability of wind contributes to better mixing than a unidirectional constant wind.

Chapter 4: Hydrodynamic Modelling

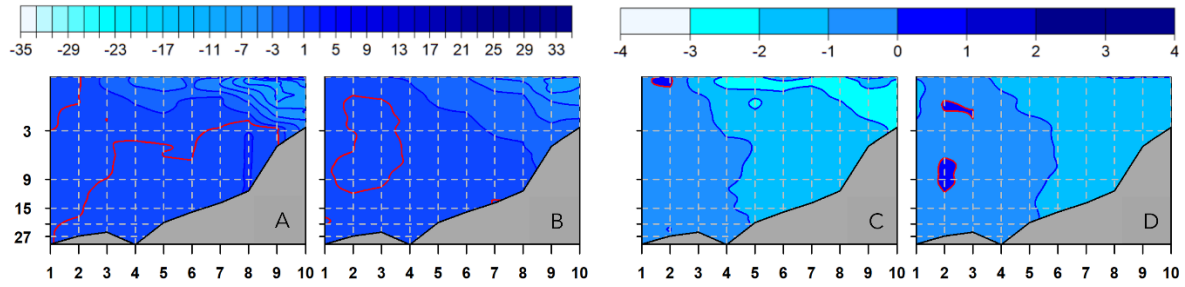


Fig 4.17 Maps showing differences in the (A~B) salinity and (C~D) temperature stratifications in the WX scenario with respect to the W0 or W8 scenarios. The differences are investigated in the (A & C) neap and (B & D) spring tides at the mid-ebb tidal level. (The x-axis represents the spatial points of investigation along the east-west at every 2 km, and the y-axis represents the water depths in metres. The legends on the top represent the scale of difference in the salinity (psu) shown on the left and the temperature (°C) on the right.)

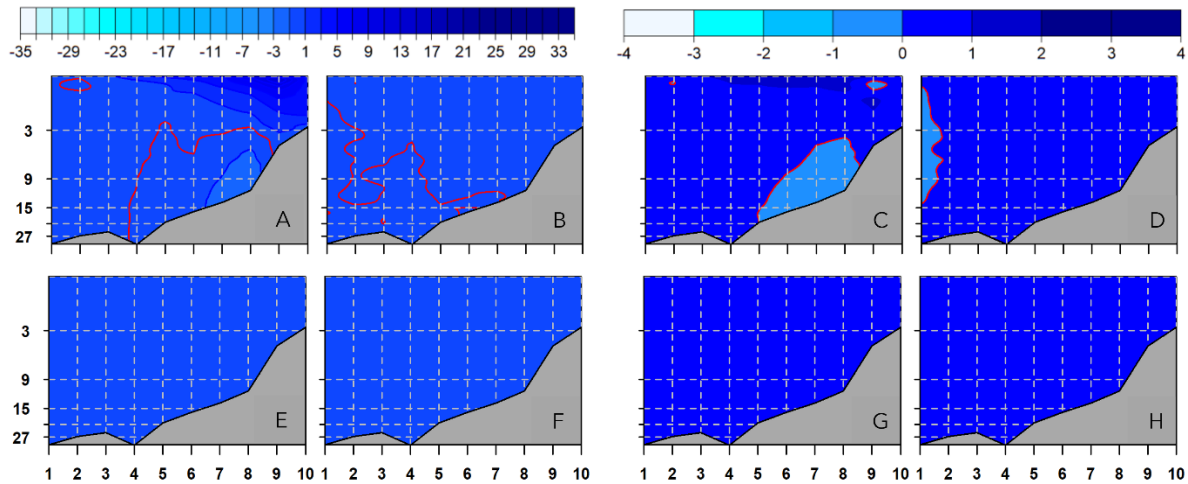


Fig 4.18 Maps showing differences in the (A~B & E~F) salinity and (C~D & G~H) temperature stratifications in (A~D) the W0 scenario with respect to the W4 or W8 scenarios and in (E~H) the W4 scenario with respect to the W8 scenario. The differences are investigated in the (A~D & I~L) neap and (E~H & M~P) spring tides at the mid-ebb tidal levels. (The x-axis represents the spatial points of investigation along the east-west at every 2 km, and the y-axis represents the water depths in metres. The legends on the top represent the scale of difference in the salinity (psu) shown on the left and the temperature (°C) on the right.)

The figures in this section, Fig 4.19 and Fig 4.20, show the differences in current flows among wind scenarios in various tidal stages and levels. According to Fig 4.19, which illustrates the relative differences in WX from W0 or W8, the surface currents are locally higher near the mouth and in the anterior of the harbour in the time-

varying wind scenario than in the time-constant wind scenarios. This difference is most noticeable during the flood tide and may be linked to changes in stratification. The difference in depth-averaged currents is relatively lower than that in surface currents. Fig 4.20 indicates that the relative difference between W0 and W4 or W8 is very low, and the relative difference between W4 and W8 is zero. These analyses suggest that wind has little influence on the tidal currents in Killary, primarily due to the time-varying wind. The time-constant winds, whether milder (4 m/s) or stronger (8 m/s), could not significantly impact the harbour currents because the wind was forced unidirectionally at constant rates, which could not overpower the tidal influence to create any difference in currents. However, a wind much stronger than 8 m/s might create different results that were not tested in this study.

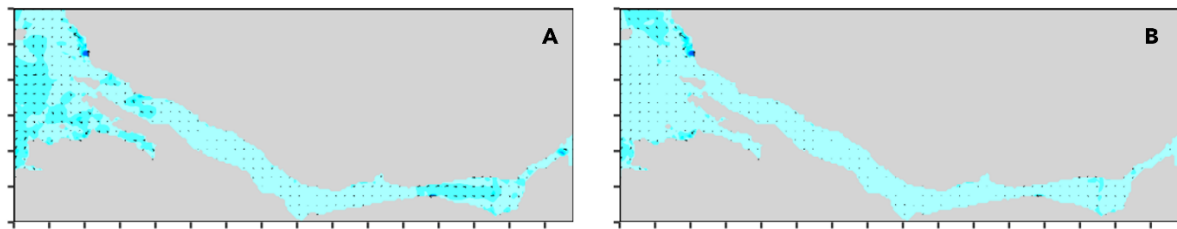


Fig 4.19 Maps showing differences in the (A) surface and (B) depth-averaged currents between the WX and the W0 or W8 model scenarios. The currents are sampled in the spring tide at the mid-flood tidal level.

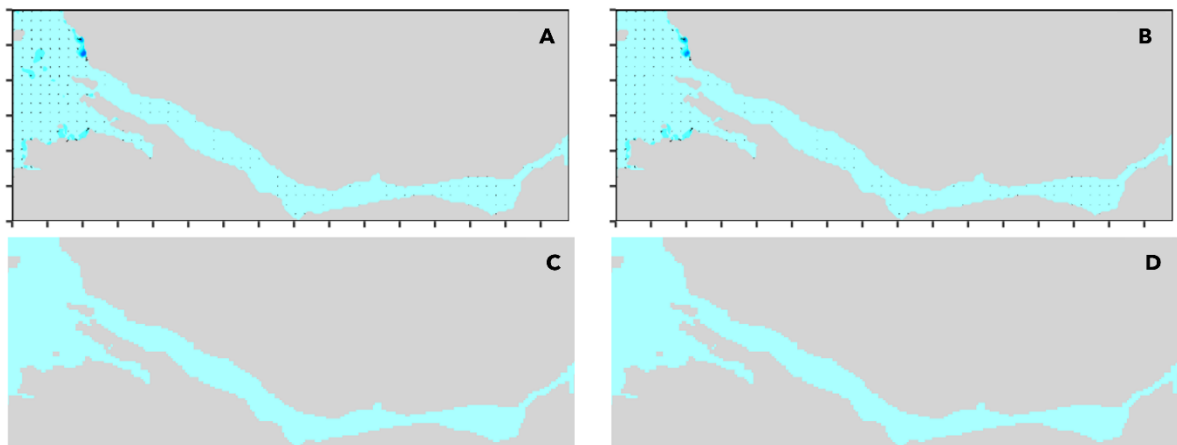


Fig 4.20 Maps showing differences in the (A & C) surface and (B & D) depth-averaged currents (A~D) between the W0 and the W4 or W8 scenarios and (E~H) between the W4 and the W8 scenario. The currents are sampled in the spring tide at the mid-flood tidal level.

4.7.2.4. River Discharge

4.7.2.4.1. Discharge Scenarios

To investigate the influence of river discharge (Q in m^3/s) on stratification and currents, four discharge scenarios were simulated and analysed through five paired comparisons, as shown in Table 4.6. The results of these analyses in terms of sensitivity are illustrated in different figures.

Table 4.6 Summary of the model sensitivity study to the river discharge.

Scenario ID	Comparative analysis	Sensitivity to Q		
		Salinity	Temperature	Currents
RX = with time-varying Q ; R0 = without Q ($0 \text{ m}^3/\text{s}$); R3 = with time-constant Q at $3 \text{ m}^3/\text{s}$; R33 = with time-constant Q at $33 \text{ m}^3/\text{s}$	RX vs. R0	Y	Y	Y
	R0 vs. R3	Y*	Y*	Y
	R0 vs. R33	Y	Y	Y
	R3 vs. R33	Y	Y	Y
	RX vs. R33	Y	Y	Y*
*Limited.				

The analysis of the reference river discharge scenario, which has a time-varying Q (RX), was presented previously in Fig 4.8 for stratifications. The stratifications of scenarios with time-constant discharge at $3 \text{ m}^3/\text{s}$ and $33 \text{ m}^3/\text{s}$ (R3 and R33, respectively) were analysed and are presented in Fig 4.21. Due to having the same or similar results of these analyses at various tidal levels, only a representative illustration of the analyses is presented here for demonstration. The scenario without the discharge (R0) did not produce any stratification, which made its illustration irrelevant here, so it was skipped. According to Fig 4.21, the analysis reveals variable stratifications across the levels of discharge and the tidal stages. The salinity and temperature are more stratified in the scenario with the higher discharge than with the lower discharge and in the spring tide than in the neap tide. Estuarine temperature is only horizontally stratified while with the low discharge at a lower

tidal influence during the neap tide; the tendency of its vertical stratification increases with increasing the discharge of the river and the tidal influence at the spring tide. However, it appears to be a bit critical to precisely interpret the extent and influence of the stratifications from the individual visualisations. So, a difference plot is illustrated and presented in the following section to properly investigate the sensitivity of the model to the river discharge.

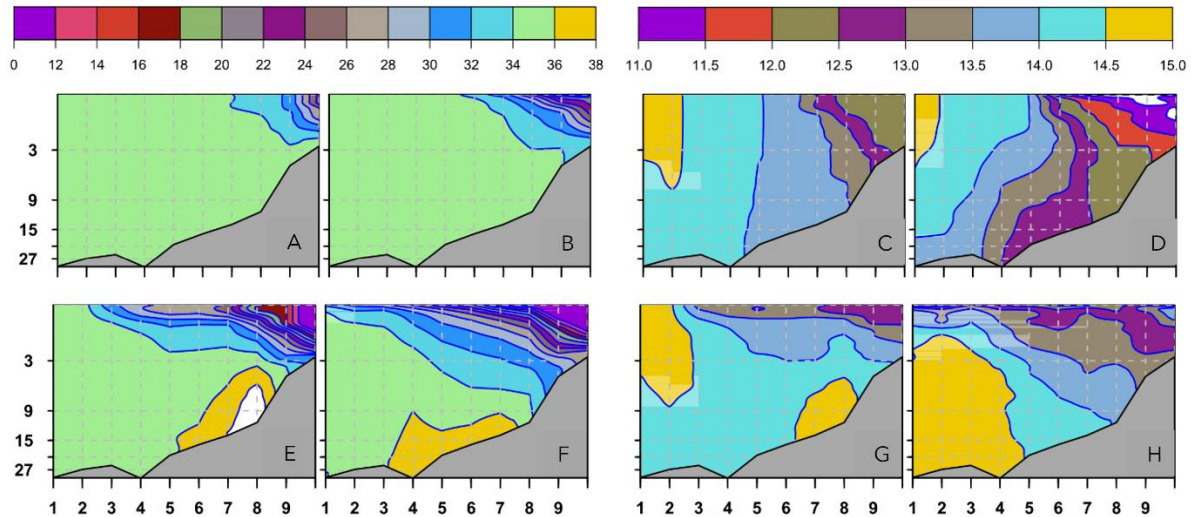


Fig 4.21 Maps showing (A~B & E~F) salinity and (C~D & G~H) temperature stratifications as per (A~D) R3 and (E~H) R33 model scenarios. The stratifications are investigated in the (A, C, E, & G) neap and (B, D, F, & H) spring tides at the mid-ebb tidal level. (The x-axis represents the spatial points of investigation along the east-west at every 2 km, and the y-axis represents the water depths in metres. The legends on the top represent the salinity scale in psu shown on the left and the temperature scale in °C on the right.)

The modelled currents at the time-varying Q (RX) have been shown previously in Fig 4.9, at no ($R0$) and low-flow ($R3$) Q are presented here in Fig 4.22, and at the high-flow Q ($R33$) in Fig 4.23. To avoid redundancy, only a representative illustration of the analyses is presented here to demonstrate similar visuals in the presentation. The visual comparisons, according to the figures, reveal that the current speeds differ among the scenarios under investigation. Both the surface and depth-averaged currents show those differences, which are noticeable in all tidal levels. A quantitative difference plot between the scenario pairs will reveal the influence of the river discharge more clearly, which is presented in the following section.

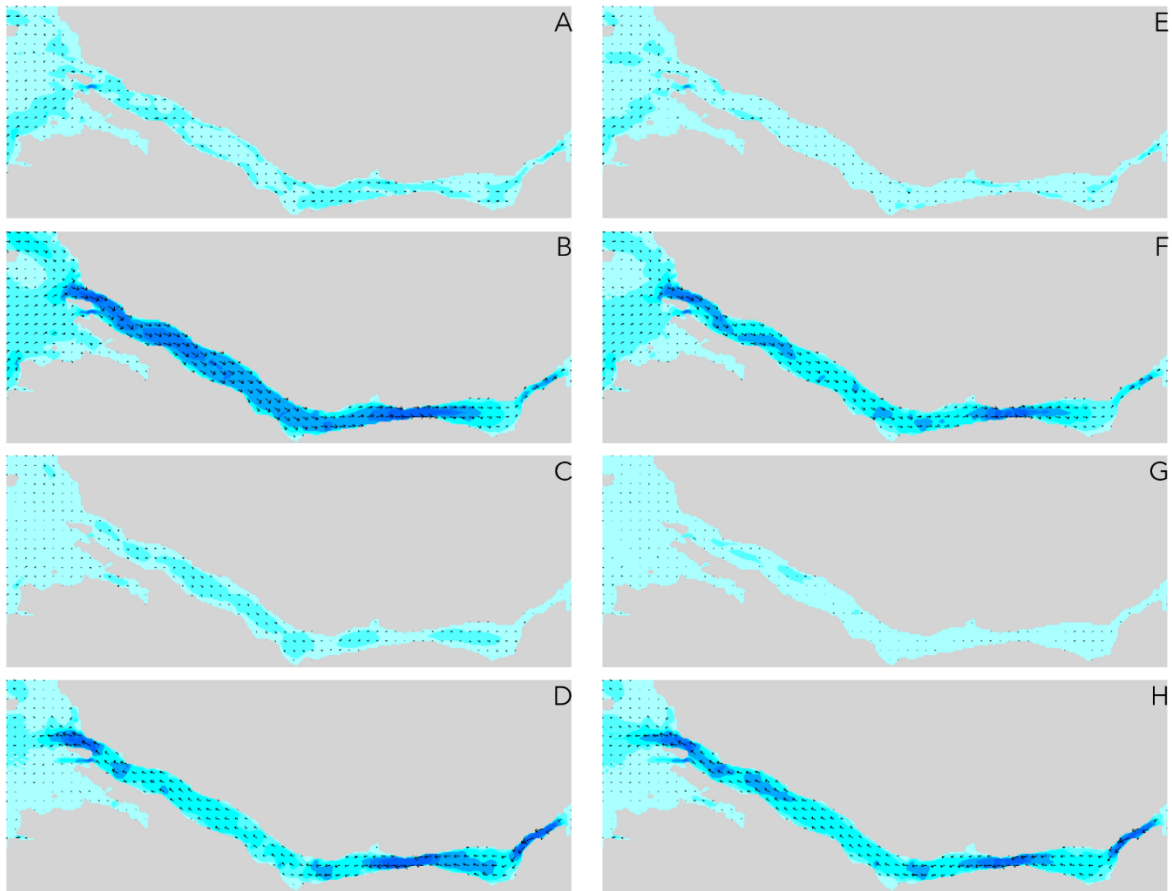


Fig 4.22 Maps showing the (A~D) surface and (E~H) depth-averaged currents in the R0 or R3 model scenario. The currents are sampled in the spring tide at the (A & E) low, (B & F) mid-flood, (C & G) high, and (D & H) mid-ebb tidal levels.

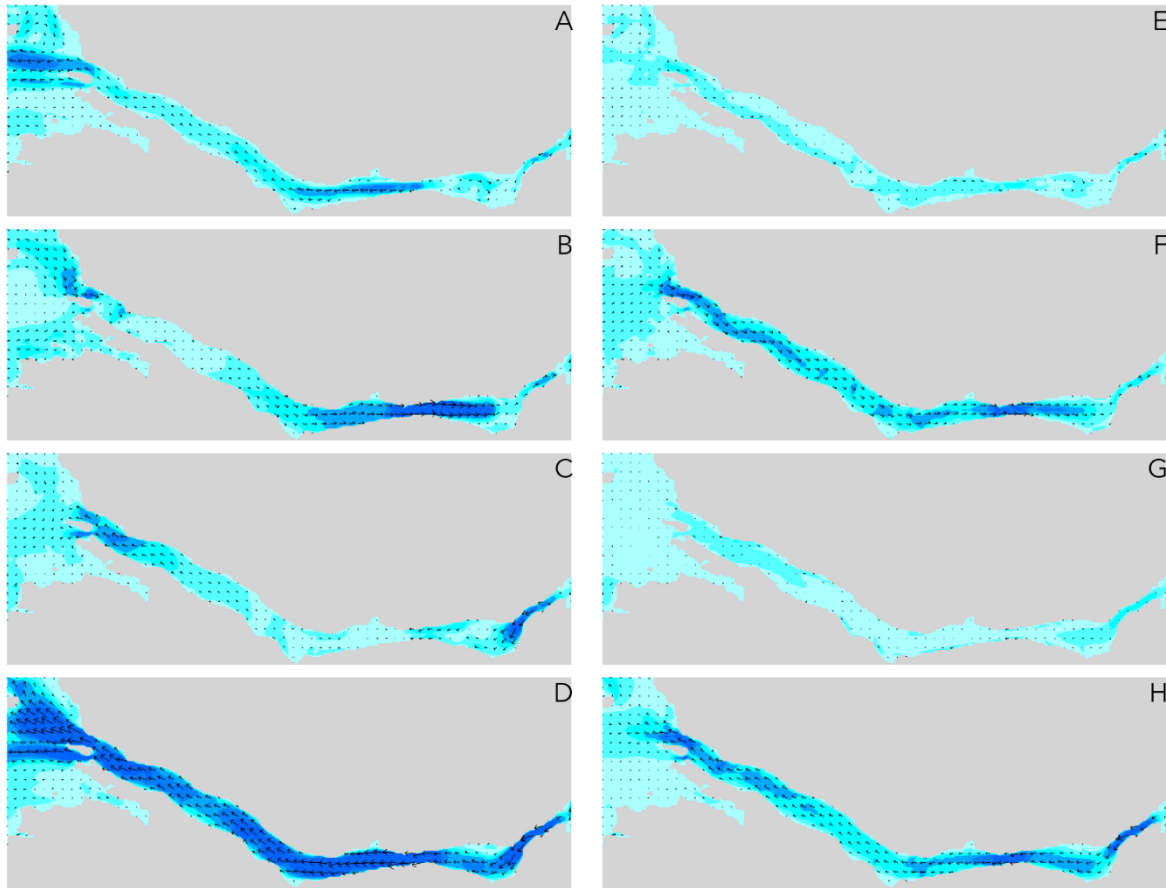


Fig 4.23 Maps showing the (A~D) surface and (E~H) depth-averaged currents in the R33 model scenario. The currents are sampled in the spring tide at the (A & E) low, (B & F) mid-flood, (C & G) high, and (D & H) mid-ebb tidal levels.

4.7.2.4.2. Differences Among The Discharge Scenarios

To investigate the influence of river discharge on stratification and currents in Killary, discharge scenarios were compared pairwise using the analysis plan in Table 4.6. Comparative analyses at various tidal levels showed no difference in stratification across tidal levels within an individual discharge scenario, but differences existed among various discharge scenarios at all tidal levels. The respective plots of difference in salinity and temperature stratification at the neap and spring tides are presented in Fig 4.24. The same or similar results are presented in the figure by a representative illustration of the analyses. Along with the tidal influence on the stratification between the neap and the spring tide, both the tidal stages individually

show variations in the stratification among the discharge scenarios, as shown in the figure. According to the figure, the difference between the scenarios having time-varying Q (RX) and no- Q (R0), as shown in A~D, reveals that the harbour salinity and temperature decrease in RX. The colder freshwater from the river discharge reduced harbour salinity and temperature upon mixing, creating a strong stratification in the harbour, as expected. The RX scenario shows an increase in salinity, but a decrease in temperature when compared with a scenario that has a time-constant discharge (e.g., R33), as shown in the figure in panels E-H. This is because the average capacity or influence of riverine freshwater input into the harbour in terms of reducing the salinity is higher in Killary with an experimental high-flow discharge than with its usual time-varying discharge, which is the opposite in reducing the temperature. Comparisons among scenarios with time-constant discharges of 0, 3, and 33 m³/s (R0, R3, and R33, respectively) show higher salinity and temperature stratification in lower discharge scenarios and vice versa (Figures I-T). An experimental zero river input characterises a more saline and warmer estuarine condition. Freshwater input from the river discharge (e.g., 3 m³/s) induces a low-level baroclinic effect by creating stratification in the harbour. Higher discharges (e.g., 33 m³/s) induce stronger baroclinic effects.

Chapter 4: Hydrodynamic Modelling

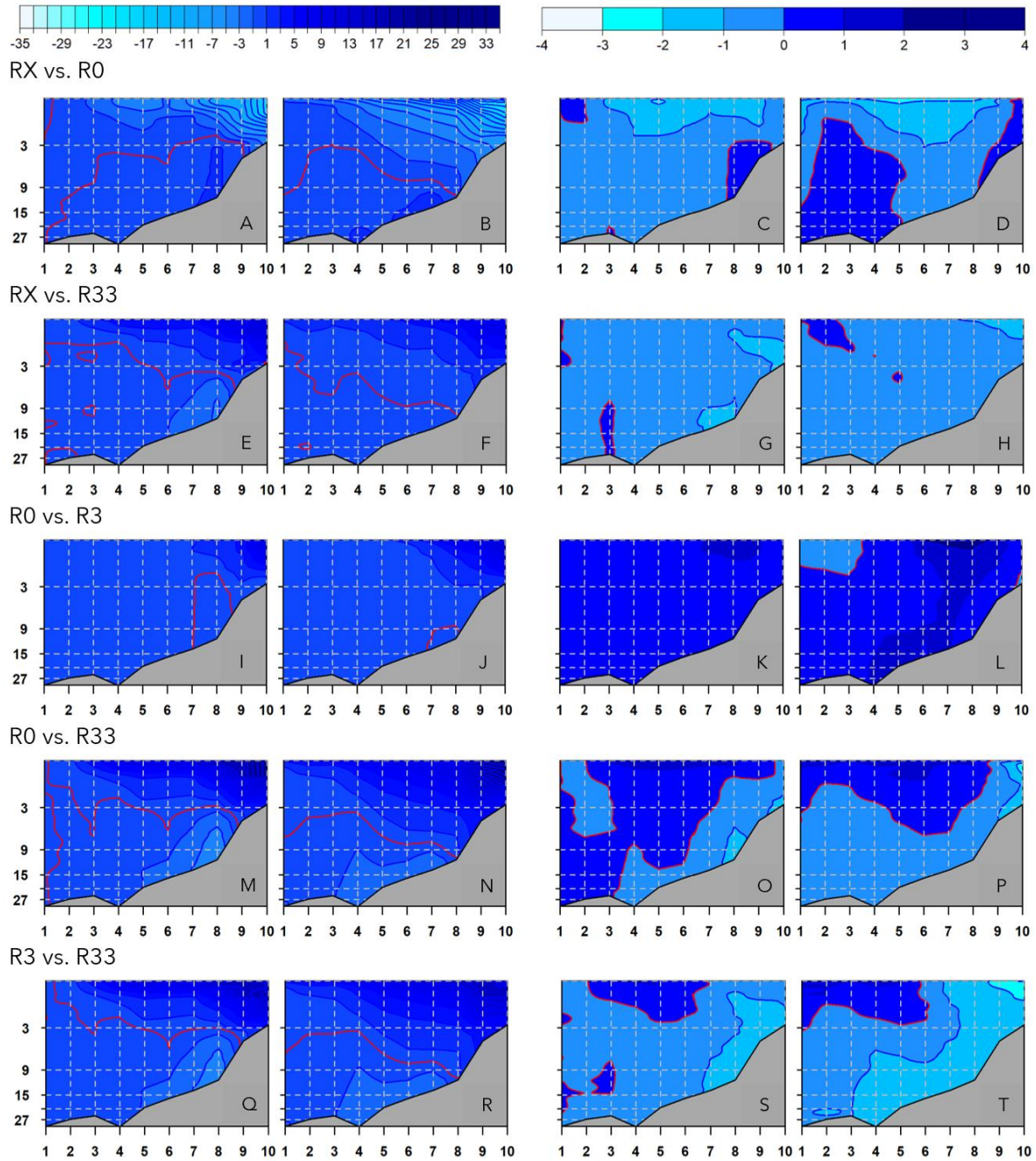


Fig 4.24 Maps showing differences in the salinity (two left-most columns) and temperature (two right-most columns) stratifications in (A~H) the RX scenario with respect to the (A~D) R0 and (E~H) R33 scenarios, in (I~P) the R0 scenario with respect to the (A~D) R3 and (E~H) R33 scenarios, and in (Q~T) the R3 scenario with respect to the R33 scenario. The differences are investigated in the neap and spring tides at the mid-ebb tidal level, and the respective figures are organised in the 1st & 3rd and the 2nd & 4th columns, respectively. (The x-axis represents the spatial points of investigation along the east-west at every 2 km, and the y-axis represents the water depths in

Chapter 4: Hydrodynamic Modelling

metres. The legends on the top represent the scale of difference in the salinity (psu) shown on the left and the temperature (°C) on the right.)

The hydrodynamic current variations due to the river discharge are plotted in Fig 4.25, Fig 4.26, and Fig 4.27. Fig 4.25 shows a representative illustration of the current variations analysed and found between the scenario pairs having a major net variation in discharge, such as RX-R0, R0-R33, and R3-R33. According to the figure, greater variations in harbour currents are observed in these scenarios, which are associated with higher discharge variations and are most noticeable for surface currents. This indicates a significant influence of river discharge in varying the harbour currents. Fig 4.26 and Fig 4.27 show the current variations in the scenario pairs separated by minor discharge variations such as R0-R3 and RX-R33, respectively. According to the figures, although the discharge variations are smaller than that shown in Fig 4.25, they still indicate sensitivity. Colder freshwater from the rivers mixed with the warmer saline water of the harbour, thereby creating a stratification by changing the harbour salinity and temperature profiles. A variable water density created by this process effectuated the flow variability within the harbour. Thus, spatiotemporally varying river discharge inputs created true baroclinic effects in the harbour through stratification and associated flow variability.

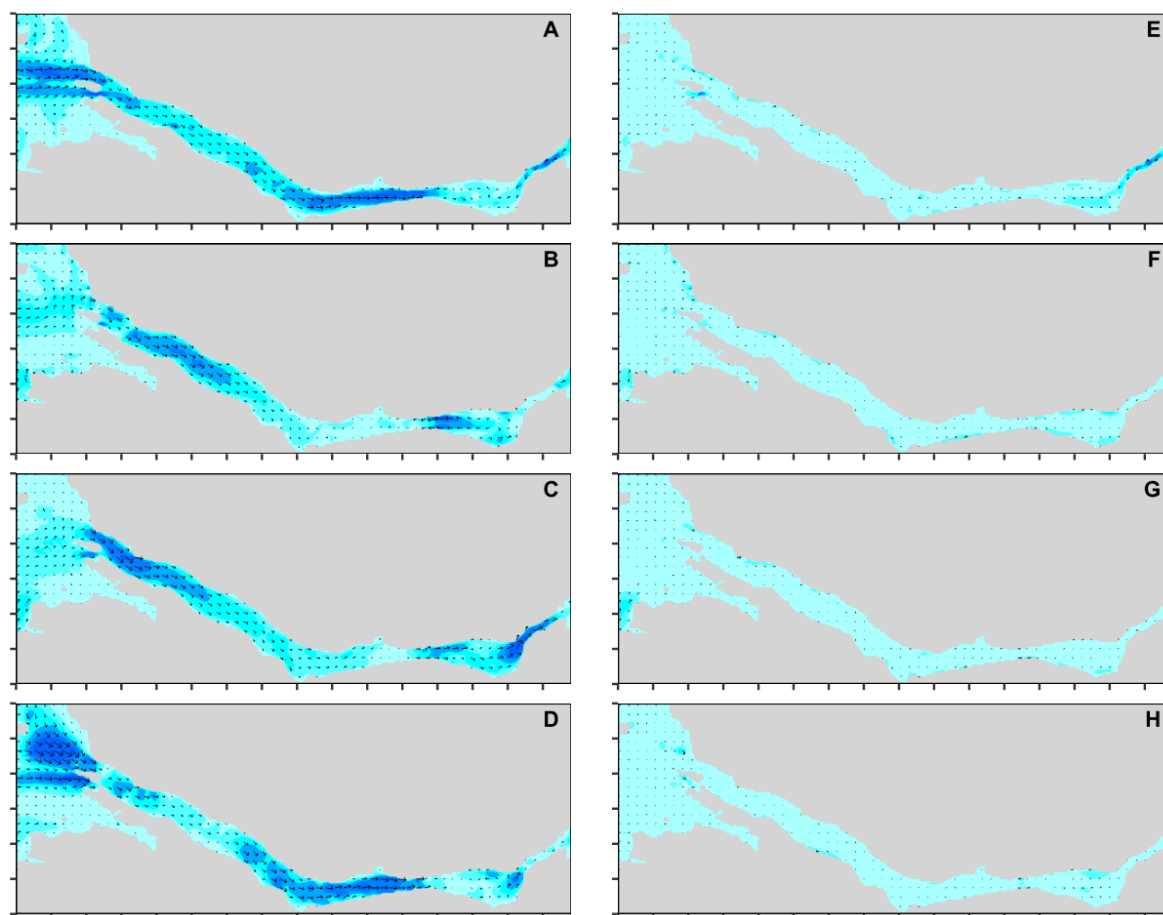


Fig 4.25 Maps showing differences in (A~D) surface and (E~H) depth-averaged currents in the discharge scenario pairs RX-R0 or R0-R33 or RR3-R33. The currents are sampled in the spring tide at (A & E) low, (B & F) mid-flood, (C & G) high, and (D & H) mid-ebb tidal levels.

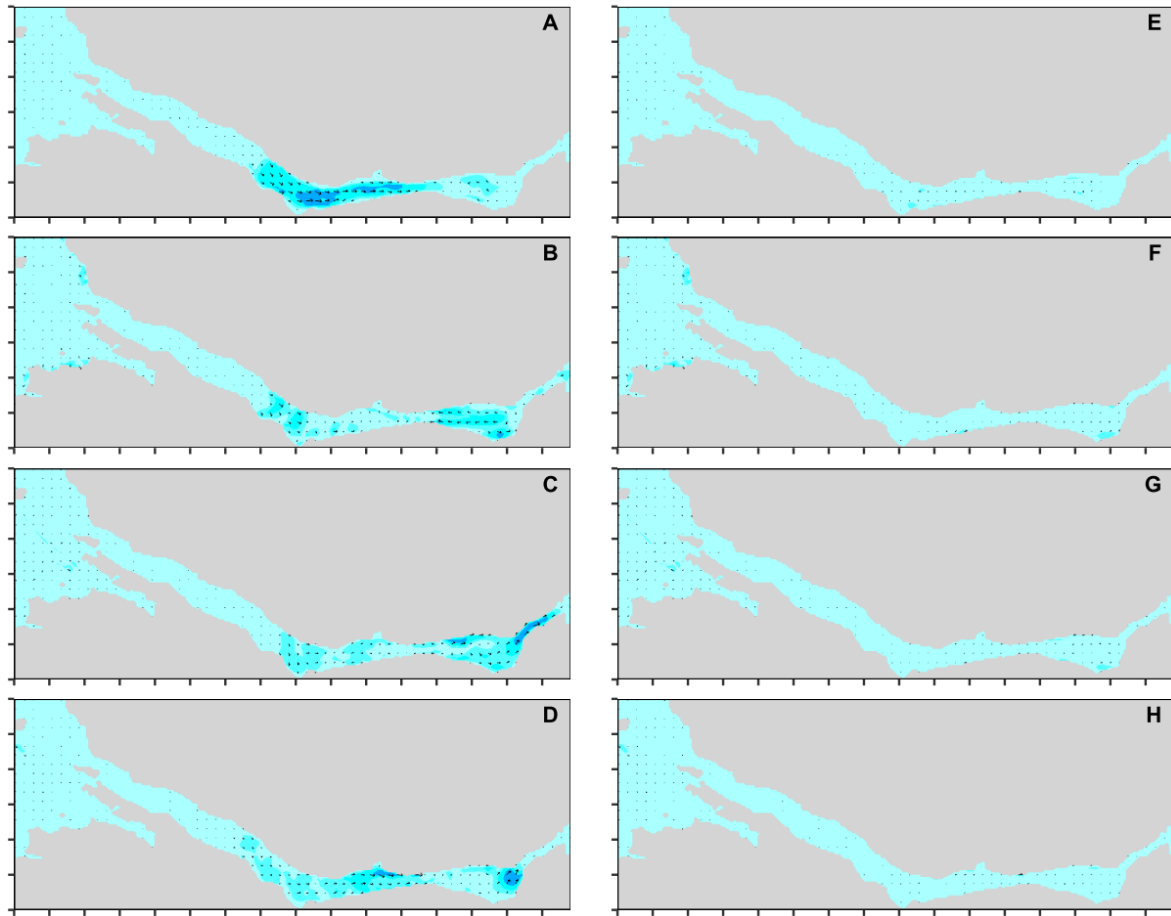


Fig 4.26 Maps showing differences in (A~D) surface and (E~H) depth-averaged currents between the R0 and R3 model scenarios. The currents are sampled in the spring tide at (A & E) low, (B & F) mid-flood, (C & G) high, and (D & H) mid-ebb tidal levels.

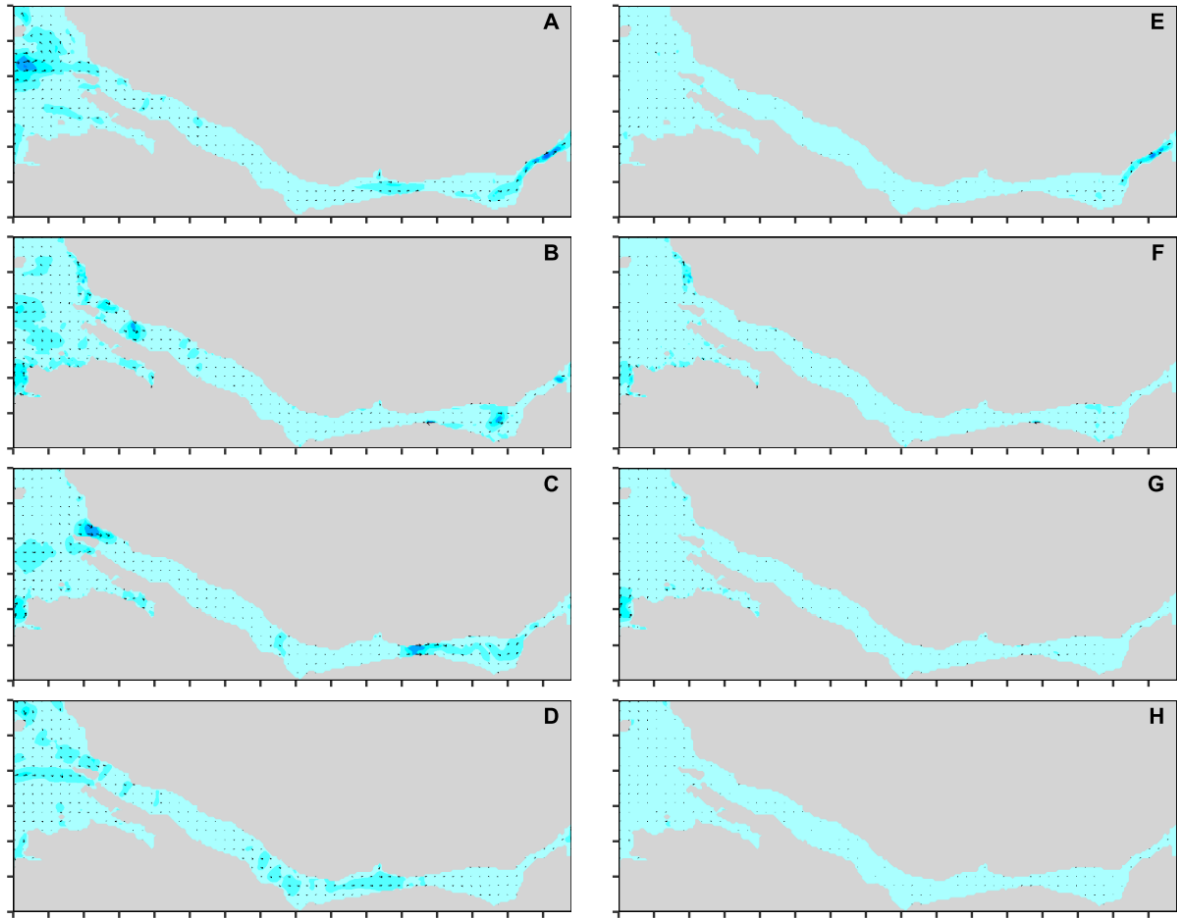


Fig 4.27 Map showing the difference in (A~D) surface and (E~H) depth-averaged currents between RX and R33 model scenarios. The currents are sampled in the spring tide at (A & E) low, (B & F) mid-flood, (C & G) high, and (D & H) mid-ebb tidal levels.

4.7.2.5. Density-driven Vertical Circulations

To investigate density-driven flows within Killary, a comparative analysis of the influence of temperature and salinity dynamics in the harbour was conducted between scenarios capable of inducing density-driven flows (baroclinic) and those lacking this capability (barotropic). This analysis, focused on vertical circulations, was carried out across various tidal levels. The results of this investigation revealed varying vertical currents at all tidal levels, highlighting differences between these levels. Figure 4.28 displays a series of illustrations depicting the current variations during spring tide attributed to temperature and salinity dynamics within the baroclinic scenario. As illustrated in the figure, the baroclinic scenario exhibits more

pronounced variations in vertical currents, particularly at the surface. These variations are closely linked to temperature and salinity inputs and fluctuations within the scenario. Notably, the variable water density resulting from the stratification caused by temperature and salinity plays a pivotal role in generating flow variability within the harbour. This underscores the substantial influence of density variation in shaping harbour currents, ultimately resulting in the manifestation of genuine baroclinic effects within the harbour, driven by stratification and the associated flow variability.

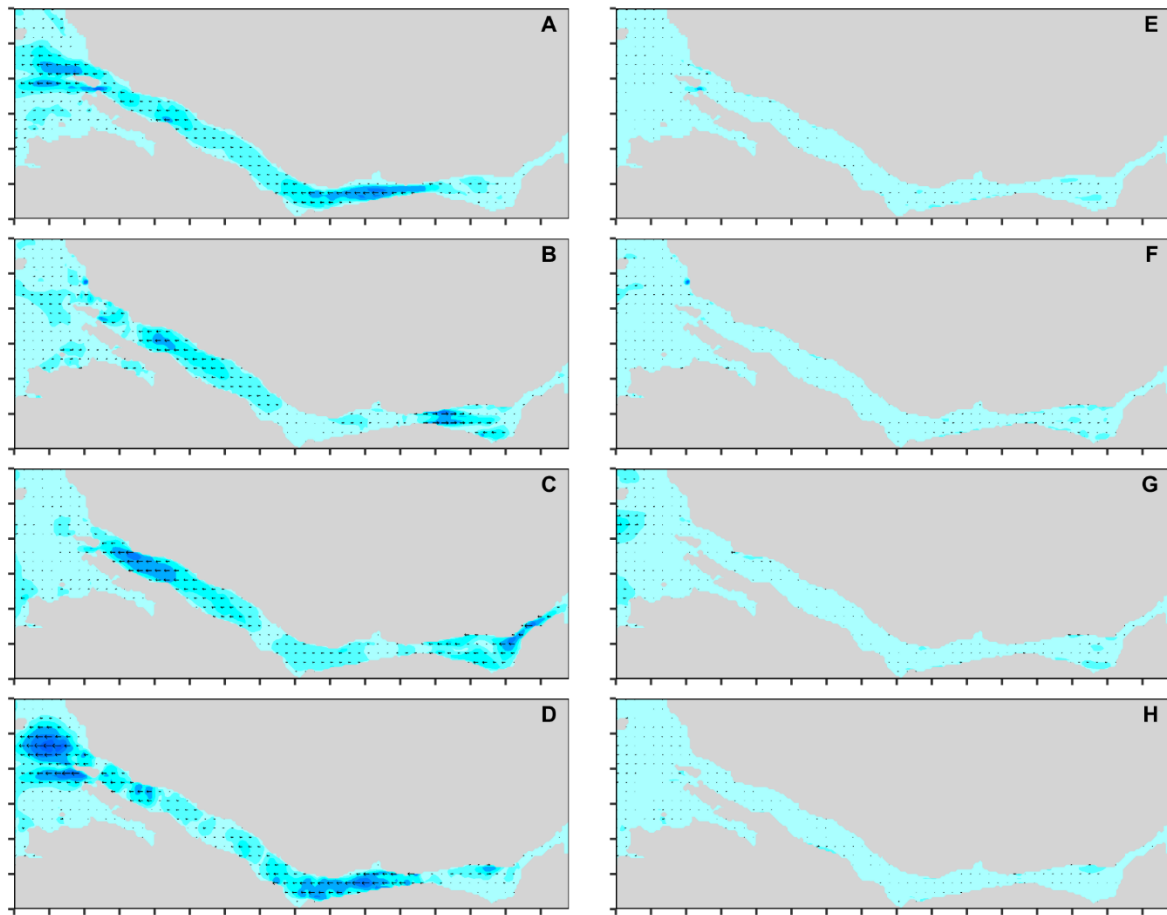


Fig 4.28 Map showing the difference in (A~D) surface and (E~H) depth-averaged currents between baroclinic and barotropic model scenarios. The currents are sampled in the spring tide at (A & E) low, (B & F) mid-flood, (C & G) high, and (D & H) mid-ebb tidal levels.

4.8. Conclusions

The hydrodynamic model of the Killary Harbour was developed using the EFDC model. The sensitivity of the model to various model forcings and parameters was investigated, and the influences of the relevant processes were analysed to characterise the Killary hydrodynamics. Some key conclusions of the study are listed and described below.

(1) The water structure of Killary Harbour was found to be stratified or partially mixed, with stronger stratification during spring tides due to increasing salinity and temperature gradients (i.e., lower salinity and colder surface water towards the upstream end of the harbour).

(2) Salinity and temperature gradients were observed during spring tides, with the values of the parameters decreasing and the horizontal gradients increasing towards the upstream end and significant vertical gradients in the form of haloclines and thermoclines occurring within a depth range of 3-10 m (as reported by Keegan & Mercer, 1986).

(3) Stratification was found to play a major role in the flow dynamics of Killary Harbour, with variable density flows induced by stratification creating a baroclinic effect in the estuary.

(4) Stratification was identified as a potential source of hydrodynamic turbulence in the harbour, with turbulence combining with advection to enhance estuarine circulations (as also noted by Keegan & Mercer, 1986).

(5) Estuarine tidal advection from the Atlantic through the west of Killary Harbour mixed with freshwater inflows from rivers in the east to increase stratification and gradients along the harbour, similar to the influence of the Gulf of Mexico through Perdido Bay demonstrated by Xia et al. (2011).

(6) The model results suggest that the baroclinic input conditions are relatively insensitive to spatiotemporal variations, likely due to limited variations in sea salinity and temperature at the model's open boundary areas. However, some stratification

Chapter 4: Hydrodynamic Modelling

was observed in temperature due to its higher variation, indicating that constant baroclinity may be used to initiate model simulations when input data are limited or uncertain.

(7) The wind was found to influence the baroclinity and hydrodynamic currents of Killary Harbour, but its impact on currents was limited, with the time-varying wind increasing surface currents inside the harbour slightly more than a constant wind of 8 m/s from the southwest.

(8) The river discharge was found to have a significant influence on stratification and current flows in Killary Harbour at various tidal levels, with higher discharge scenarios inducing stronger effects that were most noticeable for surface currents.

CHAPTER 5: PASSIVE-DRIFT MODELLING OF JELLYFISH

5.1. Introduction

Jellyfish transport modelling has been researched for many years to understand and predict their transport and swarm formation. However, making these predictions is complicated due to the dynamic nature of the waters through which jellyfish travel (i.e., the hydrodynamics) as well as the stochastic locomotive behaviour of the jellyfish induced by multiple biophysical factors (Ruiz et al., 1997). Although some of these models can predict jellyfish transportation with different levels of success, the mechanisms of jellyfish transport and in particular their own motility are still uncertain (Carlton, 1996). Spatial tracking of the transport of a jellyfish population is also difficult, which, in turn, complicates coastal ecosystem management efforts (Johnson et al., 2005).

The sudden appearance of many jellyfish inside coastal waters in the vicinity of economic and other human activities has presented an interesting set of problems in the study of jellyfish transportation. Worldwide, many jellyfish distribution studies have been conducted through field-observation research using underwater acoustics, drone monitoring, aerial photography, and underwater video profiling. Numerical modelling of jellyfish movements has the capacity to hindcast, nowcast, and forecast their transportation and distribution, an advantage over field observation, which is limited to supplying their existing status for only the period of the survey. In addition, besides the limitations of these surveys on the spatial and temporal scale, they also cost a lot of time, money, and effort and so may not always be worthwhile or feasible. Numerical modelling has no such spatial limitations and is much cheaper, and it allows investigation of transport hypotheses through scenario modelling to provide better understanding of jellyfish transportation. Such modelling prediction is also important as knowledge of jellyfish transportation dynamics can help ensure that appropriate management measures can be designed and implemented to avoid the potential adverse consequences of jellyfish invasions.

Numerical modelling has been successfully applied to simulate jellyfish transportation in coastal waters (Rahi et al., 2020 and the respective references therein). Although they are known to be motile, jellyfish have primarily been known as ocean drifters. Thus, the modelling of their passive drifting is a fundamental step towards an understanding of their transportation. The EFDC hydrodynamic model's drifter module offers the Lagrangian particle tracking (LPT) scheme by which the passive transportation of jellyfish can be modelled. A jellyfish within this model is simulated as a passive drifter and a Lagrangian particle as a virtual jellyfish. Since the LPT relies on a hydrodynamic model and the simulated current flows supplied by the model, a ready-to-use hydrodynamic model of the study site is necessary to support the LPT module.

LPT has been used in many passive transport investigations of sea-borne masses including the modelling of the tracking of plastics in the Mediterranean (Liubartseva et al., 2018), pollution transport in Tangdao Bay in China (Zhao et al., 2018), grass carp fish egg transport in a river (Heer et al., 2020), flounder fish larvae distribution in the English Channel (Sentchev & Korotenko, 2007), algal bloom (Wu & Xu, 2011). It has also been used for jellyfish studies including, but motility limited to, the distribution and stranding of *Pelagia noctiluca* jellyfish (Rahi et al., 2020), non-indigenous jellyfish transport into the Gulf of Mexico (Johnson et al., 2005), and current-oriented swimming of jellyfish (Fossette et al., 2015). These LPT studies are classified into three groups based on the agent to be modelled - (1) non-living non-motile masses like microplastic, marine debris, litter, pollutant, sediment, material, nutrient, chemical, oil slick, water residence etc., (2) living non-motile masses like fish eggs, algae, water-borne microbes, pathogens etc., and (3) living, motile masses like larvae, planktons, jellyfish, etc..

When modelling motile, living masses, various biophysical factors responsible for their motility (e.g., life cycle, individual variation, behaviour etc.) have sometimes been incorporated within the model in addition to LPT (e.g., Fossette et al., 2015; Rahi et al., 2020). While some of these models were advanced in terms of the fundamental drift investigation, some over-simplified the process by ignoring the effect caused by the lateral or vertical transports or by the diffusive transport. Pure

passive drifting by jellyfish on tidal flows, which substantially contributes to their transport, can be worthy of investigation on its own to provide an understanding of its proportionate contribution to the transport process. However, an exclusive investigation of this basic tidal effect on jellyfish transportation in modelling is ignored to some extent in many of the published studies.

From the above viewpoints, the objective of this study was to explore the extent and nature of the relationship between the tidal movements and the jellyfish movements in Killary by establishing a simple three-dimensional advection-diffusion inclusive passive drift model and comparing the model outputs with the field observations. An investigation of tidally influenced transport could be done by (1) conducting a field observation and subsequently including the observed tidal effect within the model (e.g., Fossette et al., 2015), or (2) conducting transport modelling followed by a post-simulation analysis exploring the associated tidal effect in the transportation by comparing with the field observation. For this research, the investigation was done according to the second strategy. This strategy appears to be a primary one in the development of a faster forewarning system for potential jellyfish swarms/blooms in coastal seas.

This chapter presents the application of the EFDC LPT module for simulation of passive drifting of jellyfish within Killary Harbour. The model was used to simulate releases of particles at the locations where tagged jellyfish were released and the particle transport results were then compared with the observed jellyfish movements. Section 5.3 presents the methodology used for (1) monitoring of jellyfish movements within Killary Harbour and (2) modelling of jellyfish based only on their passive drifting. With regard to the modelling, application of EFDC's LPT module required some modifications to the code and input data files which are described, as are the model settings. Section 5.4 presents the results of the jellyfish monitoring and an analysis of the observed movements with regard to stage of tide. Section 5.5 presents the results of the passive drift modelling simulations of jellyfish in Killary, analysis of the simulation outputs and comparisons of modelled and monitored jellyfish transport. Section 5.6 presents the key conclusions from the passive drift modelling including insights into the mechanisms of jellyfish transport.

based on the comparative analysis. The model does not include any biophysical factors of jellyfish either online or offline since this is exclusively a passive drift model.

5.2. Study Site

Please see Chapter 4, Section 2 for the study site.

5.3. Methodology

5.3.1. Monitoring of Jellyfish Transport in Killary Harbour

Transport of jellyfish within Killary Harbour was recorded in Aug-Sep 2015 by Dr Tom Doyle of University College Cork and his research team. The team caught and electronically tagged 10 jellyfish before releasing them again and tracking their movements with 8 geostationary receivers distributed along the shores of the harbour (Fig 5.1). Each receiver had an approximate detection radius of 500 m and recorded a 'ping' whenever a jellyfish was detected, thereby revealing their movement information. The approximate detection ranges of the receivers are shown in Fig 5.1.

The tagged jellyfish were released on the same date, but at different times and locations and so they were those exposed to different release conditions, and tide and wind events. The release times and locations are presented in Table 5.1 along with other key tracking information including the stage of tide at time of release and the tracking period. The tide and wind conditions for the release events are illustrated in Fig 5.2. The jellyfish were released over a 7-hour period starting on a high tide, and continuing through the following ebb, low and flood tides during which time a southerly wind prevailed with speeds of about 9 m/s. From Table 5.2, it can be seen that not all of the tagged jellyfish were successfully monitored. Some became entangled or sank (e.g. J-18494 and J-18848) and one had to be removed as it was swimming erratically (J-1164). Of the ten jellyfish released, only 10 were

successfully monitored, the monitoring periods varied significantly from 1 day for J-1160 to 6 days for J-18495.

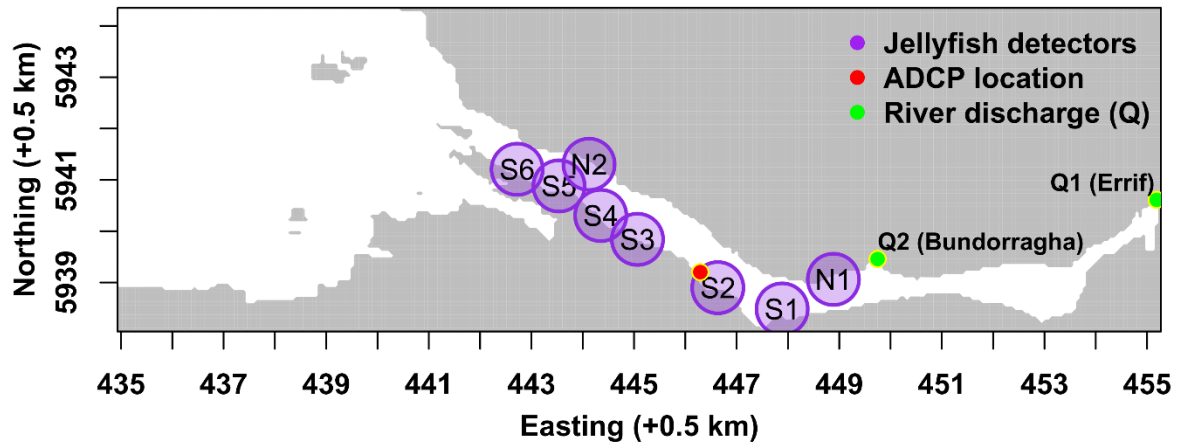


Fig 5.1 Map showing 500 m radius detection zones for 8 geostationary receivers deployed to monitor the jellyfish transportation in Killary.

Table 5.1 Information on jellyfish release for observation in Killary

ID	Release time		Release location			Bell Diameter (cm)	Tracking info.
	Time	Tidal stage	Easting (m)	Northing (m)	Rec.		
J-18500	09:00	High tide	443811.88	5941372.32	S5	-	3 days
J-18494	11:20	Mid-ebb	444161.96	5941260.00	S5	-	Sank
J-18508	11:25	Mid-ebb	444561.23	5941076.04	S4	-	Entangled
J-18499	12:00	Mid-ebb	446076.74	5940193.02	S3	-	4 days
J-1160	13:10	Late ebb	443994.99	5941360.90	S5	30	1 day
J-18501	14:10	Low tide	445070.47	5940606.42	S4	16	Sank
J-18495	14:40	Low tide	444215.55	5941327.35	S5	15	7 days

Chapter 5: Passive-drift Modelling

J-1164	14:40	Low tide	444215.55	5941327.35	S5	18	Removed
J-1162	16:00	Early flood	444270.45	5941326.70	S5	-	2 days
J-1161	16:30	Early flood	444285.04	5941329.64	S5	-	No record

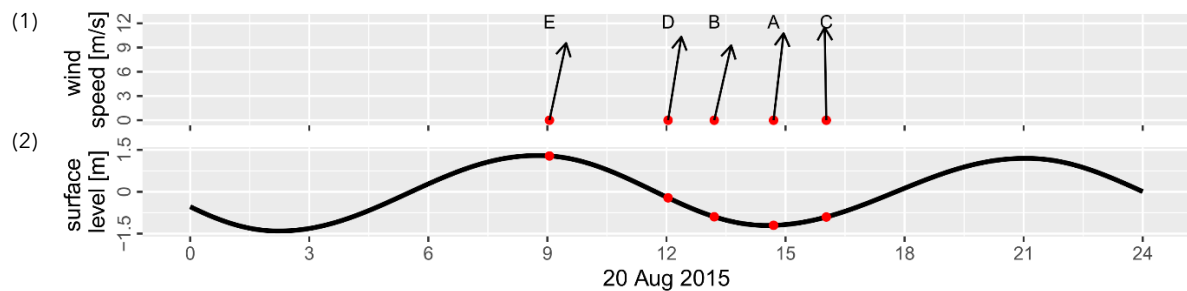


Fig 5.2 Conditions of (1) wind and (2) tide at the release events of the jellyfish (A) J-18495, (B) J-1160, (C) J-1162, (D) J-18499, and (E) J-18500 tracked in the Killary harbour. The top indicates the north as a reference for the wind direction.

It is important to note that the receivers were not capable of obtaining the exact geographical locations of the jellyfish, thus a 'ping' simply indicates that a jellyfish was present somewhere within the detection range of a receiver at a particular instance of time. The pings from all receivers were provided in a single raw data file; a sample of this data file is shown in Table 5.2 showing the type and format of the jellyfish records. These data were processed, analysed, and illustrated for exploring the jellyfish movements. The data were first separated into separate files for each jellyfish which were then processed to determine (1) resident events and (2) transport events. The ping time and receiver for each pair of consecutive detections were analysed. Residence events were identified by comparing pairs of consecutive pings. Where the difference in consecutive ping times was less than 30 minutes, a jellyfish was considered to be resident within a particular receiver's detection zone. The duration of the residence event was calculated as the difference between the times of the first and last of these closely-occurring pings. Transport events were

Chapter 5: Passive-drift Modelling

identified where consecutive pings were recorded by different receivers with the direction of travel indicated by the relative positions of the receivers and the travel time calculated as the time between the detections. The movement within a detection zone could not be investigated from the records available as geographical position was not recorded by the receivers.

Table 5.2 Sample of raw data file which contained sequential records of all pings from all 8 receivers for all jellyfish.

Date	Time	Receiver Serial No.	Transmitter Serial No.	Receiver Name	Receiver Latitude	Receiver Longitude
20/08/2015	13:32	VR2W- 125380	A69-1601- 18499	South 4	53.613157	-9.833623
20/08/2015	13:33	VR2W- 122624	A69-9004- 1160	South 5	53.618249	-9.846029
20/08/2015	13:37	VR2W- 122612	A69-1601- 18500	South 6	53.621075	-9.858418
20/08/2015	13:38	VR2W- 122612	A69-1601- 18508	South 6	53.621075	-9.858418
20/08/2015	13:38	VR2W- 122624	A69-9004- 1160	South 5	53.618249	-9.846029
20/08/2015	13:39	VR2W- 122612	A69-1601- 18508	South 6	53.621075	-9.858418
20/08/2015	13:40	VR2W- 122624	A69-9004- 1160	South 5	53.618249	-9.846029

5.3.2. Setup of the Particle-track Model

A particle-tracking model was developed for Killary harbour using the EFDC hydrodynamic model. The development and validation of the hydrodynamic model was already described in Chapter 4. The version of EFDC's drifter module that was used is that enhanced by Chung & Craig (2009). The computational cost was minimised by implementing parallel execution according to the modifications made by O'Donncha et al. (2014). The control of some model operations was made more convenient by modifying some of the model code. The implementation of the drifter module is described below.

First, the method of approximation for solving the Lagrangian transport equations was specified within EFDC's master control file. There are three numerical schemes available in the code which differ based on the order of approximation to be executed. These are: (1) the Explicit-Euler (first order), (2) the Predictor-Corrector (second order), and (3) the Runge-Kutta (fourth order). In the present passive drift model, the first-order Explicit-Euler method was used due to its relative simplicity and lower computational cost; however, all three schemes were compared to check the model sensitivity to the scheme. The simplest scheme was used so that implementation of new swim code described in later chapters would be a little easier. Next, the drifter control file was configured by specifying the operational or functional option for parameters namely, buoyancy, randomness, vertical reference, time, tracking, and location. The specification befitting the purpose of the tracking (e.g., for jellyfish transport investigation) was chosen from the panel of multiple choices for each parameter. Table 5.3 presents the various options one can choose from for the setup.

Chapter 5: Passive-drift Modelling

Table 5.3 Operational and functional settings for the particle-track sub-model.

Model Setting	Specific articulation	Options for the specification
Buoyancy	Controls particle's ability to rise, float, or sink within the water	0 for setting particles fixed at seeding depth
		1 for setting particles neutrally buoyant
Diffusion	Random walk movement (RWM) of the particles	0 for no RWM
		1 for horizontal only RWM
		2 for vertical only RWM
		3 for full 3D RWM
	Diffusion source	0 for model computed
		1 for user-specified
	Diffusion coefficients (if 1 is selected for diffusion source)	Specify horizontal diffusivity
		Specify vertical diffusivity
Particle depth reference level	Reference level for particle vertical position within the water column	0 for elevation above bed
		1 for depth below water surface
Release Time	Start time of release	Julian date
	End time of tracking	Julian date
	Output interval time	sec
Particle Number	Number of particles to be released	Integer number
Release Location	Longitudinal	Easting (m)
	Transverse	Northing (m)
	Vertical	Depth or elevation (m)

When a Lagrangian particle reaches either an open boundary or the coastline within the hydrodynamic model, its destiny is contingent upon the model's specific configuration and the inherent physical processes being simulated. In the present model, if the net transport of a particle during a particular timestep is such that it is transport across an open sea/river boundary, then the particle is removed from the simulation, symbolizing their departure from the area of primary interest. While in reality jellyfish departing the area of interest may be brought back into the area of interest by ambient currents at a later stage, in the present model, this is not possible; once a particle leaves the domain, it cannot re-enter. Upon reaching the coastline, Lagrangian particles are also removed from the simulation. This step is necessitated by the fact that the coastline serves as a tangible boundary within the model domain, and particles are not anticipated to traverse or exist on terrestrial surfaces. In this context, it is conceptually akin to envisaging that the virtual jellyfish, symbolized by these particles, have become stranded or beached.

The dynamic life cycle of jellyfish was not incorporated into this model. So, the potential impacts of changing shape and size throughout their growth on their movement and transportation cannot be explored instantly using this model. Alternatively, in a subsequent stage of jellyfish transport modelling, Lagrangian particles with variable movement speeds, reflective of the size fluctuations in jellyfish, has been introduced. This methodological strategy enables the model to investigate the effects analogous to those stemming from the jellyfish life cycle on their transportation.

5.3.3. Code Modifications

Some modifications were made to the model code to incorporate additional functionalities and streamline input of the particle release information into the model. The modifications are as follows:

Chapter 5: Passive-drift Modelling

1) An option was created in the drifter control file to allow the release of multiple particles from the same location without having to enter the release location for each particle as was the case with the existing code.

2) The model has to be provided with the depth at which particles are to be released. In the existing model, this required a manual consultation of the bathymetry at the release location, e.g., for a particle to be released at the water surface, the bathymetry file needed to be checked to find the respective water depth. The code was therefore modified so that the release depth would automatically be calculated by the model for the respective release location as per the given specification in the form of normalised elevation (0 = bed, 1 = surface and 0.5 = halfway). The modification has avoided the cumbersome process of manual consultation of the bathymetry file prior to providing the particle-releasing depth information into the model. The code was also modified to allow release of particles at specific coordinates within a grid cell rather than just at the centre of a grid cell as per the original model; code was included to obtain the coordinate-specific depth/elevation via interpolation from surrounding grid cells.

3) In the drifter module, the vertical displacement of a particle due to passive drift at a particular timestep is computed as either a positive or negative value depending on the vertical component of the respective hydrodynamic current. The computed value is then added to the particle's previous vertical position. This addition determines the vertical direction of the particle being downward if positive or upward if negative. For a model setup where particle positions were specified as elevations, this computation is referenced from the seabed and determination of the ultimate vertical position (elevation) of the particle must therefore consider changes in bed elevation due to the horizontal movement of the particle. Such consideration was not included in the existing model and required an adjustment of the vertical displacement equation.

5.3.4. Model Scenarios - Sensitivity of LPT Module

The particle-tracking model was assessed for its suitability for jellyfish transport investigation by carrying out a sensitivity study. The sensitivities of particle transport to variations in (1) particle tracking model set-up, (2) particle release conditions, and (3) hydrodynamic processes were investigated. As shown in Table 5.3, there were various options available regarding the setup of the particle-tracking module such as the choice of numerical solution scheme, specification of diffusive transport and inclusion of vertical diffusion. The sensitivity of model results to all of these was assessed. There were also various options for specification of the release of particles, e.g. the number of particles released, the release depth, the specification of release location via exact geographical coordinates or more simply by grid cell; again the sensitivity of model results to all of these settings was assessed. Finally, scenarios were also run to gain insight into the relative importance of transport processes (e.g. tide, wind, river flow). The full details of the sensitivity studies are presented in Table 5.4 showing the types and bases of the investigations carried out, their qualitative or quantitative specifications, and the approaches used for the assessment of particle modelling output.

For modelling investigations in general, batches of one hundred particles were released at the surface, first-quarter, mid, and third-quarter depths at the same locations and times that the tagged jellyfish were released. The particles were tracked based on their release depth for the duration of the jellyfish monitoring period to help either compare the agreement of particle transportations with observed jellyfish movements or assess the model performance.

Chapter 5: Passive-drift Modelling

Table 5.4 Details of LPT module sensitivity study.

Sensitivity Studied	Specification	Method of assessment of output
LPT Model Setup		
LPT numerical solution scheme	Explicit-Euler	RMSE of the centroids of particle transports
	Predictor-corrector	
	Runge-Kutta	
Transport process (horizontal diffusion)	Model-computed dynamic diffusivity	Particle density or dispersion
	User-defined diffusivity of $7\text{E-}3 \text{ m}^2/\text{s}$	
	User-defined diffusivity of $7\text{E-}5 \text{ m}^2/\text{s}$	
Vertical movement (VM) of the particles	With VM	Particle trajectory and net transport
	Without VM	
Particle Release Conditions		
Particle release depth	Surface	RMSE of the centroids of particle transports
	First-quarter	
	Mid	
	Third-quarter	

Chapter 5: Passive-drift Modelling

Spatial sourcing of particle releasing depth data	Manually consulted grid-cell general location	Particle trajectory
	Model-interpolated coordinate specific location	
Particle release number	10	RMSE of the centroids of particle transports
	100	
	1000	
Particle releasing location across the water/channel (longitudinally same as the jellyfish released)	Jellyfish release location	Particle transport distribution at the end of the simulation
	South inshore	
	At the one-third distance	
	At the two-thirds distance	
Hydrodynamic Processes		
Wind	With wind	Particle density or dispersion
	Without wind	
River discharge (Q)	With Q	Particle density and net transport
	Without Q	
Individual-based Modelling		
Particle release according to the observed jellyfish in Killary fjord	Individual time and location of releasing five agent jellyfish	Transport agreement

5.3.5. Analysis of Model Results

The primary output from the particle tracking model was particle positions (in the x-, y- and z-directions) at set intervals during the course of model simulations. These were used to produce snapshots of particles positions. The following analyses were also conducted using the particles position outputs.

5.3.5.1. Particle Centroid and RMSE

At a given time, the centroid of a particle distribution was determined in terms of their geometric median. The centroid was determined for the distributions in the east-west (zonal), north-south (meridional), and water column (vertical) dimension, yielding x, y and z coordinates for the centroid of the particle cloud. Following tests, geometric median was preferred here over arithmetic mean since median effectively finds the central location of a distribution while mean may be skewed depending on clustering of the particles. The longitudinal and vertical centroids were measured directly from the spatial values of the distribution, but due to the meandering nature of the harbour, the transverse centroid was measured by first normalizing the northing values within the banks of the channel with respect to a straight rectangular channel. The centroids were determined every half-hour across the particle tracking period, so that the centroid trajectory in each dimension could be plotted over the period of the simulation. The Root Mean Square Error (RMSE), which is an excellent general purpose error metric for numerical predictions (Christie & Neill, 2022), was calculated between the centroid trajectories of different scenarios to determine relative sensitivities or difference between them. RMSE was calculated after Hodson (2022). For a sample of particles having n observations O_i ($i = 1, 2, 3, \dots, n$) and n corresponding model predictions P_i , the RMSE is

$$RMSE = \sqrt{\frac{1}{n} \sum_{i=1}^n (O_i - P_i)^2} \quad (5.1)$$

5.3.5.2. Transport Diffusivity

Diffusivity, which is the coefficient or measure of the diffusion of particle transport, is usually computed within the model from the simulated flows by EFDC's built-in function. However, the drifter module additionally facilitates an external specification of the diffusivity, which overrides the model-sourced diffusivity if applied. The module supports specification of both horizontal and vertical diffusivity constants (denoted by D_H and D_V , respectively). Prior to modifying the model-sourced diffusivity by user-specification, an idea of its level was necessary, which was determined from the mean square displacements of the modelled particles using Fick's second law of diffusion (described in Park et al., 2017; Tyrrell, 1964). The sensitivity of the horizontal transport distribution to the respective diffusion coefficient was investigated by simulating the particle transport at constant D_H values of 0.007 and 0.00007 m²/s without any D_V . The results were compared with each other and with those from the model-calculated diffusive transport scenario. The comparisons were made by analysing the density of the particle distribution for the different diffusion scenarios. The particle density was illustrated upon Kernel density estimation (KDE) (Parzen, 1962; Rosenblatt, 1956), which is a spatial technique for estimating probability distribution or density function (Węglarczyk, 2018) by analysing the relative locations of features (here, particles) (King et al., 2016). The tool has been used widely in research (King et al., 2015, 2016; Kloog et al., 2009). A built-in function 'kde2d' (developed after Venables & Ripley, 2002) in R 'MASS' package (Brian et al., 2022) was used here for illustrating the density of the Lagrangian particles.

5.3.5.3. Transport Agreement and Ranking

Transport agreement of the modelled particles with the observed jellyfish was investigated by using both single-criterion analysis (SCA) and multi-criteria analysis (MCA). As per SCA, a particle detected at a time and location which matched an observed detection was considered as an agreement event and the number of particles detected among the total available determined the percentage of the

agreement. For the MCA), a total of seven criteria indicative of particle transport agreement were devised. The criteria and the steps used to develop and implement the analysis are presented in Table 5.5. According to the table, the steps were as follows:

- 1) Agreement criteria were devised based on the percentage of particles within the correct detection zone at the correct time and the proximity of the centroid of the particle cloud to the correct detection zone.
- 2) The devised criteria were classified as beneficial and non-beneficial groups; percentage detection being considered beneficial and centroid detection distance being considered non-beneficial.
- 3) The SCA of each criterion is determined in terms of true detection by percentage of particles agreed and centroid detection by distance of geometric median from the respective detector.
- 4) Each SCA score is normalised (using the formulae presented in Table 351).
- 5) Weightings were devised and attributed to each criterion based on their significance with regard to agreement (subjectively) with the weightings totalling to 1.
- 6) Weighted, normalized SCA scores were determined for each criterion by multiplying (4) and (5).
- 7) Finally, the weighted normalized values were summed to obtain the final MCA score.

Performance ranking of the passive drift modelling across the jellyfish models was evaluated based on the SCA and MCA assessments.

Table 5.5 Multicriteria analysis (MCA) for quantifying transport agreements.

			Steps					
1			2	3	4	5	6	7
Criteria for agreement			Classification of criteria	Estimation of criterion values (Cr_i)	Normalisation	Weight assignment	Multiplication	Summation
1)	Presence of the particles (%) at a detection time	within the detector's range (500 m)	Beneficial	Calculated from half-hourly-tracked particle positions	$NCr_i = \frac{Cr_i}{\max(Cr_i)}$	0.45	Weighted normalised agreement per criteria, $WNCr_i = NCr_i \times weight_i$	Final MCA Score = $\sum_{i=1}^n WNCr_i$
2)		within an extended range (750 m)				0.20		
3)		within the adjacent detectors' range (500 m)				0.05		
4)		within the domain				0.05		
5)	Centroid-detector distance (m)	at the time of detection	Non-beneficial	Calculated from half-hourly centroid of the particle distribution	$NCr_i = \frac{\min(Cr_i)}{Cr_i}$	0.15		
6)		at the previous time of detection				0.05		
7)		at the next time of detection				0.05		
TOTAL						1.00		

5.4. Results and Discussion

5.4.1. Results - Jellyfish Monitoring

Jellyfish transportation in Killary was observed by monitoring the movements of tagged and released jellyfish. Out of the ten tagged jellyfish released, five resulted in transport information of reasonable data quality; the rest were either lost from the receivers' signal, removed due to erratic swimming behaviour, entangled with mussel ropes, sank to the bottom or stranded on the shore.

The raw monitoring data were analysed to determine times when jellyfish were resident within a particular detector zone and times when they moved between zones. This resulted in a table of residency events and a table of movement events for each jellyfish. By way of example, Table 5.6a shows the residence events determined for J-18495. This jellyfish was detected a total of 51 times over a six-day period before the signal was lost. During this time, ten residence events were determined. The processed jellyfish tracking records were used to investigate the observed transport of the jellyfish and to compare with the modelled transportations of jellyfish in Killary, thereby allowing evaluation of the performance of the particle-tracking model. Table 5.6b shows the table of movement events determined for J-18495. The direction of the movement was determined from the relative positions of the respective detectors and is presented in the form of either westerly towards the sea (and thus with the ebb tide) or easterly towards the harbour (and thus with the flood tide). The extent of movement is either within or between detectors; only the latter can be used to discover the direction. The time of each movement event was tracked on the tide level graph to reveal the prevailing tidal state at the time of the movement so that the movement could be classified as either tidal (with the tide) or non-tidal (against the tide). It can be seen that for this jellyfish, there were a number of non-tidal movements suggesting some motility on behalf of the jellyfish.

Chapter 5: Passive-drift Modelling

Table 5.6 Transport events determined for J-18495 - (a) residence and (b) movement.

(a) Residence events for J-18495 ('End reason' describes the reason for the ending of a particular residence events and is classified as: (1) 'receiver' meaning the jellyfish was next detected by a different receiver, (2) 'timeout' meaning the maximum time between pings was exceeded and (3) 'signal lost' meaning there were no more pings recorded.)

Start	End	Duration (sec)	Detector	Residence event	End reason	Ping (num)
20/08/2015 17:47	20/08/2015 20:46	10740	S4	1	receiver	22
20/08/2015 23:09	Unknown	-	S5	2	timeout	1
21/08/2015 00:02	21/08/2015 00:05	180	S5	3	timeout	2
21/08/2015 01:17	21/08/2015 01:21	240	S5	4	receiver	2
25/08/2015 14:25	25/08/2015 14:25	0	S1	5	receiver	1
25/08/2015 20:00	25/08/2015 20:03	180	N1	6	timeout	4
25/08/2015 23:35	Unknown	2940	N1	7	timeout	1
26/08/2015 00:24	26/08/2015 00:29	300	N1	8	timeout	3
26/08/2015 01:21	26/08/2015 01:43	1320	N1	9	receiver	9
26/08/2015 03:30	26/08/2015 03:40	600	S1	10	signal lost	6

(b) Movement events for J-18495.

Start	End	Duration (sec)	Detectors (from-to)	Direction	Tide ¹	Movement		
						event	type ²	behaviour
20/08/2015 20:46	20/08/2015 23:09	8580	S4-S5	Westerly	ET	1	BD	Tidal

Chapter 5: Passive-drift Modelling

21/08/2015 00:05	21/08/2015 01:17	4320	S5-S5	Unknown	ET	2	WD	Non-tidal
21/08/2015 01:21	25/08/2015 14:25	392640	S5-S1	Easterly	MT	3	BD	Non-tidal
25/08/2015 14:25	25/08/2015 20:00	20100	S1-N1	Easterly	ET	4	BD	Non-tidal
25/08/2015 20:03	25/08/2015 23:35	12720	N1-N1	Unknown	FT	5	WD	Non-tidal
26/08/2015 00:29	26/08/2015 01:21	3120	N1-N1	Unknown	FT	6	WD	Non-tidal
26/08/2015 01:43	26/08/2015 03:30	6420	N1-S1	Westerly	ET	7	BD	Tidal
¹ ET represents ebbtide, FT represents floodtide, and MT represents multi-tides. ² BD represents 'between-detectors', and WD represents 'within-detectors'.								

An attempt was made to visualise the residency and movement events of Tables 5.6a and 5.6b. This is presented in Fig 5.3. The figure shows the measured movements of the jellyfish by the multi-coloured rings. The numbers represent sequential detections by detectors and the thickness of the rings is representative of the time spent within a detector's range. The white void area adjacent to the rings is representative of the non-detection or movement period.

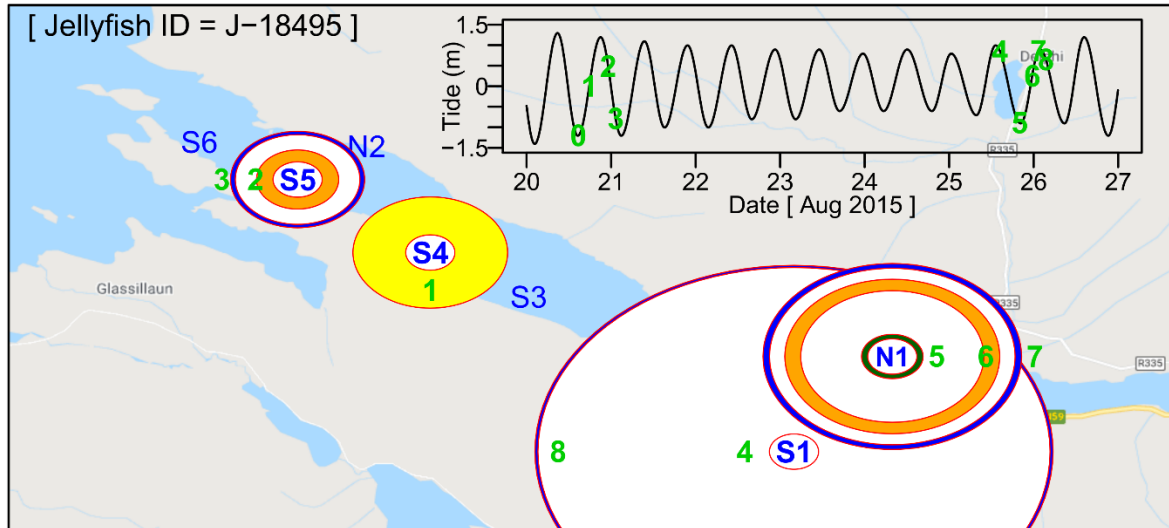


Fig 5.3 Sequential detections of J-18495 according to tide (inset) across 8 detectors along Killary harbour.

Fig 5.4 presents an overview of the movements of the 5 valid jellyfish showing the times at which jellyfish were detected by particular detectors. The tide levels during the monitoring period are also shown for reference. In the figure, the detectors are ordered based on their locations in the harbour moving from west to east from the mouth of the harbour towards the inner harbour. Since the literature suggested that one of the primary mechanisms of transport of jellyfish was by advection on tidal currents, Fig 5.4 was analysed to determine any correlation between the jellyfish movements and the stage of the tide. This is now described.

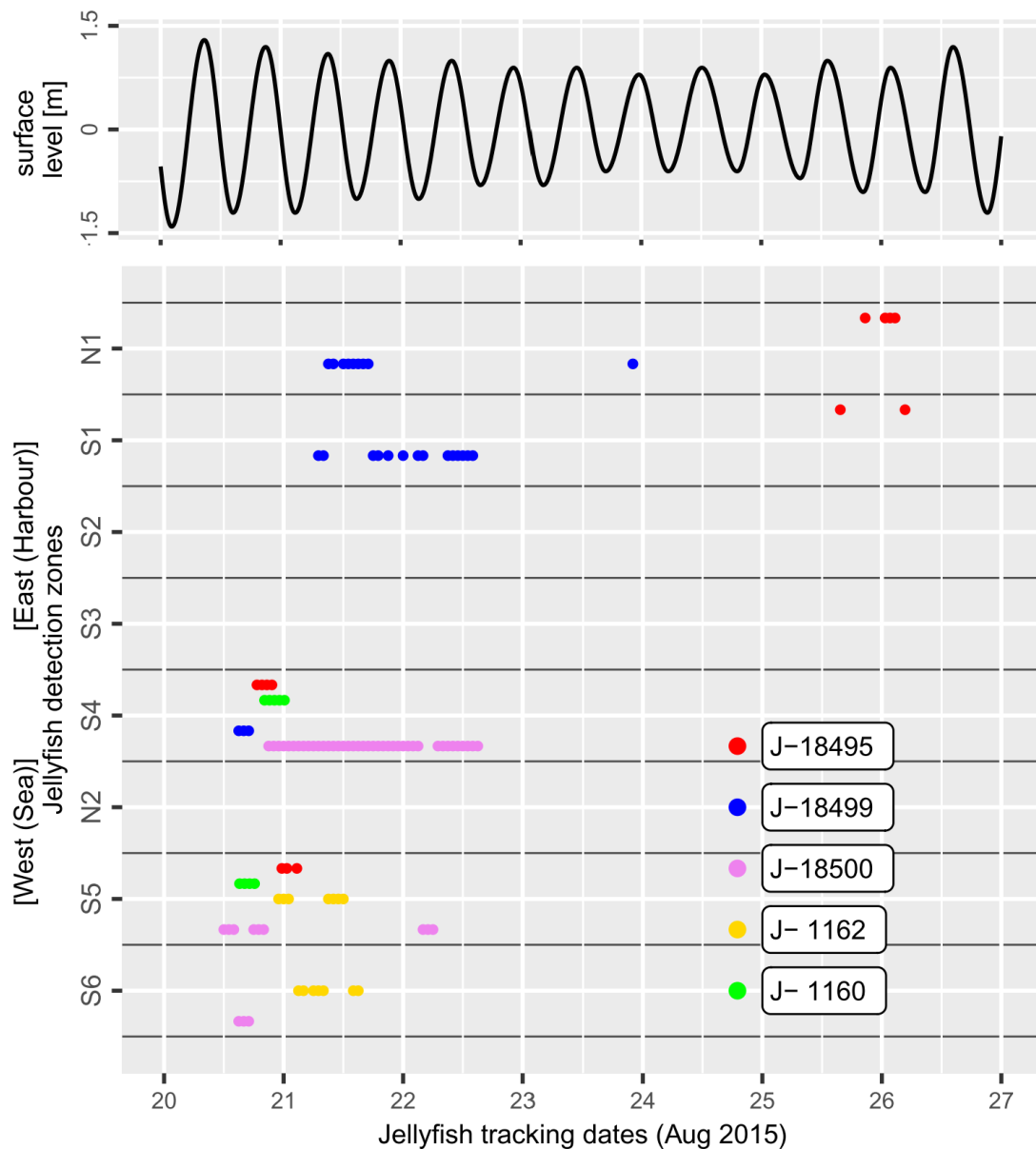


Fig 5.4 Times and locations of jellyfish detections in Killary Harbour for 5 jellyfish and the corresponding tide levels. [Legends are in order of simulation period of the respective jellyfish.]

The jellyfish J-18495 was released at 14:40 hr on 20 Aug 2015 within the detection zone of receiver S5. After 3 hrs, the jellyfish was detected by receiver S4 further to the east. Looking at the tide level graph, it can be seen that the jellyfish was released at low tide, after which the water would be flooding from west to east; thus, this transport appears to be correlated with the tidal currents and can therefore be considered a passive drifting movement. The jellyfish stays in range of S4 for the next 3 hrs and after which the detection terminates. The tide subsequently turns so

that water flows back into the sea in a westerly direction on the ebb tide. After 2 hrs of the termination of detection in S4, the jellyfish is detected by S5 to the west where there are multiple detections for another 2.5 hrs. This westerly movement of the jellyfish while on the westerly ebb tide also corresponds to the tidal influence of the jellyfish movement. There is a subsequent long period (approximately 109 hrs) before the next detection when the jellyfish must have been travelling outside any of the detectors' ranges. Tidal influence cannot be investigated for this period of non-detection. The record shows the resumption of the jellyfish detections at 14:25 on 25 Aug, with the jellyfish detected by S1 which is at least 4-6 km east of the previous detection in S5. There are multiple detections for the next 25 hrs in the easternmost detectors of S1 and N1 inside the harbour. At the beginning of the detection period on 25 Aug, the jellyfish is first detected within S1 at high tide, i.e. at the beginning of an ebb tide when currents would be flowing west towards to the sea. However, 5.5 hrs later, it appears next within N1 further northeast of S5, meaning it has travelled east against the westerly ebb tide; this indicates another non-tidal transport of the jellyfish. It is assumed that the jellyfish is using its own motility in this period, which contributed to its transport against the tide. The tide subsequently turns so that water flows back into the harbour in an easterly direction on the next flood tide. However, the jellyfish stays within N1 even though the water is flooding. There may also be motility involved here, which might restrict the tidal movement of the jellyfish and might cause the jellyfish to stay within the same detector's zone. As the flood tide ends and the tide turns for ebbing, the jellyfish returns to S1 southwest of N1 on the westerly ebb, which again correlates with the direction of the tidal currents.

Jellyfish J-18499 was released within the detection zone of receiver S3 at 12:00 hr on 20 Aug 2015, the same day that all of the jellyfish were released. It was tracked for 4 days before the signal was lost. After 2 hrs of release, it was first detected by S4 which is west of S3. Looking at the tide level graph, it can be seen that the jellyfish was released on an ebbing tide when water would be flowing from east to west; thus, this transport appears to be correlated with the tidal currents. The ebb tide subsequently ends, and the tide turns so that water flows again into the harbour in

an easterly direction on the floodtide. However, the jellyfish still stays within range of S4 through the early flood tide, possibly indicating some non-tidal activity of the jellyfish. By halfway through the flood tide, as the tidal current speed approaches its peak, the detection terminates for approximately the next 13.5 hrs while the jellyfish is travelling outside the detector's area. When next detected, it has moved to S1 some 3-5 km to the east. As this distance is covered in the space of one tidal cycle, it appears that there is some self-motility involved. There are multiple detections within S1 in the next 2 hrs while on the flood tide. The next hour until the easterly flood tide ends, the jellyfish moves further east to N1 indicating a tidal movement. The tide subsequently turns through the slack water so that water flows back in a westerly direction on the ebb tide. During the whole ebb tide period, through slack water, until the subsequent floodtide (approximately 8 hrs), there are multiple detections of the jellyfish within N1. The jellyfish next moves back to S1 against the floodtide and stays there for almost 2 tidal cycles. There are multiple detections in S1 until mid-ebb of the next tidal cycle. This residence through multiple tides would also seem to indicate some jellyfish motility. For the next 31 hrs, or approximately 2.5 tidal cycles, there are no detection until the jellyfish is detected again within N1 to the east halfway through the easterly floodtide. This eastward movement detection confirms another tidal movement of the jellyfish.

Jellyfish J-18500 was released within the detection zone of receiver S5 at 9:00 hr on 20 Aug 2015 and was tracked for 3 days before the signal was lost. It was released shortly after high tide at the start of an ebbing tide and approximately 1.5 hrs after its release, it was first detected within its release zone of S5 where it continued to stay for another 2 hrs and at the end of the ebbing tide near low tide it moved west to S6. This transport appears to be correlated with the tidal currents. Looking at the tidal graph, the tide subsequently turns so that water flows again into the harbour in an easterly direction on the flood tide. At the start of the flood tide, the jellyfish shows an easterly movement moving back to S5, thus indicating passive tidal drifting. However, its pings are alternately detected by S5 and S6 through the floodtide until the time before the tide level approaches high water. As the detection zones of S5 and S6 slightly overlap, this suggests that the jellyfish was active in the

Chapter 5: Passive-drift Modelling

overlap zone between these two detection areas before it subsequently moved to the east to S4 just prior to the next subsequent high tide. Although the alternating movements between S5 and S6 appear to be non-tidal, the last connected movement to S4 correlates with the direction of the tidal currents indicating passive drifting. Subsequently, there are multiple detections in S4 for approximately 31 hrs through almost 2.5 tidal cycles; during this time its tidal correlation cannot be investigated but the fact that it remains within S4 for multiple tides may suggest some motility against the tides. This event terminates near the end of a westerly ebbside when the jellyfish was detected to the west at S5 indicating another tidally influenced movement. The tide subsequently turns for easterly flooding and on the floodside the jellyfish moves back east again to S5; this also correlates with tidal drift. The jellyfish detection then remains within S4 for approximately 8.25 hrs, which appears to be non-tidally influenced again. The signal was then permanently lost.

Jellyfish 1162 was released at 16:00 hr on 20 Aug 2015 in the detection zone of receiver S5. Immediately after its release, there are multiple detections by receiver S5, as would be expected. After 3.5 hours, detections by S5 terminate and the jellyfish is instead detected by receiver S6 further to the west. Looking at the tide level graph, it can be seen that the jellyfish was first detected on a slack water during high tide when water would be ebbing from east to west; thus, this transport appears to be correlated with the tidal currents. The jellyfish next stays with the range of receiver S6 for 5 hours through slack water. The tide subsequently turns so that water flows back into the bay in an easterly direction on the flooding tide. By the later of the flood tide, as the tidal currents approach high speed, the jellyfish moves to the east from the zone of S6 back to the zone of S5; again, this movement correlates with the direction of the tidal currents. The jellyfish stays there for 3.5 hours. Another 2.5 hours later, approximately next to halfway through the ebbing tide, the jellyfish detections again move from S5 to S6, indicating westerly transport which also correlates with the ebbing tide.

Jellyfish J-1160 was released at 13:10 hr on 20 Aug 2015 in the detection zone of receiver S5 and was tracked for just 1 day before its signal was lost. Initially, for

almost 3 hrs, there are multiple detections by S5, as might be expected. Looking at the tide level graph, it can be seen that the jellyfish was released on a late ebb tide when water level would be approaching low water. The jellyfish remains within S5 through slack water; thus, this residence appears to be correlated with the tide. Meanwhile, the tide subsequently turns so that water flows into the harbour in an easterly direction on the flood tide. After 2 hrs, detections by S5 terminate and the jellyfish is instead detected by S4 further to the east on the mid-flood indicating tidally influenced transport. The jellyfish then remained in S4 for a couple of hours until its signal was permanently lost.

The jellyfish movements demonstrated tidal influences in general, which further corroborates the literature. However, the counter-tide (non-tidal) movements were also evidenced. For example, around day 6 of the tracking between N1 and S1, J18495 exhibited a with-tide movement at an instance and an against-tide movement at a previous instance, although both instances occurred during ebb events (Fig 5.3). The current flow patterns during both ebb instances are depicted in Fig 5.5. The illustration reveals consistent current directions throughout the channel during two consecutive ebb tides, both directed seawards. However, despite this uniformity in current direction, variations in jellyfish movements were observed. The time interval between these two events was reasonably sufficient (1.0-1.5 tidal cycles) to rule out the chance that the outcome was based on a quick atypical movement or local flows. Similar analyses for all the jellyfish across the tracking period reveal that the jellyfish transportation was partly tidally influenced, and a part of the movements was not tidal (Fig 5.3). So, the results are mixed. This helped surmise that the jellyfish are not completely passive drifters that merely move on the tide. This indicates the involvement of active swimming or motility of jellyfish in their transportation. This investigation further helped in the research in planning scenarios and assessing and evaluating the particle-track model performance.

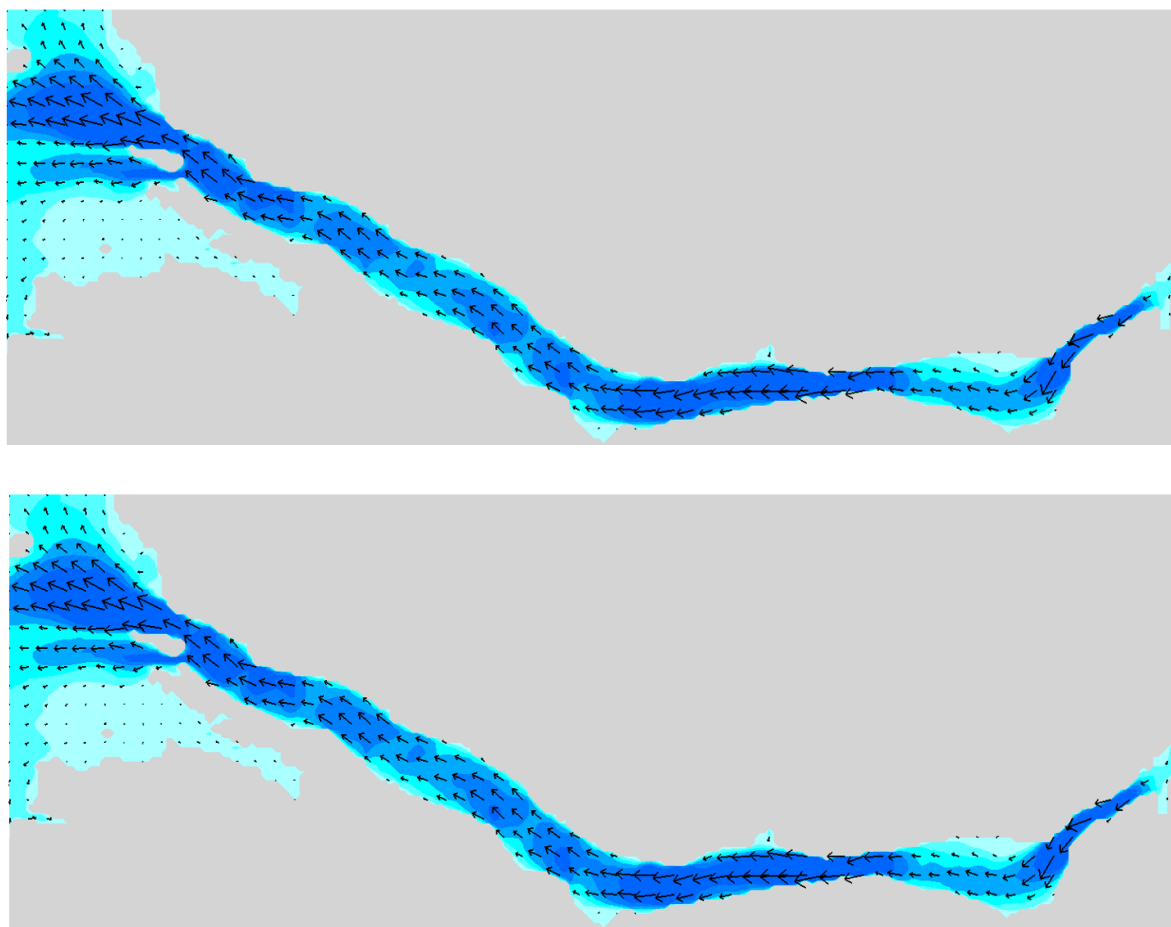


Fig 5.5 Illustration of current vector plots for two consecutive ebb tide events, depicting current directions at 17:00 hr on August 25, 2015 (top) and 05:00 hr on August 26, 2015 (bottom).

5.4.2. Results - LPT Model Sensitivity

Since the observed jellyfish movements appeared to be at least partly influenced by tidal currents and the modelled hydrodynamics in Killary agreed reasonably well with the measured data (Chapter 1), the Lagrangian particle track (LPT) model within EFDC could be used in conjunction with the hydrodynamic model to try and reproduce the jellyfish movements.

Particle transport within the model is realized through a combination of advection and diffusion processes. Advection propels the particles, driving their displacements. Meanwhile, the incorporation of particle diffusion, through the random walk process, enriches the model's ability to emulate realistic transport

behaviours and enhance prediction accuracy. In numerous real-world scenarios, particle movement is influenced by stochastic fluctuations stemming from factors such as turbulence, molecular interactions, and environmental variabilities. Numerical simulations often struggle to faithfully replicate small-scale turbulence and intricate physical phenomena. Deterministic approaches may inadequately forecast these processes or exhibit limitations. The introduction of random walk diffusion, however, addresses these issues by capturing the inherent stochastic nature of particle motion, thereby yielding more precise outcomes. Moreover, diffusion, a foundational and ubiquitous process within hydro-environmental systems, facilitates the simulation of critical phenomena like particle dispersion and mixing—effects stemming from random motion. This accounts for the inherent variability, subgrid-scale impacts, and uncertainty intrinsic to particle trajectories. Additionally, diffusion stands as a pivotal parameter for model calibration. The manipulation of diffusion coefficients enables the alignment of model predictions with real-world observations, thereby refining overall accuracy (further details in Section 5.4.2.1.2).

To investigate the implications of incorporating or omitting diffusion in particle transport modelling, we explored multiple model scenarios. These scenarios encompassed both the inclusion and exclusion of diffusion. In Figure 5.6, a vertical profile of particle transport is depicted, showcasing various diffusion conditions. This visualization highlights both instances where diffusion was included and where it was omitted. As depicted in the figure, a batch of one hundred particles was released from a depth close to the surface. These particles were allowed to move under conditions of full or partial random walk motion (RWM), or without any RWM influence. The figure reveals that in the absence of RWM, all particles follow identical trajectories. Realistic and dispersive behaviour is only achieved when the model incorporates full RWM. This observation validates the significance of including particle diffusion or RWM within our jellyfish transport model.

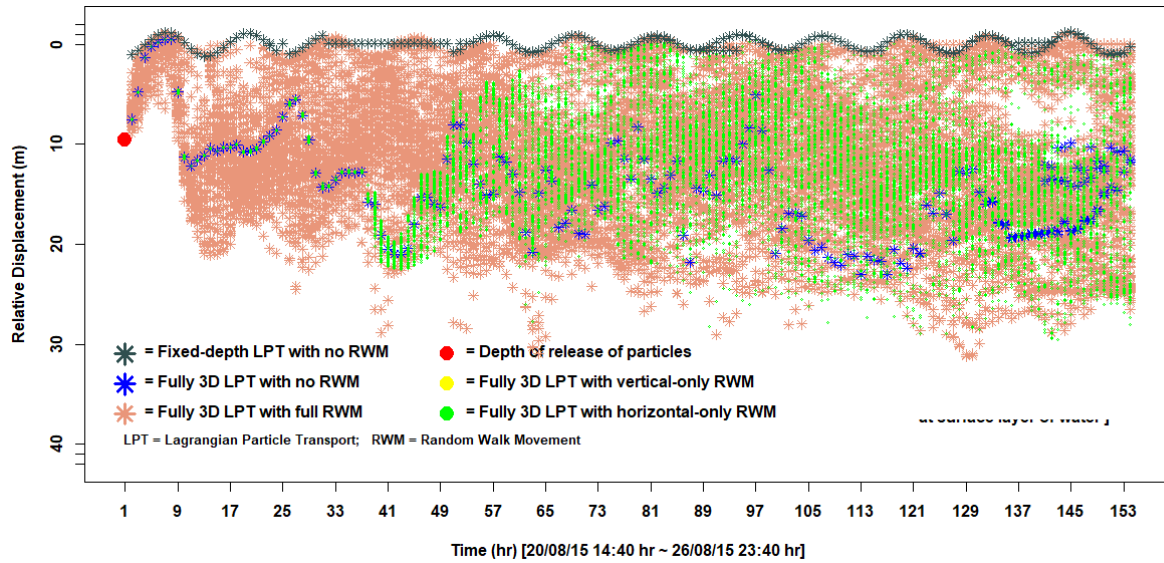


Fig 5.6 Particle transport at various RWM conditions.

The LPT model performance was initially investigated through the analyses of various sensitivity and scenario modelling simulations and carried out on the following factors.

The following sections present results which demonstrate the sensitivity of the particle tracking results to (1) various aspects of the model setup such as the numerical solution scheme and the diffusion coefficients, (2) particles release variables such as number of particles and depth of release, and (3) hydrodynamic forcings such as wind and river flow.

5.4.2.1. LPT Model Setup

5.4.2.1.1. Numerical Scheme

In the LPT sub-model, particle movements are computed based on the selection of one of three numerical schemes available. Fig 5.7 shows the centroid trajectories of the particle transports simulated using the three numerical schemes. RMSE between the centroid trajectories in the short-term (≤ 75 hrs) and long-term (> 75 hrs) of the simulations were calculated and are presented in the figure to help measure their

relative sensitivity. The trajectory lines and the RMSE between them show transport variations (i.e. differences in article positions) among the schemes being smaller in the short term and higher in the long term, as might be expected.

While the Predictor-corrector and Runge-Kutta schemes produced similar centroid trajectories and by extension particle transport distributions, the Explicit-Euler scheme differed somewhat from approximately 75 hours onwards when it had a more westward transport tendency than the other schemes and later from 125 hours when it had a more eastward transport tendency.

For LPT, schemes having a higher order of approximation may be preferred (Chung & Craig, 2009). However, in this research, simplicity of the model code (to facilitate later modification) and computational cost were considered most important, so despite the slightly different particle trajectory of the Explicit-Euler scheme, it was preferred over the other two schemes for all future modelling.

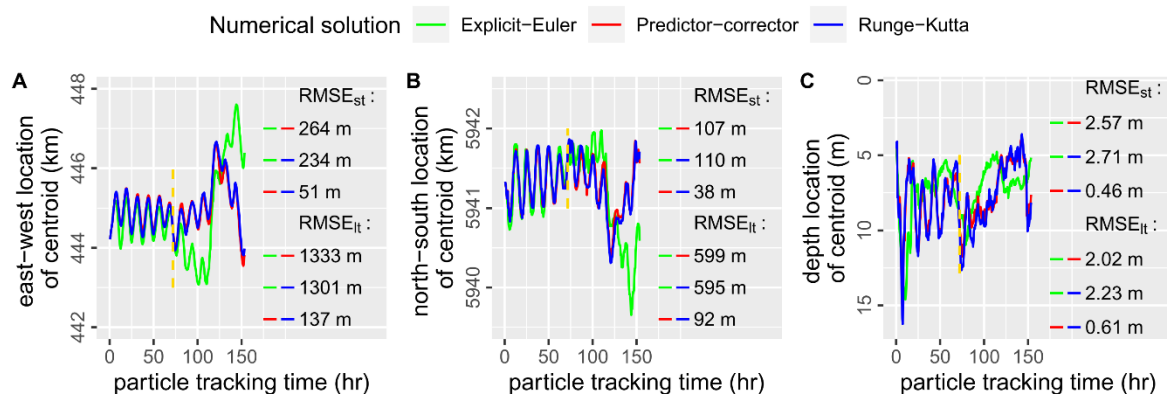


Fig 5.7 Spatiotemporal trajectories of particle centroid and RMSE of trajectory-pairs along the (A) east-west, (B) north-south, and (C) vertical directions illustrated upon three LPT numerical scheme scenarios as per J-18495 model. The RMSE is calculated for the short-term (st) and long-term (lt) periods of the simulation, which are separated by the golden vertical dash being st on its left and lt on its right side.

5.4.2.1.2. Transport Processes: Horizontal Diffusion

The results from the scenarios which used different horizontal diffusion coefficients are presented in Fig 5.8. The figure shows snapshots of Kernel density plots of the particle distributions produced by the models at a sample output time of 91.5 hrs after their release for model-sourced diffusivity (A) and user-defined diffusivities of

0.007 m^2/s and 0.00007 m^2/s (B & C, respectively). The figure also shows a comparison of kernel density estimate timeseries over the whole simulations. According to the figure, the diffusion scenarios differed between the time-specific (91.5 hr after releasing the particles) and time-varying densities (A~C and D, respectively). The comparison of the density shown in the figure reflects that the model-sourced D_H contributed to a higher dispersion of the particles, and the user-defined D_H facilitated the congregation of the particles. The density difference between D_H 0.007 and 0.00007 m^2/s was not noticeable in the time-specific plots; however, it was clear in the time-varying plot D, which demonstrates a bit higher congregation in the previous than the latter. This indicates that the diffusion, along with the advection, determines the distribution of the particles. Since the functional property of a diffusive transport is particle dispersion, the dispersion behaviour of a Lagrangian transport in modelling can be controlled by diffusivity. Thus, the diffusivity to be used in the LPT model would also be an important calibration parameter. The model was found to be sensitive to diffusivity. The diffusion coefficient can be tuned within a particle-track model for a functional purpose, for example, simulating jellyfish swarm formation, or for an operational purpose, for example, model calibration.

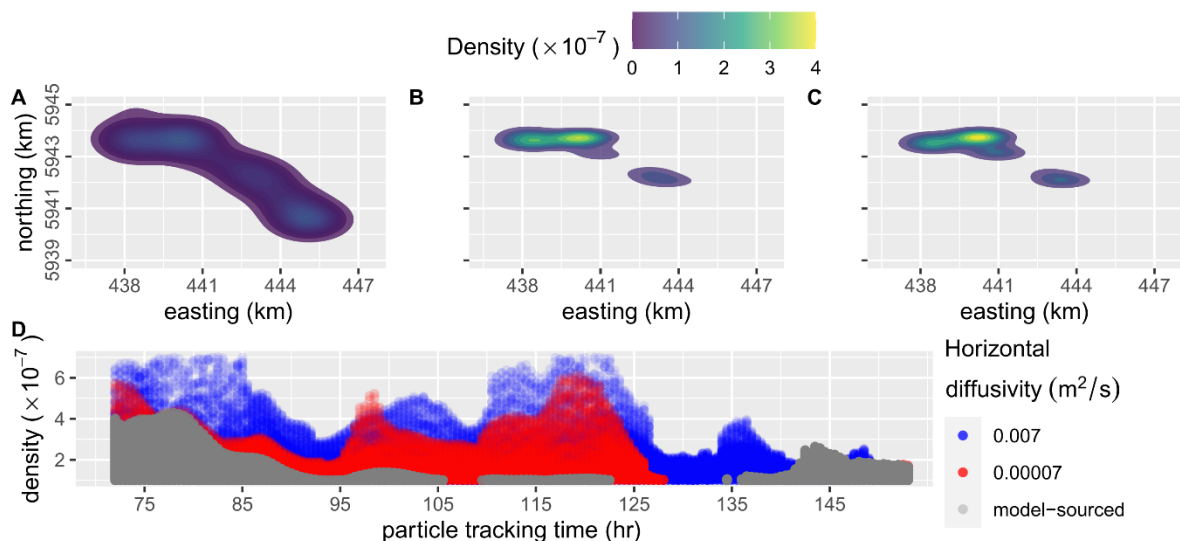


Fig 5.8 Particle density plots upon simulations at D_H (A) sourced within the model, (B) 0.007 m^2/s , (C) 0.00007 m^2/s , and (D) combined. A~C indicate the time-specific KDE at 91.5 hr after releasing the particles, and D indicates the time-varying KDE over the model domain.

5.4.2.1.3. Transport Processes: Vertical Transport

To investigate the influence of vertical transport processes (advection and diffusion) on the particles' net transport, two surface-release scenarios were run, one with vertical movements allowed and the other without vertical movements allowed. Fig 5.9 shows a graph of the east-west locations of all of the particles in the scenarios over the simulation period. According to the figure, in the early stages of both scenarios, particles travel east and west on the directions of the prevailing tides but in the scenario without vertical motion, the particles are gradually transport westward towards the sea from about 70 hrs onwards, whereas in the scenario with the vertical movement particles are distributed fairly evenly to the east and west. The particles are also travel more closely together in the absence of vertical movement - their exposure to different horizontal flow fields at different depths when vertical transport is allowed results in more spreading of the particles. The results demonstrate the influence of vertical movements on the horizontal transport of a passive drifting agent like a jellyfish and that it is therefore important to include vertical transport mechanisms. Furthermore, it implies that customization of the vertical movement (e.g. by including vertical swim behaviours) can be used to potentially improve horizontal transport calibration within the jellyfish transport model.

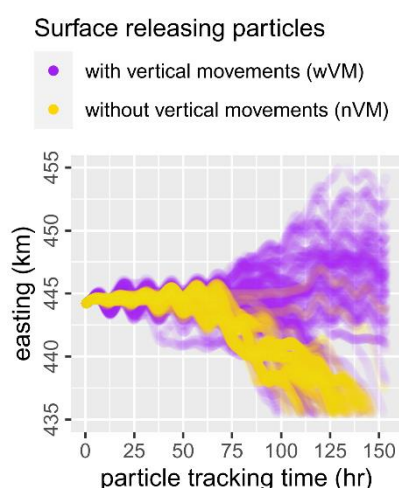


Fig 5.9 Map of distribution of the particles released at the surface with and without vertical movements.

5.4.2.2. Specification of Particle Releases

5.4.2.2.1. Depth of Release

Four simulations were conducted to investigate the effect of release depth on particle transport. Particles were released at the surface, at the bottom of the first quarter of the water column, at mid-depth and at the bottom of the third-quarter depth. Particle positions were tracked at every half-an-hour time instance. Pair-wise comparisons of the particle transports and their distributions were made among the depth scenarios. Fig 5.10 shows the particle cloud centroid trajectories for the different release depth scenarios. RMSE between the transport trajectories of different scenario pairs were calculated and are presented in the figure to help assess differences in particle movements and distributions. The trajectory lines (qualitatively) and the RMSE between the depth pairs (quantitatively) show relative transport differences between the different release depth scenarios. In all four scenarios, the particle centroids follow similar trajectories, however, the levels of RMSE in the figures ranging from 284-520 m for east-west transport (A) and 187-260 m for north-south (B) shows there is spatial variation in particle locations between the scenarios. As might be expected, the scenarios where particles were released at adjacent depth layers show the smallest transport variations (e.g., 284 m east-west between the surface and the first-quarter release scenarios). Conversely, the largest differences were observed for the scenarios where the release depths were furthest separated, i.e. surface and third-quarter with 520 m RMSE in east-west centroid trajectory. Since the particles released at any particular depth diffused and distributed gradually in the water column, their vertical centroids appear to be almost the same and the initial depth variations converge over time in the long run (Fig C). The results show that the model is sensitive to the release depth and this should be considered in future scenarios.

In all four scenarios, the particle centroid undergoes a significant shift in east-west and north-south location at approximately 120 hours. This shift is not due to the particle cloud suddenly moving across a very large distance, rather, it is due to the particle cloud having split in two earlier in the simulation with a large number of

particles moving westward to the sea and the rest travel east inside the harbour. At approximately 120 hours, the particles that travelled towards the sea leave the model domain as most of the remaining particles are far to the east inside the harbour, the centroid undergoes a large shift in location.

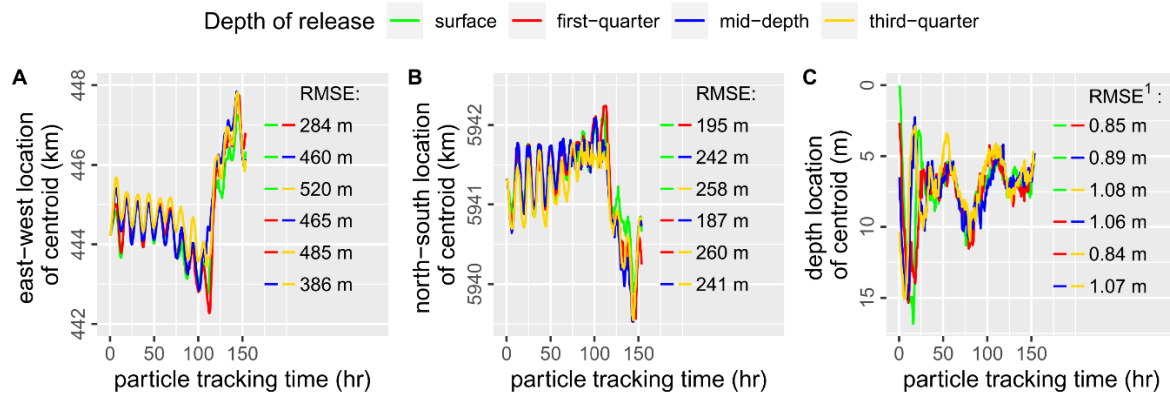


Fig 5.10 Spatiotemporal trajectories of particle centroid and RMSE of trajectory-pairs along the (A) east-west, (B) north-south, and (C) vertical directions illustrated upon four different particle releasing depth scenarios as per J-18495 model.

(¹ based on an RMSE estimation at only long-term from 57.5 hr)

5.4.2.2.2. Depth Sourcing

Originally, for releasing the particles, the EFDC drifter module sources a depth, which is manually copied from the model bathymetry and general to a model grid cell. The development of automation of this process in this study has made sourcing the particle-releasing depth within the model more efficient, and its new depth interpolation strategy has made the depth sourcing specific to the model grid cell or the release site. To investigate whether the depth sourcing strategy has any influence over particle transportation, two model scenarios were executed by varying the strategy upon spatial generalisation (grid-cell general) and spatial precision (site coordinate specific), and their outputs are presented in Fig 5.11. The figure shows distribution maps of the particles released at surface and mid-depth waters (A and B, respectively) and simulated as per those depth sourcing scenarios. The respective outputs are compared as per the depth conditions regarding the

particle distribution. The figure reveals a difference in the net longitudinal transport (east-west) of the particles between the releasing depth scenarios in the long run caused by particularly the grid-general depth. This demonstrates the implications of depth sourcing as one of the particle release specifications. The site-specific depth sourcing is logically more precise and reliable than the general one, and its implementation is even made semi-automatic and user-friendly within the model. These relative advantages justify the adoption of site-specific depth sourcing in this study for the other scenario investigations.

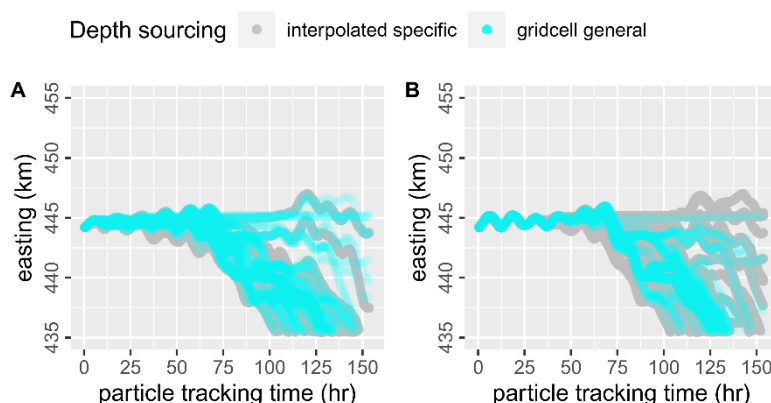


Fig 5.11 Map of distribution of the particles simulated without any vertical movement comparing depth sourcing induced transport variability between (A) surface and (B) mid-depth releasing scenarios.

5.4.2.2.3. Number of Particles Released

It was anticipated that beyond a certain large number of particles, the number of particles released would not have any major impact on the general transport of the particles or their distributions. A batch of 100 particles was employed not to investigate swarm behaviour but rather to simulate a single jellyfish. The use of a batch of 100 particles aimed to address uncertainties arising from model accuracy, including factors such as turbulent diffusion or inaccuracies in current representations, as well as uncertainties in jellyfish behaviour. To test this, three scenarios were run for 10, 100 and 1000 particles released under identical conditions. The comparisons of centroid trajectories are presented in Fig 5.12. The

trajectory lines provide a visual representation, and the RMSE between the number pairs offers a numerical indication of relative transport variations among the scenarios. A lower variation, considered insignificant here, justifies the release of 100 particles instead of a higher number. The transport differences are much higher between the 10 and 100 particle release scenarios than they are between the 100 and 1000 particle release scenarios. This indicates that releasing a small number of particles (e.g., only 10) cannot create an average and representative effect in transportation modelling and for this to be practical, the particle releasing number in modelling should be at least 100. Releasing 1000 particles produces almost the very same particle distributions as 100 particles, but with much reduced computational effort. For all future simulations, 100 particles was there adopted as the particle release number.

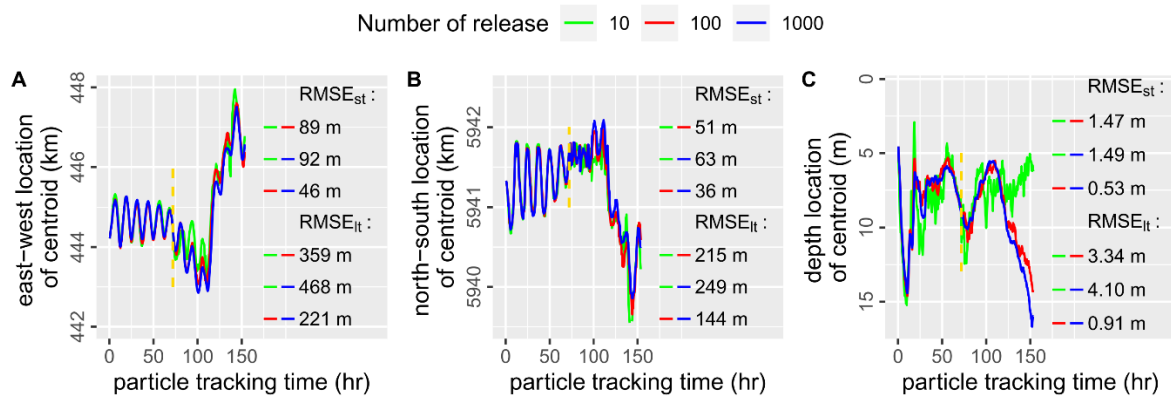


Fig 5.12 Spatiotemporal trajectories of particle centroid and RMSE of trajectory-pairs along the (A) east-west, (B) north-south, and (C) vertical directions illustrated upon three particle releasing number scenarios as per J-18495 model. The RMSE is calculated for the short-term (st) and long-term (lt) periods of the simulation, which are separated by the golden vertical dash being st on its left and lt on its right side.

5.4.2.2.4. Particle Release Location

It was thought that the starting location of a particle's travel set within the three-dimensional model grid might be important to consider in the sense that the particle would be exposed to a specific flow based on that location and the fact that the model grids cells may not exactly replicate the current velocities at the release

site. The jellyfish release locations were all close to the shore; however, in a model, grid cells adjacent to a shoreline might not be under-predicted if the spatial resolution is not of suitable resolution. To investigate the sensitivity of the jellyfish transport patterns to the specific release location, three additional scenarios were executed which released particles (1) closer to the south shore than the actual release location, (2) one-third of the channel width from 1, and (3) two-thirds of the channel width from 1.

A map showing the release locations and the particle distributions from the three scenarios above as well as the actual release location scenario (as per J-18495) is shown in Fig 5.13. The time of output is at the end of the simulation, 153 hrs after particle release. Although there were differences in the distributions, their extents were quite similar, and it was therefore difficult to draw any conclusions regards differences in transport based on visual inspection alone. To quantitatively analyse the differences, a statistical Kolmogorov-Smirnov (KS) test was carried; the results are presented in Table 5.7. Differences in the particle distributions were estimated based upon two statistical measures of the KS test, namely, (1) the maximum critical value (D_{\max}) and (2) the significance level (p). The variation between two distributions is deemed significant when $D_{\max} = 1$ and $p = 0$. Pair-wise KS tests between the actual jellyfish release scenario and the other release location scenarios presented in the table reveal that none of the test statistics shows a significant variation in the distributions. The results confirm that the distance of the release location from the shore does not significant affect transport distributions and so for all future runs the actual release location was used.

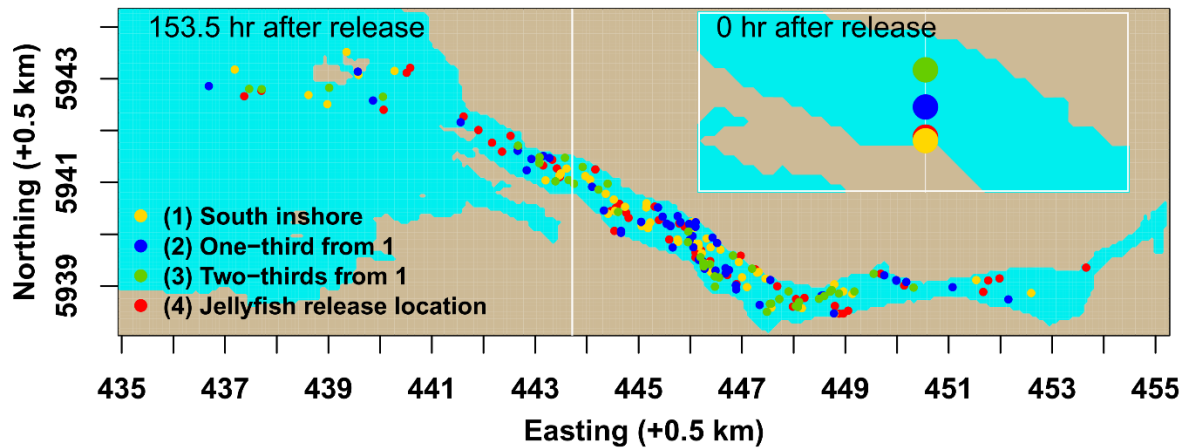


Fig 5.13 Map showing the distributions of modelled particles released at the exact release location (red) and three other locations at different distances from the shore. Inset plot shows particle locations at the time of release.

Scenarios Compared	KS test statistics	
	D_{\max}	p
Actual release location vs South shore (1)	0.13462	0.739
Actual release location vs One-third channel width from (1)	0.17308	0.421
Actual release location vs Two-thirds channel width from (1)	0.19139	0.311

5.4.2.3. Hydrodynamic Forcings

5.4.2.3.1. Wind

To investigate the wind influence on particle transportation, the basic LPT scenario which included time-varying wind was compared with an alternative scenario with no wind. Once again, the Kernel density was used to quantify the spread of the particles with time throughout the harbour. A comparison of the Kernel density estimation for the wind and no wind scenarios is shown in Fig 5.14. According to the figure, the temporal distribution of the particles exhibits a much lower density and thus a higher dispersion, or spread, in the scenario where wind was included. This

demonstrates that the wind has an obvious influence on the particle transportation and should be included in jellyfish transport models. Additionally, the variation in the figure confirms the capturing of wind influence on the particle transportation by the model developed. It can be assumed that wind speed variation would have a variable influence on the particle transportation where a strong wind event has a potential to dissociate or break any potential swarm formation provided that any other forces are constant. The wind can therefore play a significant role in changing particles' transport and their concerted movements.

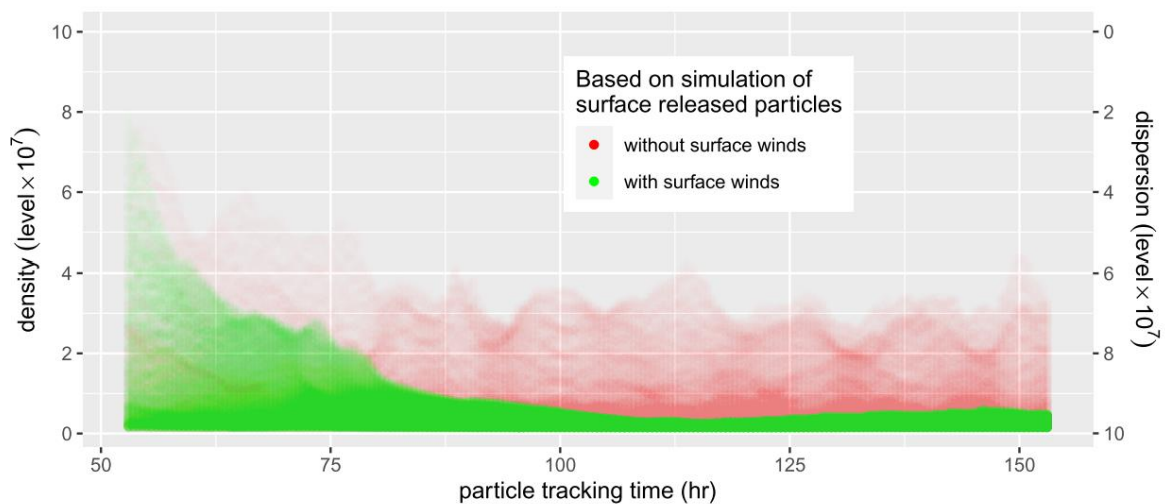


Fig 5.14 Variation of Kernel density estimation of the model particles with and without wind for J-18495.

5.4.2.3.2. River Discharge

River discharge (Q) influences the estuarine flows by creating a density stratification resulting from the differences in the density of the riverine freshwater and the estuarine saline water; this is potentially an important phenomenon for passive drifting of particles in the harbour. To investigate the influence of river discharge on particles' passive transportation, the basic J-18495 jellyfish LPT model which included time-varying river discharges was compared with a scenario without any river discharges. Fig 5.15 compares the net particle transports in terms of centroid trajectories plotted over the 153 hours of the simulation. The figure shows the

release location of the particles (displayed by the black vertical line) and the trajectories of the particle cloud centroids for the with and without Q scenarios with particles released at both surface and mid-depth. The east-west ranges (displayed by the coloured bars) of the respective centroid trajectories (displayed by the coloured lines) show the variations in the centroid location. According to the figure, the river-free condition results in many particles being transported relatively westward towards the sea while the river discharge pushes the net transport further inside the harbour, which is true irrespective of the particle releasing depth. Some particles might be trapped inside the harbour due to any turbulence or flow variations induced by the river discharge, which influences the calculation of the net transport. The results confirm that the river discharges can have a significant influence on the particles' net transport and confirms the importance of capturing river discharges in the model developed.

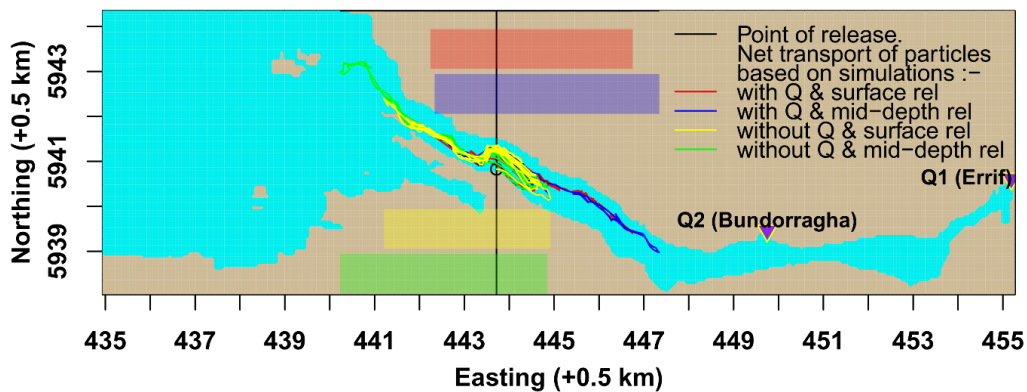


Fig 5.15 A comparison of the net transport of particles between with and without river discharge (Q) scenarios combined with the depth of release.

The link between local hydrodynamics and particle transport results is demonstrated by the presentation of current vector plots in Figure xxx. This illustration presents the differences in modelled current velocities obtained with and without the main river discharge (Q) at mid-ebb (top) and low tide (bottom). The vectors were calculated by subtracting the velocities obtained for no river discharge from those obtained with the river discharge. The vector maps show that at both stages of the tide the inclusion of the river induces stronger currents that are directed into the harbour. These local flow differences result in an increased

transport of particles eastward into the harbour when the river discharge is included in the model, as demonstrated in Fig 5.16.

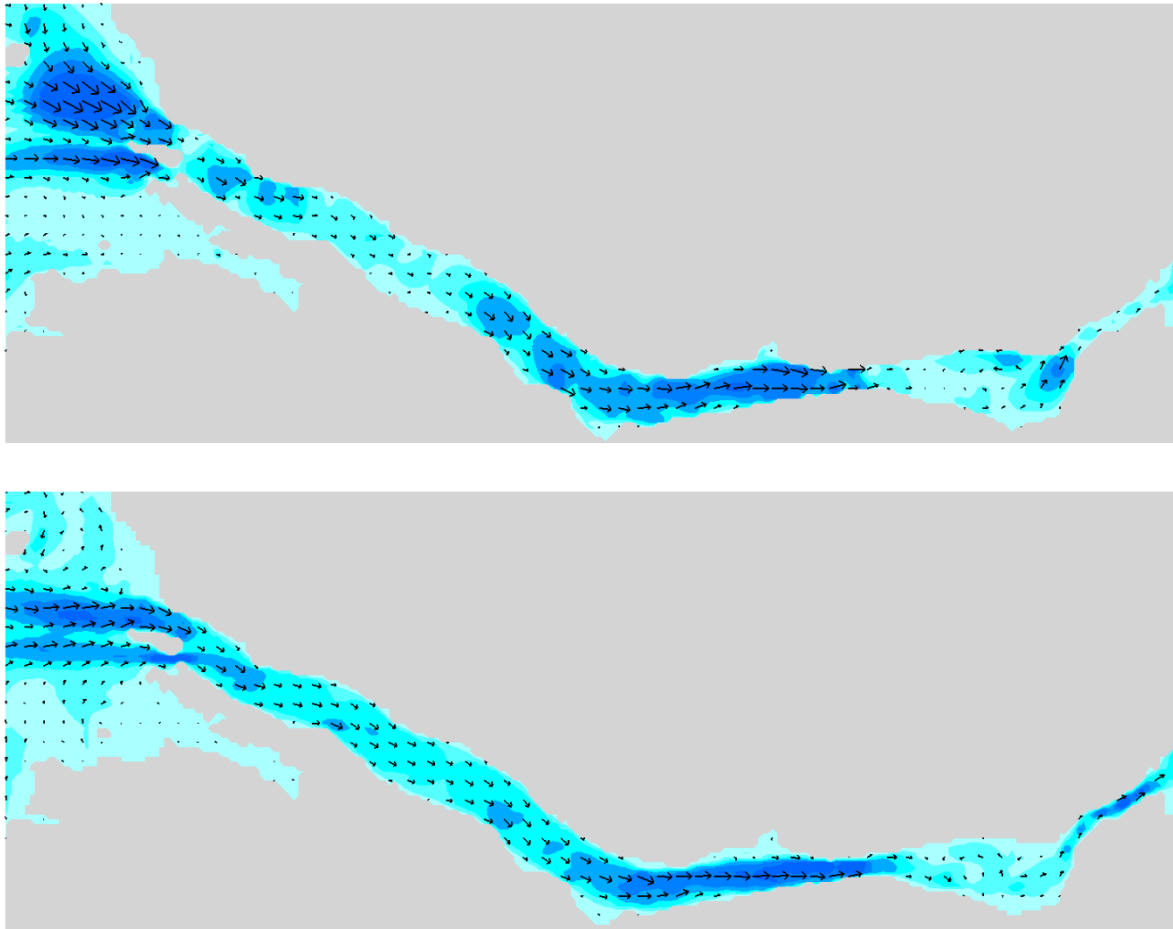


Fig 5.16 Depiction of current differences between conditions with and without river discharge illustrated for mid-ebb (top) and low-tide (bottom), highlighting higher current speed in the mid-channel where potential particle entrapment may occur.

5.4.3. Results - Comparison of Modelled and Observed Movements

Jellyfish were first modelled as passive drifters in the LPT model. Their agreement with tagged jellyfish transport is presented based upon the following four types of analyses:

- 1) qualitative spatiotemporal agreement,
- 2) snapshots of particle locations, .i.e. particle spatial distribution map,
- 3) quantitative spatiotemporal agreement by SCA, and

4) quantitative spatiotemporal agreement by MCA.

For the qualitative spatiotemporal agreement analysis, modelled particle locations were analysed at an hourly timestep and the presence of particles a detectors range was recorded. The results of this analysis were then compared with the observed locations at the times at which observations were recorded, again on an hourly basis. In this way, it was possible to determine whether a modelled particle was present within the range of the correct detector at the correct time. The results of the analysis are presented in Fig 5.17 and show particle and jellyfish occurrences across all zones at the times of jellyfish detection. A colour coding was used for the detection zones as follows:

- light green: the model predicted the presence of particle(s) at the same time at which a jellyfish was observed in that detection zone, i.e. modelled particles were in the correct location
- yellow: the jellyfish was observed in this zone but there were no model particles present at the observation time, i.e. modelled particles were in the wrong location
- green: zones in which only model particles were present at times of jellyfish observation. i.e. modelled particles were in the wrong location
- grey: neither modelled particles nor jellyfish were observed in these zones.

The spatiotemporal analysis results show mixed levels of agreement across the model jellyfish scenarios. Passive drift modelling could effectuate agreement in the models at all detection instances for J-18495, J-1160, and J-18500, the majority of time for J-1162, but could not predict any of the observations of J-18499. While these results are positive, it must be remembered that they are purely qualitative and merely indicate that the model was correctly predicted the position of at least one particle.

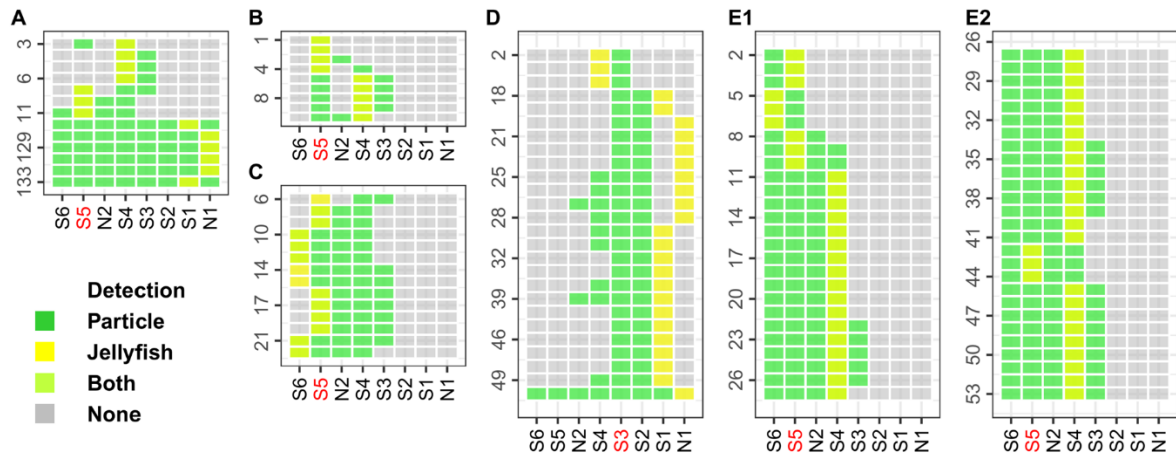


Fig 5.17 Qualitative spatiotemporal transport agreement between the particles and the model jellyfish (A) J-18495, (B) J-1160, (C) J-1162, (D) J-18499, and (E) J-18500.

Snapshots of particle locations at times of jellyfish observations provide a second qualitative evaluation of the passive drift modelling of jellyfish. An example for J-18495 is presented in Fig 5.18. The figure shows the spatiotemporal tracking of the jellyfish with reference to water level (A) and detection zones (B) along with two snapshots at two different times of jellyfish observation corresponding to the first and final detections (C and D). The agreement snapshots in the figure show particle distributions (marked by the points) at two time-instances separated by 128 hrs interval and the detection zone of the receiver that detected the jellyfish at those times (marked by the purple-coloured circle). The first snapshot (C) was just 3 hours after the particle release and the second (D) was 128 hours (almost eleven tidal cycles) after the first detection. After 3 hours, the particles have not travelled far, and transport processes have had limited time to act on them so they are still gathered quite closely near the release location. Almost all of the particles are within the detection zone of the correct detector. After 128 hours, the transport mechanisms have spread the particles throughout the harbour with some individual particles travelling both very far upstream to the east and outside of the harbour to the west. There are some particles present at these time-instances within the correct detection zone even though the detectors are at least 3-5 km apart. This confirms that the

passive drifting alone was capable of transporting at least some of the particles in a manner similar to the observed jellyfish transport. However, these snapshots still only assess the model performance qualitatively; further quantitative assessment of the transport agreement was therefore conducted using SCA and MCA strategies.

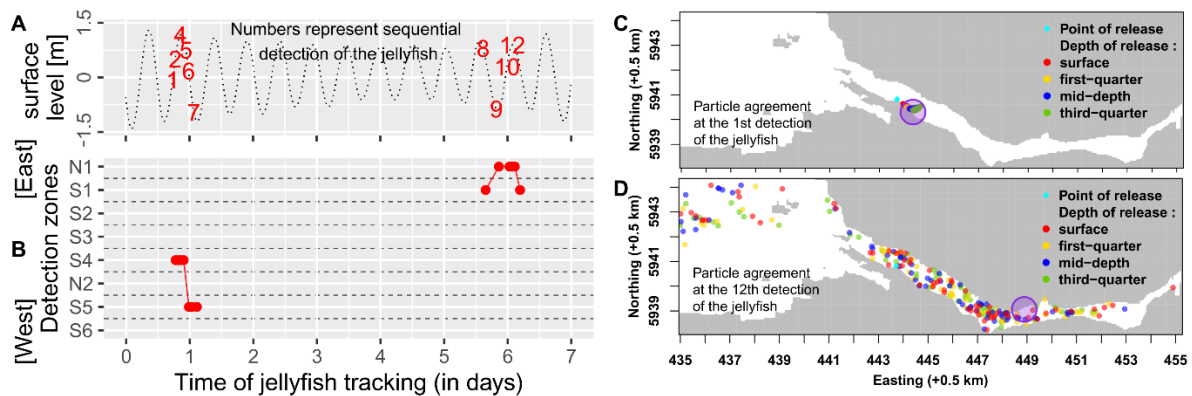


Fig 5.18 Observed transport of jellyfish (J-18495) detections based on (A) tidal stage and (B) detection zone, and snapshot agreement of modelled particles with the correct detection zone at (C) 3 hrs and (D) 128 hrs after particle release.

Although the snapshots in Fig 5.18 show that some modelled particles were indeed present at the locations and instances where J-18945 was detected, for the purpose of comparing different model scenarios upon transport agreement, it was necessary to develop a method of quantifying the level of agreement. For this, SCA is used to give a basic quantification based on one agreement criterion. Later, MCA is used to incorporate other agreement criteria. The criterion used in the SCA was the presence of a particle within the correct detection zone at the correct time of observation. SCA thus involved calculation of the percentage of particles within the model domain that agreed with a jellyfish detection. It is important to note that the effect of particle retention within the domain over the simulation has been included in the SCA.

Fig 5.19 shows the SCA percentage agreements for five jellyfish model transportations at the various detection instances. The colour represents the percentage of agreement. The figure shows percentage agreements for two

particles released at the surface and at mid-depth for each jellyfish. For all five jellyfish, and for both surface and mid-depth releases, the agreement was higher in the earlier hours of the simulation than later. Generally, percentage agreements are greater than 50% up to 10 hours after release but they reduce significantly in the longer term. This is because the particles immediately after their release tend to move as a cluster while the advective and diffusive transport processes take some time to have their influence on the particle spread. The model based on J-18495, which has much longer tracking records than the other jellyfish, produces 9.52 % and 11.29% agreements for the surface and mid-depth releases, respectively, at 133 hrs after their release. The J-1160 model produces agreements of 44-65% 10 hrs after the particle release (tracking is not available after this time) while the J-1162 and J-18500 models show 8% and 53% respectively at the same time instance. Conversely, at 22 hrs, J-1162 shows 38% agreement while J-18500 produces only 1 % agreement. The J-18499 model could not produce any agreement in the early hours of the simulation but achieved some level of agreement from 20 hours onwards; this might be because the jellyfish travelled under its own motility after release rather than simply passively drifting on the prevailing currents.

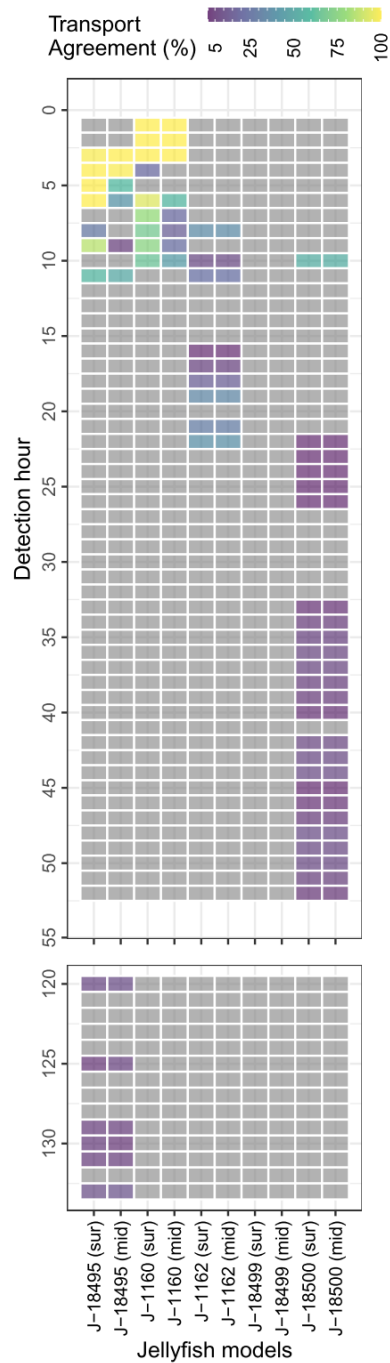


Fig 5.19 SCA determined percentage agreements of the modelled particle locations with observed locations of jellyfish for five jellyfish models for surface and mid-depth releases.

MCA was used here to assess LPT model performance, i.e. transport agreements, based on seven criteria. The first criterion was that used in the SCA, i.e. the percentage of particles in the correct detection zone at the correct time. Since some

particles might not be detected exactly within the correct detector's zone but may be located nearby; the second and third criteria were devised based on these grounds. The second criterion counts the percentage of particles within 250 m of the correct detection zone while the third includes particles in adjacent detector zones. Finally, the fourth criterion is the number of particles still remaining in the domain at a given time. The other three criteria are based on the location of the centroid of the particles relative to the correct detection zone; the closer the particle centroid to the correct detection zone, the higher the MCA weighting and thus score assigned. Centroid distance measured at pre-detection, detection, and post-detection instances of time have been included. The first criterion was considered a true measure of model agreement while the other criteria were all considered to indicate potential model agreement. The MCA analysis is considered to be a better measure of model performance than the SCA since it considers multiple potential criteria for measuring the agreement. Therefore, it allows a better assessment of the LPT model performance by revealing more insights into the transport agreement.

Fig 5.20 illustrates the particle transport agreement of the five jellyfish models at their respective detection instances and locations based on the calculated MCA scores. Each dot corresponds to a detection of a jellyfish and indicates the observation time and corresponding detection zone. The agreements are displayed in the figure by the dots having colours varying. The level of model agreement is then indicated by the colour of the dots; the colour represents the MCA score ranging from 0 to 1 with 0 indicating no agreement and 1 indicating perfect agreement. Since the particles' tracking periods and detection instances across the models are different, it is important to compare their agreements.

According to the figure, the modelled particles show a higher agreement in the first 10 hrs of their tracking, except for the J-18499 jellyfish model. While the SCA showed no true agreement for the J-18499 model, the MCA shows some potential agreements in this model over the simulation at low-levels. After approximately 10 hrs of the simulations, agreement levels drop, particularly in the longer term. Although the model jellyfish J-18495, J-1160, and J-1162 were released relatively close to each other in terms of time and location and were therefore exposed to

similar tidal currents, wind speed, and wind direction (Fig 5.2), their agreements differ in level (Fig 5.20). This suggests that some other important transport mechanism may be at play, such as active swimming by the jellyfish (Fossette et al., 2015; Matanoski & Hood, 2006; Neil & Askew, 2018; Rakow & Graham, 2006).

Two very important proofs can be seen here. One, the jellyfish is not merely a passive drifter. Two, the modelled transport cannot be expected to end up in high agreement with the observed transport under the current analytical design where the gradually diffused particles are to agree merely a single jellyfish transport and detection. The results suggest improving the model agreements by including jellyfish motility within the LPT modelling approach may be possible.

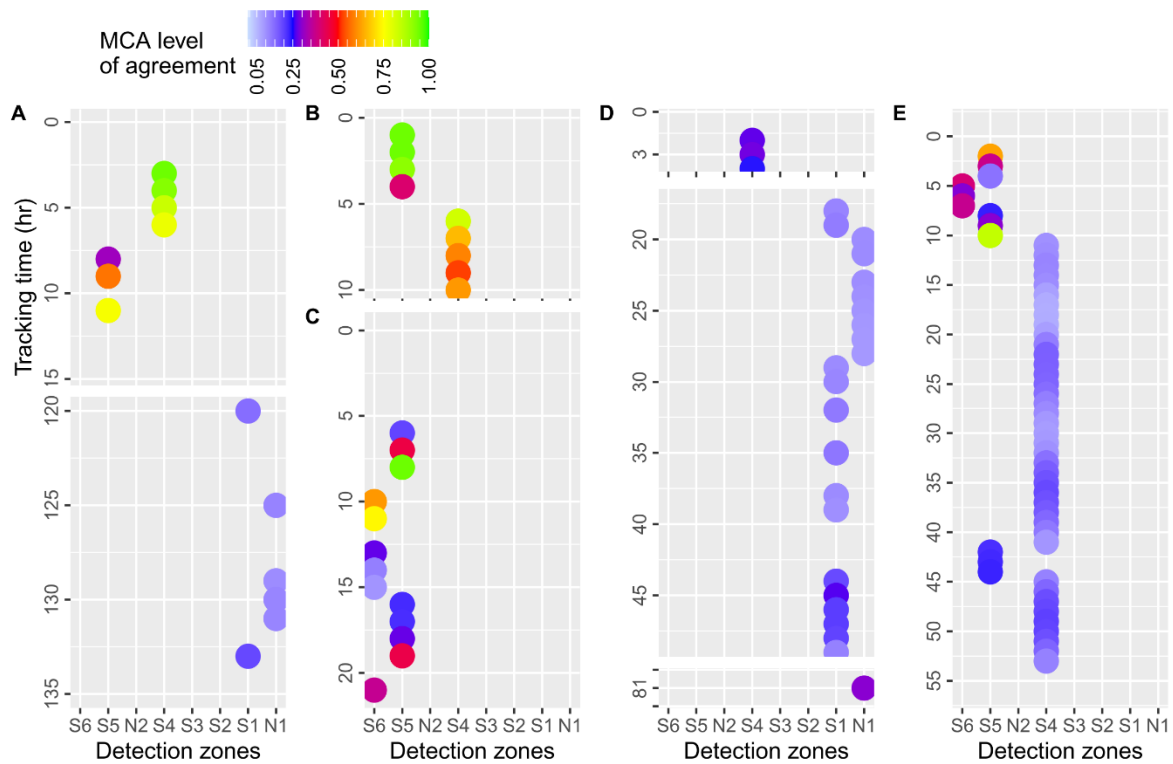


Fig 5.20 MCA-based quantitative spatiotemporal transport agreement of the particles as per the jellyfish model (A) J-18495, (B) J-1160, (C) J-1162, (D) J-18499, and (E) J-18500 to the respective jellyfish.

5.5. Summary and Conclusions

A LPT model was developed and used to simulate passive drifting of jellyfish in Killary harbour. Batches of 100 particles were released at the same times and locations as tagged jellyfish releases in the Harbour. The jellyfish monitoring data were processed and analysed to determine any particular trends in their movements. The LPT model was first assessed for its sensitivity to particle tracking model setup, particle release conditions and hydrodynamic forcing and, subsequently, the model performance was assessed by comparing modelled particle locations with observations of five tagged jellyfish using qualitative and quantitative analyses. The key conclusions of this research are described as follows.

- 1) Based on the jellyfish monitoring data, jellyfish transport in Killary was found to be partially influenced by the tidal currents with jellyfish transported with the tide for some of the time. However, movements against the tide were also observed for some periods of time. The latter non-tidal movements might be attributed to the jellyfish's motility. The investigation was only based on a qualitative analysis of tidal influence; however, a quantitative analysis is presented later in Chapter 7.
- 2) The integration of the EFDC LPT submodel within the base hydrodynamic model was successful. The model particles could move three-dimensionally by both advection and diffusion on the tidal currents.
- 3) As expected, the LPT model for jellyfish transport was found to be sensitive to the model diffusion coefficient analysed in terms of particle swarm or dispersion formation. The swarming or dispersing behaviour of a jellyfish population in modelling can be controlled by diffusivity making this an important model calibration parameter.
- 4) The particles' ability to move vertically had an influence on their net transportation. Particles being exposed to and sampling various horizontal advection levels by changing their vertical positions within the water column using the vertical advection-diffusion process resulted in significantly different transport patterns and more particle spreading than in the absence of vertical

transport. Using different particle release depths resulted in broadly similar transport patterns but there were some differences in the centroid location of the particle clouds; this difference was largest for particle released at the surface compared to those released near the bottom.

- 5) The model was found to be relatively insensitive to the particle releasing number only when it was 100 or more, a number which could create an average and representative effect of transportation modelling. Thus, the number should practically be at least 100, which is also a statistically justified sample size to achieve a meaningful result out of the transport modelling.
- 6) Particle distribution was found not to be influenced by variation of the release location laterally across the channel.
- 7) The model results demonstrated that the surface wind forcing caused a higher particle dispersion, and the river discharge created an influence on the particles' net longitudinal transport. Given the observed correlation between the long-term net longitudinal transports of jellyfish or modelled particles and the tidal currents, it was concluded that there is no substantial influence of local flows on their net transportation. However, it's important to acknowledge that local flows might impact the spatial distribution of individual particles on occasion. Nonetheless, it is crucial to emphasize that this study did not encompass the examination of these specific influences resulting from local flows, rendering them irrelevant to our current discussion.
- 8) Jellyfish transport agreement varied among models and within simulations over time. Initial hours post-release showed higher agreement, decreasing with particle spread. Non-agreement with the LPT model suggested individual jellyfish motility misaligned with passive drifts, supported by monitoring data. In Killary, partial agreement with passive drifts was observed, particularly in early hours post-release. Subsequent chapters explore integrating jellyfish motility, including diel migration and swimming, into the transport model.

CHAPTER 6: DIEL VERTICAL MIGRATION MODELLING OF JELLYFISH

6.1. Introduction

Jellyfish transportation is driven by a combination of physical hydrodynamic processes (e.g. horizontal and vertical currents) and biological locomotive functions in the organism (e.g. bell pulsation). Although traditionally, the jellyfish was said to be more of a drifter than a swimmer, some recent studies have shown their ability to either transcend or resist the current flows and their ability to orient themselves during their movement (e.g. Fossette et al., 2015). On a preliminary observation in an Irish fjord, we have also found a similar indication for some non-specific jellyfish, reported in Chapter 5 (Passive-drift Modelling). Passive drifting of jellyfish occurs continuously as the jellyfish are exposed to the local hydrodynamic circulation; however, active swimming is more deliberate and intermittent on behalf of the jellyfish. An understanding of the conditions that lead the jellyfish to be either simply passive at the mercy of the flow or simultaneously motile by actively responding to external cues is so far lacking in the literature. However, certain factors are empirically found to be responsible for jellyfish motility; light sensitivity is one of those causing diel vertical migration (hereinafter DVM) in jellyfish movement (Garm & Ekström, 2010; Martin, 2002; Nilsson et al., 2005).

Jellyfish and many other gelatinous zooplanktons participating in DVM, which is an irradiance response-based movement behaviour across the water column, spend the sunlight hours of the day in darkness at depth and return to the surface as the sun sets (Longhurst et al., 1990; Steinberg & Landry, 2017). Diving deep to take refuge during the day may be a reactive anti-predator behaviour intended to survive the risk of detection and encounters by visual predators, as mentioned in various DVM study literature, e.g. Dupont et al. (2009). According to them, it may also be a phototactic behaviour to minimise any potential photodegradation due to exposure to the light on the surface water (Dupont et al., 2009). Rising at night into the food-rich shallower water may be intended to secure a meal garnished with

photosynthetic prey foods (Bandara et al., 2021; Freer & Hobbs, 2020; Seo, 2021). Jellyfish even take refuge across the depth from adverse environmental conditions such as strong winds, heavy rain, or rapid flow (Yin et al., 2019). Since a jellyfish's survival and growth opportunities are asynchronous across the water column, there is a tendency to trade off, causing the jellyfish to migrate vertically. There are available studies on in-situ species-specific observations of DVM behaviour and its corresponding effects on the distribution of jellyfish; the DVM modelling investigations are limited though (also mentioned by Rahi et al. (2020)). However, its modelling may be advantageous as it can allow multiple scenario investigations to explore the impact of DVM on the ultimate movement of jellyfish.

Studies such as Dupont et al. (2009) and many others suggest that the sensitivity of the jellyfish to light and its due response through the avoidance and preference for certain intensities can explain the important features of their vertical distribution. However, such a model's desired output can be achieved by understanding the organism's proximate vertical behaviour, devising rules of their mechanisms, translating these numerically within a submodel, and integrating the submodel within the base particle drift model. Dupont et al. (2009) modelled the vertical migration of deep-water jellyfish *Periphylla periphylla*, where they experimented with a couple of assumptions on its related behaviour cued by the avoidance, preference, or tolerance for light. These cues require the water surface irradiance and its attenuation through the water column to be known in advance at each location, time, and water depth and be processed within the model. As per their assumption, the particles (jellyfish) lying within a depth range of preferred irradiance were randomly free-swimming with an equal probability towards up or down though how this was translated within their model is unclear. Furthermore, particles crossing the water column boundaries were mirrored back within the water area. However, there is a chance that this strategy might create repetitive hit-and-reflect by the particle on the boundaries, although this issue is not discussed much in their paper.

Berline et al. (2013) modelled the transportation and stranding of *Pelagia noctiluca* in the Mediterranean Ligurian Sea by incorporating a fixed-depth vertical migration

behaviour with a diel cycle. Recently, Rahi et al. (2020) modelled the distribution and stranding of the same species in the Mediterranean Balearic Sea by incorporating the DVM with speed adjusted upon buoyancy and its due effect at various lifecycle stages. They claimed their biophysical model predicted better than the simple drift and fixed diurnal behaviour models. However, in both models, particles' advective transport was modelled by the horizontal-only currents to force the horizontal advection, where the random walk movements and flow-governed vertical advection were ignored. Checks for the transport agreement of free-moving particles were absent in both models since their comparisons were based on stranding events only. Insights into their travel-halt-residence-travel patterns as well as the conditions that led to their gradual agreements over a period could otherwise be explored. Both models assumed a maximum depth limit for the vertical migration of jellyfish, being either fixed in Berline et al. (2013) or adjusted according to the bathymetry in Rahi et al. (2020). However, per our logic, this is an exaggeration since a jellyfish cannot adjust its vertical limit by remotely sensing the total water depth.

Our newly developed DVM model for non-specific jellyfish in Killary fjord attempts to rationally handle the limitations of the previous DVM models as detected and mentioned above. Since the exact photo response by jellyfish, either at the individual or population level, is unknown, setting a fixed light intensity threshold for triggering the vertical migration may be an overconfident approach. Even opting for such processing by a jellyfish on a continuous basis on frequent spatiotemporal changes of light intensity along the water column may not reflect a true energy-efficient behaviour. So, instead of irradiance, we rather assume a water depth threshold for DVM, which is thought to be determined by jellyfish through their experience and evolution as a depth complying with their light-induced instinct at best. Since this threshold depth is unknown, we assess its sensitivity to the model.

Here, the chapter highlights (1) the modelling of jellyfish DVM, (2) the implications of the light-induced behavioural transport of jellyfish in modelling, (3) the simplification of the dynamic DVM process for modelling, (4) the synchronisation of the DVM with the routine passive drift, (5) the integration of the DVM submodel with the base hydrodynamic model, 6) the transport simulations using the developed

DVM modelling method, (7) the analysis and comparison of the simulation outputs, (8) the insights into the jellyfish transport simulated on DVM, and (9) the comparative agreements to the observation between the passive and the DVM transport across jellyfish models. However, the model does not include sex, reproduction, mortality, individual size variability, hunger, life stages etc. of jellyfish online during the modelling. Non-specific individual variations of jellyfish were investigated offline through multiple scenario modelling.

The chapter is structured as follows. Section 2 shows the link to the description of the study site, Section-3 provides the methodology, which consists of model description, DVM submodel development, scenario and sensitivity modelling, and methods of transport analysis and comparison, Section-4 provides the results of the model development, transport simulations, model sensitivity to DVM properties and parameters, particle distributions and insights on transport pattern due to DVM, and agreement of the modelled transports to the observation. Finally, Section 5 provides the conclusions of integrating DVM in jellyfish transport modelling.

6.2. Study Site

Please see Chapter 4, Section 2 for the study site.

6.3. Methodology

A novel modelling approach for jelly transportation was developed by merging the light-induced vertical motility of jellyfish with their advective transport by the ambient tidal currents. Their movements in the vertical direction regarding diel vertical migration (DVM) were integrated with the primary advective drifting of the EFDC model using several behavioural rules. For simplicity, all jellyfish were assumed to have the same vertical motility rate, buoyancy, and diurnal migration behaviour. The hypothesis was that DVM would affect the horizontal distances travelled by jellyfish because the particles are subjected to different horizontal flow fields (and thus rates of advection) as they travel up and down through the water

column. This approach of DVM modelling is effective in investigating jellyfish transport patterns under the influence of environmental cues like currents and abiotic factors like luminosity. Much of the research involved modifications to the EFDC source code to incorporate the jellyfish DVM. The following sections describe the conceptual development of the DVM model and its implementation within the particle drift module of EFDC. The input data required to run the DVM, as well as the various model simulations executed, are both described in detail.

6.3.1. DVM Model Development

The purpose of the DVM model was to test the hypothesis that a combined effect of hydrodynamic forcing and vertical behavioural motility could predict the jellyfish transport in Killary harbour better than the passive-drift model and thus improve the particle transport agreement with the observed jellyfish detections.

6.3.1.1. Simple Conceptual Model

The transport processes to be included in the DVM model were advection, diffusion, and DVM, all of which were to be spatiotemporally synchronised. The DVM model was created by incorporating new code into the existing particle transport module of EFDC. The existing particle transport module included horizontal and vertical advection and horizontal and vertical diffusion. The new code would enable additional vertical transport of particles controlled by a set of prescribed rules. The basic concept of the DVM model is summarised graphically in Fig 6.1 and is described as follows.

The DVM model is started with the release of neutrally buoyant particles representing adult jellyfish which respond to luminosity by migrating downward to, and remaining in, the lower part of the water column during the day and migrating upward to, and remaining in, the upper part of the water column during the night (see Fig 6.1). Migration up or down through the water column is carried out at a fixed vertical motility rate. The water column is divided into upper and lower sections by specifying an invisible and idealised horizontal boundary - the DVM threshold depth. Vertical transport is the result of a combination of vertical advection, vertical diffusion, and customised vertical behavioural migrations. On the

other hand, horizontal transport depends exclusively on advection and diffusion from horizontal currents.

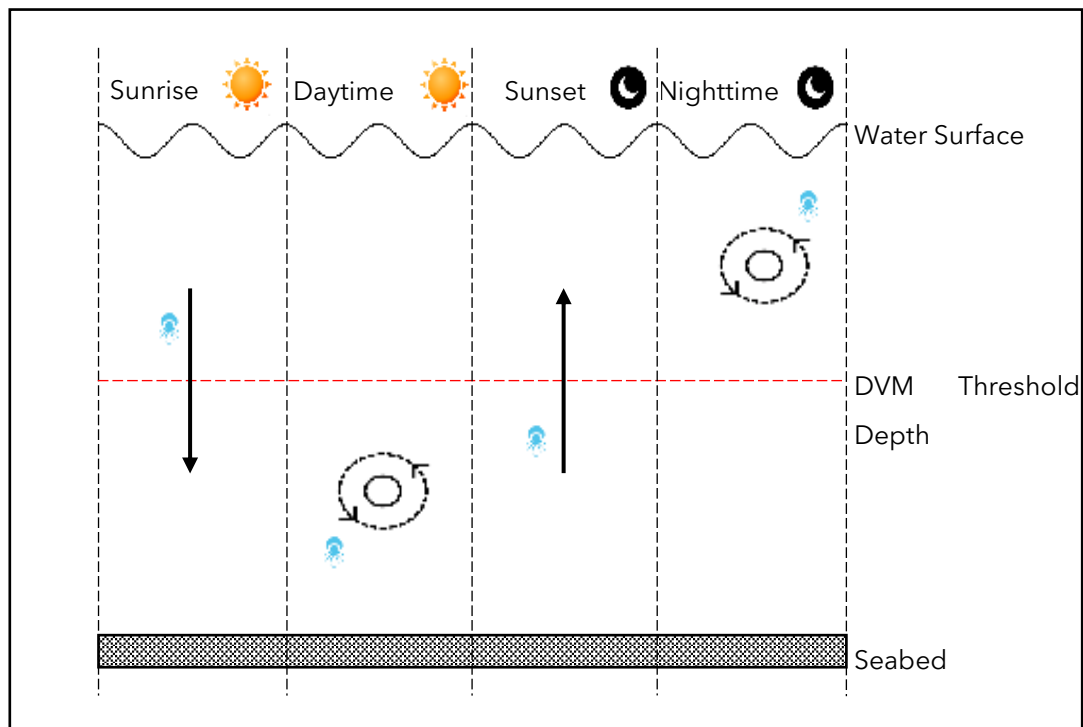


Fig 6.1 A simple graphical conception of jellyfish DVM model.

6.3.1.2. Model Processes and Rules

The DVM model is designed to capture the vertical migration behaviour of jellyfish and integrate it with passive drifting. Implementing the simple conceptual DVM model required a full understanding of the processes at play during the various stages of the idealised migratory behaviour and identification of the rules required to instigate and control the behaviour. Looking at Fig 6.1, which shows a complete daily migratory cycle, it can be seen that there are four primary stages of transport in the cycle. Moving from left to right in the diagram, we have:

- 1) Daytime vertical migration (occurring at sunrise)
- 2) Daytime normal transport (occurring during daylight hours)
- 3) Nighttime vertical migration (occurring after sunset)
- 4) Nighttime normal transport (occurring during nighttime hours)

Horizontal advection and diffusion normally occur during all four stages of the cycle, but for vertically, only independent jellyfish motility applies during daytime/nighttime vertical migration, while vertical advection and diffusion occur outside these times.

Different transport rules also apply to the four primary stages of the migration cycle depending on the particular position of a jellyfish particle and the time of day (i.e. daytime/nighttime). A total of 20 different jellyfish conditions (both real and virtual) were identified across the four stages (see Fig 6.2) of the migration cycle for which rules were required to enforce appropriate jellyfish behaviour. The aim of these rules is to ensure that a particle (i.e., jellyfish) stays above the specified threshold depth during the night and below it during the day based on its preferred luminosity across the water column, mimicking light-induced diel migration behaviour. This migration model differs from that implemented by Rahi et al. (2020) in the scale of vertical distance a jellyfish will cover during their transportation. Their model supports a particular dive distance, however, variable according to the total water depth, whereas, in this model, the particles were set free to dive to the maximum possible vertical distance across the full water depth.

As well as specifying the DVM threshold depth, buffer zones were introduced near the water surface and the seabed to prevent particles from being transported across the water surface and seabed interfaces. Rules were developed to actively prevent particles from travelling into the buffer zones. Although the buffer zones did not completely eliminate the issue of particles crossing the water/seabed interfaces, they did help to significantly minimise instances where this occurred. The threshold depth and buffer zones are shown in the water column schematic on the left of Fig 6.2. The limit of the buffer zone was specified at 0.5 m for both water margins.

Four types of vertical transport can occur during the course of the migration cycle. These are shown in Fig 6.2 and described as follows:

- 1) Diel Vertical Migration (DVM) – vertical transport of particles at a constant vertical motility speed.

- 2) Hydrodynamic Vertical Advection (HVA) – vertical advection of particles due to the vertical components of the tidal currents.
- 3) Movement at Motility Rate (MMR) – vertical movement of particles out of the DVM-exclusive session.
- 4) Movement for returning particles Back to the correct Range (MBR) – a vertical displacement of the particles to return them to the correct depth range if their current transport will bring them into the buffer zones or across the water surface/seabed interface. A variation of MBR is also implemented in terms of Ping-Pong Reversing (PPR) of the particles where a movement correction is required within the water column.

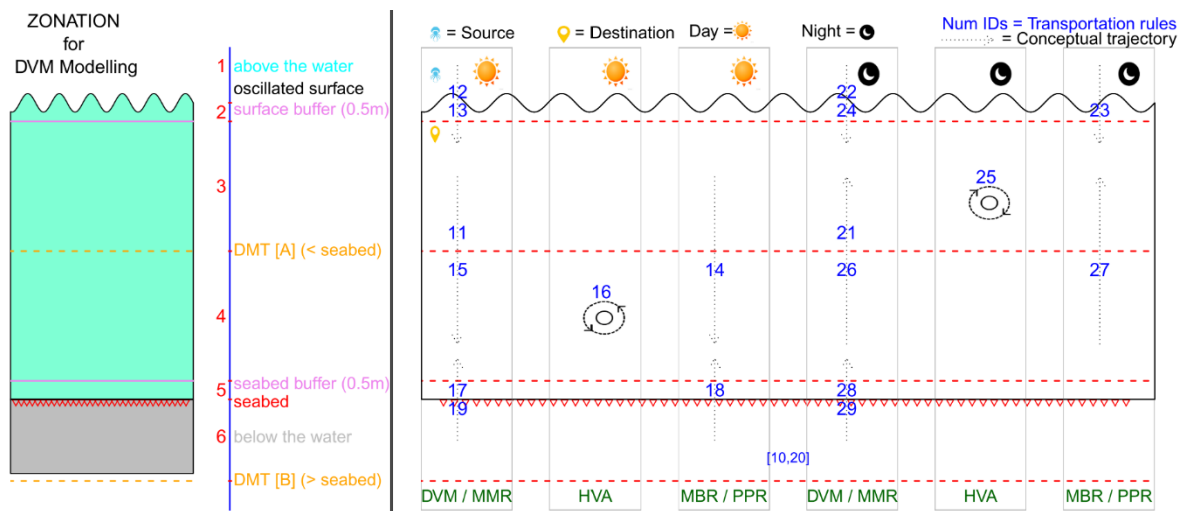


Fig 6.2 Schematic representation of DVM conditions and rules. The open end of the trajectory arrow indicates the source, and the pointed end indicates the destination of the transport. The vertical transport strategies are represented by Number IDs (blue), and their abbreviated terms (green) are defined in the following paragraph.

Chapter 6: DVM Modelling

Fig 6.2 shows which of the rules applied to each of the particle conditions. Table 6.1 provides a description of these conditions and the associated rules.

Table 6.1 A summary of DVM conditions and respective rules.

ID Num	Jellyfish particle (JP) condition [C = sequence of checks]				Rule
10	Daytime	C-7: Unidentified	If no pre-set conditions match JP's vertical position in the water column, then JP uses ordinary passive drifting.		HVA
11		C-1: JP within surface water to DMT	If JP is above the DMT, then it is set to move downwards until below the DMT.		DVM
12		C-2: JP above the bottom limit of surface buffer ¹	If JP is discovered above surface water (virtually), then it is brought back below the surface and subsequently set to move downwards at a motility rate.		MBR + MMR
13			If JP is discovered within the surface buffer, then it is set to move downwards at a motility rate.		MMR
14		C-3: JP below surface buffer up to DMT	If JP is discovered above the DMT while it is supposed to be below the DMT, it is set to return below the DMT.	If JP is found rising, it will jump back to its previous position.	PPR
15				If JP is found diving, it will move downwards at a motility rate.	MMR
16		C-4: JP below DMT	If JP is discovered within from DMT until the seabed buffer, then it is set to drift passively within the zone.		HVA

Chapter 6: DVM Modelling

17		C-5: JP within the seabed buffer	If JP is found rising, then it is set to leave the buffer at a motility rate.		MMR
18			If JP is found diving, it can jump back to its previous position.		PPR
19		C-6: JP below the seabed	If JP is discovered below the bottom limit of the seabed buffer (virtually), it is brought back above the seabed and subsequently set to move upwards at a motility rate.		MBR + MMR
20	Nighttime	C-7: Unidentified	If no pre-set conditions match JP's vertical position in the water column, then JP uses ordinary passive drifting.		HVA
21		C-1: JP within DMT to seabed	If JP is below the DMT, then it is set to move upwards until above the DMT.		DVM
22		C-2: JP above the bottom limit of the surface buffer	If JP is discovered above surface water (virtually), then it is brought back below the surface and subsequently set to move downwards at a motility rate.		MBR + MMR
23			If JP is found rising, it will jump back to its previous position.		PPR
24			If JP is found diving, then it is set to leave the buffer at a motility rate.		MMR
25		C-3: JP below surface buffer up to DMT	JP is set to drift passively within the zone.		HVA
26		C-4: JP below DMT up to the top limit of the seabed buffer	If JP is discovered below the DMT while it is supposed to be	If JP is found rising, it will move upwards at a motility rate.	MMR

Chapter 6: DVM Modelling

27			above the DMT, then it is set to return up above the DMT.	If JP is found diving, it can jump back to its previous position.	PPR
28		C-5: JP within seabed buffer	JP is set to move upwards at a motility rate.		MMR
29		C-6: JP below the seabed	If JP is discovered below the bottom limit of the seabed buffer (virtually), it is brought back above the seabed and subsequently set to move upwards at a motility rate.		MBR + MMR
¹ User-defined (here, 0.5 m)					

6.3.1.3 DVM Model Algorithm

An algorithm of the DVM model implemented in the EFDC model is presented in Fig 6.3. During each time step, the processes are executed in the following order:

- 1) luminosity (day/night) check
- 2) condition check for vertical transport rule
- 3) rule selection
- 4) particle's depth of occurrence check
- 5) vertical direction based on light and/or rule
- 6) vertical displacement based on user-defined depth-threshold
- 7) vertical speed at a user-defined motility rate
- 8) vertical limit based on the luminosity and the threshold depth and water column boundaries
- 9) vertical transport calculation and its subsequent adjustment upon bathymetry.

As a result, state variables are updated and thereby directly affect the movement of the particle agents.

Chapter 6: DVM Modelling

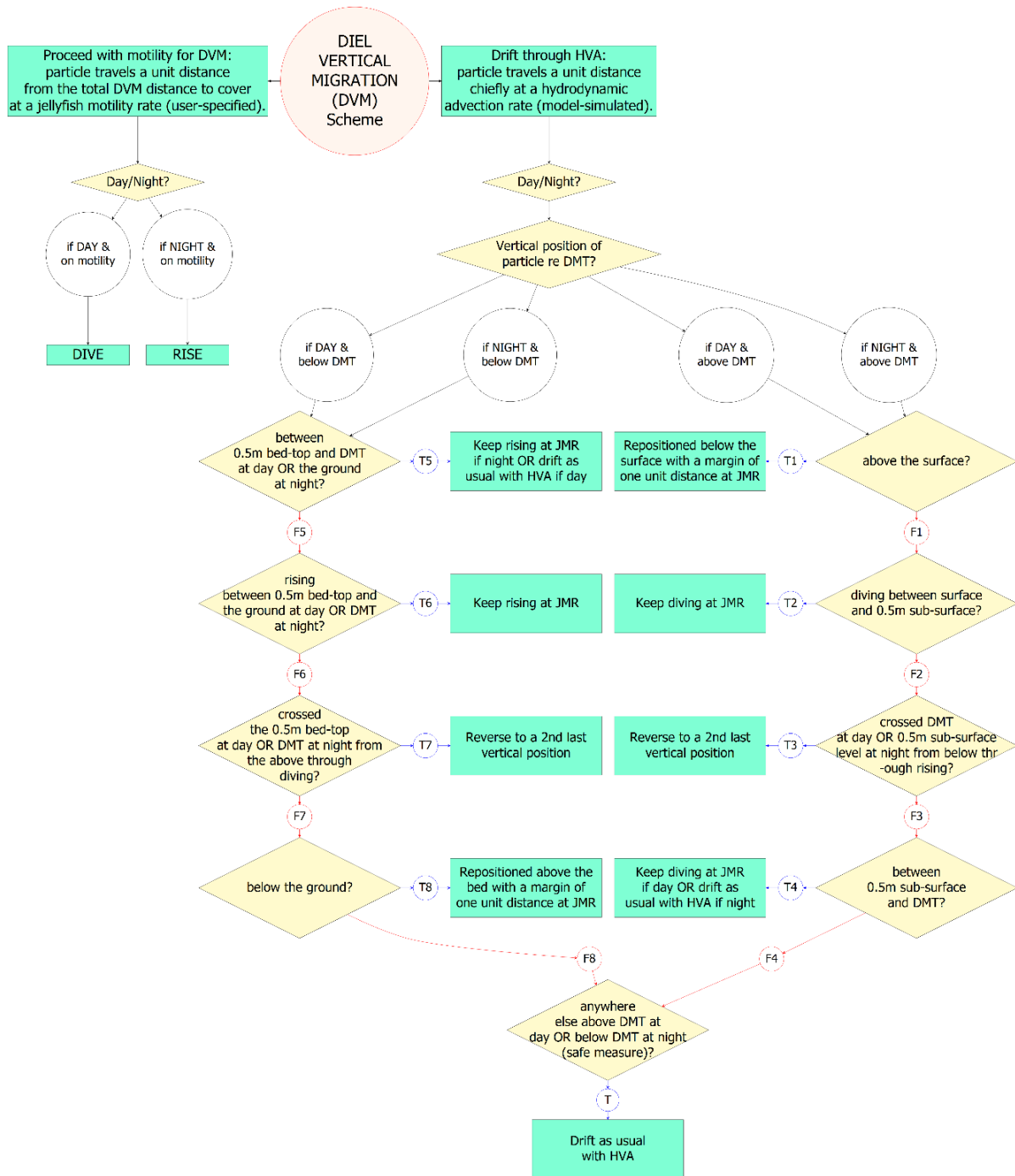


Fig 6.3 DVM model algorithm implemented in EFDC.

6.3.1.4. Implementation and Governing Equations

The DVM algorithm shown in Fig 6.3 was coded into EFDC's parallelised (O'Donncha et al., 2014) drifter module of Chung & Craig (2009). The code was extensively tested during development to ensure the various rules and processes were working correctly. Some outputs from this testing are shown in the results section. The new Drifter module code is attached electronically with this thesis as Digital Appendix.

As mentioned previously, four types of vertical transportation rules were devised and coded:

- 1) diel vertical migration (DVM),
- 2) hydrodynamic vertical advection (HVA),
- 3) movement at motility rate (MMR), and
- 4) movement for being back to the range (MBR) or ping-pong reversing (PPR).

The vertical transport is calculated upon the following basic equation.

$$z_t = z_{t-1} + \Delta z_t \quad (6.1)$$

where z_t and z_{t-1} are the vertical positions (m) of the particle undergoing DVM at the current and previous timesteps, respectively, and Δz_t is the vertical displacement (m) at a unit timestep (t), which is calculated according to the vertical transport rules mentioned above.

The vertical transport rules are now described textually and mathematically.

Rule-1: DVM

The DVM rule assumes that a particle must travel a particular vertical distance to a target depth in either an upward or downward direction. This process is captured in the model by using an incremental approach, where the particle's position is incrementally adjusted upward or downward across successive model timesteps until the target depth (100% migration) is reached. This transport is calculated upon

Eq. (1), where the vertical transport component of the equation is calculated for the current timestep in terms of diel vertical migration (*dvm*) displacement as follows:

$$\Delta z_t(dvm) = |z_{t-1} - z_{tvd}| \times \frac{dmi_t}{100} \times dir \quad (6.2)$$

Here, *dmi* is the diel migration increment adjustment factor (in percent format), and *dir* is a behavioural variable determining the direction of the DVM, which takes the value of either +1 for rising and −1 for diving if the depth is specified and vice-versa if the elevation is specified. Finally, *z_{tvd}* is the ultimate vertical position upon the target vertical distance (m) to be travelled.

dmi in Eq. (2) is the percentage (max. 100 %; if crosses, then corrected to the limit) of the target vertical distance at a duration (s) of unit timestep (*tsd*), which is set to perform at a specific velocity (*r* in m/s; same as the jellyfish motility rate, and read in the model as an input), and is calculated in the following ways:

$$dmi_t = \frac{r \times tsd}{|z_{t-1} - z_{tvd}|} \times 100 \quad (6.3)$$

At each timestep, the model recalculates the distance left to travel and the share to cover per timestep until the particle reaches the target depth. The target vertical distance is gradually reduced to 0, and diving or rising is completed within a migratory cycle.

Rule-2: HVA

Once the diel migration is completed using Rule-1, it is stopped by a switch and made ready to restart at a subsequent migratory cycle. At this time, passive vertical drifting is activated so the particle keeps moving vertically with the hydrodynamic advection until the next migratory cycle. The passive vertical drifting rule is also expressed upon Eq. (1) with its vertical transport component for the current timestep to be calculated upon advective currents as follows:

$$\Delta z_t(hva) = tsd \times \omega \quad (6.4)$$

where *hva* is the displacement due to hydrodynamic vertical advection (m) and ω is the vertical current velocity (m/s).

Rule-3: MMR

There are three vertical limits set within the water column for movements of the particles – the DVM threshold that divides the water column into two layers of preferred luminosity for the day or night and the other buffer zone limits for the water surface and seabed. There may be times when a particle moves beyond these limits but still remains within the water or when an assigned shift for a particle is not truly followed due to dynamic model computations. If so, then it is brought back within the correct extent by moving at the defined motility rate (*mmr*). This corrective rule of transport is also formulated based upon Eq. (1), where the vertical displacement is calculated for the current timestep as follows:

$$\Delta z_t(mmr) = tsd \times r \quad (6.5)$$

Rule-4: MBR / PPR

There may be times when the computed travel distance for a particular timestep may mean that the particle travels beyond the water column boundaries. If so, it is returned longitudinally to within the water column through the immediate boundary. The rule for this movement to bring the particle back into the correct range is expressed as follows:

$$z_t = z(\text{surface boundary}) \text{ or } z(\text{seabed boundary}) \quad (6.6)$$

The rule has got another formulation. There may be times when two consecutive vertical positions of a particle at a particular timestep may mean it is crossing through a boundary with a potential tendency of undesired rising or diving. If so, it is returned to its depth from two timesteps previous ($t - 2$). The particle transport at this variation in transport condition is ruled by a ping-pong reversing strategy (PPR), which is as follows.

$$z_t = z_{t-2} \quad (6.7)$$

6.3.2 Model Details

The model uses a data-driven approach to capture the transport of jellyfish (agent particles). Horizontal transport is determined by the horizontal advection of hydrodynamic variables (currents), while vertical transport is determined by vertical advection and vertical migration influenced by environmental (luminosity and water depth) and behavioural (diel migration) variables. The horizontal transport part is executed under EFDC's drifter module, and the vertical transport part is executed under the newly developed DVM submodel described in the previous sections.

Life cycle variables are not part of this model. For simplicity, transports influenced by biological trait variations (e.g. variations in the response of jellyfish to luminosity or motility speed due to their size or sex) are ignored, with the same behavioural traits being assigned to all particles. However, the sensitivity of transport patterns to variations in either biological or behavioural traits is investigated through scenario modelling. Each particle is capable of locally sensing the luminosity, its corresponding depth threshold, the water surface and the seabed. For vertical transport, luminosity (day/night) dictates the direction of migration, the threshold depth and buffer zone limits dictate the swimming depth range, the vertical motility rate dictates the speed of vertical migration, and the individual particle conditions dictate the rules that are applied. Particles are mutually exclusive; there is no interaction or communication among them that may affect each other's transport.

The vertical movements of the particles are composed of a sequence of light-induced vertical migration and flow-induced vertical advection repeated twice daily. The former is a fixed-distance type of transport determined in combination with the luminosity condition and corresponding water depth limits, while the latter follows the former and runs indefinitely until the emergence of the cue for a switch back to migration. The switch between these two processes occurs with the change of luminosity in terms of day or night. Transport outcomes are computed at each timestep, and the particle locations are output three-dimensionally at half-hour intervals.

The DVM model is composed of two main entities:

- (1) the particles, each representing a single jellyfish, where a batch released together makes a population, all having the same migratory behaviour.
- (2) the model grid cells representing the host environment (described previously in the hydrodynamic model development section).

Particles are characterised by the following variables:

- unique identity number
- time
- location
- x, y, z position
- vertical motility rate

The properties that characterise a grid cell include:

- location [x,y,z],
- current speed [m/s],
- current direction [°],
- water depth/elevation [m],
- luminosity simplified to time of sunrise and sunset [time]

Though the hydrodynamics are resolved on a grid cell resolution, the particles are tracked at sub-grid resolution and are available at half-hourly intervals over the whole model domain. The DVM model runs in discrete time steps, with state variables updated at each timestep.

6.3.2.1. Input data

Five types of input data are required by the DVM model:

- (1) hydrodynamics to impart advection to the model particles,
- (2) particle release information (e.g. location, time and depth of release)
- (3) exact times of sunrise and sunset (luminosity) to cue the diel vertical migration (DVM),

- (4) diel migration depth threshold (DMT) that divides the water column into two preferred,
- (5) buffer zone limits which determine the extent of the water surface and seabed buffer zones
- (5) jellyfish vertical motility rate (JMR), which specifies the DVM speed

The DVM submodel was coupled online with the EFDC model's hydrodynamic data to supply the hydrodynamic information needed at every time step to resolve the drift-induced displacements of the particles within three-dimensional space. The particle release data were taken from the observed reference jellyfish releases. A database of daily sunrise and sunset times for the simulation period for the study site (here the Galway-Mayo area where the Killary fjord is located) was sourced online (here <https://sunrise.maplogs.com> although data from a local weather station could also be used if available) to let the model distinguish the daylight cycles for initiating the DVM of the virtual jellyfish (particles). The DMT and JMR values were varied for different modelled scenarios and were manually defined. The buffer zone limit is also manually defined but was kept constant at 0.5 m below the water surface and above the seabed. With the exception of the hydrodynamics, all input data were communicated into the model through input files using distinct subroutines.

6.3.3. Scenario Modelling

For scenario planning and initialisation of particle transport simulation in the model, we use the reference from a prior field investigation in Killary (described in Chapter 5), where every released jellyfish featuring a uniqueness constitutes an individual reference for the model simulation at the required stages of the investigation. Particles representing adult jellyfish were released into the DVM model according to the reference. To investigate how individual variations in jellyfish influence their transport patterns, each reference jellyfish was modelled individually by scheduling a single release event per simulation to help compare with the individual reference. Batches of 100 particles, each representing a single reference jellyfish, were released in the model on 20 Aug 2015 at their corresponding tide time, and

simulations were run for a period corresponding to the tracked record of the reference jellyfish ranging from 1 to 7 days.

6.3.3.1. Assessing Model Sensitivity

Upon developing the DVM submodel of jellyfish, its sensitivity to behavioural integration, particle release conditions, DVM parameters, and indirectly the individual variation of jellyfish was tested by varying their specifications in various scenarios. A summary plan of the sensitivity study is presented with their specifications and assessment strategies in Table 6.2.

Table 6.2 Sensitivity study plan for the DVM model.

Sensitivity Studied	Specification	Method of assessment of model output
DVM parameters		
JMR (with 5 m DMT)	0.005 m/s	RMSE ¹ ; Transport agreement
	0.010 m/s	
	0.020 m/s	
DMT (with 0.02 m/s JMR)	2.5 m	RMSE ¹ ; Transport agreement
	5.0 m	
	7.5 m	
Particle release conditions		
Particle releasing depth	Surface	RMSE ¹
	First-quarter	
	Mid	
	Third-quarter	
Model setup		
Jellyfish behaviour	Without DVM	Transport agreement
	With DVM	
¹ RMSE of centroid trajectories of transported particles		

No studies specifically document the routine vertical swimming speed of a population or progressive swarm of jellyfish. So, estimations from other publications and studies performed on various species-specific jellyfish were used in the current scenario planning, mainly based on field observation of *Periphylla periphylla* in a Norwegian fjord by Kaartvedt et al. (2007). Thus, a JMR of 0.02 m/s was used here, irrespective of the time of the day, the state of the tide, and the vertical direction of the migration. The speed rate was lowered (Table 6.2) to investigate if the migration pattern was sensitive to the parameter. A similar drifter experimentation protocol, which was used earlier for the non-DVM jellyfish transportation (described in Chapter 5), was also followed in this case.

6.3.3.2 Assessing Model Performance

Analysis of transport agreement with the observations and comparison of DVM model outputs with that of the basic passive drift model was done following the protocol previously used and described in Chapter 5.

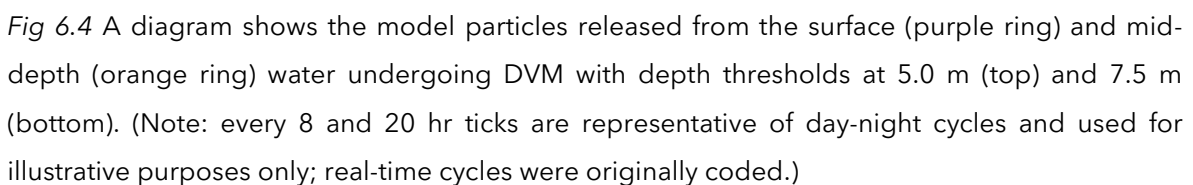
6.4. Results

The results section is divided as follows. Before proceeding with any DVM model scenarios, the competence of the newly developed biophysical model in simulating the diel vertical migration (DVM) of jellyfish was first assessed to ensure the new model code was appropriate and the sensitivity of the DVM model to swim speed, and threshold depth was assessed. The effect of DVM on the particle transport pattern and distribution was then assessed by comparison with the passive drift scenario results. The results of these assessments are presented in the following sections.

6.4.1. Testing the DVM Code

Following the development of the DVM model code, primary attention was given to checking if the DVM behaviour of jellyfish was being simulated properly so as to provide confidence in the development of the sub-model and its integration with

the base hydrodynamic model. This was done by visual inspection of the modelled particles' depth distribution by illustrating their vertical positions over a series of day-night cycles for the period of simulation. Three model scenarios were run using different threshold depths of 2.5 m, 5.0 m, and 7.5 m; the latter two were used for visualisation purposes. Fig 6.4 shows the variation of particle depths with time over a 7-day period from their time of release. They are initially released during daylight hours, so they immediately swim downwards until below the threshold depth. After that, their sequential ascent and descent with night and day can be clearly seen as they mimic the jellyfish DVM behaviour. The pattern of the particle distribution in the figure confirms that the particles dive to a deeper depth during the day and rise again during the night according to a defined threshold depth of luminosity and the time of sunrise and sunset. The plots provide clear evidence that the developed DVM model can simulate the light-induced movement of the virtual jellyfish (particles) and their roaming within the layers of preferred luminosity, thus confirming the validity of the new model code.



In biological entity modelling, individual variations of the entities, such as variations of their physical or biological properties with growth, can be hard-wired into the model code; this is popularly known as IBM (individual-based modelling). However, variations in physical or biological properties can also be investigated indirectly at the scenario modelling stage of the simulation by changing such properties in the

input data file. This can create a simple way of investigating the effects of individual variations. The current biophysical model is based on this indirect approach.

Among individual variations in traits, jellyfish size may be of the main interest as this has both direct (e.g. bell pulsation) and indirect (e.g. buoyancy) influence on the swimming speed and migration depth, respectively (Rahi et al., 2020). Other non-specific variations among individuals may also have similar modulation potential on these properties. IBM handles this process in two stages: (1) a variable (e.g. growth) modulates a property (e.g. swimming speed) according to the process equation coded in the model, and (2) the modulation, in turn, influences transportation as an effect of their correlation. In contrast, in the current biophysical model, a range of property values (e.g. range of swimming speeds) is assigned by the user manually at the model data input stage, and multiple simulations are conducted to investigate their influence on transport via comparative output. We call this approach 'fixed' or 'static' IBM. Some major properties relevant to the DVM are parameterised. Details of those scenario investigations and analyses are presented in the following subsections. The model sensitivities were assessed for Jellyfish IDs 18495, 18500, and 1162.

6.4.2.1 Jellyfish Motility Rate (JMR)

The sensitivity of the horizontal and vertical transport to the vertical migration speed of the jellyfish (parameterised as jellyfish motility rate (JMR)) was investigated to check how the individual variation in motility influences their transport. An acoustic survey of *Periphylla periphylla* species by Kaartvedt et al. (2007) resulted in the vertical migration velocity of the jellyfish being 0.02 m/s at any time in both directions. Based on this, three different JMRs were simulated in this study:

- DVM Scenario 1 - JMR = 0.005 m/s
- DVM Scenario 2 - JMR = 0.010 m/s
- DVM Scenario 3 - JMR = 0.020 m/s

For each simulation, 100 particles were released at a water depth (surface, first-quarter, mid, and third-quarter) from the release location of jellyfish ID 18495, and

the simulations were run for 7 days. The diel migration threshold depth was set to 5 m for all three DVM simulations. To compare the differences in particle locations, the centroid of the 100 particles was computed and plotted every 30 minutes. The easting, northing and depth of the centroids of the particle clouds from the 3 DVM scenarios plotted against time are presented in Fig 6.5. The results from the corresponding passive drift scenario are also included for comparison. The graphs show a significant difference between the DVM and passive drift scenarios. Within about the first 75 hrs of the particle release, the centroid locations are all quite similar, as shown by the overlaying trajectory lines; however, after that, the DVM centroids move much further westward and northward. Particles were pushed farther on the side of the sea than the passive particles, which moved the DVM centroids further west. Fig 6.6 shows a comparison of all particle locations for a DVM scenario with those from the passive drift scenario at 109 hrs after particle release. The figure shows that the differential transport in the centroids of the centroids of the particle clouds was because many DVM particles were separated from the main body of particles and moved by the stronger surface current flows towards the sea. As the clusters of the DVM particles move apart, their centroid starts moving west and north (Fig 6.5). Later in the simulation, at about 120 hrs, the seaward moving particles in the DVM scenarios start to leave the domain across the open sea boundary. When this happens, the particles are removed from the simulation, and so the DVM centroids move back eastward and southward since most of the remaining particles are in the inner harbour at this stage. Based on the centroid trajectories, the model was sensitive to the inclusion of DVM, as it significantly influenced the particle distribution and their net transport.

The above observations are further corroborated by the RMSE values shown in Fig 6.5, which compare the mean RMSE in easting, northing and depth of the particles' centroids between the different simulations. The first three RMSEs listed in each figure compare the passive drift model with the three DVM models, while the bottom three values intercompare the DVM models. The first three values are much larger than the second three for easting, northing and depth, confirming the significant influence of DVM on particle transport. Looking at the bottom three

values for the DVM inter-comparison, there is relatively little difference between these, suggesting that the DVM model is not very sensitive to the JMR. Finally, looking at the depths of the centroids, it can be seen that there is much more variation in the depth of particles for the DVM scenarios compared to the passive drift. This was expected as the passive drift particles can only be transported vertically by the ambient vertical velocities, but the DVM particles are imparted with vertical migratory swimming ability.

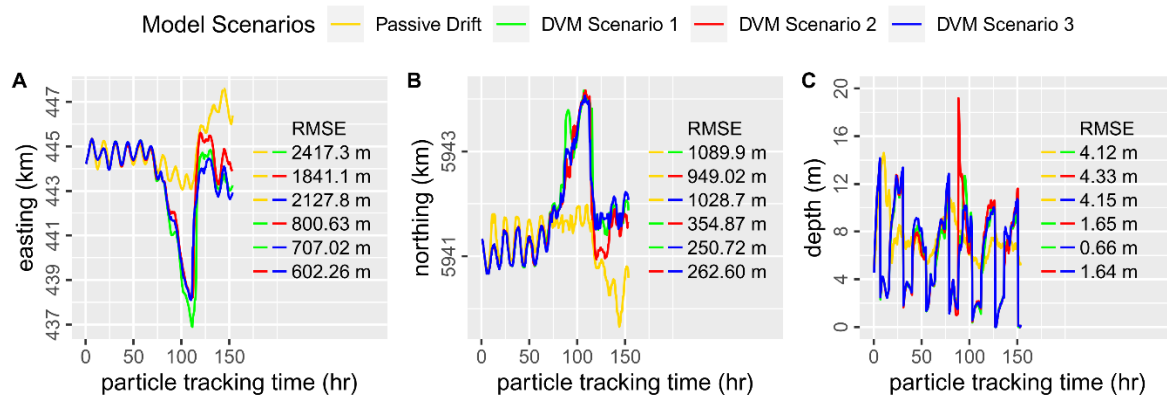


Fig 6.5 Centroid trajectories and RMSE of JMR scenarios in the (A) east-west, (B) north-south, and (C) vertical directions.

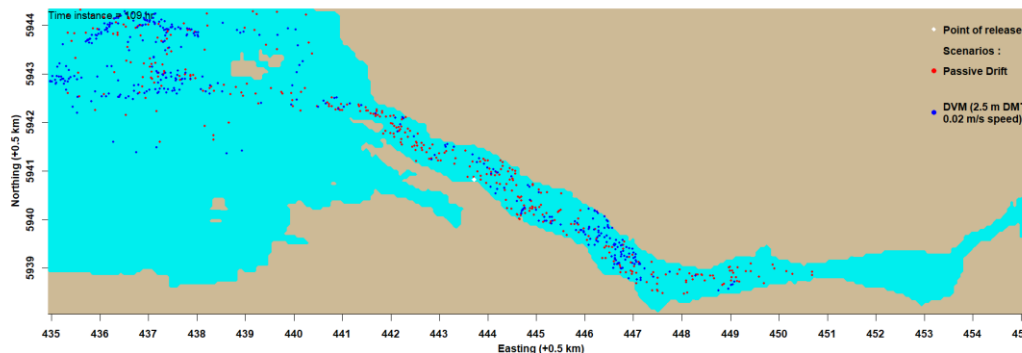


Fig 6.6 Snapshot of distributions of the passive drift and DVM particles at 109 hr after their release.

6.4.2.2 Diel migration depth threshold (DMT)

The sensitivity of the horizontal and vertical transport to the vertical migration threshold depth of the jellyfish (parameterised as the diel migration threshold (DMT)) was investigated to check how individuals featuring variable buoyancy-

regulated depth migration might influence transport. Three different DMTs were simulated:

- DVM Scenario 3 - DMT = 5.0 m
- DVM Scenario 4 - DMT = 2.5 m
- DVM Scenario 5 - DMT = 7.5 m

During the daytime, jellyfish were forced to swim downward and remain below the DMT, while at nighttime, they were required to swim upward and remain above the DMT. For all three scenarios, 100 particles were again released from four depth quarters from the release location of jellyfish ID 18495, and the JMR was set to 0.02 m/s. Fig 6.7 shows the eastings, northings, and depths of the centroids of the particle clouds from the 3 DMT scenarios plotted against time. Once again, the DVM scenarios show a significant difference from the passive drift scenario. We see a similar trend to the JMR scenarios where the eastings and northings are quite similar up to about 75 hrs, after which they deviate quite significantly. As with the JMR simulations, the DVM particles split at about 75 hrs with a cluster of particles moving seaward. However, this only happens for Scenarios 3 and 4 but not for Scenario 5. The centroid trajectories of Scenarios 3 and 4 subsequently remain quite similar until about 125 hrs, where a noticeable difference occurs. For both these scenarios, the breakaway particles have now left the model domain across the seaward boundary, and the remaining particles are spread across the inner harbour; however, the remaining particles from Scenario 4 are clearly located more eastward and southward than those of Scenario 3. The results clearly indicate the model is sensitive to the DMT and that variations in its value can significantly affect particle distribution and transport.

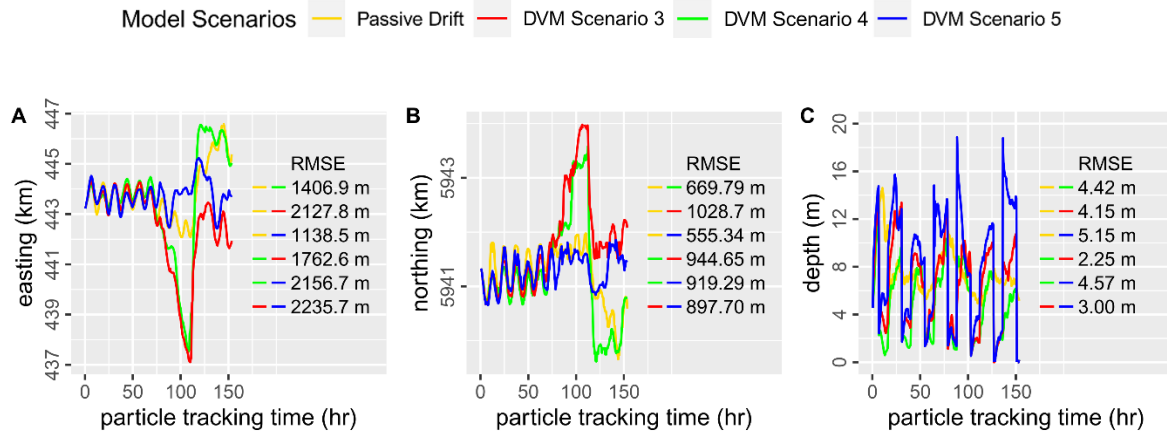


Fig 6.7 Centroid trajectories and RMSE of DMT scenarios in the (A) east-west, (B) north-south, and (C) vertical directions.

6.4.3. Sensitivity to Particle Release Depth

It would be expected that jellyfish positioned at different depths of water and, therefore, driven by different horizontal currents will be transported differently. This was one of the reasons for investigating the influence of DVM on model performance. However, another important stage of the model simulation with regard to the depth of the particles is the moment of particle release. Depending on whether a particle was released at the water surface or further down in the water column, it was hypothesised that the varying currents at different depths would likely result in different transport patterns. DVM scenario 4 was used to investigate this hypothesis by rereleasing 100 particles at four different depths as follows:

- 1) At the surface
- 2) At one-quarter of the total water depth below the water surface
- 3) At mid-depth
- 4) At three-quarters of the total water depth below the water surface

For the four scenarios, the centroid trajectories of the particle clouds were tracked every half an hour and are plotted in Fig 6.8 with an estimation of RMSE between the trajectory coordinates.

The trajectories and RMSE estimations in the figure show the sensitivity of the DVM-induced transport patterns to the particle-releasing depth. The results show that the release depth does indeed affect particle transport; more interestingly, it does so in both the short term and the long term. According to the figure, the differences in centroid location are greatest in the east-west direction; the differences are relatively minor along the north-south and vertical directions. This is understandable as the primary direction of particle transport is east-west. Looking at the easting centroid coordinate plot, there is a noticeable trend with release depth. Easting locations are quite similar for the release locations in the upper half of the water column (surface and 1st quarter release depths). They are also quite similar for the release locations in the lower half of the water column (mid-depth and 3rd quarter-release depths). Still, the easting trajectories for the upper and lower-half release depths are noticeably different. This is most likely due to wind influence on the surface currents. The RMSEs confirm this observation, with RMSEs being lowest between the surface and 1st quarter release depths (719.34 m for easting) and the mid-water and 3rd quarter release depths (716.55 m for easting) and highest for and highest for 1st quarter versus 3rd quarter release depths (1,901.6 for easting).

One can see some differences in centroid trajectories during the first tidal cycle after particle release, but apart from these, the centroid locations are all quite similar within the first 70 hrs of their release, as shown by the overlying trajectory lines in Fig 6.8. As discussed in the previous sections, about 70 hours after their release inclusion of DVM resulted in the particles splitting into two clusters which moved apart in opposite directions causing the centroid of the particles to move westward, as shown in the easting plot. There is a clear difference in the easting location of the centroids of the particles released in the upper half of the water column compared to the bottom half. Upon investigation, it was found that for the upper-half releases, the number of particles in the cluster that left the harbour was smaller than that of the clusters that left the harbour in the lower-release scenarios. This was due to differences in the spatial distributions of the particles as they neared the mouth of the harbour.

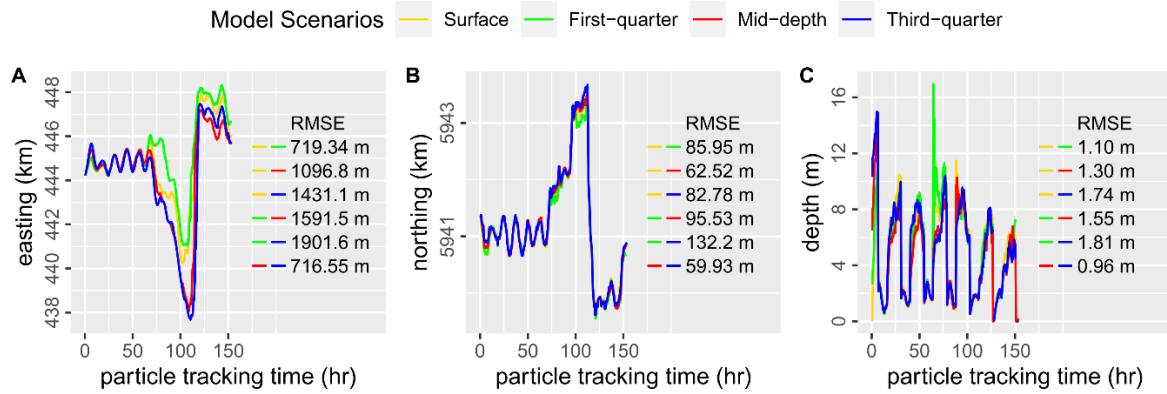


Fig 6.8 Centroid trajectories and RMSE of release depth scenarios in the (A) east-west, (B) north-south, and (C) vertical directions.

6.4.4. Assessment of DVM Accuracy Versus Passive Drift

The hypothesis for including diel vertical migration in the model was that coupling any behavioural transport with the basic passive drift would improve the agreement of modelled transport with the observed jellyfish transport. At the very least, it was intended that the results would provide learning and insights into the influence of DVM on jellyfish transport. Thus, the transport patterns and agreement of the modelled particles with the observed jellyfish were compared across the 5 DVM models presented in the previous sections and with the passive drift models. While five different jellyfish releases were simulated, just three are presented here. These were selected as they were the three jellyfish with the longest sets of observations. Based on the trajectories and RMSE in Fig 6.8, the model was sensitive to the particle releasing depth, and the sensitivity was most apparent for particles released in the upper half of the water column versus particles released at mid-depth or below. Thus, for the following performance assessments, particles were released at both the surface and mid-depth.

6.4.4.1. Jellyfish J-18495

Observation records for J-18495 were for 139 hours, covering multiple tidal cycles. Sample snapshots of the distribution of particles 120 and 133 hrs after their release

are shown in Fig 6.9 and compare the distributions of particles released at different depths between DVM Scenario 4 and the passive drift scenario. The black circle at Easting 448.5 km shows the range of the location and the range of the detector (S1) that observed the jellyfish at that time. While the snapshots show lots of variation in particle locations between the scenarios and for different release depths, there is clearly a higher density of particles near the detector for the DVM scenario than for the passive drift scenario. In the DVM scenario, the particle cloud in the harbour is approximately centred around the detector, while in the passive drift scenario, the particle cloud is centred west of the detector. Passive drift relies solely on the influence of currents and wind forces to direct particles toward specific destinations at particular times. A more realistic hypothesis takes into account the possibility that jellyfish exhibit forms of motility, such as Diel Vertical Migration (DVM), in addition to passive drift. The fact that particles sample different horizontal velocities at different water depths as they migrate results in difference in their overall transport relative to a simple passive drift scenario. In the provided snapshots, it becomes evident that the behaviour of particles undergoing DVM-driven passive transport differs significantly from those undergoing passive transport alone. DVM particles tend to aggregate, forming localized density patterns, in contrast to the more diffuse spreading observed in passive transport. These DVM particles appear to align themselves with the prevailing current flows and adapt their movements according to their motility strategy. This snapshot offers qualitative evidence that the DVM scenario is better able to predict the transport path of this particular jellyfish; however, it was also important to try to assess model performance using quantitative measures, which was not trivial given the large variations in particle locations.

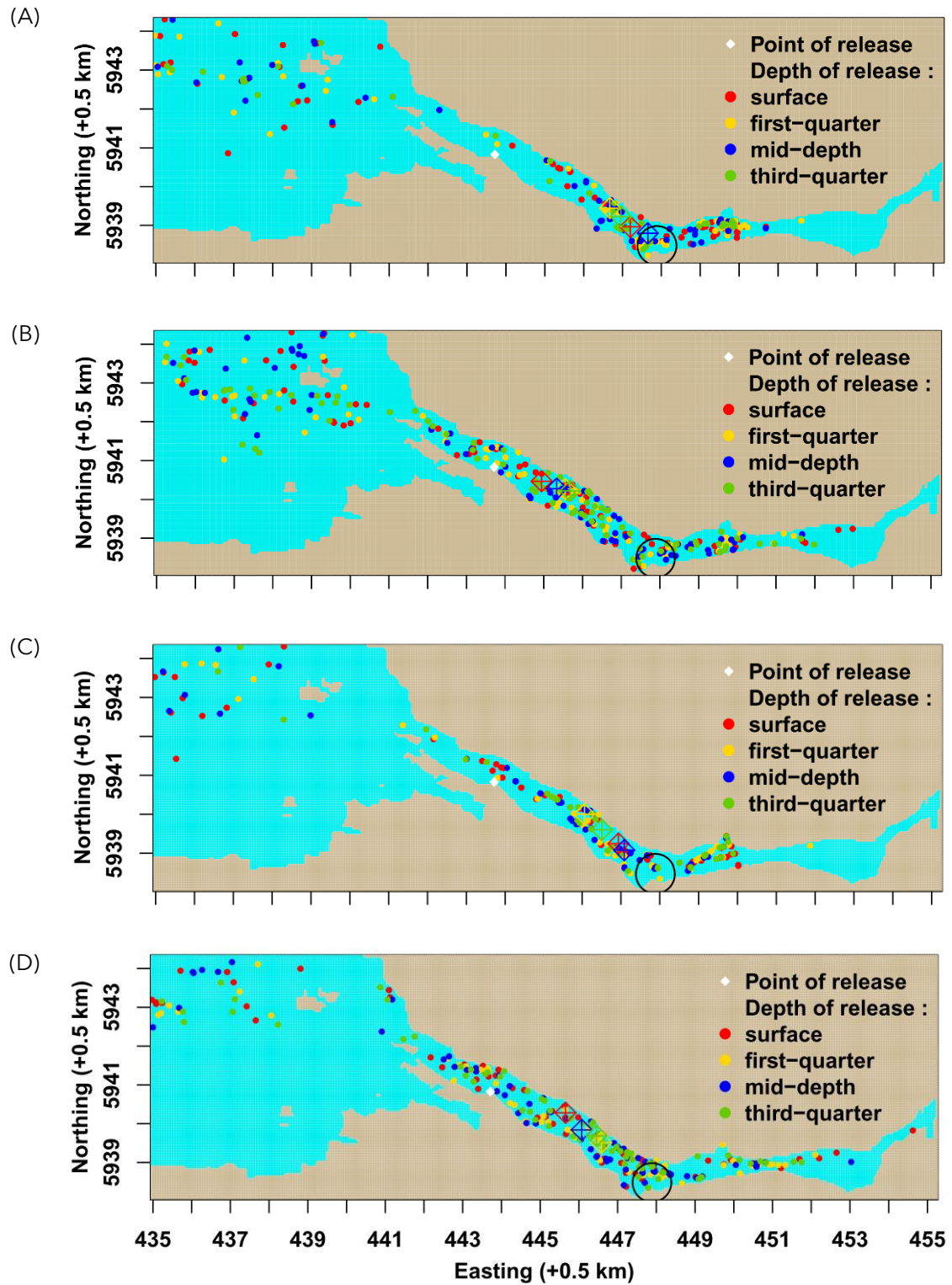


Fig 6.9 Snapshots of particle locations 120 and 133 hr after their release for (A & C) DVM Scenario 4 and (B & D) passive drift scenario. The black circle marks the S1 detector range. The centroids of the particles released at different depths are marked by coloured diamonds (some are overlapping).

Chapter 6: DVM Modelling

Two main measures of model performance were developed. These were: (1) the percentage of particles within the model domain that were located within the range of the detector that recorded the presence of J-18495 at a particular time, and (2) the distance of the centroid of the particles in the domain from the centre of the relevant detector's range. The first is used to determine the percentage of modelled particles that are present at the correct location at the correct time, and the second is used to determine how close all of the particles are to the correct location at the time of observation. Some particles may leave the domain during a simulation by passing across the sea boundary. These are permanently removed from the simulation. Some particles may become beached. Therefore the number of particles in the domain may reduce over time. The number of available particles in the domain is an important factor because the percentage agreement performance metrics are calculated based on this number; therefore, it was also calculated. Tables 6.3a and 6.3b present the quantitative for the DVM and passive drift scenarios for surface-released and mid-depth released particles, respectively.

As Table 6.3 shows, in the short term (up to 11 hours), 100% of the particles were present within the domain. This is to be expected as the particles have not travelled far from the release point at this stage. Longer-term (after 120 hours of approximately), between 23~76 % of the surface released particles and 14~79 % of the mid-depth released particles left the domain, depending on the scenario. For all DVM scenarios except the mid-depth release for DVM Scenario 5, particle retention is lower for the DVM scenarios than the corresponding passive drift scenario. This is due to the observation in previous sections that the introduction of DVM causes a cluster of particles to leave the harbour and travel westward towards the sea boundary, where they eventually leave the domain. This is likely due to the diel migration forcing particles to spend longer times near the surface than in the passive drift model, where they are exposed to stronger currents. Of all the DVM scenarios, those for Scenario 5 with the deepest migration threshold give the highest retention levels and are similar to those of the passive drift scenarios. This is like due to particles spending more time in deeper water where they are exposed to lower currents. The particle retention is seen to be impacted by a combined effect

of relative exposure and time spent within high, moderate, and low flow speeds regulated by depth migration and horizontal travel, and different initial drives at different depths mapping particles in horizontal space. Different particle retention capacities of different scenarios indicate that a higher capacity would increase the chance of transport agreement. Thus, this factor has important consequences for jellyfish transport modelling performance.

Percentage agreement is considered here the most important measure of the transport model performance as it directly estimates a one-to-one match of the modelled and observed jellyfish locations. According to Table 6.3, the percentage agreement of modelled particles with observations varied significantly during simulations and across the scenarios. In the time shortly after particle release (3~11 hr after particle release), agreement is at its highest and was between 70~100 % in 60 % of detection instances; however, longer term (120~133 hr after release), the percentage agreement was significantly lower, ranging from 0~15.56 % with the highest agreement of 15.56 occurring for DVM Scenario 4. To make it easier to compare the metrics of performance (i.e. percentage agreement and centroid distance) between scenarios, the values are plotted against time for the short term (3-11 hrs) and longer term (120-133 hrs) in Fig 6.10. Looking at Fig 6.10A, which shows percentage agreement, it can be seen that for the surface releases, the passive drift model performance is better for most of the short term than the DVM scenarios, but at hour 11, DVM agreements are all slightly higher (70-80%) than the passive drift (56%). For the mid-depth releases, there is very little difference in the performance of the DVM and passive drift models in general, but the DVM agreements are again mostly higher at hour 11. In the longer term, DVM Scenario 4 is the best-performing scenario. It yields consistently higher agreements for surface releases and for most of the time for mid-depth releases, although its performance does deteriorate in the latter stages for the mid-depth releases.

The second measure of model performance was the centroid distance, which measures model performance by assessing the proximity of particles to the desired (i.e. the observed) location rather than by assessing a direct match of modelled and

observed positions. The best part of this strategy is that it takes account of the positions of those particles that may have travelled generally in the same direction as the jellyfish but did not make it into the desired detector's range. The distances presented in Table 6.3 a and b are presented graphically in Fig 6.10. Looking at Fig 6.10, it can be seen that the centroids of modelled particles are much closer to the desired detector range in the short term than in the long term. This is to be the primary influencing process in the short term is passive drifting due to horizontal currents. For surface release, the passive drift and DVM Scenario 4 models perform best in the short term, with centroid distances being close to zero, indicating that the centroid of the modelled particles is just outside the detector range. For mid-depth releases, the centroid distances are very similar, with a short-term mean distance of approximately 200 m. Looking at the long-term model performance, there is significant variation in centroid distances, but regardless of the depth of particle release, DVM Scenario 4 outperforms all other DVM models and the passive drift model, particularly for the surface release scenarios. The mean distance of the centroid of DVM Scenario 4 modelled particles from the desired detector range is 1.5 km for the surface release scenario and 1 km for the mid-depth release. The centroid distance results are broadly in line with the percentage agreement results and confirm that DVM Scenario 4 gives better model performance than the passive drift model.

Chapter 6: DVM Modelling

Table 6.3a A comparison of model performance metrics for surface particle releases for J-18495.

Detector	Detection time (hr)	Model scenarios																	
		Scenario 1 JMR = 0.005 m/s, DMT = 5 m			Scenario 2 JMR = 0.010 m/s, DMT = 5 m			Scenario 3 JMR = 0.020 m/s, DMT = 5 m			Scenario 4 JMR = 0.020 m/s, DMT = 2.5 m			Scenario 5 JMR = 0.020 m/s, DMT = 7.5 m			Scenario 6 Passive drift		
		1	2	3	1	2	3	1	2	3	1	2	3	1	2	3	1	2	3
S4	3	100	100.0	0	100	100	0	100	100	0	100	100	0	100	100	0	100	99	0
S4	4	100	100.0	0	100	100	0	100	100	0	100	100	0	100	98	0	100	100	0
S4	5	100	93.0	0	100	93	0	100	93	0	100	100	0	100	43	31	100	100	0
S4	6	100	70.0	0	100	69	0	100	72	0	100	100	0	100	27	153	100	100	0
S5	8	100	0.0	594	100	0	583	100	0	585	100	0	298	100	0	863	100	27	110
S5	9	100	0.0	313	100	0	305	100	0	307	100	3	106	100	0	524	100	86	0
S5	11	100	74.0	0	100	81	0	100	79	0	100	62	0	100	74	0	100	57	0
S1	120	37	2.7	4045	52	0	9517	34	2.94	4521	64	7.81	338	72	2.78	3275	77	7.79	3048
N1	125	27	0.0	4878	32	3.12	4581	26	0	4812	58	15.52	1271	56	0	4010	68	2.94	3847
N1	129	27	0.0	4660	29	3.45	4268	25	0	4588	56	10.71	1068	55	0	4054	65	4.62	3384
N1	130	27	0.0	4640	29	0	4223	25	0	4587	55	9.09	972	55	0	3980	65	4.62	3110
N1	131	27	3.7	4814	29	3.45	4427	25	0	4759	55	7.27	1108	55	0	4143	65	4.62	2948
S1	133	26	0.0	4691	27	0	4381	24	0	4663	55	10.91	791	54	1.85	4198	63	9.52	2367
Column headings: [1] Number of particles available in the domain, [2] Percentage of available particles agreed to the reference jellyfish (calculated with respect to the column of the block marked by 1), [3] Centroid distance (m) from the periphery of the respective detector																			

Chapter 6: DVM Modelling

Table 6.3b A comparison of model performance metrics for mid-depth particle releases for J-18495.

Detector	Detection time (hr)	Model scenarios																	
		Scenario 1 JMR = 0.005 m/s, DMT = 5 m			Scenario 2 JMR = 0.010 m/s, DMT = 5 m			Scenario 3 JMR = 0.020 m/s, DMT = 5 m			Scenario 4 JMR = 0.020 m/s, DMT = 2.5 m			Scenario 5 JMR = 0.020 m/s, DMT = 7.5 m			Scenario 6 Passive drift		
		1	2	3	1	2	3	1	2	3	1	2	3	1	2	3	1	2	3
S4	3	100	100.0	0	100	100	0	100	100	0	100	100	0	100	100	0	100	99	0
S4	4	100	99.0	0	100	99	0	100	99	0	100	99	0	100	99	0	100	100	0
S4	5	100	59.0	0	100	59	0	100	59	0	100	59	0	100	51	0	100	100	0
S4	6	100	39.0	75	100	40	70	100	40	68	100	41	67	100	27	127	100	100	73
S5	8	100	0.0	769	100	0	772	100	0	762	100	0	768	100	0	807	100	27	800
S5	9	100	0.0	457	100	0	455	100	0	452	100	0	472	100	0	519	100	86	489
S5	11	100	52.0	1	100	55	0	100	64	0	100	19	79	100	61	0	100	57	0
S1	120	41	0.0	10463	51	0	4604	64	3.12	3661	49	6.12	1047	86	18.6	1933	76	7.89	2433
N1	125	26	0.0	5078	37	0	3980	59	0	4973	45	15.56	2199	77	0	2742	69	2.90	3070
N1	129	23	0.0	4897	36	2.78	3779	57	1.75	4665	41	14.63	2224	76	0	2678	65	4.62	2272
N1	130	23	0.0	4907	36	2.78	3740	57	1.75	4597	41	4.88	2143	76	2.63	2723	66	4.55	2185
N1	131	22	0.0	4977	36	0	3827	56	1.79	4729	41	2.44	2188	76	2.63	2873	66	4.55	2126
S1	133	21	0.0	4955	35	2.86	3789	55	3.64	4689	41	4.88	1874	76	0	2650	62	9.68	1165
Column headings: [1] Number of particles in the domain, [2] Percentage agreement of modelled particle locations with observations (calculated with respect to column 1), [3] Distance (m) of the centroid of all particles from the desired detector.																			

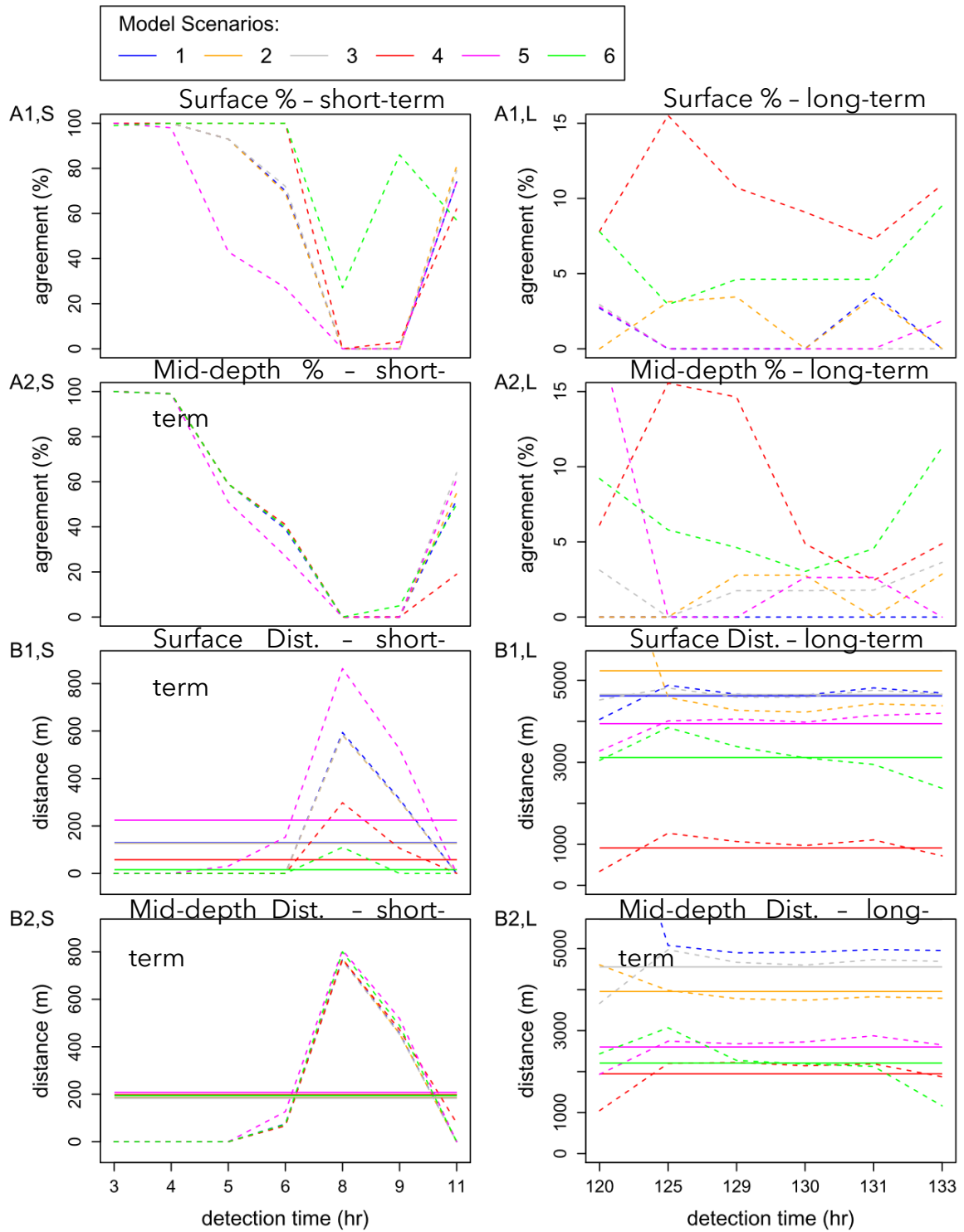


Fig 6.10 Comparing agreements as per J-18495 among the transport scenarios in terms of (A) percentage and (B) centroid distance for (1) surface and (2) mid-depth released particles over the short-term (S) and long-term (L) simulation periods. Real estimations are represented by the dashed lines and calculated means by the solid lines. [Notes: Specifications for the model scenarios are in Table 6.3. Centroid distances are from the periphery of the respective detectors.]

To gain some insight into the reasons for the differences in model performance metrics, Fig 6.11 shows the percentages of particles located within a detector's range at the times of the jellyfish observation for (1) the passive drift model, (2) the DVM Scenario 4 and (3) DVM Scenario 3. The figure helps to explore the variability in particle distribution patterns across the model scenarios. While particle distributions are similar in the short term, distributions in the longer-term period vary. For the passive drift model, particles have spread almost uniformly in both directions along the length of the harbour, while for DVM Scenario 4, particles are more concentrated in the inner harbour nearer the desired detectors S1 and N1. By contrast, comparing these distributions with DVM Scenario 3, which performed poorly, it can be seen that for DVM 3, the particles are more concentrated in the outer half of the harbour resulting in its poorer performance.

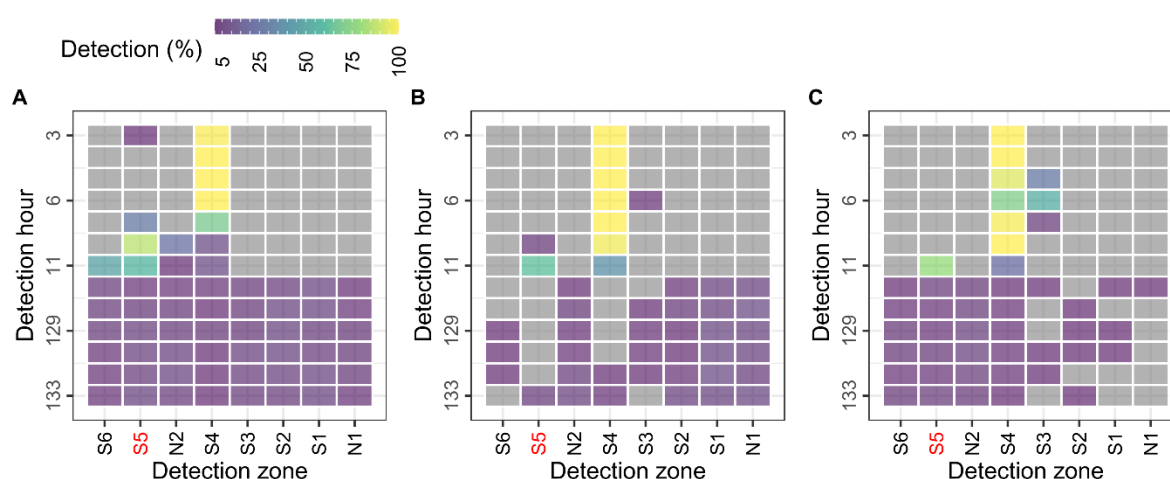


Fig 6.11 Spatiotemporal detections of the surface-released particles as per J-18495 model jellyfish detections in (A) passive drift, (B) DVM with 2.5 m threshold (Scenario 4), (c) DVM with 5.0 m threshold (Scenario 3) scenarios.

6.4.4.2. Jellyfish J-18500

Jellyfish J-18500 had 52 hours of observational records for comparison with model data. Its release was simulated using the passive drift model and DVM Scenario 4, which was determined as the best-performing DVM model for both short-term and longer-term modelling of J-18495. Particles were again released at the surface and in the middle of the water column. The percentage agreements of particles with the

Chapter 6: DVM Modelling

desired detector location and the centroid distances of the particles to the desired detector are presented in Table 6.4 and summarised graphically in Fig 6.12.

Given the relatively short length of observational data (52 hrs), no particles left the domain across the sea boundaries, so 100% of particles were present in the analyses. Looking first at the percentage agreement of particle locations with observed location, it can be seen that model performance was noticeably poorer than for J-18495. In particular, the DVM model performed very poorly, with percentage agreements of zero or close to zero for most of the 52 hours of particle transport. Release depth had no noticeable effect on DVM model performance. The passive drift model performed noticeably better than the DVM for surface-released particles, but its performance was only marginally better than the DVM for mid-depth release. By hour 52, the percentage agreement of the surface release passive drift model was just 16%, and the maximum agreement reached during the 52 hours was just 40% at hour 4.

Table 6.4 A comparison of model performance metrics of surface and mid-depth particle releases for J-18500.

Detector	Detection time (hr)	Model scenarios											
		Surface released particles						Mid-depth released particles					
		Scenario 4 JMR = 0.020 m/s, DMT = 2.5 m			Scenario 6 Passive drift			Scenario 4 JMR = 0.020 m/s, DMT = 2.5 m			Scenario 6 Passive drift		
		1	2	3	1	2	3	1	2	3	1	2	3
S5	2	100	0	437	100	37	229	100	0	476	100	0	489
S6	4	100	0	301	100	40	59	100	0	334	100	0	354
S6	6	100	3	106	100	25	0	100	0	168	100	0	201
S5	8	100	0	254	100	18	88	100	0	248	100	0	294
S4	10	100	0	674	100	3	725	100	0	684	100	0	731
S4	12	100	0	643	100	9	706	100	0	648	100	0	803

Chapter 6: DVM Modelling

S4	14	100	0	1197	100	12	1006	100	0	1239	100	0	1401
S4	16	100	0	1576	100	1	1780	100	0	1615	100	0	1985
S4	18	100	0	1579	100	1	1674	100	0	1588	100	0	1990
S4	20	100	0	1435	100	20	1029	100	0	1588	100	0	1537
S4	22	100	0	1400	100	24	626	100	0	1263	100	1.00	800
S4	24	100	0	1266	100	18	665	100	0	1182	100	1.00	699
S4	26	100	0	1670	100	15	845	100	0	1495	100	0	1237
S4	28	100	0	1849	100	9	1277	100	0	1888	100	0	1990
S4	30	100	0	1853	100	9	1350	100	0	1877	100	0	2063
S4	32	100	0	1523	100	23	949	100	0	1546	100	2.00	1625
S4	34	100	2	1031	100	22	663	100	1	1056	100	6.00	1010
S4	36	100	2	936	100	18	782	100	2	950	100	7.00	825
S4	38	100	0	1353	100	22	878	100	0	1439	99	4.04	1217
S4	40	100	0	2022	100	9	1387	100	0	2055	99	0	1943
S5	42	100	3	1245	100	25	543	100	1	1280	99	8.08	1193
S4	44	100	0	2079	100	15	1171	100	0	2075	99	1.01	1952
S4	46	100	1	1699	100	23	768	100	1	1740	98	4.08	1339
S4	48	100	2	1569	100	17	729	100	1	1424	98	8.16	1041
S4	50	100	1	1981	100	20	727	100	0	1915	97	5.15	1302
S4	52	100	0	2711	100	16	1053	98	0	2542	93	1.08	2016
<p>Column headings: [1] Number of particles in the domain, [2] Percentage of available particles agreed to the reference jellyfish (calculated with respect to the column of the block marked by 1), [3] Centroid distance (m) from the periphery of the respective detector</p>													

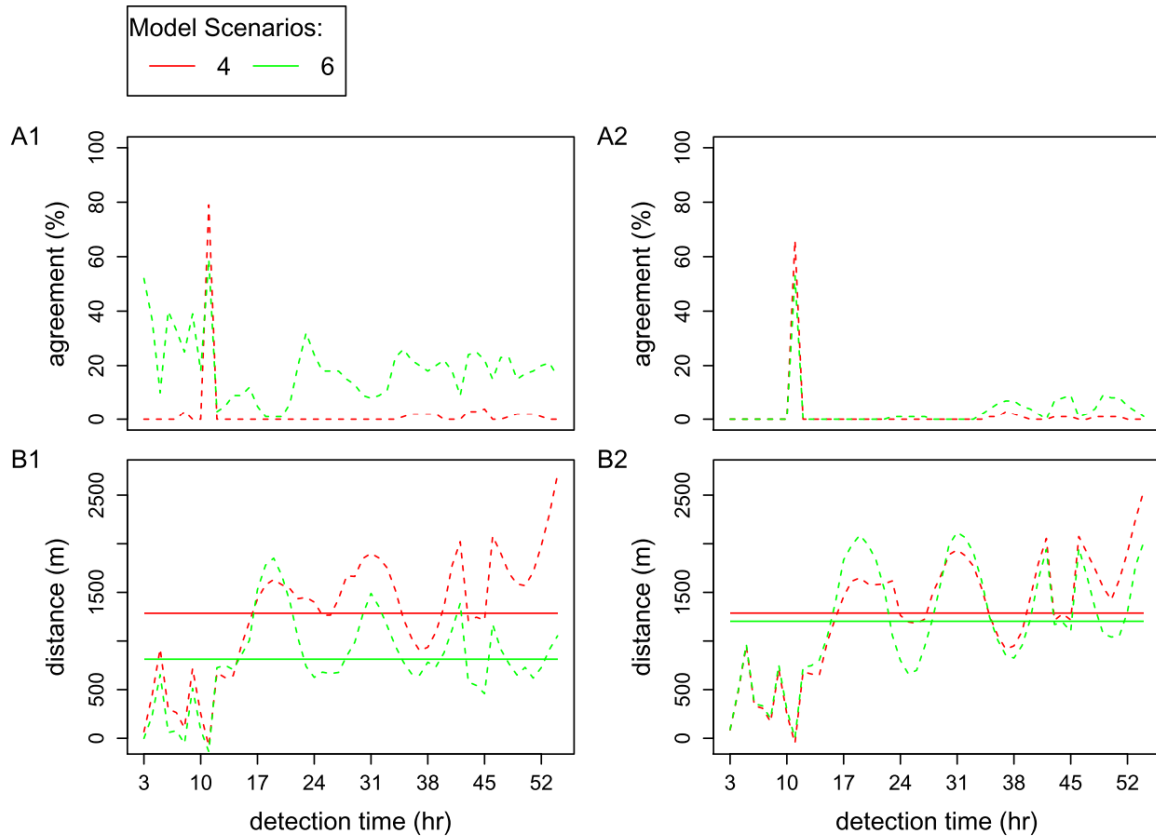


Fig 6.12 Comparing agreements as per J-18500 between the DVM and the passive drift transport scenarios in terms of (A) percentage and (B) centroid distance for (1) surface and (2) mid-depth released particles over the short-term (S) and long-term (L) simulation periods. Real estimations are represented by the dashed lines and calculated means by the solid lines. [Notes: Specifications for the model scenarios are in Table 6.4. Centroid distances are from the periphery of the respective detectors.]

A snapshot of the distribution of transporting particles can be illustrative of the performance results discussed above. For instance, the surface-releasing particles tracked at 52nd hr after the simulation show significant differences in percentage agreement and centroid distance. Fig 6.13 presents a snapshot of the modelled particle locations output from both models at that time. For both models, it can be seen that particles have spread a significant distance along the harbour. Passive drift particles have spread east and west of the release location (shown in white), and although they have travelled further in the westerly direction, there are still a sizable number of particles in the vicinity of the correct detector to the east of the release location. By contrast, the DVM particles are almost all located to the west of the

release location – this may be due to them being exposed to stronger surface currents on the ebbing tide.

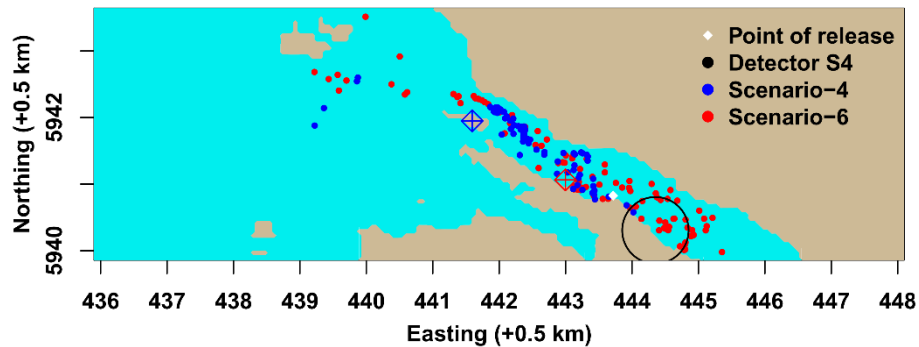


Fig 6.13 Snapshot of J-18500 modelled particle locations 52 hr after their release in Scenario 4 (DVM) and Scenario 6 (passive drift). The black circle marks the respective detector (S4) range. Coloured diamonds mark the centroids of the particles released at different depths.

The trend observed in the snapshot above is also apparent in Fig 6.14, which shows the percentages of particles located within a particular detector's range during the course of the simulation. Like the patterns in J-18495, the relative spreading of the particles was more extensive in the passive drift model than in the DVM. In the particle drift model, particles spread across five adjacent detectors from S3 to S6, whereas the spread of particles within the DVM was limited mostly within S5 and S6. This is the primary reason for the poor DVM performance; S5 is where the jellyfish was released, and S6 is west of that, but the jellyfish actually spent most of its time within the range of detector S4, which is to the east of release location. The conclusion is that the transport of this jellyfish appears to be more closely correlated to passive drifting.

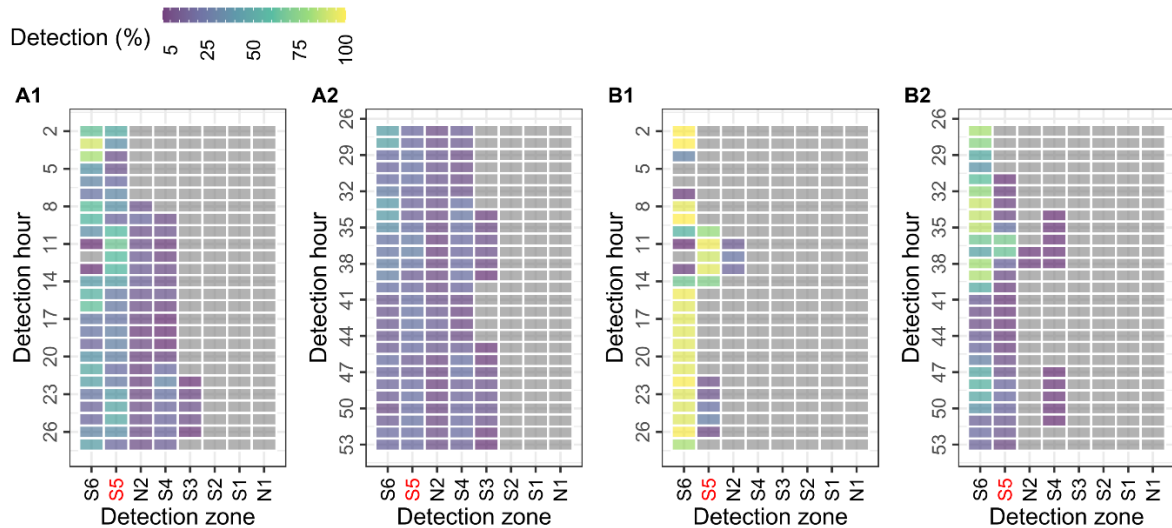


Fig 6.14 Spatiotemporal detections of the surface-released particles as per J-18500 model jellyfish detections in (A) passive drift, (B) DVM with 2.5 m threshold (Scenario 4) scenarios.

For J-18495, the models achieved very high levels of agreement with observed jellyfish location in the short-term, i.e. less than one tidal cycle after particle release, and lower levels of agreement in the longer term, i.e. multiple tidal cycles after particle release. By comparison, for J-18500, the model agreement was poor for both the long-term and short-term. This is possibly less surprising for the DVM model than for the passive drift, given that the length of a tidal cycle (approx. 12.5 hrs) is equivalent to a day or night diel cycle. If the jellyfish, in reality, is not following any diel migration or a migration pattern different to that programmed into the model, then modelled particle position may not correlate well with observations.

6.4.4.3. Jellyfish J-1162

J-18495 had 22 hrs of observation records. Particle releases to reproduce this jellyfish's transport were again conducted using (1) the passive drift model and (2) DVM Scenario 4. Agreement analyses of these scenarios are presented in Table 6.5 and visualised in Fig 6.15.

Particle retention was 100 % in all scenarios, which did not change due to the short period of simulation. Looking firstly at the percentage agreement of modelled particles with observations, agreement varies widely at different times during the 22

hours of observational records, and there were a number of times when the agreement was zero. Irrespective of the depth of release of particles, the passive drift model gives higher agreement than the DVM model in the early hours of the simulation (hrs 7-11), the DVM model gives better agreement for hrs 16-18, and then the passive drift model gives better agreement for hrs 21-22. Looking at the sensitivity of results to the release depth, DVM model agreement was higher for surface release than for mid-depth release, while for the passive drift model, surface particle release agreement was higher than mid-depth release agreement in the early hours, but this trend was reversed in the later hours. The latter suggests that there is some depth element at play in the transport of J-1162 rather than simple passive drifting. Overall, for surface particle release scenarios, location agreement levels were higher for the passive drift model, but for mid-depth releases, the DVM and particle drift agreement levels were similar.

With regards to the second performance metric - centroid distance - there was also much variation in this parameter over the course of the 22 hours after particle release. There were no discernible trends other than the centroid distances being low when the agreement levels were high, which is to be expected. Looking at the mean values over the 22 hours, the values for both models were quite similar for the surface releases at approximately 500 m, but the mean value for the passive drift model (approx. 500 m) was slightly lower than that for the DVM (approx. 600 m) for mid-depth releases.

Chapter 6: DVM Modelling

Table 6.5 A comparison of model performance metrics for surface and mid-depth particle releases for J-1162.

Detector	Detection time (hr)	Model scenarios											
		Surface released particles						Mid-depth released particles					
		Scenario 4 JMR = 0.020 m/s, DMT = 2.5 m			Scenario 6 Passive drift			Scenario 4 JMR = 0.020 m/s, DMT = 2.5 m			Scenario 6 Passive drift		
		1	2	3	1	2	3	1	2	3	1	2	3
S5	6	100	0	327	100	0	233	100	0	692	100	0	718
S5	7	100	0	168	100	54	0	100	0	459	100	0	452
S5	8	100	44	9	100	92	0	100	5	163	100	36	63
S6	10	100	0	750	100	54	0	100	0	726	100	8	247
S6	11	100	0	720	100	56	0	100	0	704	100	23	163
S6	13	100	0	903	100	3	515	100	0	901	100	0	478
S6	14	100	0	992	100	0	937	100	0	1028	100	0	841
S6	15	100	0	993	100	0	1293	100	0	1079	100	0	1155
S5	16	100	18	196	100	3	670	100	7	296	100	1	446
S5	17	100	18	199	100	3	788	100	7	319	100	6	519
S5	18	100	21	173	100	3	837	100	14	295	100	16	468
S5	19	100	37	71	100	15	717	100	27	185	100	34	322
S6	21	100	0	722	100	14	904	100	0	772	100	29	537
S6	22	100	0	580	100	29	622	100	0	586	100	38	277
Column headings: [1] Number of particles in the domain, [2] Percentage of available particles agreed to the reference jellyfish (calculated with respect to the column of the block marked by 1), [3] Centroid distance (m) from the periphery of the respective detector													

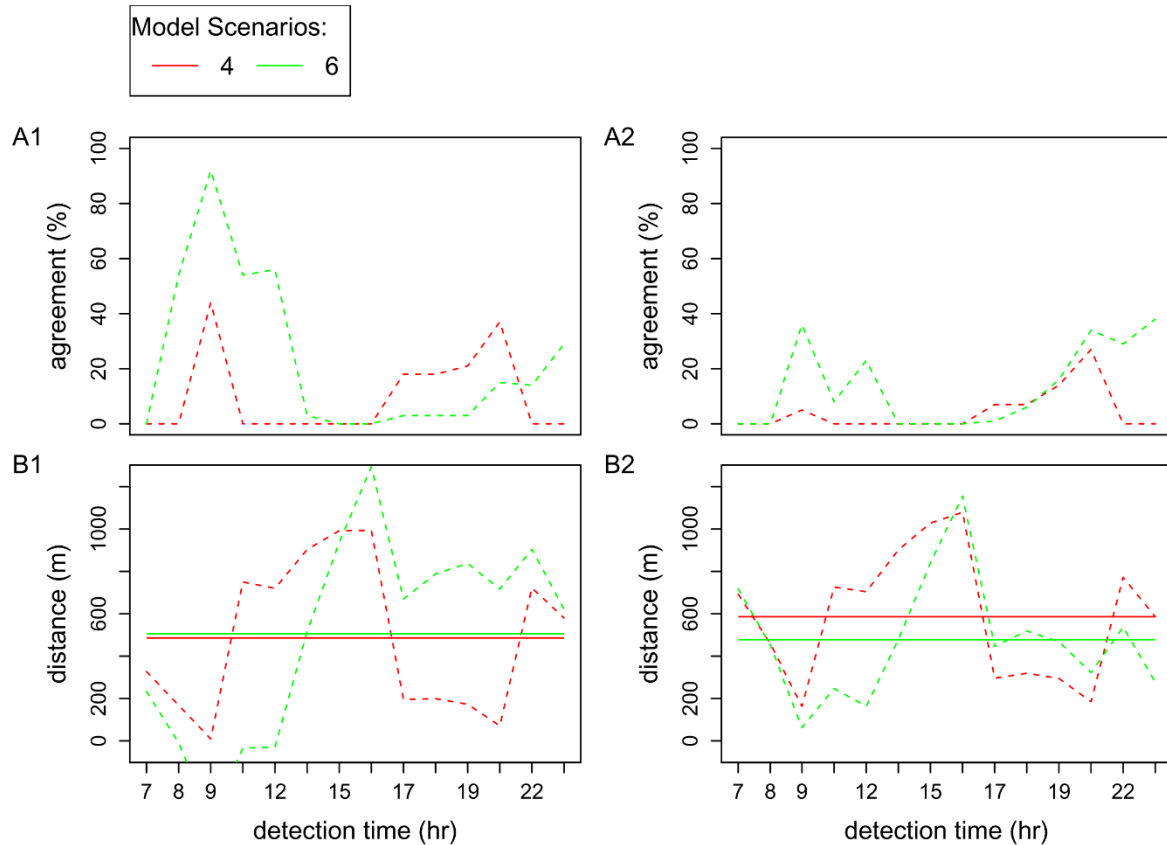


Fig 6.15 Comparing agreements as per J-1162 among the transport scenarios in terms of (A) percentage and (B) centroid distance for (1) surface and (2) mid-depth released particles over the simulation period. Real estimations are represented by the dashed lines and calculated means by the solid lines. [Notes: Specifications for the model scenarios are in Table 6.5. Centroid distances are from the periphery of the respective detectors.]

A snapshot of the distribution of transporting particles can be illustrative support of the results discussed above. For example, at the end of Scenario-4, the centroid distances of the surface releasing particles from the respective detectors at two consecutive detection instances of 19 and 21 hr were significantly different, earlier 71 m while later 722 m (Table 6.5). This is demonstrated in Fig 6.16. The figure shows that the reference jellyfish was detected at different detectors, S5 and S6, in those instances, respectively, where the ranges of the detectors themselves were apart by more than 1 km centre-to-centre.

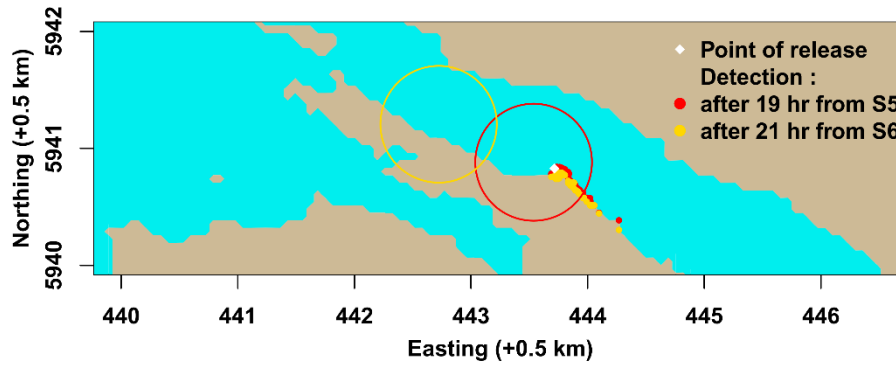


Fig 6.16 Snapshot of J-1162 modelled particle locations 19 and 21 hr after their release in Scenario 4 (DVM). Respective colour circles mark the respective detectors (S5 and S6) ranges.

Fig 6.17, which shows the percentages of particles located within a particular detector's range during the course of the surface release simulations. Similar to the previous jellyfish simulations, the passively drifted particles spread more along the harbour, while the particles in the DVM model show much less spreading and are concentrated at two adjacent detectors, S4 and S5. The observed jellyfish cycled between their release location within S5 and S6 to the west of S5; however, both the passive drift and DVM particles are transported predominantly to the east of S5.

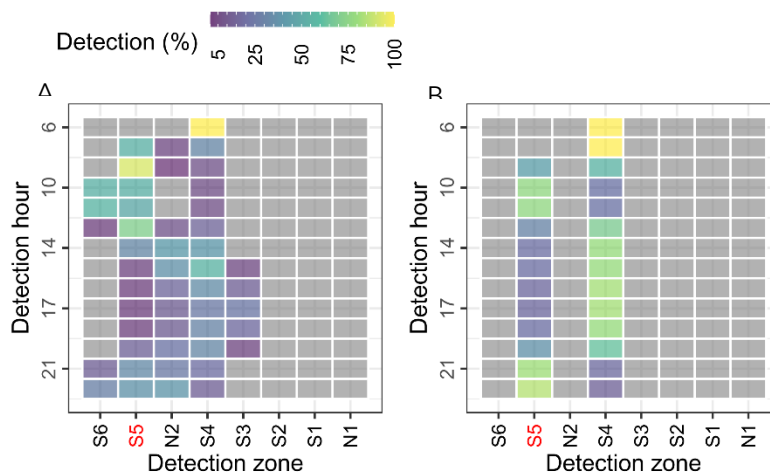


Fig 6.17 Spatiotemporal detections of the surface-released particles as per J-1162 model jellyfish detections in (A) passive drift, (B) DVM with 2.5 m threshold (Scenario 4) scenarios.

6.4.5. Multicriteria Analysis (MCA) of Model Performance

Above, several metrics were investigated separately to investigate the transport agreements of the modelled particles with the observed jellyfish movements. Those metrics were combined to compute a single model performance score through Multicriteria Analysis (MCA). The method has previously been described in Chapter 5, Section 5.3.5.3. For an overall comparison of the performance of DVM Scenario 4 across the jellyfish model, the MCA was calculated for each jellyfish model simulation, and these are presented graphically in Fig 6.18. The figure shows coloured dots on a spatiotemporal map to represent the relative agreements of particle transport with the model jellyfish across jellyfish detection instances and locations. The dots are coloured to indicate the strength or likelihood of the agreement. The simulations were based on the DVM transport of the particles ruled by a DVM threshold depth of 2.5 m and a motility rate of 0.02 m/s (Scenario 4). This was chosen here for the MCA based on the DVM performance shown in Fig 6.8. According to Fig 6.18, the agreements were better immediate to the release of the particles in all three jellyfish models visible by the colours of the dots on the colour scale for the MCA level of agreement; the agreements over time reduced near to the minimum like for the passive drift model transport (Chapter 5 Section 5.4.3). Yet, the DVM produced relatively better agreements in the long term (20~135 hr) in the J-18495 model, as shown in Fig 6.18A, and in the short term (16~19 hr) in the J-1162 model, as shown in Fig 6.18B. Individual variations in the observed jellyfish might promote a transport mechanism differently at different times over the journey.

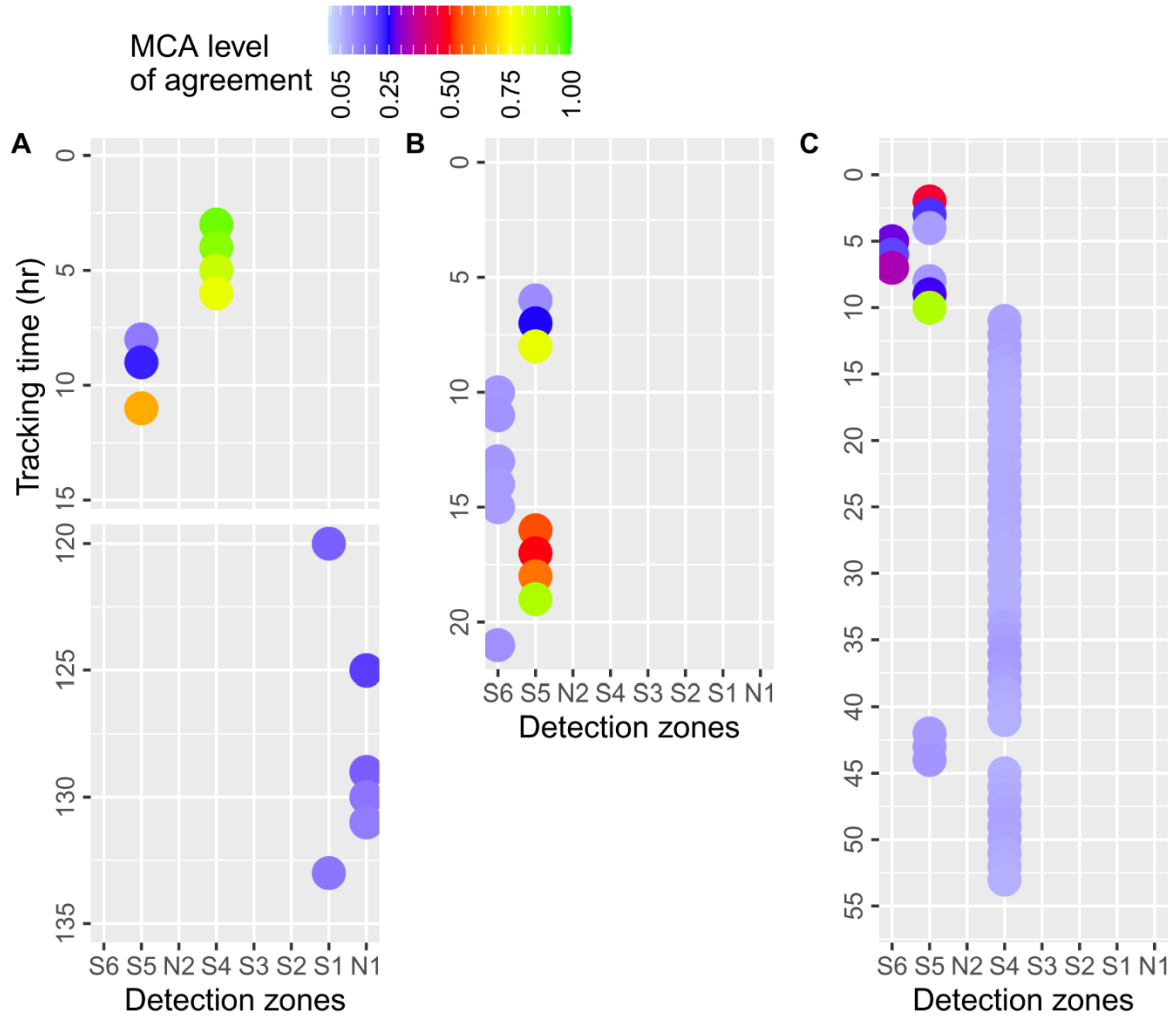


Fig 6.18 MCA of Scenario-4 (DVM at 2.5 m threshold depth and 0.02 m/s motility rate) simulated for (A) J-18495, (B) J-1162, and (C) J-18500 models.

6.5. Conclusions

Diel vertical migration was incorporated into the passive drift model to simulate the diel migration of jellyfish in response to daily and nightly changes in luminosity, thus creating a new DVM model. Four different diel migration behaviours were tested using different vertical migration swimming speeds and migration threshold depths. The DVM models were used to simulate the jellyfish release with the longest observational data record, J-18495. The best-performing DVM was then used to simulate two other jellyfish releases. In all cases, the DVM results were compared with those from the basic passive drift model and performance metrics were used to quantify their levels of agreement with the observed jellyfish movements.

The key conclusions based on this work are described as follows.

- 1) The installation of the DVM submodel within the base hydrodynamic model was successful. The submodel was successfully tested to give confidence in the development of the DVM submodel code. The modelled particles were able to move actively in the vertical direction in combination with their flow-induced passive drifting. The DVM model was able to reproduce the idealised diel migratory behaviour of jellyfish in terms of diving during the day and rising at night based on the depth of luminosity and motility rate.
- 2) The transport of the virtual jellyfish (particles) was not sensitive to the specified vertical motility rates. This might be because the submodel was applied to a shallow waterbody like the Killary Harbour, where the particles had to move too limited a vertical distance for a limited time to induce an impact of their speed. However, modelled particle transport was sensitive to the DVM threshold depth, which changed the limits of their migration and residence across the water column. The particle-releasing depths were also shown to contribute to variation in particle transport over the simulation by exposing the particles to different flow fields across the water column right after their release.
- 3) For the modelling of jellyfish J-18495, the DVM Scenario 4 model showed better agreement with observed jellyfish movements than the passive drift model

suggesting that diel migration, or at least some independent vertical motility, did play a role in that jellyfish's transport. However, for the other jellyfish models, the results were mixed, but overall, the DVM model did not yield improved agreement over the passive drift model. However, the observational record lengths were much shorter for these jellyfish; thus, diel migration would naturally have less influence over the shorter period. In addition, it is quite likely that migratory behaviour will not be the same for all jellyfish, so the diel migration rules used for J-18495 may not have been suited to the other two jellyfish.

- 4) In general, unlike the passive particles, most of the DVM particles of the J-18495 simulations tended to divide into clusters, and the newly formed clusters tended to be separated by distance. Thus, the diel migratory particles had a higher clustering and more limited spreading tendency depending on the resultant effect of their threshold depth and drifting speed, which might influence the development of a potential jellyfish bloom.
- 5) The results provided here showed that DVM could better replicate the transport of some model jellyfish observed in Killary better than the basic passive drift for particular specifications of the DVM properties (vertical motility rate and migration depth). Therefore, coupling any behavioural transport (e.g. DVM) with the basic passive drift process in jellyfish transport modelling could potentially improve transport agreement with the observation. The results also provide learning and insights into the potential effects of DVM on jellyfish transport, not least that it can produce significantly different transport patterns than a simple passive drift model.

CHAPTER 7: SWIM MODELLING OF JELLYFISH

7.1. Introduction

Swimming is an integral part of the movement of most aquatic organisms. It is an active behavioural response shown by individuals mainly to search for food, capture prey, locate mates, avoid predators and pollution, or find a suitable environment (Manning & Dawkins, 2012). Aquatic organisms are nearly always in constant motion due to the movement of the water surrounding them and/or their active behavioural responses. Although some movements may simply involve passive drifting due to fluid flows (e.g., wind or currents), many may involve active swimming. Both forms of movement determine the oceanic transportation and distribution of aquatic organisms. Individuals' movements play a major role in the transport dynamics of the population (Turchin, 1998). So, a good understanding of their mechanisms and associated contributions to the transportation of the organism is very important in predicting the transportation.

Since this research investigates the modelling of jellyfish transportation, it is necessary to identify and address all the main drivers and associated processes acting behind their transportation and consider them in the modelled processes. Swimming appears to be an important driver of their transportation (Fossette et al., 2015). Many jellyfish are not merely passive drifters; they are advanced in their orientation ability, making them strong swimmers. Evidence on barrel-jellyfish shows that they possess a remarkable ability to detect the direction of ocean currents and orient themselves against them in response to drifts (Fossette et al., 2015). Unlike many migrating animals either on land or in water, such as birds or fish, which use their vision to detect and direct orientation, jellyfish use non-visual mechanisms for the purpose and detect ocean currents without a fixed visual reference point (Fossette et al., 2015). Although the mechanism(s) they use is not yet fully understood, it has been hypothesised that they might detect current shear across their body surface or assess the flow speed and direction using other cues,

such as magnetism or infrasound (Fossette et al., 2015). This advanced orientation skill in jellyfish allows them to navigate at their own will instead of simply drifting passively in the ambient flows.

Transportation models may better predict the distribution and potential blooms of jellyfish if the swimming behaviours of jellyfish can be modelled and coupled together with their flow-driven drifting. Swimming mechanics can be incorporated into transport models based on understanding gained from jellyfish behavioural studies. Studies have shown that swimming may be more common when jellyfish travel in school, while drifting is more common when they are solitary. They modify their swimming behaviour in response to changes in the environment, such as hydrodynamics, illumination, and chemical gradients (Fossette et al., 2015; Mackie et al., 1981). Swimming is directed both horizontally and vertically. Vertical swimming was already captured in the model by the Diel Vertical Migration (DVM) mechanism cued by the presence or absence of light in the water column (discussed in Chapter 6). According to Fossette et al. (2015), the speed and direction of swimming may be dependent or independent of references, such as tidal stages or tidal currents, and thereby may be oriented with or against the currents. Whether on an ebb or a flood tide, the swimming may either follow the tide direction (unidirectional) or defend the tide (stable) or be independent of the tide (bidirectional). Swimming behaviour may vary with the depth at which jellyfish lie in the water column. The rate of swimming may be either constant or variable over time. All these factors working towards the jellyfish swimming behaviour may function either separately or jointly.

Swimming in jellyfish may lead to their swarm formation, which may be caused by the combination of their passive drifting and active swimming (Graham et al., 2001); however, there is very little understanding of the functional combination of these processes or the best strategy for implementing their interactions in numerical models. Various studies have found a strong relationship between the direction of jellyfish swimming and the currents (Matanoski & Hood, 2006). However, this multifaceted relationship was not explored further to investigate how many ways they can be related and how their influences would be on the jellyfish swimming.

Chapter 7: Swim Modelling

Directional swimming against vertical shears was demonstrated in the jellyfish *Aurelia aurita* (Rakow & Graham, 2006). A coupled hydrodynamic-behavioural model of jellyfish by Fossette et al. (2015) provided evidence that jellyfish orientation was modulated by tidal currents and that current-oriented swimming contributed to jellyfish being able to form swarms. Incorporation of swimming behaviours in their model also contributed to improving their predictions of jellyfish transport in coastal waters. According to their field observations, the average swimming speed of tracked jellyfish was 0.05 m/s (SD = 0.02 m/s; range 0.03–0.08 m/s), which was slower than the measured tidal currents (~0.2–0.5 m/s). They used this swim speed in their model implementation of swimming behaviour, with the model allowing jellyfish to swim over tides continuously. However, this was the only swimming behaviour they tested in their model, so that the resulting transport predictions may be ambiguous. Most of the previous studies on jellyfish swim modelling addressed merely the horizontal swimming of jellyfish. But jellyfish appear to demonstrate diel migration as an active mode of motility or swimming in the vertical direction (discussed in Chapter 6). Jellyfish transport modelling by coupling jellyfish diel migration with their horizontal swimming or adapting their vertical migration as their vertical swimming still remains virgin in the jellyfish transport investigation studies.

In this research, a novel swim modelling strategy was developed within the particle-tracking module of EFDC, i.e. the jellyfish transport model. The developed swim model covers a wide spectrum of swimming principles, which reflects a number of individual swimming behaviours of jellyfish arising from multiple behavioural cues, such as flow dependence, tidal relation, depth variation, orientation ability, and directional stability of jellyfish swimming. The model was developed by testing multiple combinations of swim speed and directional factors and then used to investigate the effects of a wide range of swimming behaviours on jellyfish transport and distributions. The swimming was synchronously coupled with the passive drifting online within the model, and the combined action of these transport processes determined the displacement of the virtual jellyfish. The novelties and advances of this research relative to the literature are, therefore:

(1) for the first time, a jellyfish swim model was developed in a way to secure a true but simple synchronization of jellyfish swimming with their hydrodynamic drifting resulting in the modelled transport being united but singular one within a three-dimensional space;

(2) many facets of swimming's relationship with currents were investigated;

(3) jellyfish swimming behaviour was simulated at multiple combinations of various behavioural cues. Although swimming behaviours may change with jellyfish sex, predation, individual size variability, hunger and life stages, the model does not include these parameters; thus, non-specific individual variations of jellyfish swim behaviour were investigated through multiple scenario modelling of different swim behaviours;

(4) finally, horizontal swimming was modelled in terms of jellyfish motility and vertical swimming was modelled in terms of DVM. The chapter is structured as follows. Section 2 provides the methodology with a strong focus on the swim model development. It includes a comprehensive analysis of the observed jellyfish transport in Killary in order to deduce any apparent swimming behaviours for inclusion in the model, the conversion of observed swimming behaviours into swimming principles to be included in the model, the development of corresponding swim algorithms and their implementation in the model, the synchronization of the swimming transport with the passive drifting and the integration of the swim sub-model within the EFDC hydrodynamic model. Section 3 provides the results of the model development, transport simulations, model sensitivity to swim properties and parameters, particle distributions and insights on transport patterns due to swim, and agreement of the modelled transports to the observation. Finally, Section 4 provides the main conclusions based on the integration of swimming in a jellyfish transport model.

7.2. Methodology

The purpose of the swim model developed here was to investigate the hypothesis that the combined effects of hydrodynamic forcing and behavioural motility could

better predict the jellyfish transport than either the passive-drift or the DVM models. Development and assessment of the swim model involved the following activities:

- (1) Analysis of the transport of jellyfish observed in Killary harbour more comprehensively than it was done previously, which was a simpler one,
- (2) Devising of rules governing active behavioural horizontal swimming,
- (3) Numerical translation of the swim rules,
- (4) Integration of swim rules into the model by the creation of a new EFDC source code,
- (5) Testing of the swim model to ensure that the model code was appropriate and bug-free,
- (6) Planning and modelling of swim scenarios, and
- (7) Analysis of model outputs to investigate the effects of jellyfish swim behaviours.

The swim rules were developed based on an analysis of the observed jellyfish movements in Killary and a review of the literature. Along with testing some conventional swim approaches and adapted versions of those, some novel modelling approaches to jellyfish swimming were also developed by merging behavioural motility along with advective transport. Jellyfish swimming movements were integrated with primary passive drifting using several behavioural swim rules. For simplicity, the biological characteristics of the jellyfish, which might affect swim behaviour, were not included in the model. Instead, the swimming behaviour of only the adult jellyfish was modelled, whereby all modelled particles/jellyfish in a simulation had the same swim speed, buoyancy, and directional migration tendency. The influence of individual variations in jellyfish on their transport was instead investigated through scenario modelling, which varied the swim speed, buoyancy, and directional migration tendency. This approach of biophysical modelling was found to be effective in investigating jellyfish transport patterns under the combined influence of environmental cues like currents and behavioural locomotion like swimming.

7.2.1. Analysis of Observed Transport of Jellyfish

This section presents a comprehensive analysis of the jellyfish observed in Killary. Fig 7.1 is a replication of Fig 5.3 (presented previously in Chapter 5 Section 5.4.1) and shows the times at which the tagged jellyfish were detected and the detection zones within which they were detected at those times. It can be seen for J-18499, for example, that it was first detected within S4 before being picked up in S1, then briefly travelling to N1, returning back to S1 and finally being picked up again in N1. It can be seen from this plot that jellyfish can spend time both within and outside of detection zones and can travel between detection zones.

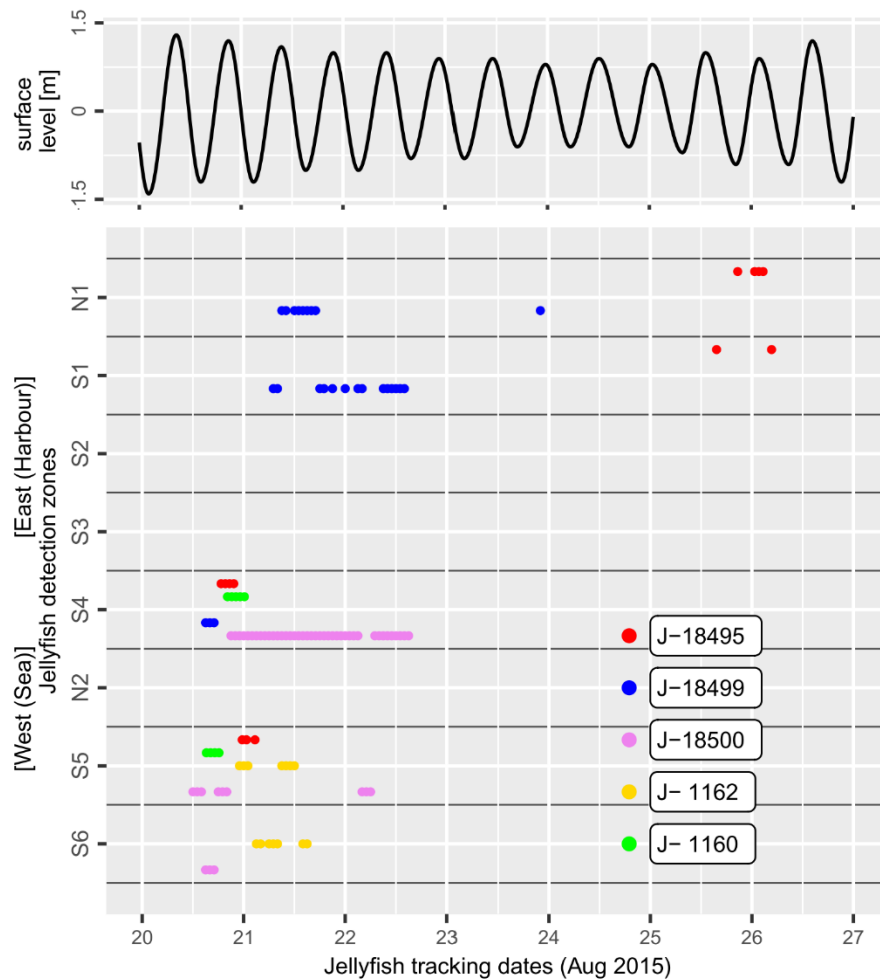


Fig 7.1 Times and locations of jellyfish detections in Killary Harbour for 5 jellyfish and the corresponding tide levels. Detections are colour-coded by tag number. (Note: It is replicated here from Fig 5.3 in Chapter 5.)

Chapter 7: Swim Modelling

With the purpose of identifying and distinguishing between tidally and behaviourally influenced movements, the analysis explores the directional travels of a jellyfish to determine whether it moves with or against the flood and ebb tides. The analysis involved four steps:

- (1) illustrating the principles of forming movement patterns by a jellyfish in various tidal situations and determining the type (active or passive) and direction (with or against the tide) of the transport (Fig 7.2), which was used as a reference in Step-3,
- (2) identifying the patterns and directions of interzone movement (from a detector's range to another) of jellyfish in the field observation (Fig 7.3),
- (3) illustrating residence and movement events of observed jellyfish on the tide (Fig 7.4), and
- (4) measuring the duration of each type and event of movements to determine their percentage distribution.

The transport patterns in Fig 7.1 were analysed in combination with the stage of the tide, with a particular focus on determining whether the movements showed any evidence of jellyfish possessing active swimming capabilities. If the jellyfish did possess horizontal swimming ability, then it was deduced that three possible transport strategies might be observed:

1. Passively drifting with
2. Swimming with the tide
3. Swimming against the tide

Upon examining the data, it was deemed that these transport strategies could be best determined at times of slack water (high tide / low tide), on flood and ebb tides, and long-term over multiple tides. For example, if jellyfish were only being passively transported by tidal currents, then they would be expected to travel in the direction of a tide, e.g. eastward towards the inner harbour on a flood tide and westward towards the sea on an ebb tide, so evidence of travel against the tide indicated swimming ability. Conversely, an absence of transport on a flood or ebb tide means

Chapter 7: Swim Modelling

the jellyfish is actively swimming against the tide to remain in the same position. At slack water, if the jellyfish were only subject to passive drifting, then they should not be observed travelling any substantial distances, so evidence of interzone travel would suggest active swimming ability. These theoretical transport strategies are summarised in Fig 7.2. Unfortunately, as the jellyfish were not fitted with GPS trackers, the exact geographical locations of the jellyfish within the detection zone were unknown so that intra-zone travel could be tracked; thus, interzone travel provided the best evidence of the presence or absence of swimming ability.

		Resultant type of transport		
		Drift with tide (no interzone travel)	Swim with tide (any intrazone travel; unspecifiable)	Swim against tide (any interzone travel)
Tidal situations	at slack tide, if			
	at flood tide, if	(east/fjord-ward travel at the mid-flood) 	(east/fjord-ward travel at the terminal-flood) 	(west/sea-ward travel)
	at ebb tide, if	(west/sea-ward travel at the mid-ebb) 	(west/sea-ward travel at the terminal-ebb) 	(east/fjord-ward travel)
	at any tide, if	Specific situations are mentioned above	(long distance travel in the direction of longer tide over multi-tides) 	(no interzone travel)

Fig 7.2 Graphic showing all theoretical transport processes of the jellyfish. The red asterisks indicate the starting point of a movement, and the blue the destination. The dashed arrows indicate the movement directions.

Fig 7.3 shows all the inter-zone travel paths observed for the 5 jellyfish based on the movements presented in Fig 7.2. Each type of inter-zone travel is assigned a travel-type ID from 1 to 8, with intra-zone travel assigned an ID value of 0. For example, looking at the inter-zone travel of Jellyfish J-18499, it first travels from S4 to S1 (travel-type ID 7) and then from S1 to N1 (travel-type ID 8). Interzone travel was directed either eastward towards the inner harbour or westward towards the sea and could be either with or against the tide. In Fig 7.3, travel-types 1-3 are westward while 4-8 are eastward. The type of transport process (e.g. passive drift, swimming with/against the tide) was determined by matching the observed travel paths with the theoretical patterns shown in Fig 7.2 **Error! Reference source not found.** For example, the movement of a jellyfish from S4 westward to S5 (Fig 7.3 travel-type 2) on an ebb tide corresponds to passive drift transport in Fig 7.2. On the other hand, a movement from S5 eastward to S4 (travel-type ID 5 in Fig 7.3) on an ebb tide indicates transport against the tide which is only possible by swimming (Fig 7.2).

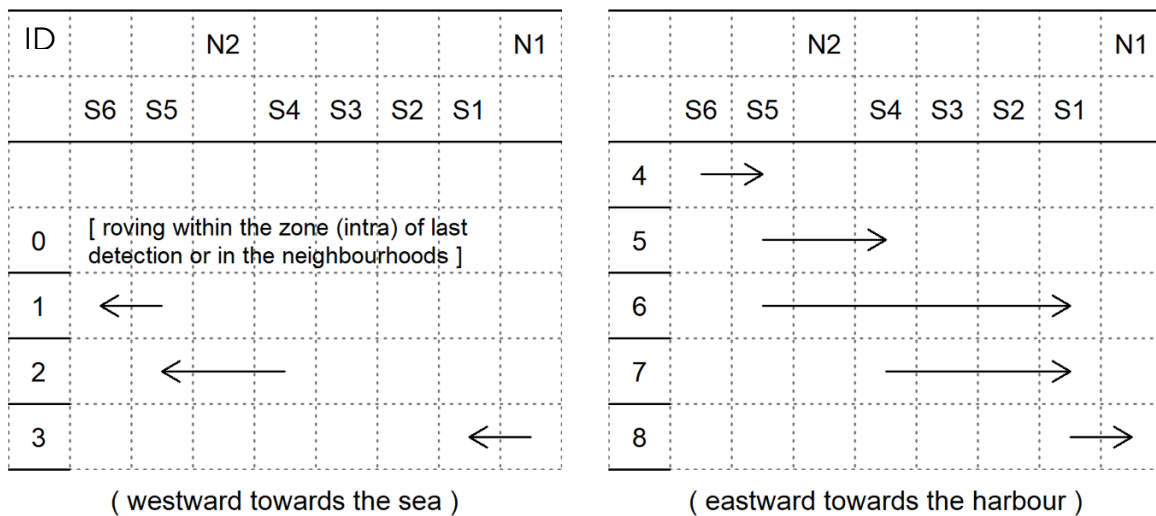


Fig 7.3 A summary of the different types of inter-zone travel observed in Killary. Each type of inter-zone travel is assigned a number from 1-8, which is used in subsequent analyses, while 0 is used to indicate intrazone travel. The eight detectors' zones are listed in order of location from east to west along the harbour. The arrow indicates the direction of transport, and the arrow length determines the specific shift.

The times and durations of the observed transport patterns of each jellyfish were analysed in relation to the tide stage to produce Fig 7.4. The figure shows the type

of inter-/intra-zone travel undertaken by each jellyfish numbered according to Fig 7.3 and coloured by the determined transport process. The transports are overlaid on the tidal water level graph to help identify any tidal influence. As such, the length of the transport mark determines the length of an individual influence. Each jellyfish detection for a period within a detector's range was characterized by an event of residence, and any undetected period was a movement event. Each movement period follows a residence period and vice-versa. The movements are divided into the following transport types: (1) drift-dominated movement with the tide, (2) swim-dominated movement with the tide, (3) swim-dominated movement against the tide, and (4) unspecifiable movement over multiple tides. Taking, J-1160 in Fig 7.4(a) as an example, it was released shortly after high tide, and its first detection was around the following low tide when it spent a couple of hours within a specific detection zone (indicated by the blue line). As indicated by the green line, it left the zone shortly and spent some time travelling to another zone. The number of the green line is the travel-type ID, and Fig 7.3 tells us that this travel-type 5 indicates interzone travel from zone S5 to S4. Fig 7.3 also tells us that this type of travel is eastwards, and since we are on a flood tide where tidal currents are directed eastwards, the travel process is assumed to be drift-dominated movement with the tide, i.e., the green coloured line as per the legend in Fig 7.4. This analysis and classification allowed the computation of the percentage contribution of the different transport processes to overall jellyfish movements.

Chapter 7: Swim Modelling

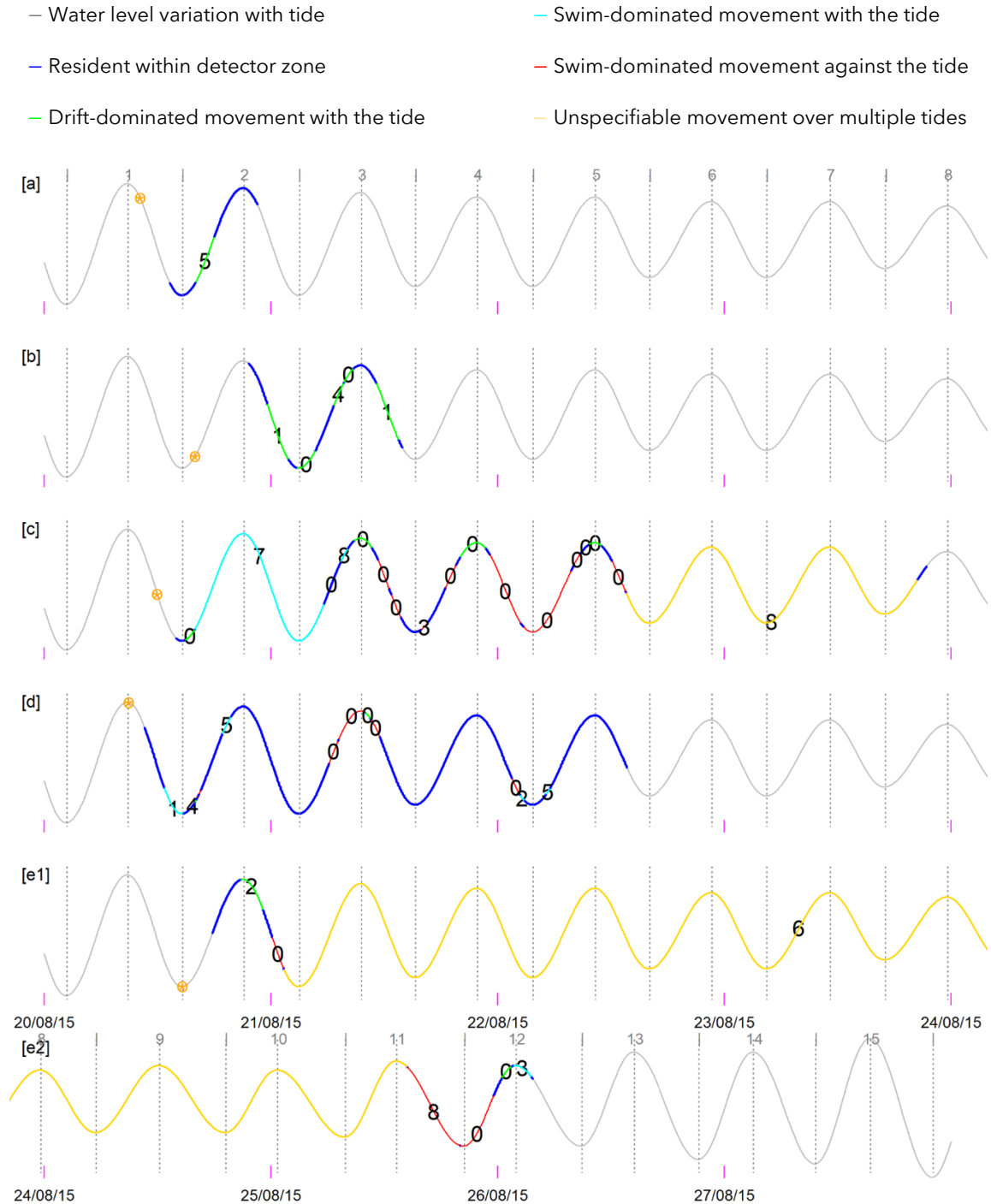


Fig 7.4 Observed jellyfish movements overlaid on water level graphs and visualised in terms of residency in particular detection zones (blue lines) or inter-zone travel (other coloured lines). The colour of the line indicates the type of governing transport process as per the legend, and the number of each line indicates the type of inter-zone travel based on Fig 7.3. **Error! Reference source not found..** Transports are shown for jellyfish: (a) J-1160, (b) J-1162, (c) J-18499, (d) J-18500, and (e) J-18495 (divided into e1 and e2 due to longer observation record). The orange circle indicates the releasing time of each jellyfish.

Finally, the durations of the individual types of jellyfish movement, as shown in Fig 7.4, were extracted for all the observed jellyfish. Then, the average periods of tidally oriented movements of the jellyfish over an ebb or a flood tide were calculated to find out the shares of the movement types (with- or against-tide) within a particular tide (flood or ebb). These calculations were made at four tidal and jellyfish movement scenarios, as found in Fig 7.4. Fig 7.5 graphically shows these scenarios distinctly helping in preparing logical equations of the calculations. According to the figure, point A and B on the tide (water level) line indicates the start and end time for the water ebbing (so is for the flooding) and point P and Q for a jellyfish moving (tide-oriented and individual-type movement), respectively. The sequence of the points thereby makes patterns distinct across the conditions and equations used for the calculations. Thus, the calculations of the period of a tidally oriented (individual type) movement of jellyfish (T) were carried out across the patterns in the figure.

Chapter 7: Swim Modelling

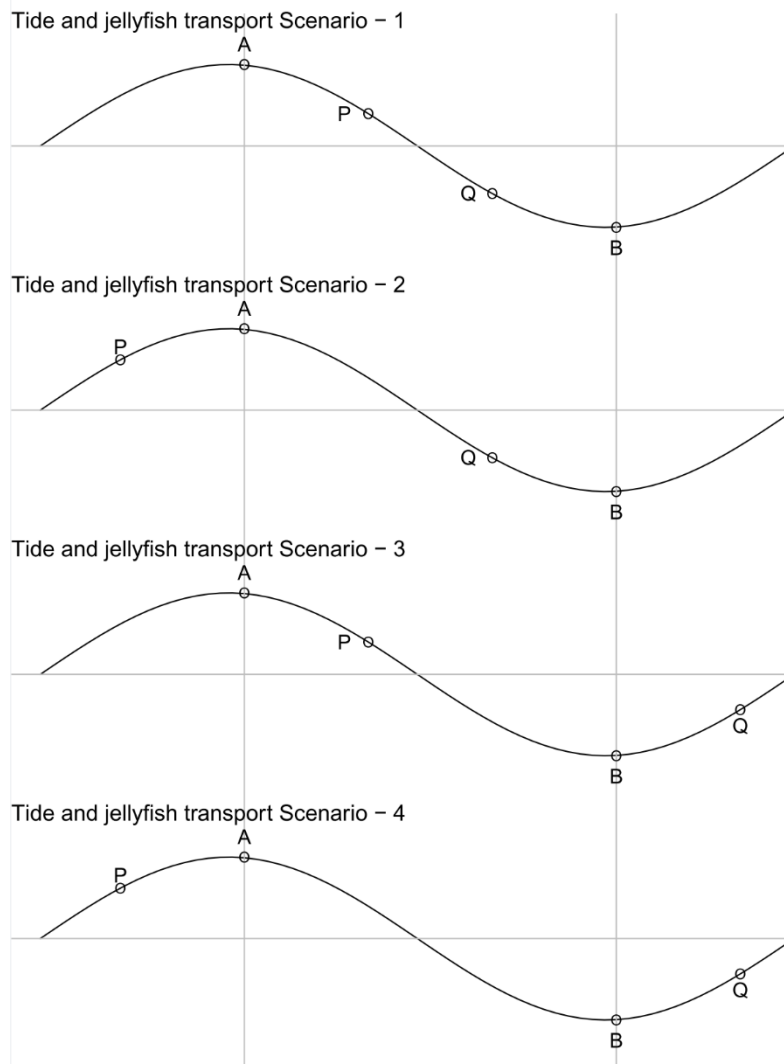


Fig 7.5 Graphic showing scenarios of tidal transport of jellyfish; point pairs A-B and P-Q indicating the start-end of the tide and the jellyfish transport, respectively.

According to Fig 7.5,

for the APQB pattern in Scenario-1,

$$T = \sum_{i=1}^n |t_{P_i} - t_{Q_i}| \quad (7.1)$$

for the PAQB pattern in Scenario-2,

Chapter 7: Swim Modelling

$$T = |t_A - t_Q| \quad (7.2)$$

for the APBQ pattern in Scenario-3,

$$T = |t_P - t_B| \quad (7.3)$$

for the PABQ pattern in Scenario-4,

$$T = |t_A - t_B| \quad (7.4)$$

where t is the time at a particular point on the tide line.

The transport periods calculated thereby per Eqs (7.1) - (7.4) were filtered in groups according to their with-tide and against-tide directions on the floodtide and ebbtide. Based on the observed jellyfish transportation, the calculations revealed average proportions of jellyfish orientations with respect to the tide, which were 35 % time with the tide and 65 % time against the tide during the flood tide and 25 % time with the tide and 75 % time against the tide during the ebbtide. Later, this was incorporated in the swim rule as one of the jellyfish swimming mechanics or strategies and tested for its performance through scenario modelling.

7.2.2. Swim Model Development

The analysis of the jellyfish data and the literature review confirmed that horizontal motility could play a role in the transport of jellyfish within Killary, and this ability was therefore incorporated into the jellyfish model to develop the swim model. The following sections describe the development of the swim model.

7.2.2.1. Swim Model Concept

There are three types of transport processes included in the swim model: (1) hydrodynamically-cued passive movements, which include advective drift and diffusion, (2) light-induced diel vertical migration and (3) biologically-cued active horizontal swimming. All these processes were spatiotemporally synchronized to let them function in combination. The Lagrangian transports in the biophysical model are resolved and updated at every model timestep. Neutrally buoyant particles representing the adult jellyfish are set to swim three-dimensionally in water space at specified speeds and directions to perform behavioural locomotion like a jellyfish.

The following steps describe the various processes carried out during each model timestep within the developed swim model; these were implemented in the model via the introduction of a new model code.

- (1) Swim rule parameters (speed, direction, etc.) are presented in the swim calculation subroutine.
- (2) Tidal current's speeds, direction, and tide stage are checked.
- (3) Particle depth of occurrence is checked to characterize them as shallow or deep (needed to apply depth-related swim rules).
- (4) The swim specification is identified based on the previous tide and/or depth-related checks.
- (5) The horizontal swim speed is identified either by selecting the user-specified values or calculating it with respect to the current speed.
- (6) The horizontal swim direction (with or against the tide) is identified based on the swim rule.
- (7) The vertical swim speed is identified based upon:
 - selecting the user-specified values, or
 - calculating it with respect to the current speed, or
 - calculating it with respect to the DVM strategy

(8) The vertical swim direction (up or downwards) is identified based on either the resultant vector of the active and passive movements or the light-induced DVM movements

(10) resolving the swim velocity into 3D vector components to combine with other transport velocity components (e.g. due to advection).

The behavioural locomotion of the jellyfish was integrated into the DVM model in this way so that the resultant transportation was a combined effect of the active and passive transport processes.

7.2.2.2. Swim Rule Development and Implementation

The swim model was designed to capture jellyfish motility behaviour regarding horizontal swimming and integrate it with the passive drift and DVM. The swimming rules were devised to be reflective of the real swimming behaviour of jellyfish and were motivated first by the literature, and second, from the comprehensive analysis of the transport observed in Killary that revealed distinguishable tidal-related movements and independent free movements of jellyfish. Swim rules were developed sequentially by varying the swim specifications depending on model results in an effort to improve model prediction of jellyfish transport. The rules were developed based on the transport patterns of J-18495, the jellyfish with the longest observed transport records. Twelve swim rules were developed in total and were coded into the EFDC model to take account of the following important behavioural aspects:

- (1) how fast a jellyfish swims,
- (2) how a jellyfish orients itself while it swims,
- (3) how swimming (speed and direction) varies with respect to the stage of the tide and water depth,
- (4) possible flow dependence of the swim, and
- (5) spatiotemporal variability of the swim.

Chapter 7: Swim Modelling

These aspects of swimming behaviour were identified for inclusion in the model based on findings from the literature, findings from the analysis of jellyfish movements in Section 2.1, and from personal hypotheses. Since a jellyfish's swimming speed depends on a poorly understood complex relationship between multiple factors (age, size, environment, food, predators, etc.), and there are no studies that specifically document the swimming speeds of a population or progressive swarm of jellyfish, it was hard to select sensible specific values or ranges of speed for inclusion in the swim rules. Estimations from publications and studies performed on various species-specific jellyfish were used, as well as estimates based on observations and personal experience.

The swim rules are structured within a suite of equations (Eqs 7.5~7.11) presented below. The basic principle of the swim rules assumes that a particle must actively travel either a fixed (known) or variable (unknown) distance at every timestep, depending on its flow dependency. Swims are oriented either with or against the tide or a combination of both, at either absolute or relative motility rates, which are either constant or variable with respect to tide and depth.

The swim rules have a similar basic structure where the swim velocity of a particle, p , (i.e. a jellyfish) at time t , $v_{sw,p}(t)$ is calculated as:

$$v_{sw,p}(t) = \alpha \times v_{ts,p} \times \beta \quad (7.5)$$

where $v_{ts,p}$ is the transport strategy swim velocity (m/s) defined by a particular swim rule. Depending on the swim rule, v_{ts} may be set to a constant value set by the user, or it may vary with the stage of the tide, water depth or flow speed at the current location of a particle. α is a behavioural variable determining the swim direction. If swimming with the tide is desired, then $\alpha = +1$; if swimming against the tide is desired, then $\alpha = -1$. Finally, β is the swim speed proportionality constant which is used to scale $v_{ts,p}$ relative to the ambient tidal current flow flow-dependent swim speed rules. It can vary from 0-2.

Depending on the swim rule, the transport strategy swim velocity may take on a different value at different tide stages or for particles at different depths in the water column.

Chapter 7: Swim Modelling

The stage of the tide, td , is identified as follows:

$$\text{If } z_{p,t-1} < z_{p,t} \quad \text{then } td = \text{floodtide.} \quad (7.6)$$

$$\text{If } z_{p,t-1} > z_{p,t} \quad \text{then } td = \text{ebbtide.} \quad (7.7)$$

$$\text{If } z_{p,t-1} == z_{p,t}$$

or

$$\text{If } z_{ts} > 0.5 \text{ m and } v < 0.03 \text{ m/s,} \quad \text{then } td = \text{slack (high/low) tide} \quad (7.8)$$

The particle depth condition in the water column, dp , is defined as follows:

$$\text{If } z_{p,t} < 5 \text{ m,} \quad \text{then } dp = 1 \text{ indicating shallow-lying.} \quad (7.9)$$

$$\text{If } z_{p,t} > 5 \text{ m,} \quad \text{then } dp = 2 \text{ indicating deep-lying.} \quad (7.10)$$

$$\text{If } z_{p,t} \geq 0 \text{ m,} \quad \text{then } dp = 3 \text{ indicating at any depth.} \quad (7.11)$$

where $z_{p,t}$ and $z_{p,t-1}$ are the vertical positions of any particle p with respect to the surface water (m) at the current and previous timesteps.

The aim of the swim rules is to allow a particle (i.e., jellyfish) to actively swim three-dimensionally within the water space under its own locomotion and for this transport to be calculated initially in the model exclusive of any other transport, e.g., passive drifting. This is then combined with the respective passive displacement to realize the total transport of the virtual jellyfish (particles). The basic principles and execution methods of the swim rules are described below.

Rule-1: Continual swimming with constant speed against the tide

This rule assumes that a particle swims at a constant speed against the tide at every stage of the tide. This process is captured in the model according to Eq (7.5) with the specification of the parameters as follows:

$$v_{ts,p} = \text{a constant swimming rate set by the user}$$

$$\alpha = -1$$

$$\beta = 1$$

A value of $v_{ts,p} = 0.05 \text{ m/s}$ was used for scenario modelling – this was informed by the literature.

Rule-2: Swimming with constant speed against the flood tide.

This rule assumes that a particle swims only on the flood tide and is subject to passive drifting only on the ebb tide. The particle swims against the flood tide. The process is captured in the model according to Eq (7.5) with the specification of the parameters as follows:

If $td = \text{flood tide}$, then: $v_{ts,p} = \text{a constant swimming rate set by the user.}$

otherwise: $v_{ts,p} = 0$

$$\alpha = -1$$

$$\beta = 1$$

As for Rule-1, a value of $v_{ts,p} = 0.05 \text{ m/s}$ was used for scenario modelling.

Rule-3: Swimming with constant speed against the ebb tide.

This rule is the opposite of Rule-2, with the particle swimming only on the flood tide and subject to passive drifting alone on the ebb tide. The process is captured in the model according to Eq (7.5) with the specification of the parameters as follows:

If $td = \text{ebb tide}$, then: $v_{ts,p} = \text{a constant swimming rate set by the user.}$

otherwise: $v_{ts,p} = 0$

$$\alpha = -1$$

$$\beta = 1$$

Values of $v_{ts,p} = 0.02, 0.05 \text{ and } 0.08 \text{ m/s}$ were used for scenario modelling.

Rule-4: Flow-dependent swim speed against the ebb tide.

Like Rule-3, this rule assumes that particles swim only on the ebb tide and that the swim direction is against the tide; however, the transport strategy swim velocity is set to the ambient local current velocity. This means that a jellyfish essentially holds its position on the ebb tide rather than being advected passively by the tidal current. It is implemented according to Eq (7.5) with the specification of the parameters as follows:

$$\text{If } td = \text{ebb tide, then: } v_{ts,p} = v(i,j)_p$$

$$\text{otherwise: } v_{ts,p} = 0$$

$$\alpha = -1$$

$$\beta = 1$$

where $v(i,j)_p$ is the ambient current velocity at the particle's location.

Rule-5: Swimming at slack tide and on the ebb tide

This rule is an adaptation of Rule-4 where particles use two swim strategies:

(1) On ebb tides, the particle swims against the tide at the local prevailing current speed, and

(2) During slack tide, the particle swims at a constant speed against the tide set by the user.

This rule is implemented using the following specification of Eq (7.5):

$$\text{If } td = \text{ebb tide, then: } v_{ts,p} = v(i,j)_p$$

$$\text{If } td = \text{slack tide, then: } v_{ts,p} = 0.08 \text{ m/s}$$

$$\text{otherwise: } v_{ts,p} = 0$$

$$\alpha = -1$$

$$\beta = 1$$

Rule-6: Continual swimming with flow-dependent speed against the tide

This rule assumes a similar principle to Rule-1, i.e. continual swimming against the tide at all stages of the tide, except that a particle swims at a flow-dependent swim velocity equal to the prevailing local current speed at a particle's location rather than the constant swim velocity of Rule-1. The scaling factor β can be set to any value by the user. If it is set to 1, then any passive drifting should be fully negated by swimming, and the particles should resist any passive drifting. For scenario modelling, it was set to 0.15, i.e. the particle swim speed was 15% of the local current speed. The specification of swim parameters is as follows:

$$v_{ts,p} = v(i,j)_p$$

$$\alpha = -1$$

$$\beta = 0.15$$

Rule-7: Depth-conditional swim direction and flow-dependent swim speed

This rule assumes a similar principle to Rule-6, except that a particle swims at a conditional motility rate with respect to tide and depth. This process is captured in the model separately in three individual conditions. The conditions and their respective specifications of the parameters are as follows:

- (1) During floodtide, particles in shallow water swim against the tide ($\alpha = -1$)
- (2) During floodtide, particles in deeper water swim with the tide ($\alpha = +1$).
- (3) During ebbtide, all particles swim against the tide irrespective of depth ($\alpha = -1$).

The swim speed is dependent on the ambient current speed at a particle's location, and the strength of the flow dependence is specified by the user via β . For scenario modelling, $\beta = 0.15$ was used.

Rule-8: Overcoming ebb tide with depth-conditional swim direction and flow-dependent swim speed I

This rule assumes a similar swimming behaviour to Rule-7 except that β is not constant; rather, it varies with respect to the behavioural (orientation) variable α , i.e., with the swim direction. Thus this rule allows particles to travel at different percentages of the ambient current speed at different tide stages. For scenario modelling under this rule, we wished to allow jellyfish swimming against the tide to not only negate the passive drifting but to achieve a net positive transport against the tide when both active swimming and passive drift were considered in combination. A β value greater than 1 is required to achieve this. For scenario modelling, the rule was implemented, such that net positive swim transport was achieved on the ebb tide. The process was included in the model as follows.

$$v_{ts,p} = v(i,j)_p$$

For flood tide swimming, $\alpha = +1$: $\beta = x$

For ebb tide swimming, $\alpha = -1$: $\beta = 1 + x$

Two scenarios were modelled where $\beta = 0.15$ and 1.15 , and $\beta = 0.2$ and 1.2 for flood and ebb tide swimming, respectively.

Rule-9: Overcoming ebb tide with depth-conditional swim direction, flow-dependent swim speed and minimum threshold swim speed

This rule assumes a similar swimming behaviour to Rule-8 except that a minimum threshold is set for $v_{ts,p}$. If the local current speed $v(i,j)_p$ falls below the minimum threshold, then $v_{ts,p}$ is set to the minimum threshold. The minimum threshold speed is decided by the user; for the implementation of this rule in scenario modelling, the minimum threshold speed was set to 0.2 m/s.

Rule-10: Overcoming ebb tide with depth-conditional swim direction and flow-dependent swim speed II

This rule assumes similar swim behaviours to Rule-8 except that the swim speed proportionality constant, β , on a flood tide is set to half the value for the ebb tide. The process was included in the model as follows.

$$v_{ts,p} = v(i,j)_p$$

For flood tide swimming, $\alpha = +1$: $\beta = \frac{1}{2} (1 + x)$

For ebb tide swimming, $\alpha = -1$: $\beta = 1 + x$

Rule-11: Overcoming ebb tide with depth-conditional swim direction and flow-dependent swim speed

This rule is identical to Rule-8 except that the against tide swim speed proportionality constant was increased to $\beta = 1.5$.

Rule-12: Continual swimming with variable directionality and flow-dependent swim speed

This rule assumes that the direction of jellyfish swimming action is independent of the tide stage, as also found by Fossette et al. (2015). Particles swim randomly both with and against the tide, irrespective of the flow direction. The proportion of time during the floodtide and the ebbtide that particles spend swimming with or against the tide was determined empirically from the analysis of observed jellyfish in Section 7.2.1. For the swim speed, β is assumed as per the strategy in Rule-8. The swim speed becomes zero while the respective current speed drops below a given low level, which is set by the user (a random low value of 0.005 m/s was used here). Due to the complexity of realising such a swim orientation strategy within the model, an equivalence determination of the swim speed (β_{eq}) was used to simplify the capturing of the process. This is explained with an example below in Box-1.

Box 1. Strategy to implement behavioural swim orientation in jellyfish transport modelling as per Rule-12.

This swim orientation strategy was motivated by the tidal transport observation of jellyfish in Killary. Passive drifts are always oriented with the tide. There are two cruising orientations in terms of the tide – (1) towards the tide or with the tide, tt/wt, (2) against the tide, at;

Suppose

$T = 10$ days, where T is the total duration of floodtide or ebbtide (equal duration assumed);

Chapter 7: Swim Modelling

P during floodtide = $P_{tt} + P_{at} = 35\% T + 65\% T$

P during ebbtide = $P_{tt} + P_{at} = 25\% T + 75\% T$,

where P is the percentage (%) of tide-specific orientations with respect to T (based on the observed transport in Killary);

$TCS = 5$ km/day, where TCS is the tidal current speed;

$TSS = 20\%$ of TCS at pre-drift stationary/neutral state, where TSS is the theoretical swim speed;

$PSS_{tt} = \alpha \times TSS$

$PSS_{at} = \alpha \times (TCS + TSS)$ [covers drift neutralization],

where PSS is the practical swim speed and α is a behavioural variable that takes the value of +1 (tt) or -1 (at);

$NS_{tt} = (P_{tt} \times \alpha \times TSS)$

$NS_{at} = (P_{at} \times \alpha \times TSS)$

$NS_{os} \text{ (total)} = NS_{tt} + NS_{at}$,

where NS is the net swim distance (actual while no drift is involved) [should not be confused with the net transport, which includes passive drifts along with the swim].

The net swim as per the equivalent strategy (NS_{eq}), which is calculated below using the above equations, was assumed to be equal to the net swim as per the original strategy above.

	<i>Floodtide</i>	<i>Ebbtide</i>
NS_{tt}	$(0.35 \times 10 \text{ days}) \times (+1) \times (0.2 \times 5 \text{ km/day})$	$(0.25 \times 10) \times (+1) \times (0.2 \times 5)$
NS_{at}	$(0.65 \times 10) \times (-1) \times (0.2 \times 5)$	$(0.75 \times 10) \times (-1) \times (0.2 \times 5)$
NS_{os}	-3	-5
	Since flood and ebb work in opposite directions, the net transport is then '-2' towards ebb OR '+2' towards flood.	

An equivalence can be calculated in either of the following ways:

(Note: 100 needs to be added as a neutralization factor to the absolute value only when PSS_{at} is to be calculated.)

Strategy-1: during the flood, TT AND during ebb, AT

NS_{eq}	Normalized upon TT: During the flood, particles swim towards a fixed direction, suppose TT, but the net swim is '-3'.	Normalized upon AT: During the flood, particles swim towards a fixed direction, suppose AT, but the net swim is '-5'.
-----------	---	---

Chapter 7: Swim Modelling

	$(1 \times 10) \times (+1) \times (TSS \times 5) = -3$	$(1 \times 10) \times (-1) \times (TSS \times 5) = -5$
TSS	-6% of TCS (absolute result; need to re-specify the sign based on the direction)	+10% of TCS (absolute result; need to re-specify the sign based on the direction)
PSS	$PSS_{tt} = (+1) \times (-6\%)$ ['+' sign since TT assumed above] $= -6\%$	$PSS_{at} = (-1) \times (+)(10+100)\%$ ['- sign since AT assumed above] $= -110\%$
Strategy-2: all AT		
NS _{eq}	Normalized upon AT: During the flood, particles swim towards a fixed direction, suppose AT, but the net swim is '-3'. $(1 \times 10) \times (-1) \times (TSS \times 5) = -3$	Normalized upon AT: During the ebb, particles swim towards a fixed direction, suppose AT, but the net swim is '-5'. $(1 \times 10) \times (-1) \times (TSS \times 5) = -5;$
TSS	+6% of TCS (absolute result; need to re-specify the sign based on the direction)	+10% of TCS (absolute result; need to re-specify the sign based on the direction)
PSS	$PSS_{tt} = (-1) \times (+6\%)$ ['- sign since AT assumed above] $= -6\%$	$PSS_{at} = (-1) \times (+)(10+100)\%$ ['- sign since AT assumed above] $= -110\%$
Strategy-3: all TT		
NS _{eq}	Normalized upon TT: During the flood, particles swim towards a fixed direction, suppose TT, but the net swim is '-3'. $(1 \times 10) \times (+1) \times (TSS \times 5) = -3$	Normalized upon TT: During the ebb, particles swim towards a fixed direction, suppose TT, but the net swim is '-5'. $(1 \times 10) \times (+1) \times (TSS \times 5) = -5$
TSS	-6% of TCS (absolute result; need to re-specify the sign based on the direction)	-10% of TCS (absolute result; need to re-specify the sign based on the direction)
PSS	$PSS_{tt} = (+1) \times (-6\%)$ ['+' sign since TT assumed above] $= -6\%$	$PSS_{at} = (+1) \times (-)(10+100)\%$ ['- sign since AT assumed above] $= -110\%$
Among the above strategies, Strategy-1 was used in the model.		

Chapter 7: Swim Modelling

All the swim rules described above are summarized in Table 7.1.

Table 7.1 Summary of the swim rules.

Swimming principles											
Rule	Swim direction ¹			Speed ²						Rule Descriptor	
	flood		ebb	S1	S2	S3	S4	S5	S6		
	dp=1	dp=2	dp=3								
1	–	–	–	Q	R	R	Q	R	R	Constant speed against the tide.	
2	–	–		Q	Q	R	Q	R	Q	Constant speed against flood tide.	
3			–	Q	Q	R	Q	Q	R	Constant speed against ebb tide.	
4			–	R	Q	Q	Q	Q	R	Neutralisation of passive drift on ebb tide.	
5			–	R	Q	Q	Q	Q	R	Neutralisation of passive drift on ebb tide and swimming at slack tide.	
6	–	–	–	R	R	Q	Q	R	R	Flow-dependent speed and reversal direction.	
7	–	+	–	R	R	Q	R	R	R	Directional stability.	
8	–	+	–	R	Q	Q	Q	R	R	Drift neutralization while cruising against the tide.	
9	–	+	–	R	Q	Q	Q	R	R	Nonzero selective minimum speed and neutralization.	
10	–	+	–	R	Q	Q	Q	R	R	Speed halving while with the tide and neutralization.	
11	–	+	–	R	Q	Q	Q	R	R	Widely diverging tide-specific speed.	
12	+ & –			R	Q	Q	Q	R	R	Proportionate orientation ³ and neutralization.	
¹ Swim orientation behaviour (direction, α) across the following tide and depth conditions: $dp = 1$ is shallow-lying (<5 m) on floodtide, $dp = 2$ is deep-lying (>5 m) on floodtide, and $dp = 3$ is lying at any depth on ebbtide ('+' represents with-tide and '–' represents against-tide).											
² Swim motility behaviour (speed, β) across the following properties: S1 = Flow dependence, S2 = Tidal stability, S3 = Temporal stability, S4 = Directional stability, S5 = Active on floodtide, and S6 = Active on ebbtide.											
³ The ratios of the with-tide and against-tide orientations (+:–) during the floodtide is 35:65 and during the ebbtide is 25:75 (resolved through the tidal analysis of the observation of jellyfish transport in Killary).											

7.2.3. Swim Model Details

The model uses a data-driven approach to simulating the transport of jellyfish (i.e., particles). Horizontal and vertical transports were determined by combining the respective advection of the hydrodynamic currents and the respective motility of the jellyfish. In scenarios, the determination of the vertical transport was varied by replacing the free-swimming vertical motility with the special light-induced DVM. The advective transport calculation was executed under EFDC's drifter module. The motility transport calculation was executed under a newly developed swim submodel, as presented in Section 2.2. Finally, the transports were joined together within the model.

Jellyfish life stages or other biological traits that might influence their transportation were not considered in this model for simplicity. Due to individual variations in size and sex, variable responses to swim speed were normalized within this model by disregarding their relative responses. However, variations in transport patterns due to individual variations in either biological or behavioural traits were investigated through scenario modelling. Each particle was capable of locally sensing the tidal currents and their depth in the water column, which were used to define the swim speed and direction. Different combinations of those swim variables were used to devise alternative swim rules for testing, as outlined in Section 2.2.2. Particles were mutually exclusive; there was no interaction or communication among them that might affect each other's transport.

Advection, diffusion, and swimming along horizontal and vertical directions as well as the DVM, wherever applicable, were synchronous throughout the simulation. The swim process was designed upon the specification of speed and direction. The specifications were pre-defined. Conditional swims varied online in real-time with respect to particle depth, current speed, and tidal direction. Swim direction was specified in the model in terms of with-tide or against-tide, irrespective of the state of the tide. However, the swims on the ebbtide were directed exclusively against the tide. Transport outcomes are computed at each timestep and outputted three-dimensionally at half-hour intervals in terms of particles' spatiotemporal occurrence.

7.2.3.1. Entities, State Variables, and Scale

Like the DVM model, this biophysical (swim) model is composed of two main entities - (1) the particles and (2) the model grid cells. In addition to the state variables previously used in the DVM model for the model entities, the swim model contains two additional variables - the particles' horizontal swim speed and swim direction. The speed was specified either independently by the user or dependent on the current speed (expressed as a percentage of the current speed), and the direction was specified with respect to the tide (with or against). The hydrodynamics were resolved on the fixed model grid, but the particle locations were refined at sub-grid resolution using standard cartesian coordinates. The particle locations were output at half-hourly intervals.

7.2.3.2. Input Data

Five types of input data were used in the swim model:

- (1) hydrodynamics to impart advection to the model particles,
- (2) particle release information (e.g., location, time, and depth of release)
- (3) swim speed to provide jellyfish motility,
- (4) swim direction to provide jellyfish orientation with respect to the tide
- (5) DVM properties to cue light-induced vertical movement.

The current data, which were generated within the main hydrodynamic module of EFDC, were useful within the swim model at every timestep to resolve the passive drift displacements of particles. The swim speed and direction data, which were supplied into the swim submodel via the input data file, were used at every timestep to determine the active swimming displacements. The swim submodel, in turn, supplied the processed information into the hydrodynamic drift model, where these data were coupled to ultimately effectuate the combined transportation due to drifting and swimming. Particle release information of the simulation specific to the reference jellyfish was useful to backtrack any individual variation causing variable impact in transport pattern. DVM specification data, specified in the input data file, were used in scenarios where the DVM replaced the passive vertical movements to

investigate the effect of light-induced vertical motility combined with horizontal swimming.

7.2.4. Scenario Modelling

A range of swim model scenarios was simulated to investigate the effect of different swimming rules and other model specifications on the model performance. For these simulations, particles representing adult jellyfish were released into the biophysical model according to the release information of the observed jellyfish. For each scenario, batches of 100 particles were released, representing a single reference jellyfish release. They were released on 20 Aug 2015 at the corresponding tide time and coordinates of the tagged jellyfish releases and at four different depths of water: surface, first quarter, mid, and third quarter. Simulations were run for a period corresponding to the tracked record of the reference jellyfish ranging from 1 to 7 days.

Swim scenarios were planned to investigate the effects of different combinations of swim properties and specifications over the tide type and particle depth. Flow-independent and flow-dependent swim speeds and directions were assessed for both constant and variable levels. Swim direction with or against the tide was universal across the scenarios; however, the relative durations of those directional swims varied in different scenarios.

7.2.4.1. Assessing Model Sensitivity and Effects of Swim Rules

Upon the development of the jellyfish swim submodel, its sensitivity to behavioural integration, particle release conditions, and the various swim parameters specified in the swim rules was tested by assessing model output from a range of model scenarios. A summary plan of the sensitivity study is presented in Table 7.2. The table lists the swim-related factors that were assessed for sensitivity. Relevant swim scenarios were grouped together to investigate a particular sensitivity. The impact of integrating the swim with the drift and varying the swim rule, speed, direction, and release condition and the dependence of swimming on tide and depth

Chapter 7: Swim Modelling

investigated through the swim sensitivity study in the jellyfish transport modelling were all assessed. The sensitivity of the model to particle release depth was also assessed. All these sensitivity studies were conducted for the same jellyfish release – J-18495. Upon completion of the sensitivity study, the effect of swim rules on model performance was assessed, again using J-18495, to determine the optimum swim rule, and that rule was then used to assess model performance for two other jellyfish – J-1162 and J-18500.

Table 7.2 List of model scenarios run for assessment of model sensitivity and accuracy.

Sensitivity Studied	Specification	Method of assessment of model output		
Particle release conditions				
Particle releasing depth	Surface	RMSE		
	First-quarter			
	Mid			
	Third-quarter			
Swim feature assessed, rules compared and parameter settings				
	Rule No.	Swim Speed		
		with-tide (wt) ['+']	against-tide (at) ['−']	
Tidal dependent swimming	Rule-1	+0 m/s	−0.05 m/s	RMSE
	Rule-2			
	Rule-3			
	No swim	+0	−0	
	Rule-3	+0 m/s	−0.02 m/s	RMSE

Chapter 7: Swim Modelling

Constant swim speed		+0 m/s	−0.05 m/s	
		+0 m/s	−0.08 m/s	
Flow speed dependence of tide explicit steady swimming orientations	Rule-7	+15 %	−15 %	RMSE
	Rule-8	+15 %	−115 %	
		+20 %	−120 %	
	Rule-10	+60 %	−120 %	
		+75 %	−150 %	
	Rule-11	+15 %	−150 %	
Flow speed dependence of analytically determined dynamic swimming orientations	Rule-12**	+20 %	−120 % −6 % and −110 %***	RMSE
		+40 %	−140 % −12 % and −120 %***	
		+50 %	−150 % −15 % and −125 %***	
		+80 %	−180 % −24 % and −140 %***	
Slack tide swimming	Rule-4	+0	−100 %	RMSE
	Rule-5	+0	−0.08 m/s*	
			−100 %	
Flood tide swimming	Rule-6	+0	−15 %	RMSE
	Rule-7	+15 %	−15 %	
	Rule-7	+15 %	−15 %	RMSE

Chapter 7: Swim Modelling

Ebb drift neutralisation	Rule-11	+15 %	−150 %	
Minimum swim speed threshold	Rule-8	with any swim speed respective to the current speed		RMSE
	Rule-9	with at least at 0.2 m/s swim speed		
Transport strategy				
Swim rules	All scenarios under the rules for the J-18495 model			Particle distribution; Transport agreement
Model setup				
	Jellyfish models	Scenarios (with vs without swim)		
Jellyfish behaviour	J-18495	All the 12 rules	Passive drift	Particle distribution; Transport agreement
	J-1162	Best performing and supplemental swim rules		
	J-18500	Best performing and supplemental swim rules		

* Speed at slack tide.

** Proportionate orientation (on flood, wt:at = 35:65 and on ebb, wt:at = 25:75).

***Execution equivalence [$\beta_{eq}(fld)$ and $\beta_{eq}(ebb)$], respectively, where eq represents the equivalence, fld represents the floodtide, and ebb represents the ebbtide]

7.2.4.2. Assessment of Model Performance

The analysis of particle transport agreement with the observed jellyfish movements and comparing the swim model outputs with that of the passive drift model were done using the protocol previously described in Chapter 5.

7.3. Results

The results section presents the competence of the newly developed swim model in simulating jellyfish locomotion. First, the capability of the new swim code was tested to ensure that it was able to execute the planned swim behaviour and was free from bugs. Next, the sensitivity of the model to particle release depth was assessed. Following this, the sensitivity of the particle transport patterns and distribution to different swim rule parameters, such as swim speed and direction, was assessed. Finally, the transports for the twelve different swim rules were assessed with respect to observed jellyfish movements to determine the optimum swim strategies, and the optimum strategies were then applied to other jellyfish releases.

7.3.1. Testing the Performance of the Swim Code and Comparison with the Passive Drift Model

The primary focus here was to check the model's ability to simulate the swim behaviour of jellyfish, to provide confidence in the development of the submodel and its integration with the base hydrodynamic model. This was done by visually comparing the spatial distributions of particles from a swim scenario with those from a basic passive drift scenario. The comparison was carried out for jellyfish J-18495.

Fig 7.6 (a-c) presents snapshots of particle distributions captured from several swim scenarios (4 & 5 in 7.6a, 6 & 7 in 7.6b, and 8(1) & 9 in 7.6c) 120 hours after release and compares them with the corresponding particle locations from the passive drift model. The time instance of the snapshots allows sufficient differences to have developed between the distributions over the transport based on the different

jellyfish behaviours modelled. The particle distributions exhibit distinct variations, underscoring how various swimming behaviours lead to different final positions and distributions for the particles. In most cases, these outcomes are notably different from the distribution observed in the passive drift transport scenario.

The particle distributions depicted in Fig 7.6(a) reveal some significant trends. Firstly, when employing an ebb neutralizing swim (rule 4), it is observed that all particles ultimately end up inside the harbour, with the majority of particles tending to congregate to the east of the release location, where the passive drift distribution was found to be more widespread across the entire domain. Secondly, in the case of slack tide swimming (rule 5), the particles exhibit a distinctive behaviour by forming a cluster within the central region of the harbour. This clustering behaviour is quite pronounced. Again, this outcome sharply contrasts with the passive drift results, where the particles dispersed both to the east and west of the release location, spanning a considerable distance. In contrast to this, swimming at a significantly slower pace relative to the current speed during ebb and flood tides (rule 6 and rule 7, respectively) as depicted in Figure 7.6 (b), did not result in any substantial impact on particle transport and distributions when compared to passive drift. Introducing an additional swim condition, which involves maintaining a minimum swimming speed when the current flows fall below a certain threshold (rule 9), as part of a combined swimming strategy that incorporates multiple swim conditions into the transport strategy (rule 8), has the potential to induce a noteworthy alteration in particle distribution. This alteration manifests as the formation of a dense cluster or swarm of particles within the harbour as shown in Fig 7.6 (c). Indeed, all these examples serve to illustrate the impact of different swimming strategies in comparison to passive drift, highlighting clear distinctions.

Fig 7.6(d) shows the particle positions 120 hrs after release for the swim rule 12 scenario. The plot shows particles released at different depths. This can be directly compared with Fig 7.6 (e) which shows particle positions at the same time from a drift-only scenario. A comparison of the two shows that the particle distributions are clearly quite different and swimming according to rule-12 results in all particles ending up inside the harbour to the east of the release location. This is in contrast

Chapter 7: Swim Modelling

with the passive drift results, which show the particles have spread east and west of the release location over a very long distance. This difference in model results is also very apparent in Fig 7.6 (f), which shows traces of the travel paths of all the released particles from the time of release to the time of the snapshots (120 hrs after release). It is clearly seen that the passively drifting particle paths extend westward to the open sea boundary and eastward to the innermost extents of the harbour, while the swim particles' travel paths are much more concentrated and only extend to the east of the release location. Since the swim model rules were developed with the aim of getting more particles to travel to the east of the release location to better match the observed jellyfish movement, the results confirm that the model code is indeed capable of enabling the particles to mimic the desired jellyfish behaviour contained in the swim rules.

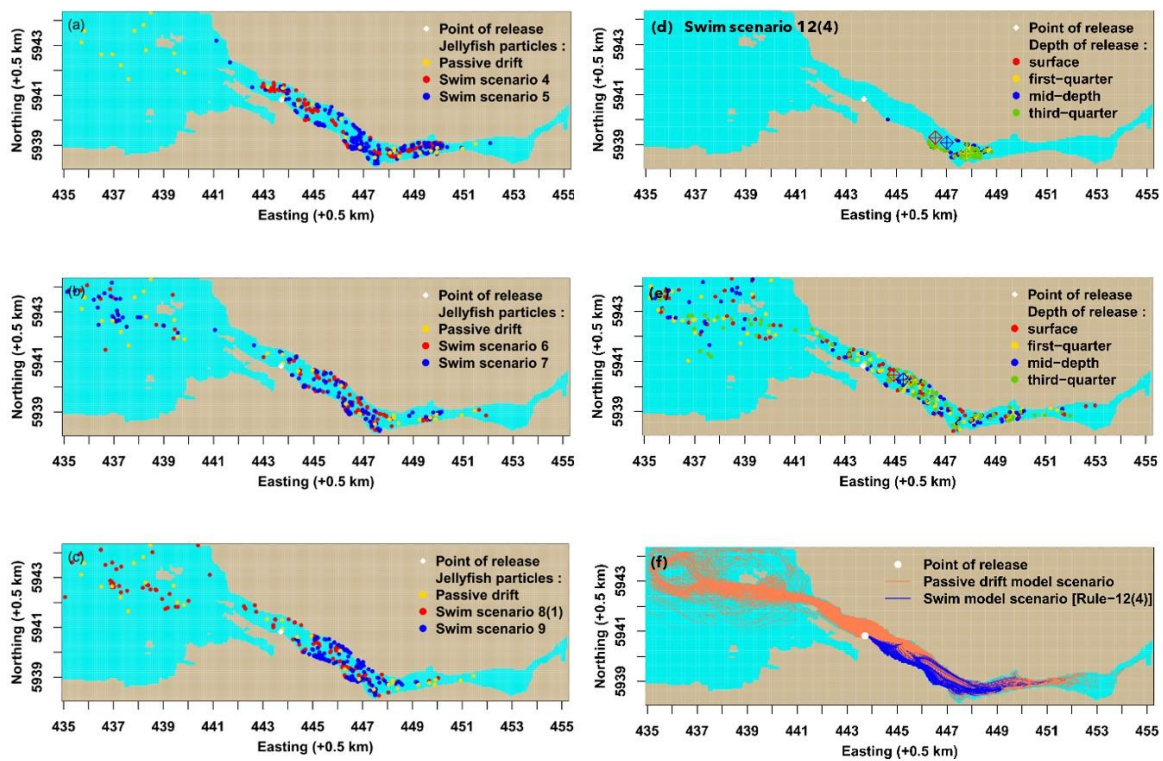


Fig 7.6 Snapshots of particle distributions captured from (a-d) multiple swimming scenarios and (e) a drift-only scenario, along with (f) representative comparative traces of their travel paths.

7.3.2. Sensitivity of Swim Model to Particle Release Depth

Jellyfish sample the depth-specific horizontal currents while they are at different depths and passive drifters. Exposure of the jellyfish to different vertical current fields would thus be expected to have an impact on their transportation. Since the release depth of the jellyfish was unknown, the sensitivity of model results to release depth was assessed by releasing the virtual jellyfish (particles) at four different depths (surface, 1st quarter, mid-depth and 3rd quarter). To investigate the differences in particle locations because of release depth, the RMSE (m) of pairwise particle centroids was calculated for the following release depth comparisons:

- Surface release versus 1st quarter, mid-depth and 3rd quarter release
- 1st quarter release versus mid-depth and 3rd quarter release
- Mid-depth release versus 3rd quarter release

The RMSEs were calculated for the passive drift model, and the 19 swim model scenarios ran in total; results are shown in Fig 7.7. In the figure, the bar heights represent the RMSE values, and the bar colours indicate the release depth comparison. Generally, RMSEs in east-west centroid positions are less than 500 m, RMSEs in north-south centroid positions were less than 300 m and RMSEs in centroid positions vertically in the water column were less than 1.5 m. The RMSEs were lowest for comparisons between the top two quarters and the bottom two quarters. They were highest for any comparisons between the top half releases relative to the bottom half releases. This is to be expected given that velocity variations will be greatest for the top half of the water column versus the bottom half, particularly for the surface versus the third quarter (i.e., bottom quarter). According to Fig 7.7, the centroid RMSE analysis shows that Scenario-12 was the most sensitive of the swim scenarios to particle release depth with RMSEs in an east-west centroid position of more than 1 km.

Chapter 7: Swim Modelling

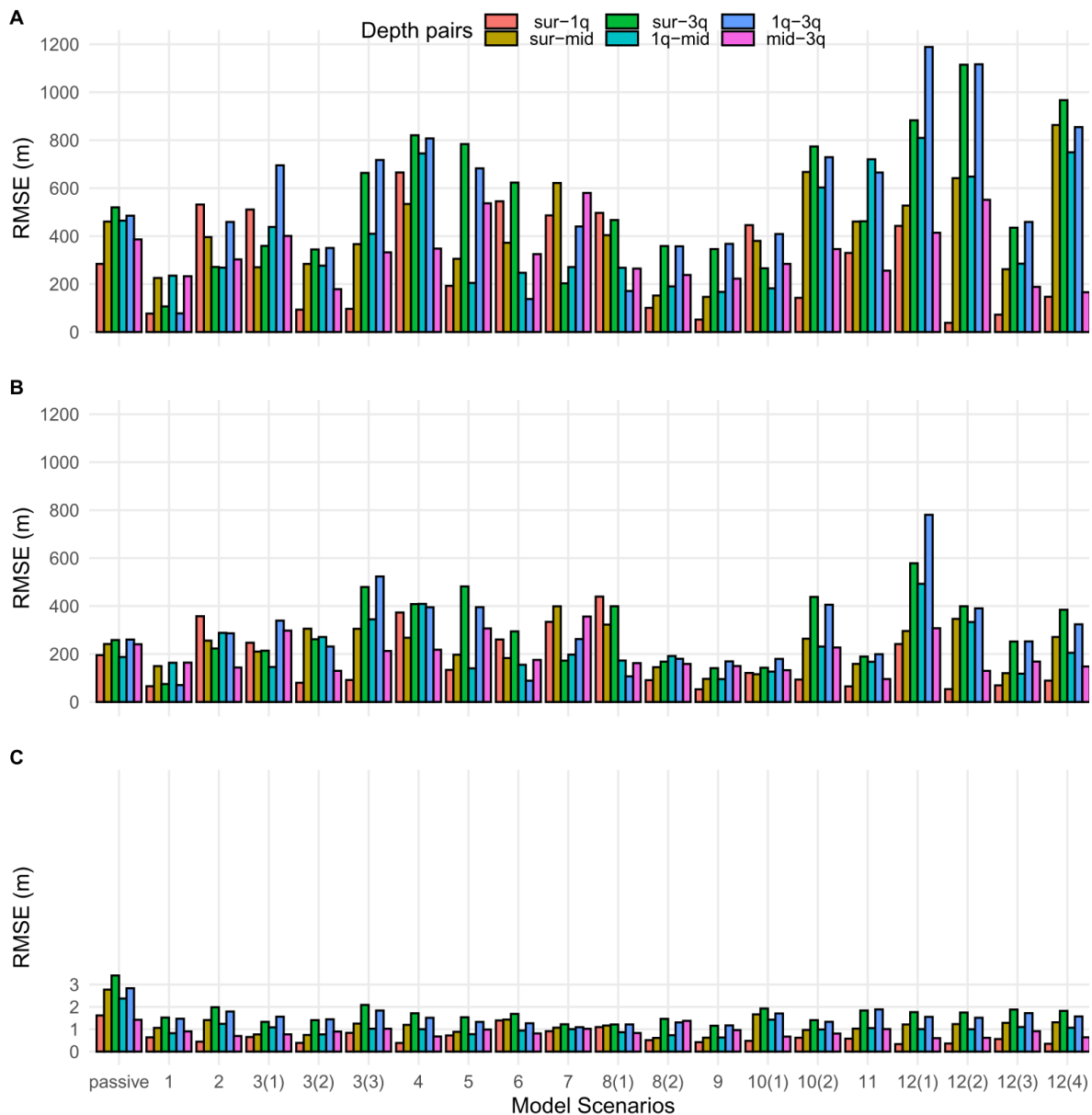


Fig 7.7 RMSEs (in meter, m) between pairs of particle centroids estimated across the (A) east-west, (B) north-south, and (C) water column depths upon releasing the particles at different water depths viz, surface, first quarter, mid-depth, and third-quarter.

7.3.3. Sensitivity of Model to Swim Parameters

In the present swim model, the effects of individual biological/behavioural variations in jellyfish swimming, such as the swimming speed and direction, were investigated using indirect IBM. Since the size is likely the most influential differentiating character in jellyfish swimming ability, scenario modelling of

variations in swim features was used to indirectly assess the effect of size variation upon transport. This section presents the results of an analysis of the sensitivity of the swim model to changes in some of the swimming rule parameters. Included in the analysis is an investigation of:

- The possible dependence of swimming on the stage of the tide
- variations in swimming speed and flow-dependent swim speed
- inclusion of swimming at slack tide
- ebbtide swim speed
- swimming direction
- neutralisation of passive drift
- inclusion of minimum threshold swim speed

In all cases, model sensitivity was assessed by comparing the differences (computed as RMSEs) in the locations of the centroids of the particle clouds over the course of the simulations. The sensitivity scenarios were conducted for J-18495 only.

7.3.3.1. Effect of Relationship Between Swimming and Stage of Tide

This sensitivity study was based on the hypothesis that jellyfish swimming behaviour may be dependent on the stage of the tide. For example, jellyfish might swim only on an ebb tide or only on a flood tide. Three swim rules (Rules- 1, 2 and 3) were therefore devised to investigate model sensitivity to tidal-dependent swimming. Rule-1 assumes that swimming is independent of the tide stage, and the jellyfish swim continually at a constant speed. By comparison, Rules-2 and 3 assume tidal dependence, so jellyfish swim only on the flood and ebb tides, respectively. In all three cases, the direction of the swim was against the tide, and the speed of the swim was constant at 0.05 m/s.

Fig 7.8 presents the results of the sensitivity analysis as a time-series of the particle cloud centroid location presented individually for the x (Easting), y (Northing) and z (Depth) component directions. Half-hourly-tracked centroid trajectories for the three swim scenarios (Rules-1, 2 and 3) are illustrated. The passive drift scenario is also included for reference. Differences in centroid location coordinates between

the swim scenarios were computed as RSMEs and are compared in the figure. The figure shows that the swim scenarios differ from the passive drift indicating that horizontal motility can have a significant influence on jellyfish transport. The figure also shows a significant influence of the tidal swims on particle transportation in all three directions revealed by the centroid trajectories and RMSE between the swim scenario conjugates. Flood swimming (Rule-2) drove the particle mass westward to the sea as the swimming negated some of the flood tide passive drifting, which would act to transport particles eastward into the harbour. In contrast, the particle mass moved more eastward inside the harbour under ebb swimming (Rule-3) as westward flood tide passive drifting was negated. Tide-independent swimming (Rule-1) kept the particle mass roughly centred on the release location as both flood and ebb tide passive drifting was negated by the continual swimming. The results provide clear evidence that any tidal influence on horizontal swimming can potentially significantly influence jellyfish transport and can result in notable different transports. The results also provided further confirmation that the swim rule model code was performing correctly.

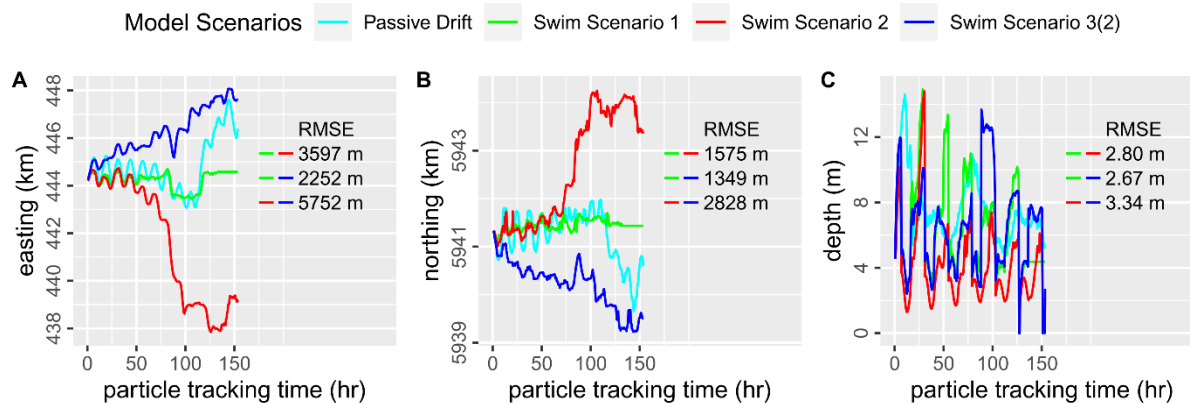


Fig 7.8 Spatiotemporal trajectories of particle centroid and RMSE of trajectory-pairs along the (A) east-west, (B) north-south, and (C) vertical directions illustrated upon passive drift and swim scenarios 1, 2, and 3(1) as per J-18495 model.

7.3.3.2. Swim Speed

Jellyfish may exhibit variable swim speeds due to their individual variations, more specifically, the size variation. A larger jellyfish is expected to swim faster due to their

larger bell pocket size, enabling them to push off the water quicker than a smaller individual. A transporting swarm of jellyfish composed of individuals of different sizes swim at different speeds, which impacts their net transportation. Swimming speed was specified in the model as either a constant value or a value which varied in relation to the ambient tidal current (i.e., flow-dependent). The model's sensitivity to swimming speed was investigated from the comparison of scenarios using the following swim rules:

- Rule-3: constant swim speed with ebb-only, against tide swimming
- Rule-7, 8, 10: flow-dependent swim speed with particles swimming with the tide on the flood tide and against the tide on the ebb tide.
- Rule-12: flow-dependent swim speed where the strength of flow dependence and direction of swimming changes over the course of a tidal cycle.

Constant Swim Speed

Rule-3 used a constant swim speed with ebb-only against tide swimming and was therefore used to assess the effect of varying the constant swim speed. Three scenarios were run using different swim speeds of 0.02, 0.05, and 0.08 m/s. The particle mass centroid trajectories are presented in Fig 7.9. The passive drift scenario is again included for reference and shows that ebb-tide swimming, regardless of swim speed, resulted in the particles travelling further east and south along the harbour. The variation in the swim speed created variations in transport in all three directions. Increasing the swim speed resulted in the particle mass travelling progressively eastward and southward as the stronger swim speeds negated more of the westerly ebb tide passive drifting. This trend is confirmed by ranking the easting and northing RMSE of the scenario conjugates. The results confirm that the model is very sensitive to swim speed when a constant swim speed is specified.

Chapter 7: Swim Modelling

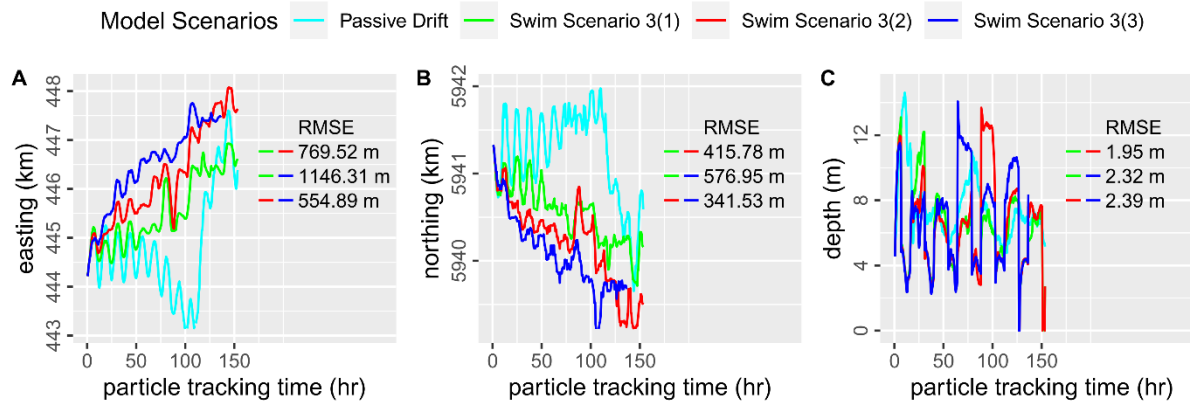


Fig 7.9 Spatiotemporal trajectories of particle centroid and RMSE of trajectory-pairs along the (A) east-west, (B) north-south, and (C) vertical directions illustrated upon passive drift and swim scenario 3 as per J-18495 model.

Flow-dependent Swim Speed

The sensitivity of the model to flow-dependent swim speed was assessed using scenarios which implemented Rules-7, 8 and 10, which were all based on the specification of a flow-dependent swim speed, i.e., the swim speed was specified as a percentage of the ambient current speed using the swim speed proportionality constant, β . For all three scenarios, particles swam with the tide on the flood tide and against the tide on the ebb tide.

Fig 7.10 compares the particle mass trajectories obtained for Rule-7 and Rule-8. According to Table 7.2, for Rule-7, β was set to a relatively low value of 15%, and the same value was specified for both the flood and ebb tides. By comparison, Rule-8 used the same value for the flood tide but used a value greater than 100% for the ebb tide. This meant that on the ebb tide, the passive drift was completely overcome, and net transport was in the opposite direction to the ebb tide - we call this ebb drift neutralisation. For Rule-8, two different scenarios were run where the second scenario - Rule-8(2) - used higher values of β than the first - Rule-8(1). For Rule-8(2), β was set to 20% and 120% for the flood and ebb tide, respectively, compared to 15% and 115%, respectively, for Rule-8(1).

Chapter 7: Swim Modelling

According to Fig 7.10, all the swim scenarios resulted in noticeably different particle centroid trajectories to the passive drift model. The low dependence flood and ebb swimming of Rule-7 resulted in the particles being transported east and west of the release location but with their centroid remaining centred around the release location. Interestingly, there was negligible difference between the trajectories simulated using Rule-7 compared to Rule-8(1), which reveals that ebb neutralization on its own was not enough to significantly impact transport relative to low ebb flow dependence.

In contrast, the results for Rule-8(2) show a significant difference from those from Rule-8(1). This implies that ebb neutralization could only create an influence above a particular threshold swim speed, dictated in this instance by the value of β . Scenario 8(2) drove the particles more east and south inside the harbour, while the lower speed scenario (Scenario 8(1)) and the speed upon the equalization strategy (Scenario-7) kept the particle mass or the net transport roughly to their release location, even at the end of a 7-day simulation period. Across depth, all the swim scenarios exhibit centroid trajectories the reflect the DVM pattern of movement.

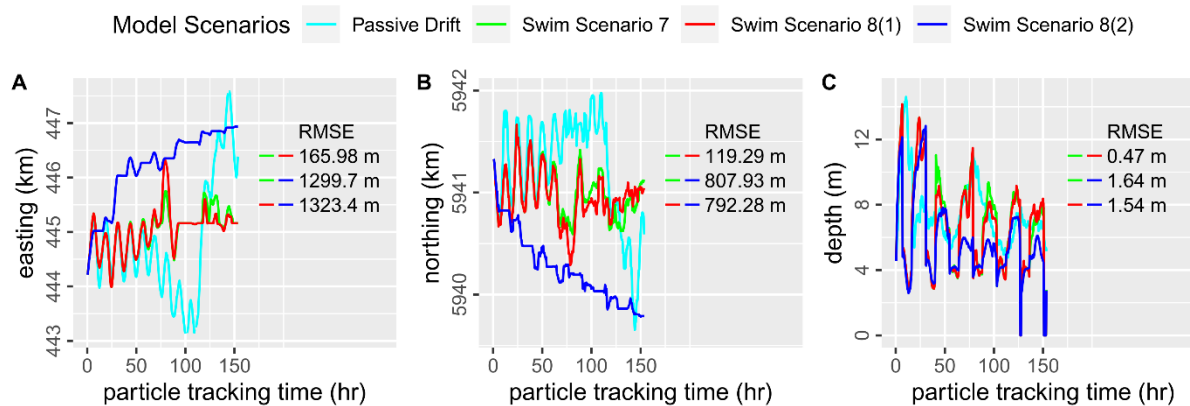


Fig 7.10 Spatiotemporal trajectories of particle centroid and RMSE of trajectory-pairs along the (A) east-west, (B) north-south, and (C) vertical directions illustrated upon passive drift and swim scenarios 7 and 8 as per J-18495 model.

Strength of Flow-Dependent Swim Speed

The sensitivity of the model to the strength of the flow-dependent swim speed was investigated by comparing results from the Rule-7 scenario ($\beta=15\%$ for flood and

ebb) with two scenarios based on Rule-10, which used values ebb drift neutralisation values for β greater than 100% and flood values of β that were half those of the ebb tide. β values for Scenario 10(1) were 60% and 120% for the flood and ebb tide, respectively, while those for Scenario 10(2) were 75% and 150%. Fig 7.11 shows the differences in the particle centroid trajectories for the three scenarios. It can be seen that the ebb neutralisation and the faster flood swim speeds of Rule-10 caused a significant easterly movement of the particles compared to Rule-7. In addition, the trajectories of the Rule-10 scenarios are very similar, as demonstrated by the RMSE of 446.04 m E and 279.25 m N between scenarios 10(1) and 10(2) compared to the RMSE values of the other scenario conjugates. Interestingly, there is less spatial variation in the trajectory for the 10(1) scenario than the 10(2) scenario; this may be due to the higher flood and ebb swim speeds.

The centroid trajectories of Scenarios 8(1) and 8(2) are compared with those from Scenarios 10(1) and 10(2) in Fig 7.12. Of particular interest here is the comparison between 8(2) and 10(1). For these scenarios, both used the same ebb tide β value of 120% but used different flood tide β values with 8(2) using a lower value of 20% compared to 60% for 10(1). The difference in the flood tide β value affected a significant difference in particle transport, as evidenced by the different centroid trajectories. The larger flood tide value, and thus faster flood tide swim speeds, of 10(1) resulted in the particles covering more distance on the flood tide and thus travelling farther eastward into the harbour.

Chapter 7: Swim Modelling

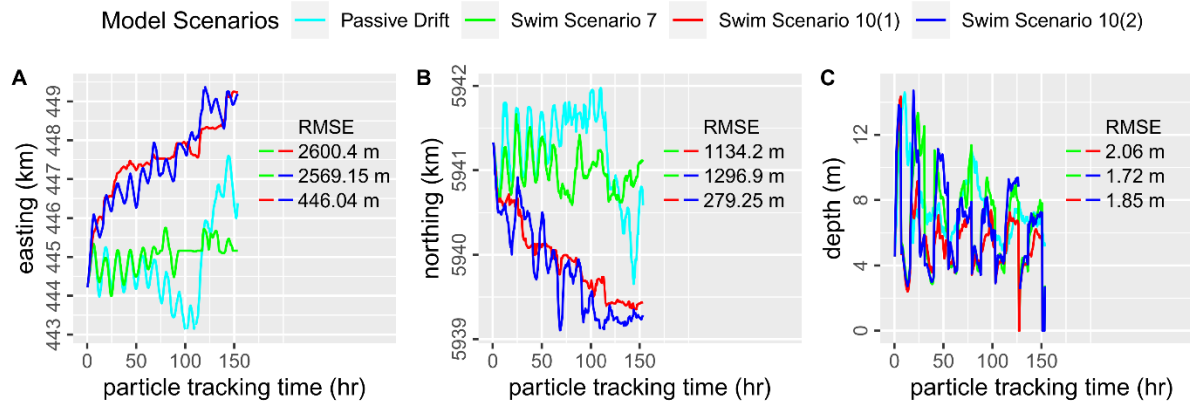


Fig 7.11 Spatiotemporal trajectories of particle centroid and RMSE of trajectory-pairs along the (A) east-west, (B) north-south, and (C) vertical directions illustrated upon passive drift and swim scenarios 7 and 10 as per J-18495 model.

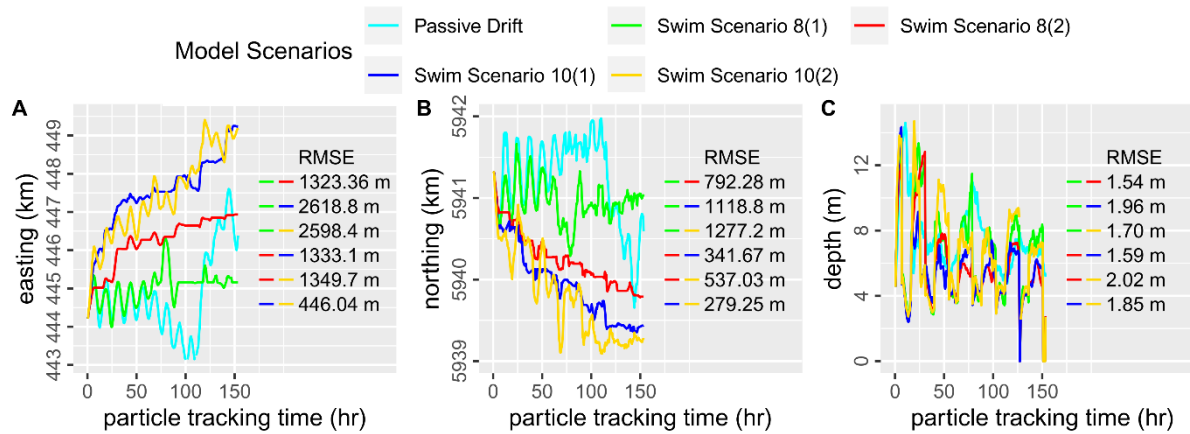


Fig 7.12 Spatiotemporal trajectories of particle centroid and RMSE of trajectory-pairs along the (A) east-west, (B) north-south, and (C) vertical directions illustrated upon passive drift and swim scenarios 8 and 10 as per J-18495 model.

Dynamic Orientation and Respective Flow Dependence of Swimming

The speed variations in the swim simulated as per the observed conditional orientation (proportionate) strategy (Rule-12) were analysed to exhibit the sensitivity of the model to variations within that strategy. The speed setting was configured by integrating the drift neutralization factor against the tide and assigning variable combinations across the scenarios at +20/−120, +40/−140, +50/−150, and +80/−180 percent of the current flows. Each combination in the configuration was composed of the tidal (flood and ebb) and orientation (with and against the tide)

Chapter 7: Swim Modelling

components at conditional proportions and simulated as per their execution equivalences (as in Table 7.2). The sensitivity analysis of the scenarios is presented in Fig 7.13. The figure shows the centroid trajectories illustrated spatiotemporally and their RMSE estimated between every two-speed combination of the strategy. Such an analysis of those four scenarios of four orderly speed combinations simulated in Rule-12 reveals their transport sensitivity to speed within the strategy. All the scenarios resulted in a south-easterly net transport with some individual transport variations at each, as shown in the figure. Their relative variations can be known from the RMSE of the scenario conjugates. The highest RMSE, 902.40 m E and 474.32 m N, are estimated between scenarios 12(1) and 12(4). This effect has a causal relationship with the fact that they are separated by the highest speed variation than the other scenario conjugates tested on this strategy. The trajectory lines and the relative RMSE in the figure reveal that the scenario transports were in order of the swim speed in the strategy. The speed combination +50/–150 in Scenario-12(3) let many particles dive deeper than the other three speed levels and created a depthwise transport variation from those, which is confirmed quantitatively by the highest RMSE levels of the respective scenario conjugates (3.24~3.31 m), as shown in Fig 7.13C. All these analyses prove that the setting and level of speed in a swim strategy are potential sources of transport variation.

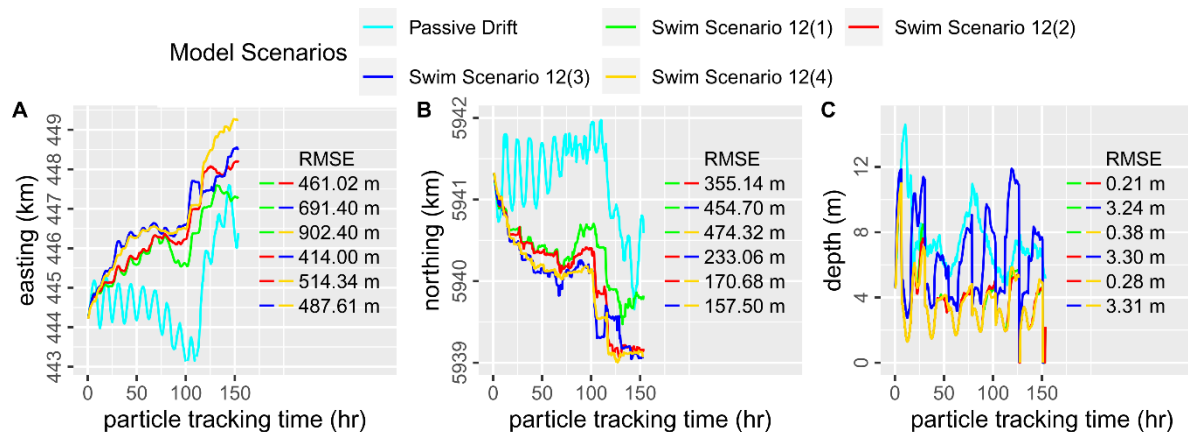


Fig 7.13 Spatiotemporal trajectories of particle centroid and RMSE of trajectory-pairs along the (A) east-west, (B) north-south, and (C) vertical directions illustrated upon passive drift and swim scenario 12 as per J-18495 model.

7.3.3.3. Swimming at Slack Tide

Rule-5 is based on the premise that a peak in swimming may occur at a time when there are little or no tidal currents (i.e. slack tide) and that this swimming at a time of minimal passive drift might have a noticeable effect on particle transport. To investigate this hypothesis, scenarios implementing Rule-4 and Rule-5 were executed. Both scenarios had no swimming on the flood tide and complete ebb neutralisation swimming on the ebb tide ($\beta=100\%$), but Rule-5 additionally allowed swimming at a constant speed of 0.08 m/s (based on the measured tidal currents in Killary) at the time around slack tide. The comparative analysis of centroid trajectories is presented in Fig 7.14. The figure shows that the incorporation of peak swimming at slack tide drove the particle mass eastward inside the harbour. The extent of the influence is ascertained by RMSE and estimated to be 1459.2 m, 937.21 m, and 2.98 m in the longitudinal, lateral, and vertical directions, respectively, proving a significant transport variation. , such behaviour of peaking the swim by a jellyfish during slack tide has the potential to result in significant transport variations.

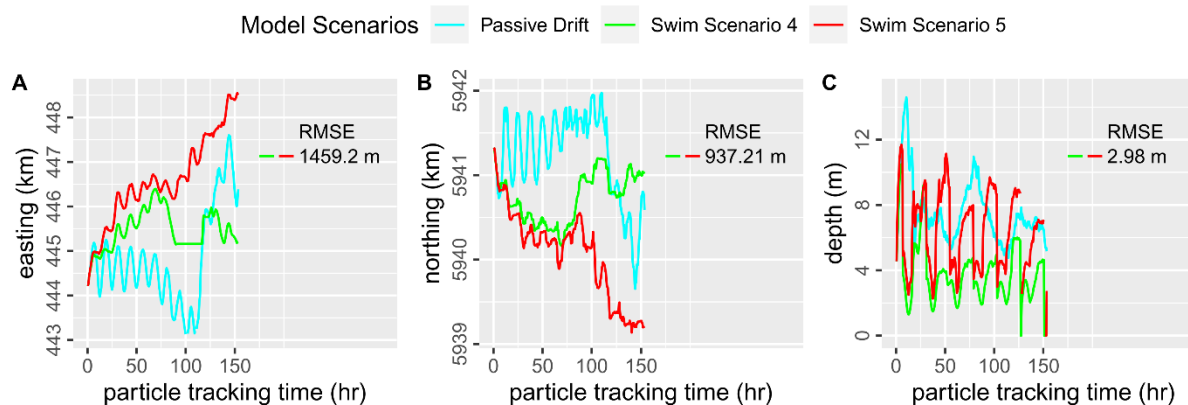


Fig 7.14 Spatiotemporal trajectories of particle centroid and RMSE of trajectory-pairs along the (A) east-west, (B) north-south, and (C) vertical directions illustrated upon passive drift and swim scenarios 4 and 5 as per J-18495 model.

7.3.3.4. Drift Neutralisation

Ebb tide swimming was of particular interest as neither the passive drift nor the DVM model affected sufficient easterly movement to particles to match the transport of J-18495. In Killary, the flood tide passively advects particles in an easterly direction

into the harbour while the ebb tide advects them in a westerly direction back out towards the sea. To negate the westerly ebb tide passive drift, particles were enabled with active swimming against the ebb tide, which was of sufficient strength to completely overcome the passive drifting, and the result allowed them to travel in an easterly direction on an ebb tide. This was achieved by specifying a value of $\beta > 100\%$. The effect of this strategy on jellyfish transportation was investigated by comparing a scenario with Rule-7, for which β was 15 % for both tides, with a scenario with Rule-11, for which β was 15 % for the flood tide but 150% for the ebb tide. The centroid trajectories are compared in Fig 7.15. The figure shows that introducing ebb drift neutralisation drove the particle mass eastward inside the harbour and provides evidence that ebb (or flood) drift neutralisation can have a significant influence on transport.

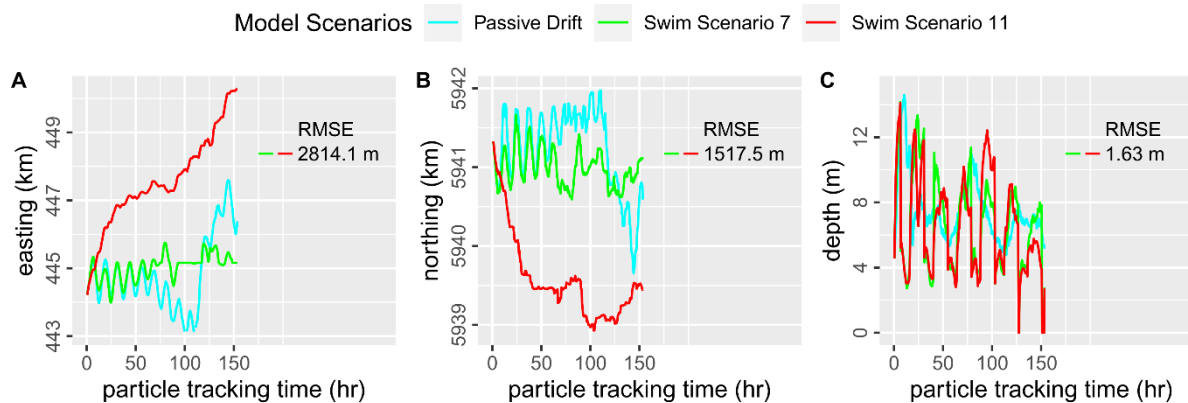


Fig 7.15 Spatiotemporal trajectories of particle centroid and RMSE of trajectory-pairs along the (A) east-west, (B) north-south, and (C) vertical directions illustrated upon passive drift and swim scenarios 7 and 11 as per J-18495 model.

7.3.3.5. Flood Tide Swimming

Varying the directional configuration of swim orientation based on tide and depth is expected to create variable impacts on jellyfish transportation. To investigate this, the ebb-exclusive swim model was modified to a universal swim model by activating the swim over both the flood and ebb tides. However, the swim configuration over the tidal orientation was made variable in two scenarios as per the swim rules 6 and 7. Its transport impact was explored by comparing the outputs of the simulations.

The swim was universally invoked against the tide at an equal speed (15 % of the flows) in both scenarios except, for a change, with the tide while the particles were lying deep in flood water. The effect of such a change in the configuration is presented in Fig 7.16 regarding the RMSE of the respective centroid trajectories. The figure shows that varying the swim configuration over the tidal orientation based on the particle depth created just some transport variation but could not influence the net transport to a level that can validate this strategy as a potential one to cause a transport impact. The transport variation caused due to this configurational variation is displayed in the figure by the trajectories. The extent of the variation is ascertained by RMSE and estimated to be 371.15 m, 222.74, and 0.70 m in the longitudinal, lateral, and vertical directions, respectively. Yet, depending on individual variation, a jellyfish may exhibit the swim orientation behaviour on any travel occasion as an adaptive strategy.

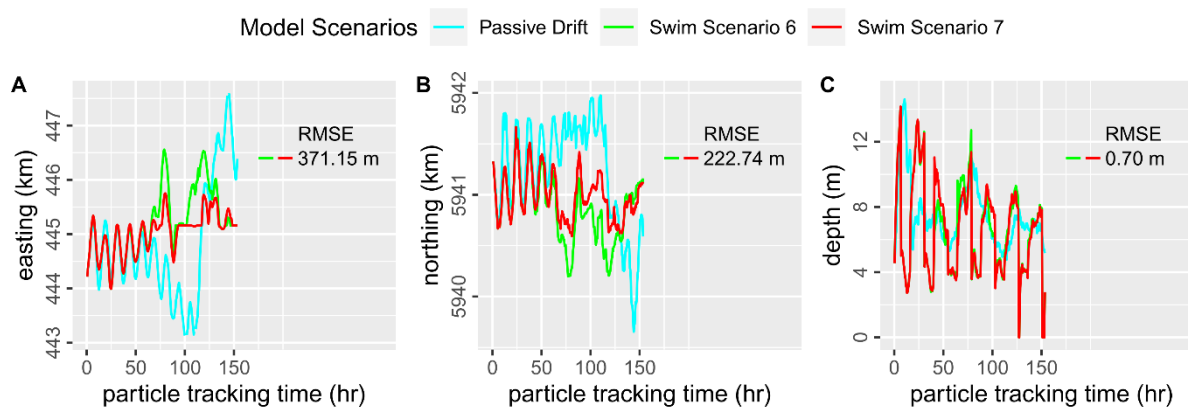


Fig 7.16 Spatiotemporal trajectories of particle centroid and RMSE of trajectory-pairs along the (A) east-west, (B) north-south, and (C) vertical directions illustrated upon passive drift and swim scenarios 6 and 7 as per J-18495 model.

7.3.3.6. Minimum Swim Speed

Maintaining swim speed relative to current flows in jellyfish is a process that calls on the energy to be utilised by them efficiently at the least possible cost of energy. At times when currents are reducing to very low values, but the water depth is still deep enough to support swimming activity, the jellyfish may want to continue moving with a minimum swim speed rather than a lower flow-dependent swim speed. Rule-9

implemented this behaviour where for the flow-dependent swim, a jellyfish may maintain a minimum speed even if the flow speed drops below a certain level. A current speed of 0.2 m/s was considered as the threshold for the Killary Harbour model, below which the swim in the model was set independent of the currents and instead maintained at 0.2 m/s. Its effect on transportation was investigated by comparing the centroid trajectories of the scenarios simulated without and with the minimum speed functionality (as per rules 8 and 9, respectively).

The centroid trajectories from the runs are presented in Fig 7.17. The figure shows that the east-west transports in Scenario-9 differ significantly from Scenario-8(2) by a very low RMSE at only 67.4 m, which represents an insignificant transport variation, whereas from Scenario-8(1) by 1293 m, which represents a significant transport variation (Fig A). It is here to note that Scenario-9 was adapted from Scenario-8(1). The outputs indicate that the strategy of using a fixed minimum swim (Scenario-9) influenced the overall transport by creating a variation from the transport that was without this strategy (Scenario-8(1)). The strategy created a transport effect like Scenario-8(2), which had a different swim speed than Scenario-8(1). Furthermore, the strategy transported the particles farther eastward inside the harbour since the transport was supplemented by the minimum swim against the ebbtide. The transport variations and trends are similar in the north-south (Fig B) and vertical (Fig C) directions.

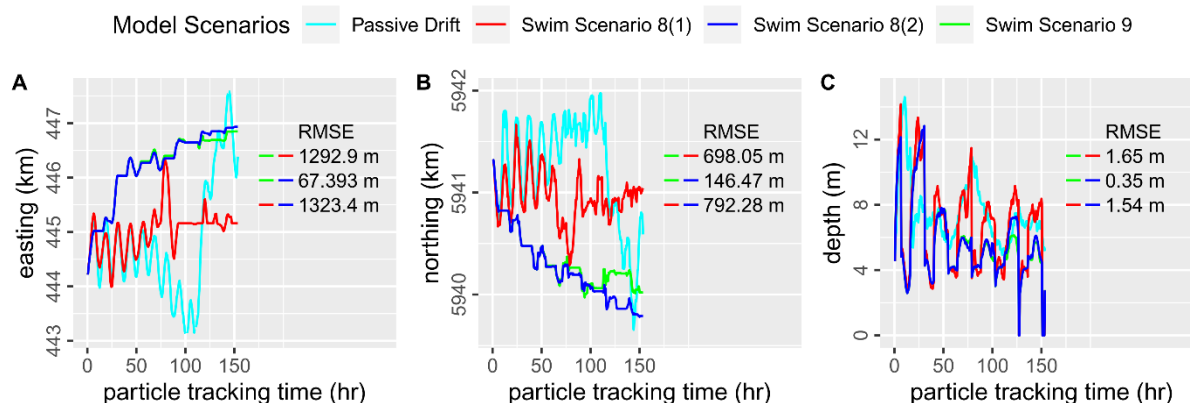


Fig 7.17 Spatiotemporal trajectories of particle centroid and RMSE of trajectory-pairs along the (A) east-west, (B) north-south, and (C) vertical directions illustrated upon passive drift and swim scenarios 8 and 9 as per J-18495 model.

7.3.4. Comparison of Model Performance Across Swim Rules

A total of twelve swim rules were devised for testing their relative performance in simulating jellyfish transport of J-18495. Using these rules, a total of nineteen scenario simulations were executed and analyzed. The same hypothesis used for the DVM modelling was used for the swim modelling, i.e., that coupling any behavioural transport (e.g., swim) with the routine passive drift could bring a positive effect on the transport agreement. Additionally, studying the transport patterns of the different swim rules would provide learning insights to better understand the effects of behavioural swimming on jellyfish transport.

7.3.4.1 Spatiotemporal Analysis of Transport

To test the hypothesis, the transport patterns of the swim-modelled particles and their agreement with the observed jellyfish in Killary were compared across the various swim scenarios and with the passive drift models. Fig 7.18 and Fig 7.19 show the spatiotemporal detections of the surface (Fig 7.18) and mid-depth (Fig 7.19) released particles which help to explore the variability in their transport distribution patterns across the model scenarios. Movements of the J-18495 jellyfish were detected in both the short-term and the long-term, indicated by the tracking periods from 3-11 hr and 120-133 hr, respectively. There was very little variability in transport results in the short term as there was insufficient time for any large movements to occur.

Fig 7.18T and Fig 7.19T show the detections of passively drifted particles over the course of the surface and mid-depth release simulations, and the recorded positions of the jellyfish are indicated by the red boxes. Model detections in the long-term period show that the passively drifted particles spread quite uniformly in both directions east and west from their initial release at S4, whereas the swimming particles showed more variable distribution patterns across the swim strategies (Fig 7.18 and 7.19 A~S). Similar long-term transport patterns to the passive drift were obtained with the swim scenarios where ebb-drifting was counterbalanced by

Chapter 7: Swim Modelling

swimming in the opposite direction to the tide (Scenarios-4, Scenarios-5 and 6) and with one of the conditional swim rules (Scenarios-12(1)).

For the tide-dependent swim scenarios (1-3), where swimming was executed at a constant rate of 0.05 m/s against the tide, the effect of tide specificity is evident from the results shown in Fig 7.18/7.19 A, B, and C. When swimming took place on both tides (plot A), particles still travelled relatively equally east and west of the release location, but they did not travel as far east or west as the passive drift particles, and none were detected at N1 in the inner harbour as per the observed jellyfish. For flood swimming (plot B), particles travelled more westward towards the sea as the swimming negated some of the eastward drifting on the flood tide; no particles were detected east of the S4 detection zone. For ebb-swimming (plot C), the particles moved more eastward inside the harbour as some of the westward ebb-drifting was negated; only a small percentage of particles were detected west of S4. Of the three scenarios, the long-term particle movements of the ebb-swimming scenario were most agreeable with the observed movements of J-18495. As might be expected, the distribution of particles for the ebb-swimming scenario also differed when the swimming speed was varied, with more particles travelling further eastward as the swimming speed was increased. Upon varying the ebb-exclusive swim speed from 0.02 m/s to 0.05 m/s and 0.08 m/s (Scenario 3(1)~3(3)), the particle distributions across detectors remained similar, but a greater proportion of particles moved further inside the harbour as the swim speed was increased (indicated by the detections in Fig 7.18C~E and Fig 7.19C~E).

Fig 7.18 and 7.19 I~O show that when swim speed is specified as a percentage of the flow speed, varying the strength of the flow dependence results in different transport distributions. All these scenarios specify against-tide swimming on the ebb tide, but on the flood tide, the swimming direction is depth dependent with particles swimming with the flood tide in deep water and against the tide in shallow water. Looking at the results, it is seen that scenarios 7 and 8(1) produced similar distributions, and scenarios 8(2), 9, 10 and 11 also produced similar distributions, which were different to those of 7 and 8(1). The latter set of scenarios all had much

Chapter 7: Swim Modelling

higher strength ebb tide swimming than scenario 7; thus, their particles could overcome more of the ebb drift, allowing them to travel further east into the harbour. This is clearly seen comparing plots K, L, M, N and O with the plot I (scenario 7). In plots, K, L, M, N and O, much greater proportions of the particles were detected east of the release zone S4. Particle release depth also had some impact on the results of Scenarios 8(2), 9, 10 and 11, with particles that were released at mid-depth travelling further eastward than those released at the surface.

The effect of flood tide swimming strength can be seen by comparing scenario 10(1) with scenario 8(2) and scenario 10(2) with scenario 11. For these respective pairs, the ebb tide swimming strengths were the same, but the flood tide swimming strengths were higher for the first-named of the pairs. Since most of the particles in the simulation reside in deep water, flood tide swimming is predominantly with the tide, so stronger flood swimming speeds result in particles travelling further eastward.

The effect of specifying slack tide as a time of peak swimming can be seen by comparing plot G for scenario (5) with plot F for Scenario 4(3). Both scenarios had no flood tide swimming, against-tide ebb tide swimming at the same strength swimming speed, but scenario 5 allowed higher speed swimming at a speed of 0.08 m/s near slack tide on the ebb tide. The plot comparisons show that the strategy of peak swim at slack tide pushed the particles further eastward inside the harbour due to additional and stronger swimming against the tide near slack tide. So, enabling jellyfish motility with peak swimming at slack tide is a potential transport strategy that might cause a swarm formation inside the harbour. Particle-releasing depth had no differential effect on this strategy, as demonstrated by comparing the effects between the surface and mid-depth released particles.

To investigate the effect of varying the against-tide ebb swim speed, two different speed levels at 15 % and 150 % of the current speed were used for scenarios 7 and 11, respectively. The transport distributions can be compared in plots I and O of Fig 7.18/7.19. The figures show that the distribution shifted farther inward within the harbour with increasing swim speed against the ebb tide, and this happened

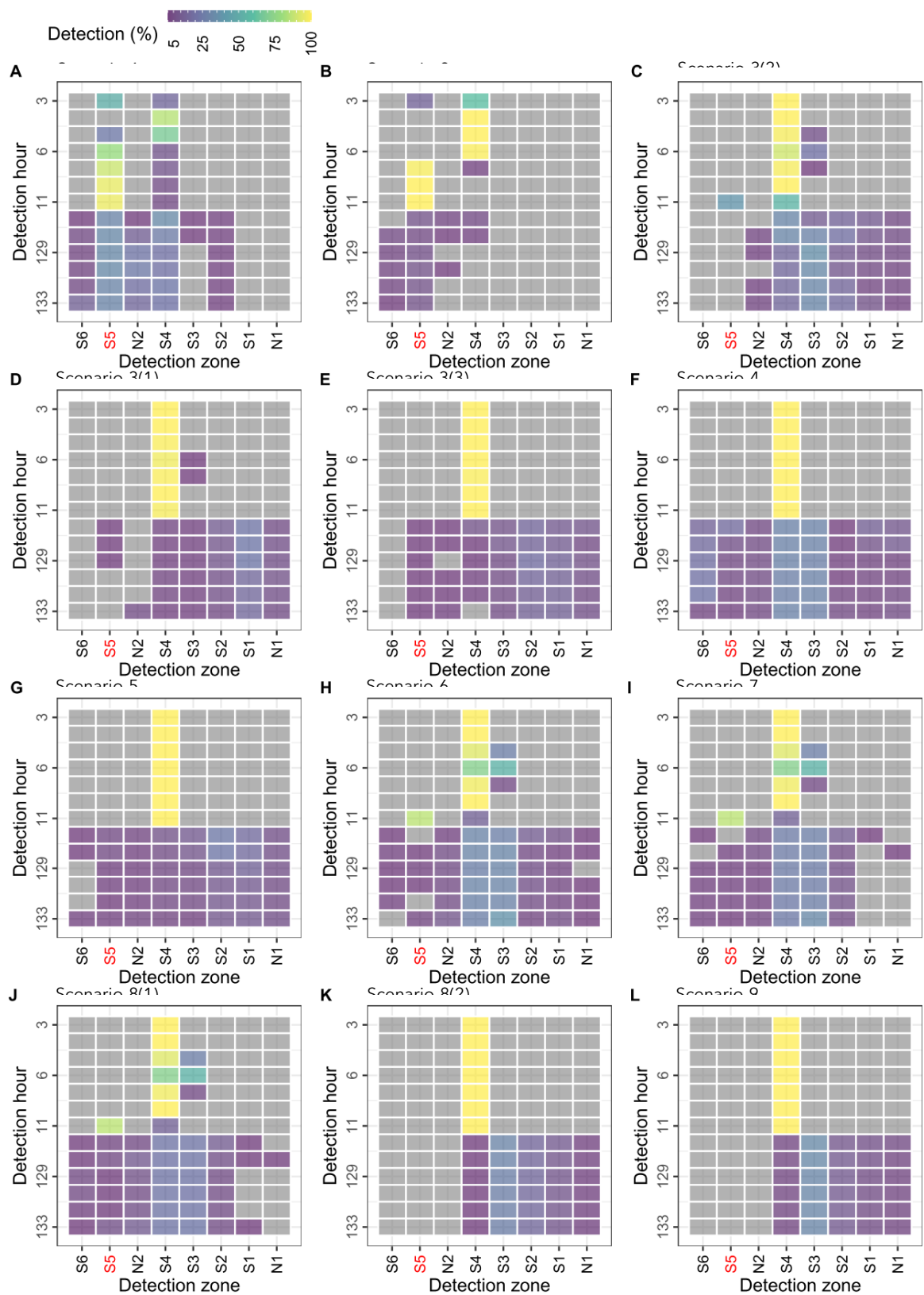
regardless of the particle release depth. Thus, the ebb swim speed can potentially contribute to a swarm formation inside the harbour.

The effect of ebb drift neutralization is demonstrated by results from Scenario-7 and Scenario-8, where Scenario-8 included ebb neutralisation and Scenario-7 did not. The strategy was based on specifying a flow-dependent swim strong enough to neutralize passive ebb drifting and was meant to create an effect that caused more particles to end up inside the harbour. The results of scenarios 8(1) and 8(2) show that this did not happen until the flow dependence was increased to 120% (Fig 7.18 and 7.19 K vs J, respectively).

Scenario 9 specified a minimum swim speed, such that the particles' swim speed could not fall below this level near slack tides. The distributions are shown in Fig 7.18 and 7.19 L. The figure shows an inclination of the particle distribution inside the harbour, which is quite similar to that of scenario 8, which does not have the minimum swim speed; thus, its effect appears negligible.

The transport distributions of the scenarios configured by variable levels of proportionate swims (Scenario-12) are presented in Fig 7.18 and 7.19 P~S. The figures show an increasing trend of easterly mobility of the particles with increasing swim speed across the scenarios within the strategy caused by the net differential effect between the easterly and westerly movements. The effect was more noticeable when the particles were released from the mid-depth water (Fig 7.18 P~S vs 7.19 P~S). The resultant easterly transport due to this swim behaviour was also more noticeable for particles released at mid-depth rather than those released at the surface, likely due to the surface currents being stronger.

Chapter 7: Swim Modelling



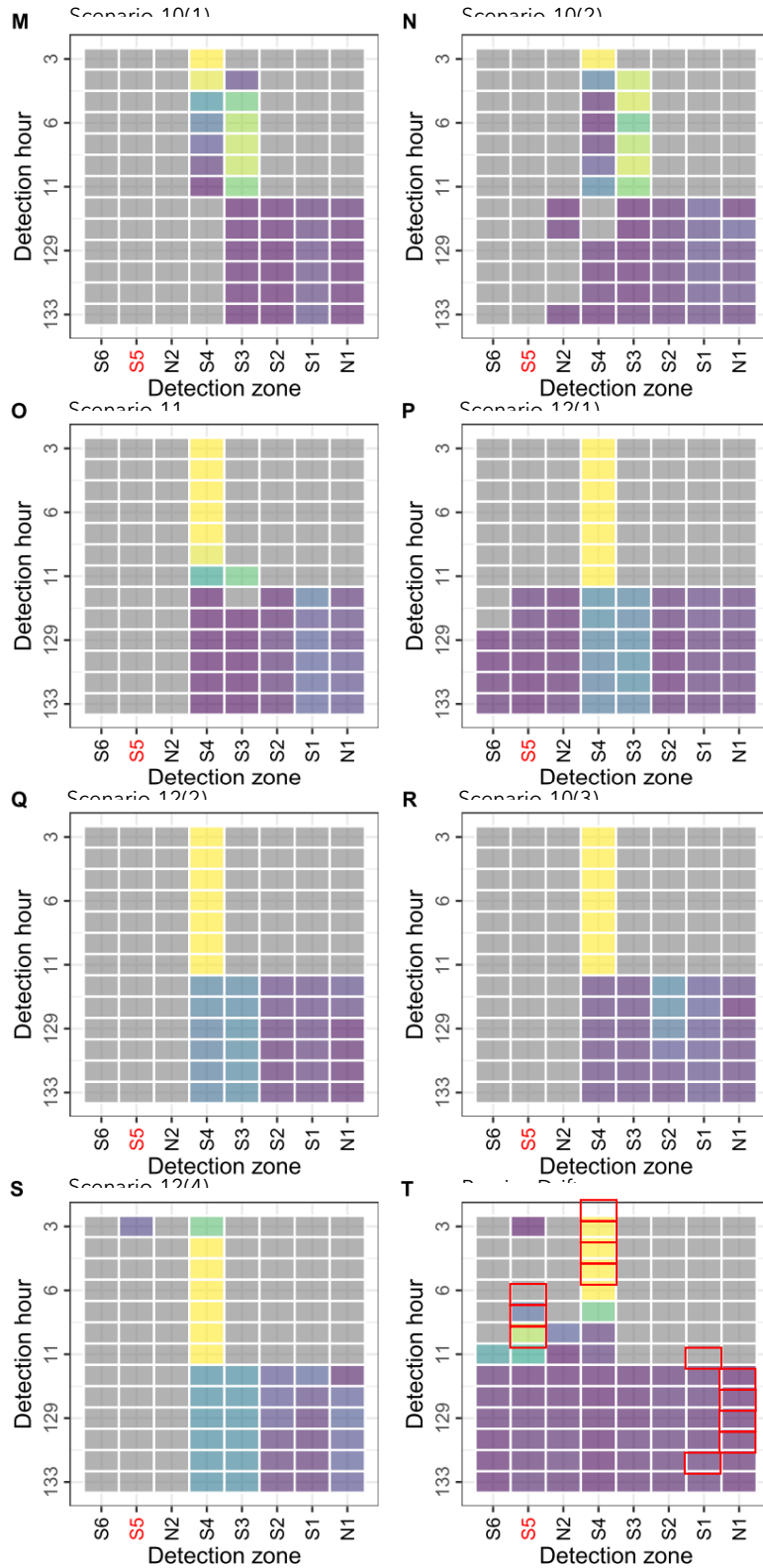
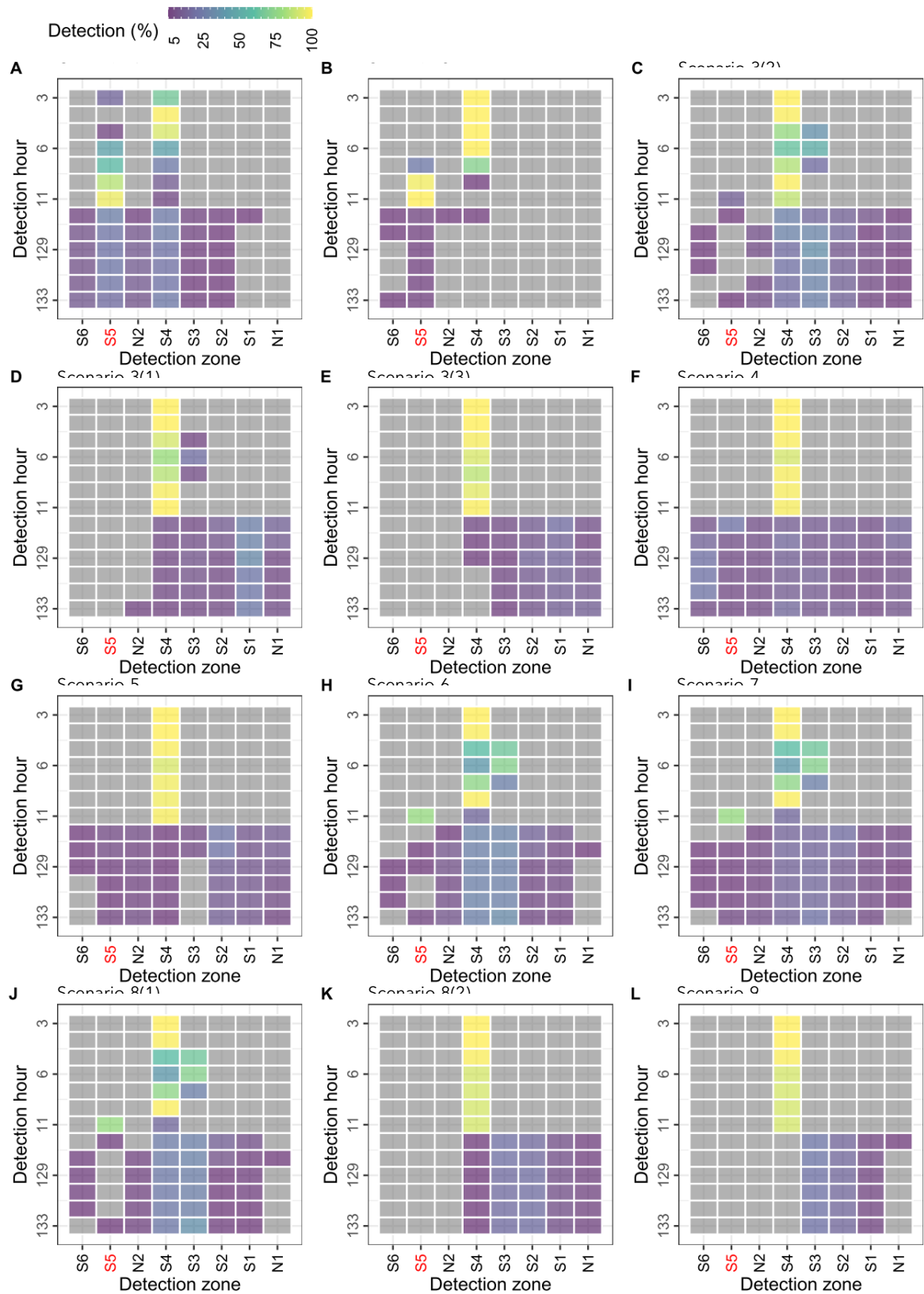


Fig 7.18 Spatiotemporal detections of surface-released particles from J-18495 scenarios.

Chapter 7: Swim Modelling



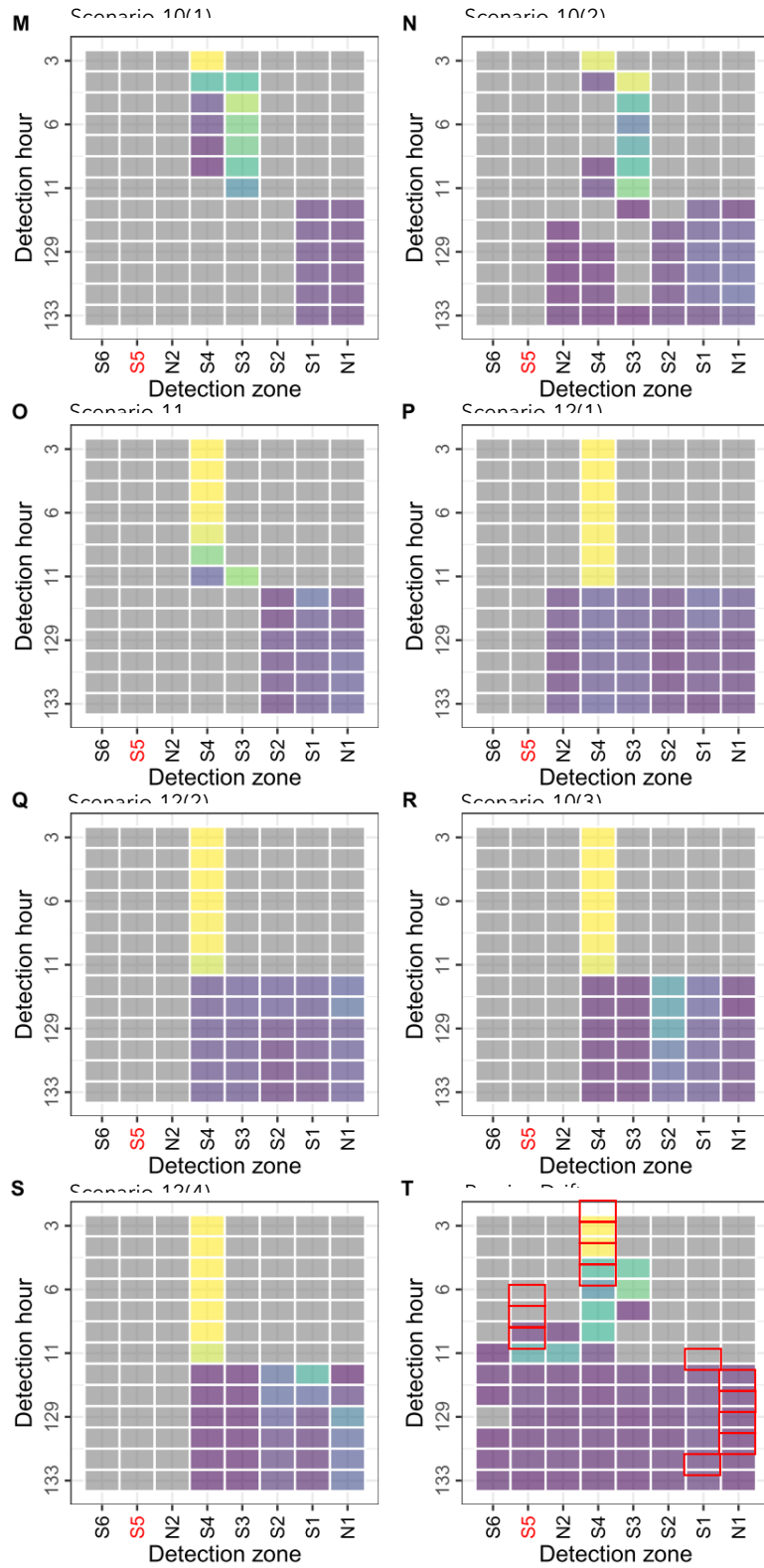


Fig 7.19 Spatiotemporal detections of mid-depth-released particles for J-18495 scenarios.

7.3.4.2. Agreement with Observations

Quantitative analysis of agreement with the scenario results with the observed detections of J-18495 are presented in Tables 7.3 and 432 for surface-released and mid-depth-released particles, respectively. The quantifications include the same statistical parameters used for the DVM modelling analysis: (1) the number of model particles present in the domain at each detection time instance, (2) the percentage agreement of the particles still present in the domain with the observed detection location, and (3) the distance of the centroid of all available particles in the model domain from the centre of the observed detection zone.

The number of particles present in the domain significantly affects the agreement statistics, as the percentage agreement is based on this number rather than on the total number of particles released. Therefore, fluctuations in this parameter over the simulation period influence the others. As Table 7.3 shows, in the short term (3-11 hrs after release, i.e., close to one tidal cycle), 100% of particles were present within the model domain. However, in the longer term (after about 10 tidal cycles), 100% of particles remained in just 12 of the scenarios; in the other 8, between 0~39 % of the surface released particles and 0~37 % of the mid-depth released particles left the domain depending on the scenario. Generally, the percentages of particles that left the domains were higher for the surface-release scenarios than the mid-depth release scenarios. The stronger surface current likely contributed mostly to transporting more of the particles out of the domain. The particle retention was seen to be impacted by a combination of relative exposure and time spent at the high, moderate, and low flow speeds regulated by depth migration and different initial drives at different depths mapping particles in horizontal space. Thus, higher retention was seen for the particles released at mid-depth than at the surface. Since the swim scenarios were developed to encourage more eastward transport of the particles, most of the swim rules devised for testing demonstrated the ability of full particle retention; the exceptions were rules 2, 6, 7, and 8(1).

Chapter 7: Swim Modelling

Percentage agreement is treated here as the most important model performance indicator, as it indicates a one-to-one match (as closely as the data allows) of the modelled and the observed transports. As can be seen in Table 7.3, percentage agreement varied with time during a scenario, as well as across scenarios. In each of the swim model simulations, the percentage agreement was higher for short-term transport (3~11 hr after particle release) compared to long-term transport (120~133 hr after release) for both surface and mid-depth releasing particles. This may be due to a combination of factors. First, the jellyfish might exhibit an initial short period of acclimatization to the hydrodynamic environment immediately after its release in the water, during which it might exhibit different, or no, swimming behaviour to normal. Similarly, in the shorter term, neither advection, diffusion, diel vertical migration, nor swimming has had sufficient time to cause any large variations in particle locations, and they generally remain quite clustered and close to their release location for that period. As a result, the modelled particles generally agree better with the observed jellyfish in this period.

At the time of the jellyfish release, it may be hypothesised that the jellyfish found itself in a phase of transitioning to a new environment and flow field, distinct from its previous conditions. During this phase, the flow dynamics exerted a greater influence on the jellyfish's movements compared to the biological cues of the jellyfish itself. Consequently, the jellyfish initially moved in alignment with the prevailing flows, representing its short-term behaviour immediately following its introduction to the new flow field. The model particles were configured to drift passively with the flows, as they are inanimate and virtual representations of the jellyfish. Hence, their transport patterns mirrored the jellyfish's short-term drifting behaviour. However, over an extended period, as the jellyfish became acclimated to the new flow field, they began to exhibit variable transport behaviour. As their transport behaviour gradually deviated from purely drift-driven movements, and instead displayed a more intricate pattern, it raises the question of whether jellyfish possess a drift-coupled swimming motility behaviour in their long-term response to the flow environment.

Chapter 7: Swim Modelling

The majority of models predicted the location of the jellyfish from hours 3-6 to a very high degree, although there were some exceptions, such as Scenario 1, which implemented both flood and ebb swimming. From hours 8-11, the percentage agreement of many swim scenarios reduced to zero, but this recovered to varying degrees in the longer term. In the short term (6-11 hrs), the highest percentage agreement was achieved by Scenario 2, with an average over this time of 94 % and 88.71 % for the surface and mid-depth released particles, respectively. In the longer term (120-133 hrs), Scenario-12(4) achieved the highest agreement with an average percentage agreement of 19.17 % and 25.67 % for the surface and mid-depth released particles, respectively; indeed, the mid-depth release for this scenario achieved the highest percentage agreement of all the swim scenarios, 55%, at 120 hr after the release of the particles.

The distances of the particle centroids from the respective detectors at the various detection instances of the observed jellyfish is the second important model performance indicator as it determines the model's tendency towards an agreement by a proximity analysis rather than a direct match. Thus, particles that are in the correct area of the harbour but are not within a particular detection zone are taken into account. In the short term, the centroids were mostly located within the correct detectors (500 m radius), with some exceptions. In the longer term, their distances range from a few hundred to a few thousand meters. According to Table 7.3, particle centroids were located at distances from the respective detectors ranging from 0.0 to 0.7 km in the short term and 0.15 to 11.29 km in the long term. Swim scenarios show high variability in this measurement in the longer term, but the scenario with the closest mean distance of the centroids with respect to the detectors had the highest probability of agreeing with the observed transportation. Multicriteria analysis of this agreement is presented later in this chapter.

Chapter 7: Swim Modelling

Table 7.3a Quantitative transport agreement of surface released particles in different scenarios.

Detector	Detection time (hr)	Swim rules and respective model scenarios																	
		Rule-1			Rule-2			Rule-3									No swim (drift only)		
		Scenario 1			Scenario 2			Scenario 3(1)			Scenario 3(2)			Scenario 3(3)			Passive Drift		
		1	2	3	1	2	3	1	2	3	1	2	3	1	2	3	1	2	3
S4	3	100	16	22	100	61	0	100	100	0	100	100	0	100	100	0	100	99	0
S4	4	100	85	0	100	100	0	100	100	0	100	100	0	100	100	0	100	100	0
S4	5	100	68	0	100	100	0	100	98	0	100	99	0	100	100	0	100	100	0
S4	6	100	8	75	100	99	0	100	90	0	100	97	0	100	100	0	100	100	0
S5	8	100	89	0	100	98	0	100	0	553	100	0	486	100	0	448	100	27	110
S5	9	100	95	0	100	100	0	100	0	299	100	0	375	100	0	442	100	86	0
S5	11	100	96	0	100	100	0	100	38	8	100	0	177	100	0	291	100	57	0
S1	120	100	0	4095	82	0	10096	100	10	1205	98	22.45	869	100	10	997	77	7.79	3048
N1	125	100	0	4844	69	0	11835	100	5	2451	97	6.19	1663	100	4	1591	68	2.94	3847
N1	129	100	0	4760	55	0	11215	98	4.08	2387	93	6.45	1506	99	7.07	1705	65	4.62	3384
N1	130	100	0	4762	63	0	11745	98	3.06	2322	93	7.53	1525	99	6.06	1742	65	4.62	3110
N1	131	100	0	4740	63	0	11737	98	3.06	2431	93	6.45	1606	99	5.05	1810	65	4.62	2948
S1	133	100	0	4123	61	0	11109	98	7.14	1816	93	17.2	824	99	13.13	1074	63	9.52	2367
Column headings: [1] Number of particles remaining in the domain, [2] Percentage of particles remaining in the domain that were located in the correct detection zone, [3] Distance (m) of the centroid of remaining particles from the centre of the correct detection zone.																			

Chapter 7: Swim Modelling

Table 7.3b Quantitative transport agreement of surface released particles in different scenarios (due part).

Detector	Detection time (hr)	Swim rules and respective model scenarios																	
		Rule-4			Rule-5			Rule-6			Rule-7			Rule-8					
		Scenario 4			Scenario 5			Scenario 6			Scenario 7			Scenario 8(1)			Scenario 8(2)		
		1	2	3	1	2	3	1	2	3	1	2	3	1	2	3	1	2	3
S4	3	100	100	0	100	100	0	100	100	0	100	100	0	100	100	0	100	100	0
S4	4	100	100	0	100	100	0	100	100	0	100	100	0	100	100	0	100	100	0
S4	5	100	100	0	100	100	0	100	93	0	100	93	0	100	93	0	100	100	0
S4	6	100	100	0	100	100	0	100	72	0	100	72	0	100	72	0	100	100	0
S5	8	100	0	241	100	0	450	100	0	579	100	0	579	100	0	579	100	0	546
S5	9	100	0	241	100	0	450	100	0	292	100	0	291	100	0	291	100	0	546
S5	11	100	0	190	100	0	419	100	86	0	100	86	0	100	86	0	100	0	545
S1	120	100	12	3395	100	17	773	80	8.75	2677	73	1.37	3279	84	1.19	3361	100	10	1374
N1	125	100	10	4019	100	6	1585	77	1.3	3858	63	1.59	3879	76	1.32	3986	100	2	2188
N1	129	100	3	4072	100	6	1522	78	0	3766	61	0	3869	74	0	3986	100	2	2092
N1	130	100	3	4067	100	5	1529	78	1.28	3746	61	0	3854	74	0	3986	100	2	2092
N1	131	100	4	4063	100	5	1513	77	1.3	3771	61	0	3868	73	0	3970	100	2	2092
S1	133	100	3	3472	100	10	783	77	6.49	3189	60	0	3151	71	1.41	3374	100	8	1306
Column headings: [1] Number of particles remaining in the domain, [2] Percentage of particles remaining in the domain that were located in the correct detection zone, [3] Distance (m) of the centroid of remaining particles from the periphery of the correct detection zone.																			

Chapter 7: Swim Modelling

Table 7.3c Quantitative transport agreement of surface released particles in different scenarios (due part).

Detector	Detection time (hr)	Swim rules and respective model scenarios											
		Rule-9			Rule-10						Rule-11		
		Scenario 9			Scenario 10(1)			Scenario 10(2)			Scenario 11		
		1	2	3	1	2	3	1	2	3	1	2	3
S4	3	100	100	0	100	100	0	100	99	0	100	100	0
S4	4	100	100	0	100	95	0	100	34	64	100	100	0
S4	5	100	100	0	100	44	11	100	4	409	100	100	0
S4	6	100	100	0	100	32	158	100	2	596	100	100	0
S5	8	100	0	546	100	0	1210	100	0	1416	100	0	527
S5	9	100	0	546	100	0	1286	100	0	1307	100	0	690
S5	11	100	0	545	100	0	1466	100	0	1097	100	0	948
S1	120	100	6	1583	100	6	63	100	15	0	100	31	0
N1	125	100	3	2273	100	3	840	100	17	690	100	11	531
N1	129	100	3	2271	100	2	806	100	8	660	100	10	78
N1	130	100	3	2271	100	2	804	100	8	646	100	15	0
N1	131	100	3	2271	100	2	790	100	11	660	100	15	14
S1	133	100	5	1588	100	13	21	100	9	0	100	22	288
Column headings: [1] Number of particles remaining in the domain, [2] Percentage of particles remaining in the domain that were located in the correct detection zone, [3] Distance (m) of the centroid of remaining particles from the periphery of the correct detection zone.													

Chapter 7: Swim Modelling

Table 7.3d Quantitative transport agreement of surface released particles in different scenarios (due part).

Detector	Detection time (hr)	Swim rules and respective model scenarios											
		Rule-12											
		Scenario 12(1)			Scenario 12(2)			Scenario 12(3)			Scenario 12(4)		
		1	2	3	1	2	3	1	2	3	1	2	3
S4	3	100	100	0	100	100	0	100	100	0	100	70	0
S4	4	100	100	0	100	100	0	100	100	0	100	100	0
S4	5	100	100	0	100	100	0	100	100	0	100	100	0
S4	6	100	100	0	100	100	0	100	100	0	100	100	0
S5	8	100	0	193	100	0	182	100	0	325	100	0	123
S5	9	100	0	239	100	0	233	100	0	419	100	0	241
S5	11	100	0	248	100	0	286	100	0	522	100	0	388
S1	120	100	10	1649	100	11	1107	100	16	570	100	24	1055
N1	125	100	9	2268	100	11	1776	100	2	1359	100	20	1758
N1	129	100	6	2339	100	2	1298	100	7	1217	100	25	1310
N1	130	100	7	2393	100	3	1209	100	8	1137	100	19	1259
N1	131	100	6	2486	100	3	1216	100	8	1091	100	21	1252
S1	133	100	6	1915	100	7	416	100	14	99	100	6	252
Column headings: [1] Number of particles remaining in the domain, [2] Percentage of particles remaining in the domain that were located in the correct detection zone, [3] Distance (m) of the centroid of remaining particles from the periphery of the correct detection zone.													

Chapter 7: Swim Modelling

Table 7.3e Quantitative transport agreement of mid-depth released particles in different scenarios.

Detector	Detection time (hr)	Swim rules and respective model scenarios																	
		Rule-1			Rule-2			Rule-3									No swim (drift only)		
		Scenario 1			Scenario 2			Scenario 3(1)			Scenario 3(2)			Scenario 3(3)			Passive Drift		
		1	2	3	1	2	3	1	2	3	1	2	3	1	2	3	1	2	3
S4	3	100	66	0	100	100	0	100	100	0	100	100	0	100	100	0	100	99	0
S4	4	100	99	0	100	100	0	100	99	0	100	100	0	100	100	0	100	100	0
S4	5	100	92	0	100	100	0	100	78	0	100	91	0	100	98	0	100	100	0
S4	6	100	44	10	100	100	0	100	63	0	100	80	0	100	92	0	100	100	0
S5	8	100	57	0	100	24	59	100	0	693	100	0	723	100	0	659	100	27	110
S5	9	100	85	0	100	97	0	100	0	484	100	0	553	100	0	619	100	86	0
S5	11	100	96	0	100	100	0	100	12	96	100	0	278	100	0	525	100	57	0
S1	120	100	1	4294	80	0	10012	99	7.07	2345	100	27	70	100	18	230	77	7.79	3048
N1	125	99	0	4749	70	0	11346	97	6.19	2918	99	11.11	1147	100	3	1087	68	2.94	3847
N1	129	98	0	4772	61	0	11222	97	1.03	2601	98	4.08	1052	100	8	1146	65	4.62	3384
N1	130	98	0	4789	67	0	11576	97	1.03	2620	98	4.08	1040	100	9	1145	65	4.62	3110
N1	131	98	0	4754	65	0	11504	97	1.03	2649	98	5.1	1036	100	10	1175	65	4.62	2948
S1	133	98	0	4035	63	0	11096	97	3.09	1968	98	24.49	0	100	12	166	63	9.52	2367

Column headings: [1] Number of particles remaining in the domain, [2] Percentage of particles remaining in the domain that were located in the correct detection zone, [3] Distance (m) of the centroid of remaining particles from the periphery of the correct detection zone.

Chapter 7: Swim Modelling

Table 7.3f Quantitative transport agreement of mid-depth released particles in different scenarios (due part).

Detector	Detection time (hr)	Swim rules and respective model scenarios																	
		Rule-4			Rule-5			Rule-6			Rule-7			Rule-8					
		Scenario 4			Scenario 5			Scenario 6			Scenario 7			Scenario 8(1)			Scenario 8(2)		
		1	2	3	1	2	3	1	2	3	1	2	3	1	2	3	1	2	3
S4	3	100	100	0	100	100	0	100	100	0	100	100	0	100	100	0	100	100	0
S4	4	100	100	0	100	100	0	100	99	0	100	99	0	100	99	0	100	100	0
S4	5	100	99	0	100	99	0	100	59	0	100	59	0	100	59	0	100	99	0
S4	6	100	91	0	100	92	0	100	40	68	100	40	68	100	40	68	100	91	0
S5	8	100	0	628	100	0	623	100	0	762	100	0	762	100	0	762	100	0	667
S5	9	100	0	628	100	0	623	100	0	447	100	0	447	100	0	447	100	0	664
S5	11	100	0	603	100	0	594	100	78	0	100	78	0	100	78	0	100	0	664
S1	120	100	6	2838	100	9	357	94	8.51	2577	80	5	1349	87	6.9	3276	100	6	1533
N1	125	100	13	3598	100	10	1257	88	1.14	3374	74	8.11	2489	78	1.28	3929	100	2	2262
N1	129	100	7	3603	100	8	1217	88	0	3467	72	1.39	2406	76	0	3779	100	3	2253
N1	130	100	7	3597	100	5	1227	88	0	3407	72	1.39	2446	76	0	3608	100	3	2253
N1	131	100	8	3606	100	5	1271	88	0	3484	72	1.39	2596	76	0	3649	100	3	2253
S1	133	100	4	3101	100	9	427	88	3.41	3306	72	5.56	2358	75	1.33	3266	100	6	1550
Column headings: [1] Number of particles remaining in the domain, [2] Percentage of particles remaining in the domain that were located in the correct detection zone, [3] Distance (m) of the centroid of remaining particles from the periphery of the correct detection zone.																			

Chapter 7: Swim Modelling

Table 7.3g Quantitative transport agreement of mid-depth released particles in different scenarios (due part).

Detector	Detection time (hr)	Swim rules and respective model scenarios											
		Rule-9			Rule-10						Rule-11		
		Scenario 9			Scenario 10(1)			Scenario 10(2)			Scenario 11		
		1	2	3	1	2	3	1	2	3	1	2	3
S4	3	100	100	0	100	100	0	100	93	0	100	100	0
S4	4	100	100	0	100	58	0	100	9	256	100	100	0
S4	5	100	99	0	100	12	248	100	0	629	100	100	0
S4	6	100	91	0	100	10	399	100	0	864	100	99	0
S5	8	100	0	667	100	0	1433	100	0	1675	100	0	656
S5	9	100	0	664	100	0	1525	100	0	1579	100	0	830
S5	11	100	0	664	100	0	1700	100	0	1373	100	0	1100
S1	120	100	3	1600	100	7	0	100	11	1199	100	24	322
N1	125	100	0	2292	100	6	162	100	15	0	100	9	0
N1	129	100	0	2286	100	6	271	100	17	0	100	12	0
N1	130	100	0	2286	100	6	303	100	19	0	100	17	0
N1	131	100	0	2286	100	6	331	100	21	0	100	17	0
S1	133	100	3	1543	100	9	0	100	7	435	100	12	708
Column headings: [1] Number of particles remaining in the domain, [2] Percentage of particles remaining in the domain that were located in the correct detection zone, [3] Distance (m) of the centroid of remaining particles from the periphery of the correct detection zone.													

Chapter 7: Swim Modelling

Table 7.3h Quantitative transport agreement of mid-depth released particles in different scenarios (due part).

Detector	Detection time (hr)	Swim rules and respective model scenarios											
		Rule-12											
		Scenario 12(1)			Scenario 12(2)			Scenario 12(3)			Scenario 12(4)		
		1	2	3	1	2	3	1	2	3	1	2	3
S4	3	100	100	0	100	100	0	100	100	0	100	100	0
S4	4	100	100	0	100	100	0	100	100	0	100	100	0
S4	5	100	100	0	100	100	0	100	100	0	100	100	0
S4	6	100	99	0	100	100	0	100	100	0	100	100	0
S5	8	100	0	586	100	0	508	100	0	467	100	0	372
S5	9	100	0	606	100	0	586	100	0	580	100	0	517
S5	11	100	0	626	100	0	650	100	0	681	100	0	717
S1	120	100	18	1150	100	15	0	100	18	620	100	55	0
N1	125	100	11	1846	100	27	694	100	1	1389	100	10	241
N1	129	100	6	1704	100	13	746	100	8	1244	100	37	34
N1	130	100	6	1788	100	16	791	100	8	1142	100	25	33
N1	131	100	6	1853	100	15	842	100	7	1106	100	22	62
S1	133	100	4	1197	100	7	0	100	14	96	100	5	185
Column headings: [1] Number of particles remaining in the domain, [2] Percentage of particles remaining in the domain that were located in the correct detection zone, [3] Distance (m) of the centroid of remaining particles from the periphery of the correct detection zone.													

Chapter 7: Swim Modelling

Further analyses of the transport agreements in the tables above are presented in Fig 7.20-437, which plot the agreement metrics (A - percentage agreement and B-centroid distance) of the modelled particles against time for J-18495. The figures help to explore the overall suitability of the swim strategies. The better performance of any scenario is indicated by higher percentage agreement and lower centroid distance.

For scenarios 1-3, where swimming was at a constant rate but depended on the stage of the tide, it can be seen from Fig 7.20 that Scenario-3(2), which specified ebb-only swimming against the tide, resulted in the highest percentage agreement and lowest centroid distances in the longer term compared to the scenarios with continual swimming (scenario 1) and flood-only swimming (scenario 2). This reveals that the jellyfish J-18495 may have used a swim strategy that helped it to limit the flow-induced westerly drift of the ebb tide to move eastward inside the harbour.

Continuing with the ebb-only swim strategy and varying the constant swim speed, Fig 7.21 shows that the higher swim speeds of scenarios 3(2) and 3(3) resulted in higher percentage agreement and lower centroid distances in the long run. While there was little difference in the results of these scenarios, the percentage agreement and centroid distances were noticeably lower and higher, respectively, for the lowest swim speed (0.02 m/s) of scenario 3(1). This demonstrates that a size variation in jellyfish which might influence their swim speed, could be significant when modelling the net transport of the jellyfish.

The transport strategy that applied swimming during slack tide (scenario 5) produced a different performance to that without any such behaviour, as shown in Fig 7.22. According to the figure, although the percentage agreements between the scenarios were similar (Fig 7.22 A1, A2 S, L), the centroid distances of scenario-5, which was based on peak swim at 0.08 m/s against the slack tide, were much lower than scenario 4 in the long term (Fig 7.22 B1, B2 L), indicating this to be a potential swim strategy.

Fig 7.23 shows transport metrics of several scenarios to allow a number of comparisons across scenarios. First, ebb-only swimming against the tide (Scenario-6; blue line) can be compared with a scenario similar to the ebb swimming strategy but allowing deep water particles to swim with the flood tide (Scenario-7; orange line), where all swimming is at 15 % of the flow speed. In the short term, the scenario metrics overly each other and are, therefore, the same. In the longer term, differences are also negligible. For Scenario 7, a lower centroid distance is demonstrated by the mid-depth released particles compared to the surface release - this might be because the with-tide effect of Scenario-7 resulted in an initial drive to the sub-surface particles to let them move eastward inside the harbour, creating a higher tendency of agreement in that direction. Second, the agreement due to the drift-neutralizing swim against the tide (Scenario-8(1) & 8(2)) was compared to an ordinary swim (Scenario-7) and marked in the figure by grey, red and orange lines, respectively. In the short term, the scenario outputs are overlaying, meaning their agreements are the same. Longer term, the relative agreements show the drift neutralization behaviour gives better performance while being used with higher swim dependence (-115% vs -120%). The drift neutralization was found to be an important swim behaviour to be used in the jellyfish transport modelling. The agreement due to the minimum swim at low (< 0.2 m/s speed) flows (Scenario-9) was compared to an ordinary flow-dependent drift-neutralizing swim (Scenario-8(1) & 8(2)), marked in the figure by black, grey and red lines, respectively. The agreements shown by the respective scenarios are very close to each other, indicating that the use of a minimum swim speed has negligible influence over the other scenario.

Specifying a flow-dependent swim speed in the model meant that the swim speed was controlled constantly by the flows. A particle thus swims faster when the ambient flows around the particle are higher in speed and swims slower when the ambient flow speed drops. The strength of this flow speed dependence varied between the scenarios in Fig 7.23, and it can be seen that Scenario-10 and Scenario-11 gave the best long-term model performance with the highest percentage agreement and lowest centroid distances. This provides an insight that the jellyfish

might not swim at a fixed speed; rather, they might use variable speeds related to the ambient flow speeds.

The performance metrics of the swim scenarios using varying combinations of the proportionate swim rule (Scenario-12) are presented in Fig 7.24. In the short term, performance metrics were the same (overlying lines), but performances in the longer term varied. Scenario-12(4), using swim speeds of +80/–180 % of the flow speed, generated the highest agreement among the combinations tested. This was supported by the centroid distance estimation of the mid-depth releasing particles. The particle-releasing depths (either surface or mid) did not have any remarkable influence on the effect of this swim behaviour. The modelled transport behaviour found thereby reveals that J-18495 might not have swum at a fixed rate of the flows and might have shown adaptive behaviour in swimming.

Chapter 7: Swim Modelling

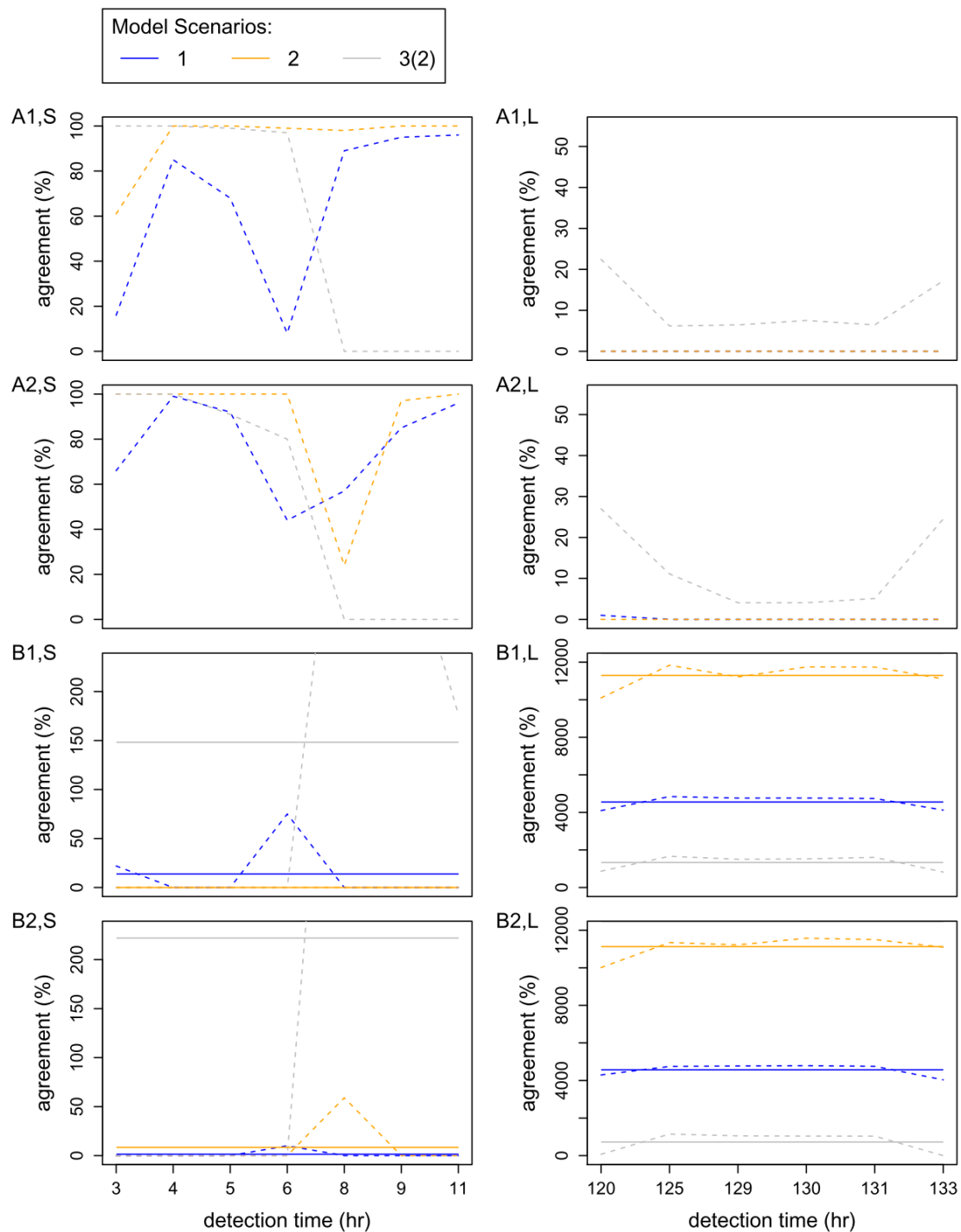


Fig 7.20 Comparing agreements as per J-18495 among the swim scenarios in terms of (A) percentage and (B) centroid distance for (1) surface and (2) mid-depth releasing particles over the short-term (S) and long-term (L) simulation periods. Real estimations are represented by the dashed lines and calculated means by the solid lines. [Notes: Specifications for the model scenarios are in Table 7.3. Centroid distances are from the periphery of the respective detectors.]

Chapter 7: Swim Modelling

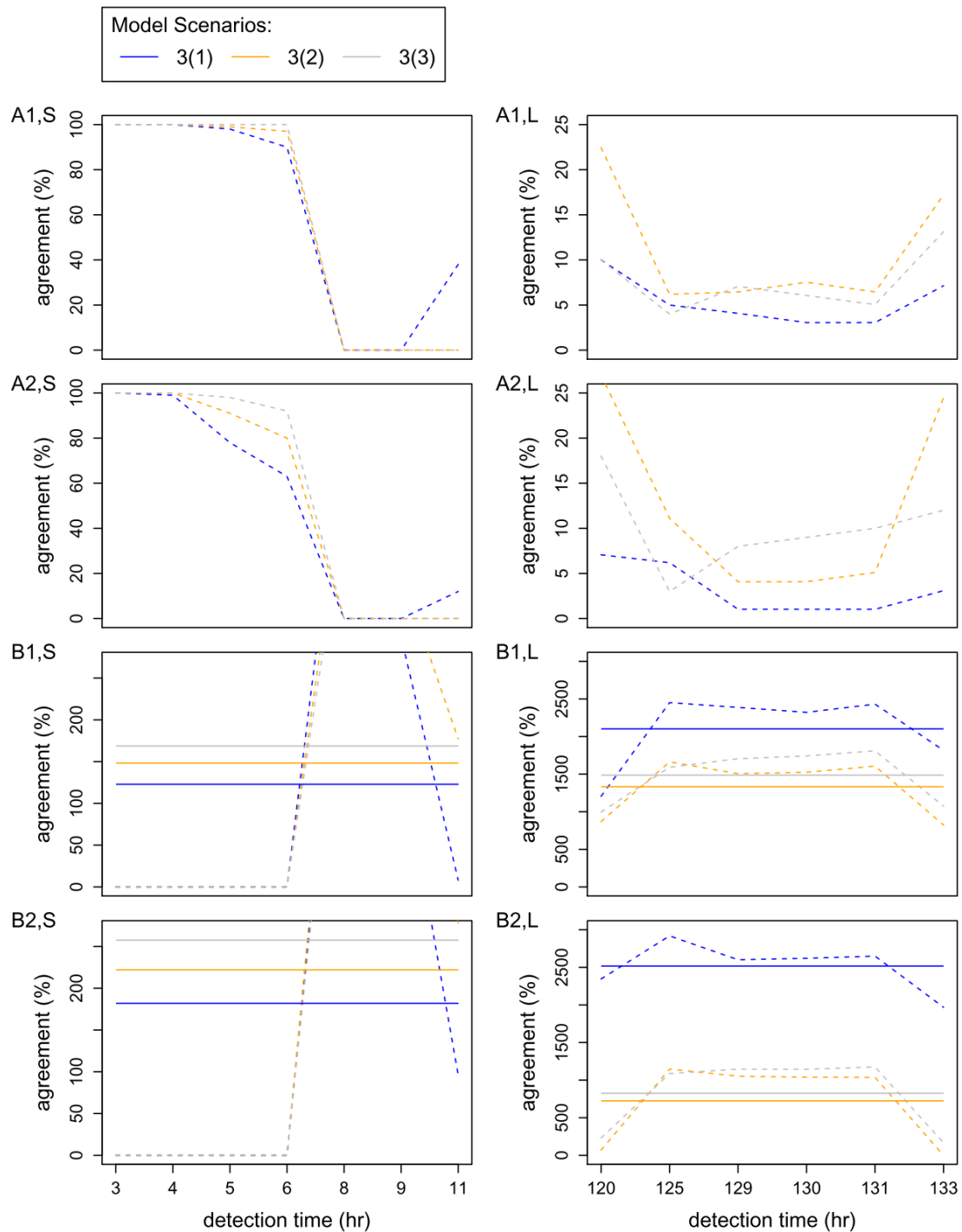


Fig 7.21 Comparing agreements as per J-18495 among the swim scenarios in terms of (A) percentage and (B) centroid distance for (1) surface and (2) mid-depth releasing particles over the short-term (S) and long-term (L) simulation periods. Real estimations are represented by the dashed lines and calculated means by the solid lines. [Notes: Specifications for the model scenarios are in Table 7.3. Centroid distances are from the periphery of the respective detectors.]

Chapter 7: Swim Modelling

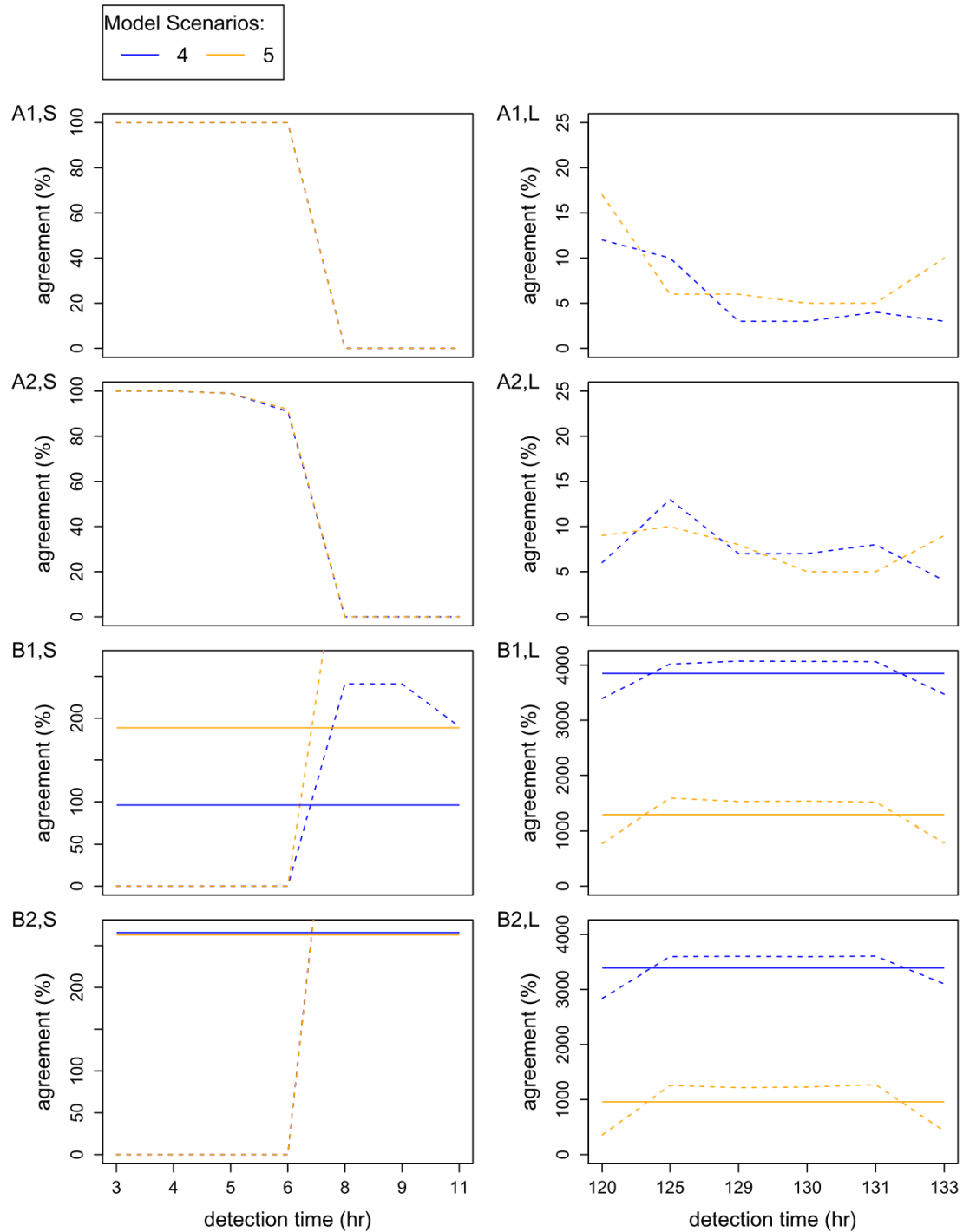


Fig 7.22 Comparing agreements as per J-18495 among the swim scenarios in terms of (A) percentage and (B) centroid distance for (1) surface and (2) mid-depth releasing particles over the short-term (S) and long-term (L) simulation periods. Real estimations are represented by the dashed lines and calculated means by the solid lines. [Notes: Specifications for the model scenarios are in Table 7.3. Centroid distances are from the periphery of the respective detectors.]

Chapter 7: Swim Modelling

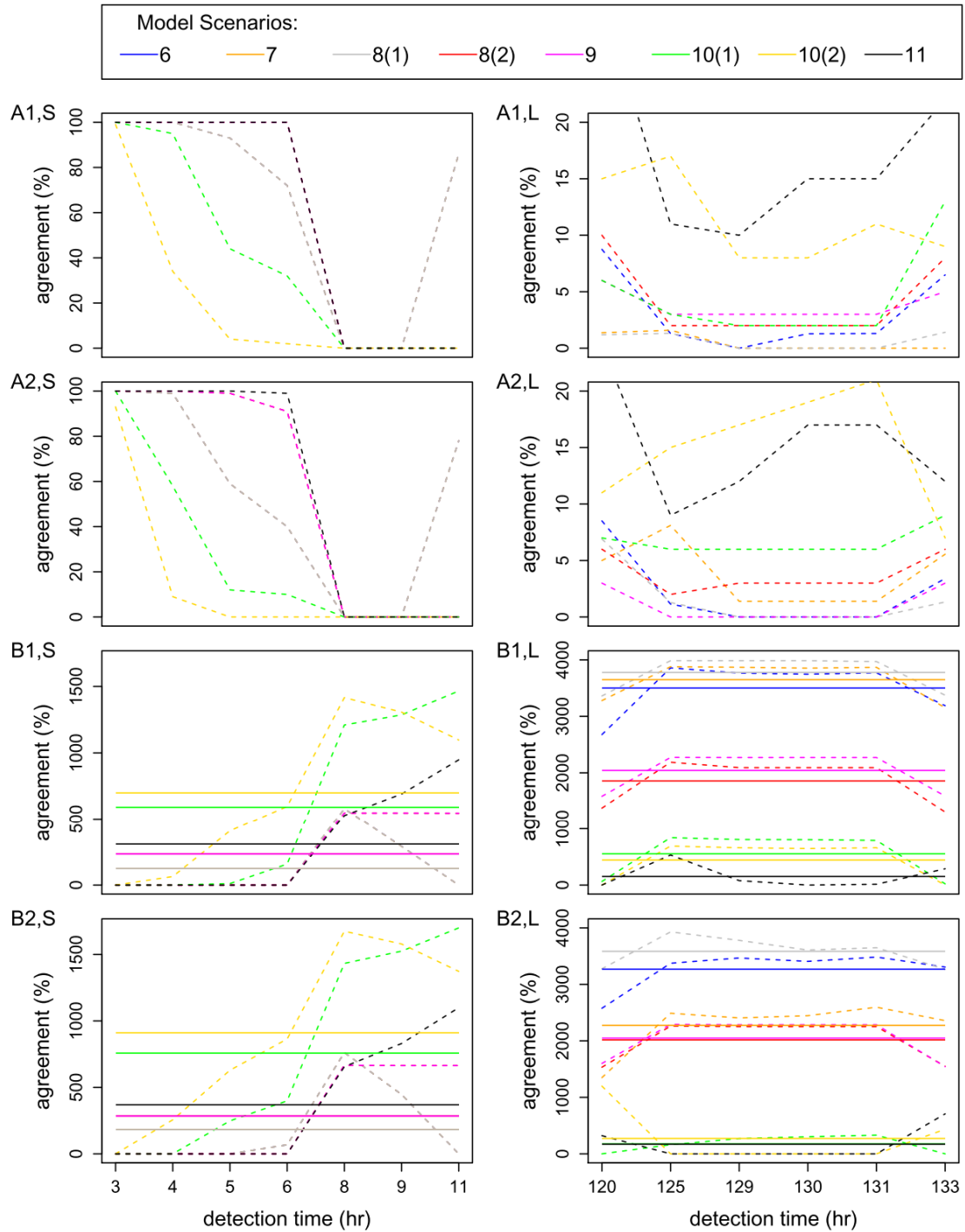


Fig 7.23 Comparing agreements as per J-18495 among the swim scenarios in terms of (A) percentage and (B) centroid distance for (1) surface and (2) mid-depth releasing particles over the short-term (S) and long-term (L) simulation periods. Real estimations are represented by the dashed lines and calculated means by the solid lines. [Notes: Specifications for the model scenarios are in Table 7.3. Centroid distances are from the periphery of the respective detectors.]

Chapter 7: Swim Modelling

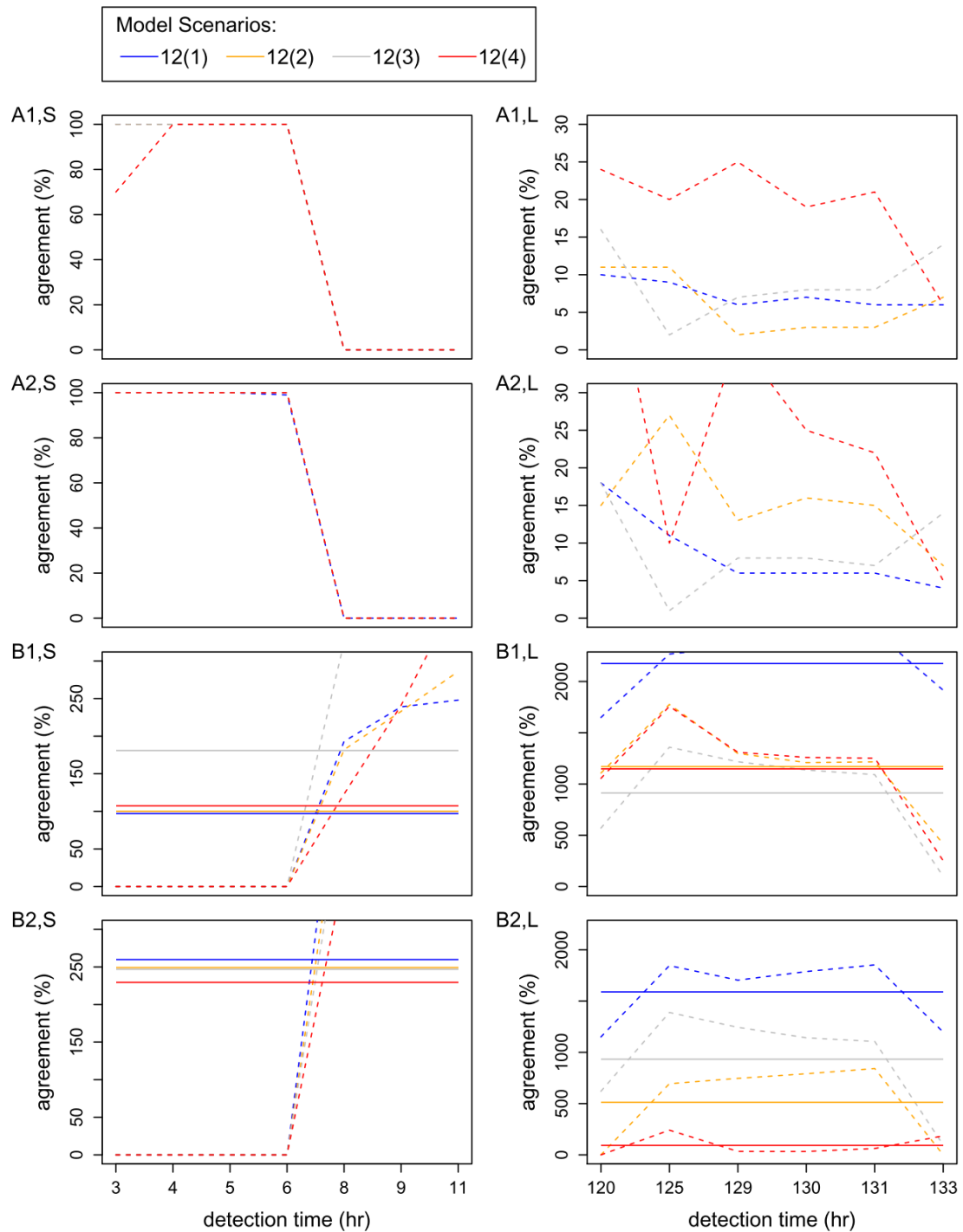


Fig 7.24 Comparing agreements as per J-18495 among the swim scenarios in terms of (A) percentage and (B) centroid distance for (1) surface and (2) mid-depth releasing particles over the short-term (S) and long-term (L) simulation periods. Real estimations are represented by the dashed lines and calculated means by the solid lines. [Notes: Specifications for the model scenarios are in Table 7.3. Centroid distances are from the periphery of the respective detectors.]

7.3.4.3 Multicriteria Analysis

Multicriteria Analysis (MCA) of model performance metrics, previously described in Chapter 5 Section 5.3.5.3, was used to assess overall model performance and determine the optimum swim rule. Fig 7.25 presents the MCA results for the different swim scenarios for jellyfish J-18495. The figure shows coloured dots on the spatiotemporal canvas where the colouring represents the MCA score which is a measure of the accuracy of the modelled particle transports at the specific jellyfish detection instances and locations. The MCA plots (A-T) are presented in order of the swim rules and scenario, as presented in Table 7.1 and Table 7.2. In the short-term of the swim simulations, the agreements were higher in all nineteen swim scenarios tested (MCA score ranges from 0.05 to 0.98 on a scale of 0-1) in the earlier hours. The cores dropped to some extent later in the short term in a few scenarios. This kind of drop in the level of agreement is seen in scenarios 5, 10, 11, and 12, which have been found to recover to some extent in the long-term period (Fig 7.25 G, M~S). This might be due to the actual swim of the jellyfish being variable over the period of transportation, e.g. they may not have actively swum immediately after their release, then began swimming with a strategy that did not match the modelled one but later changed to a strategy the matched the modelled one.

The swim mechanisms devised for testing by model simulation were usually characterized to generate mutually exclusive transport patterns. In an individual scenario simulation, the modelled transport influenced by a particular swim may not fully comply with the observation in all instances of the period. However, the model is considered better performing when such compliance is achieved to a higher extent in the long-term transport simulation. So, the analysis will now be focused on the long-term MCA agreement investigations. As per the long-term investigations and the corresponding MCA scores ranging from 0.05 to 0.65 in Fig 7.25, the scenarios can be classified into lower and higher groups in terms of the level of agreement. Here, the effort of this analysis involves determining the closest swim strategy that agreed the best to the observed transportation and the gradual improvement of the strategies during their development. Among the tidal-stage-

Chapter 7: Swim Modelling

dependent swim scenarios, Scenario-3(2) and Scenario-3(3) with 0.05 m/s and 0.08 m/s swim speed, respectively, against the ebbtide show some agreements in the long term. But the strategies have been ruled out at this stage as specifying a fixed speed for the swim would be an overconfident and imprudent approach. Yet, insight may be built up into this finding that the model jellyfish might have travelled with a swim speed of around 0.05-0.08 m/s against the ebbtide for a significant period of time.

Chapter 7: Swim Modelling

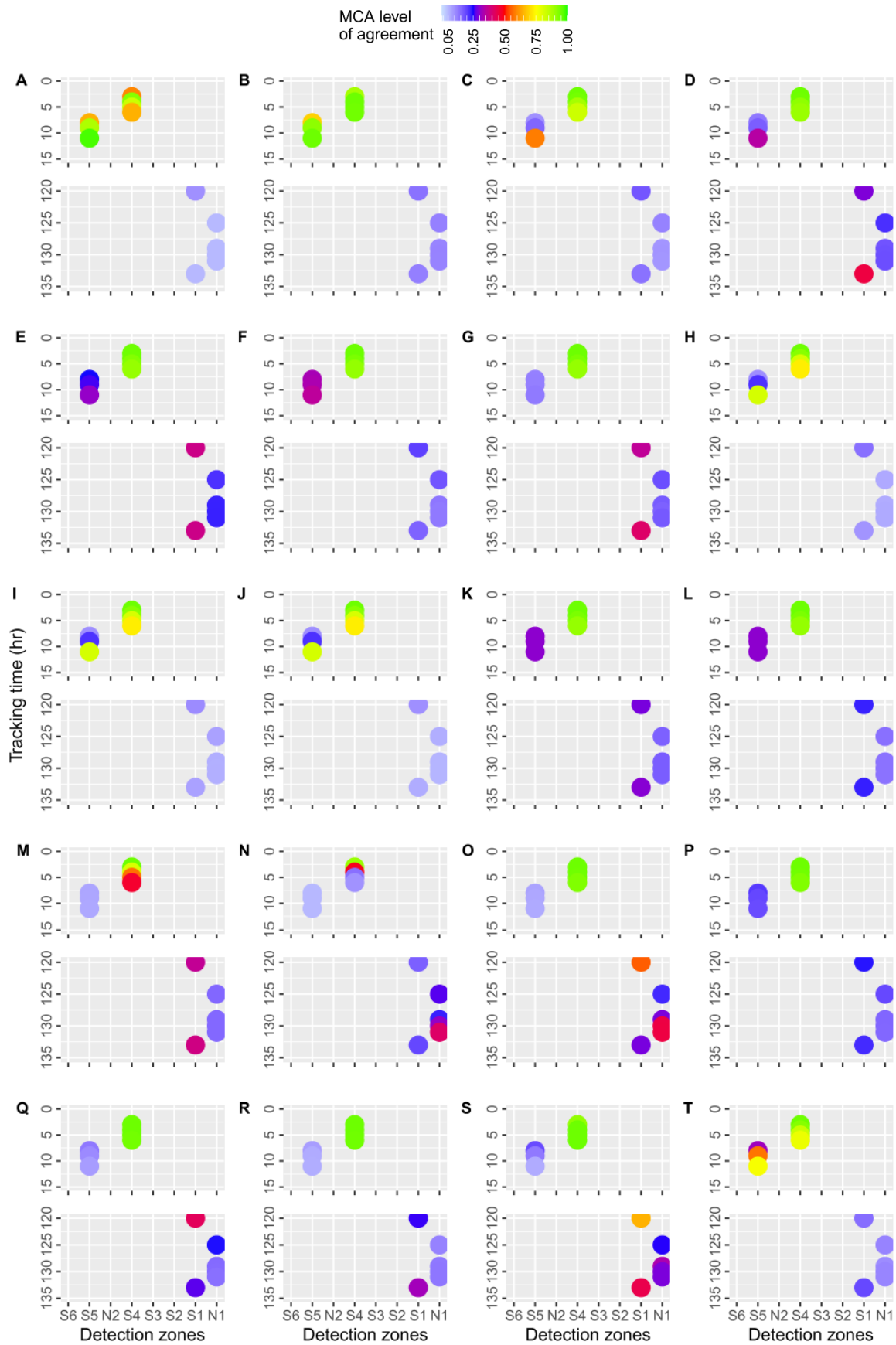


Fig 7.25 Graphical representations of MCA of active swim scenarios (A~S) and passive drift scenario (T) for J-18495 jellyfish model.

Chapter 7: Swim Modelling

The percentage agreement and centroid distances of the group of scenarios with the highest long-term MCA scores - scenarios 5, 10, 11, and 12 (Fig 7.25 G, M~S) - are presented separately in Fig 7.26 to assess their ranking. Time-averaged MCA scores, indicated by the horizontal lines, were computed here to explore the ranking among the scenarios. From Fig 7.26 A and B, it is seen that for Rules 10 and 12, Scenarios 10 (2) and 12(4) achieved the highest time-averaged MCA scores. These are compared to the MCA scores of the other higher-performing scenarios (5 and 11) in Fig 7.26-C, which reveals that Scenarios 11 and 12(4) showed the highest potential in reproducing the observed transport of J-18495. Both scenarios achieved similar time-averaged MCA scores of 0.38, but scenario 12(4) achieved the highest score of any scenario - 0.65 at 120 hrs - and was thus considered the optimum strategy. The inclusion of jellyfish swimming and the optimisation of the swim rules meant the model was able to improve the transport agreement in the long term, compared to the passive drift model; long-term MCA scores for the passive drift model ranged between 0.11 and 0.19. Another notable observation is that the swim strategy of Scenario-12 was devised based on analysis of the observed jellyfish movements (for example, the extent of their tidal transports) and so is possibly more realistic compared to the other hypothesised strategies.

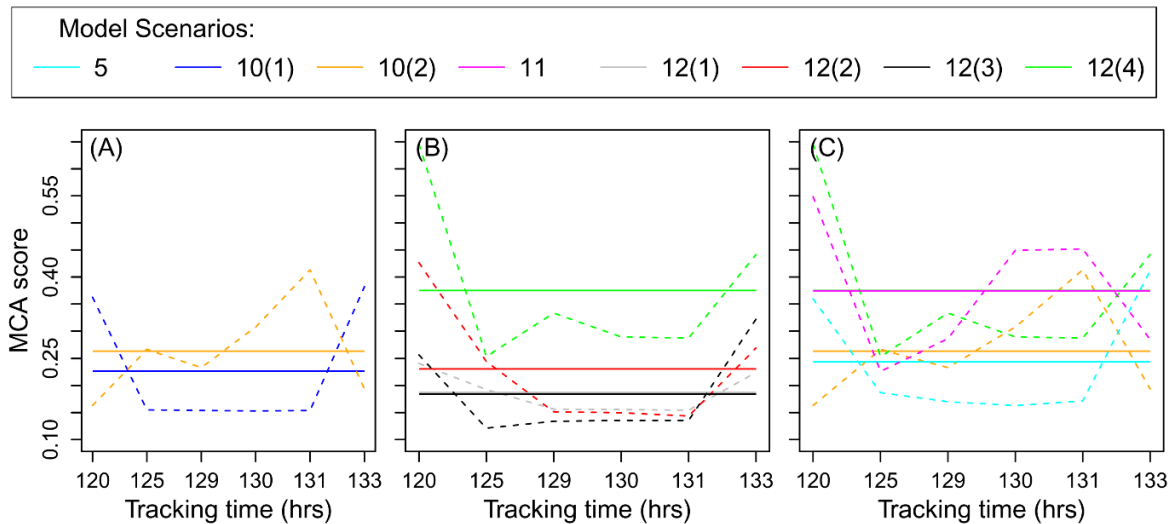


Fig 7.26 Comparing long-term MCA scores for J-18495 for (A) Scenario-10(1, 2), (B) Scenario-12(1, 2, 3) and (C) their bests along with scenarios 5 and 11 modelled. Real estimations are represented by the dashed lines and calculated means by the solid lines. [For the scenario specifications, please see Table 7.3.]

7.3.5. Behavioural Integration: Comparison across the Jellyfish Models

In the field, the tagged jellyfish were released back to the water at different locations and were therefore exposed to different current fields, which would have affected their transports. After identifying the best-performing swim strategy for J-18495, it was then tested for the two other jellyfish with the next longest observational records - J-1162 and J-18500. A small number of other swim rules were also assessed for these jellyfish.

7.3.5.1. J-1162 Swim Scenarios

To assess the suitability and performance of swim rule 12(4) for J1162, spatiotemporal distributions of model particles within the various detection zones at times of recorded detections are presented in Fig 7.27. The figure shows the percentage detection of the particles (Fig A & B) and the observed detections of the jellyfish (Fig C). recorded data were only available up to 22 hours after the jellyfish release. According to Fig C, the jellyfish initially moved west from detection zone S4 where it was released to S5, then moved back east to S4 and finally moved back west to S5 at its last time of detection 22 hours after its release. However, according

Chapter 7: Swim Modelling

to Fig A and B, the swim model transported the particles in the opposite direction to the recorded jellyfish transportation; the particle cloud initially moved eastward inside the harbour within the ranges of S4 and S3 detectors. This indicates that the speed and direction of the swim specified in the model were not able to mimic the jellyfish movements, possibly because swim rule 12(4) was devised based on the observed movements of a different jellyfish. Scenario-12(4) was therefore modified based on the transport analysis of J-1162. The new swim scenarios are presented in Table 7.4. Rather than swimming occurring on both the ebb and flood tide, as in scenario 12(4), the swim was only executed on the ebb tide. Flow-dependent swim speeds of 30, 60, and 80 % of the current speed were trialled.

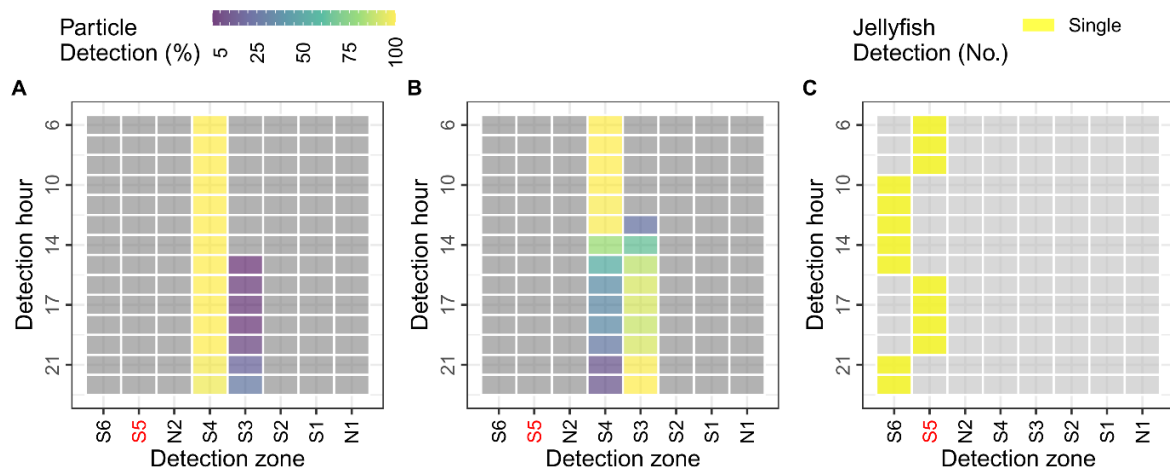


Fig 7.27 Modelled spatiotemporal detections of J-1162 for (A) surface and (B) mid-depth released particles and (C) observed spatiotemporal detections.

Table 7.4 Customized swim scenarios for the J-1162 jellyfish model.

Model scenario		Tidally oriented swim period (%)				Swim speed	
		Floodtide		Ebbtide		(% current speed)	
		WT	AT	WT	AT	WT	AT
Ref	Scenario-12(4)	35	65	25	75	80	-180
Tailored	Scenario-12(5)	0	0	100	0	30	0
	Scenario-12(6)	0	0	100	0	60	0
	Scenario-12(7)	0	0	100	0	80	0

Chapter 7: Swim Modelling

The spatiotemporal distributions and detections for the new swim model scenarios are presented in Fig 7.28. The figures show that while some particles still travel east of the release zone, a greater number of particles remain within the release detection zone and some travel to the west to S6 in the later hours. This distribution was more like the movements shown by the observed jellyfish.

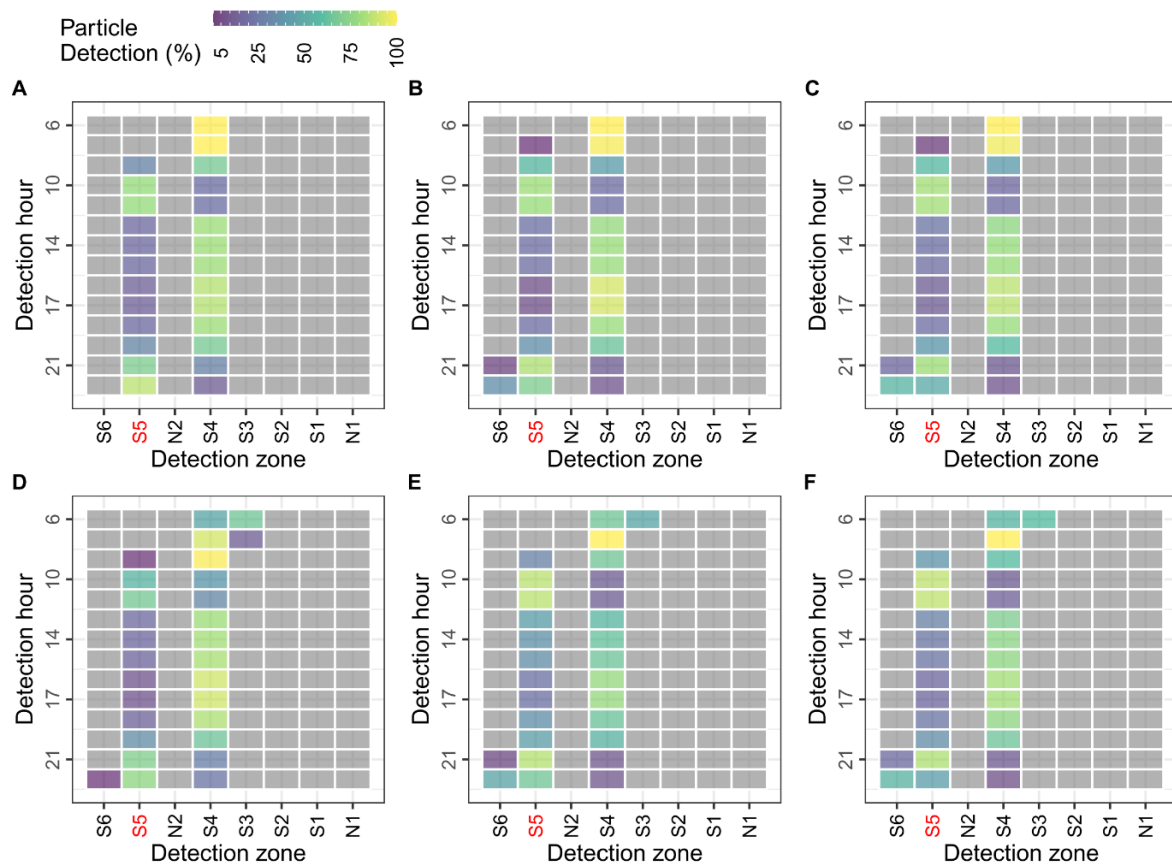


Fig 7.28 Spatiotemporal detections of (A~C) surface and (D~F) mid-depth released particles of J-1162 jellyfish model across scenarios.

The transport agreements of the modelled particles for the new J-1162 scenarios are presented in Table 7.5. Agreement data for scenario 12(4) are not shown because it resulted in 0% agreement across all hours of detection. According to the table, the particle retention was 100 % in all scenarios due to the short period of simulation. Transport agreements varied across the swim scenarios, detection instances, and particle-releasing depths. In the first two-third period of particle tracking (0~15 hr), with the exception of hour 8, the model failed to achieve any match in detection instances; a maximum agreement of 58 % was achieved in hour

8. Later in the simulation (16~22 hr), the level of agreement improved, but it is difficult to distinguish which scenario produced the highest levels of agreement overall.

Fig 7.29 helps to determine an overall ranking of the scenarios based on percentage agreement (A) and centroid distance (B). It shows that Scenario-12(5), having the lowest swim speed, was the poorest performing scenario. Scenario 12(6) was the best performer for surface-released particles, and scenario 12(7) was best for mid-depth released particles.

Chapter 7: Swim Modelling

Table 7.5 A comparison of quantitative transport agreement of surface and mid-depth releasing particles (as per J-1162) among different swim scenarios

Detector	Detection time (hr)	Swim model scenarios																	
		Surface released particles									Mid-depth released particles								
		Scenario 12(5) SP (% CS) = 30			Scenario 12(6) SP (% CS) = 60			Scenario 12(7) SP (% CS) = 80			Scenario 12(5) SP (% CS) = 30			Scenario 12(6) SP (% CS) = 60			Scenario 12(7) SP (% CS) = 80		
		1	2	3	1	2	3	1	2	3	1	2	3	1	2	3	1	2	3
S5	6	100	0	432	100	0	422	100	0	475	100	0	1007	100	0	840	100	0	946
S5	7	100	0	247	100	1	119	100	3	105	100	0	740	100	0	458	100	0	465
S5	8	100	31	26	100	57	0	100	58	0	100	1	394	100	30	69	100	39	54
S6	10	100	0	747	100	0	734	100	0	733	100	0	865	100	0	511	100	0	515
S6	11	100	0	716	100	0	709	100	0	711	100	0	827	100	0	621	100	0	632
S6	13	100	0	1016	100	0	976	100	0	980	100	0	996	100	0	936	100	0	1012
S6	14	100	0	1070	100	0	1118	100	0	1067	100	0	1000	100	0	969	100	0	1193

Chapter 7: Swim Modelling

S6	15	100	0	1204	100	0	1295	100	0	1090	100	0	1004	100	0	1005	100	0	1387
S5	16	100	15	437	100	9	456	100	14	310	100	10	208	100	22	186	100	18	592
S5	17	100	15	454	100	9	460	100	14	401	100	10	251	100	22	186	100	18	625
S5	18	100	19	427	100	20	437	100	20	307	100	16	187	100	36	107	100	24	538
S5	19	100	32	248	100	36	180	100	40	102	100	35	109	100	45	67	100	35	281
S6	21	100	0	771	100	5	315	100	18	208	100	0	772	100	6	309	100	19	234
S6	22	100	0	591	100	36	174	100	56	0	100	1	550	100	47	33	100	55	0

SP = Swim speed; CS = Current speed; Swim direction = with the ebbtide;

Column headings: [1] Number of particles available in the domain, [2] Percentage of available particles agreed to the reference jellyfish (calculated with respect to the column of the block marked by 1), [3] Centroid distance (m) from the periphery of the respective detector

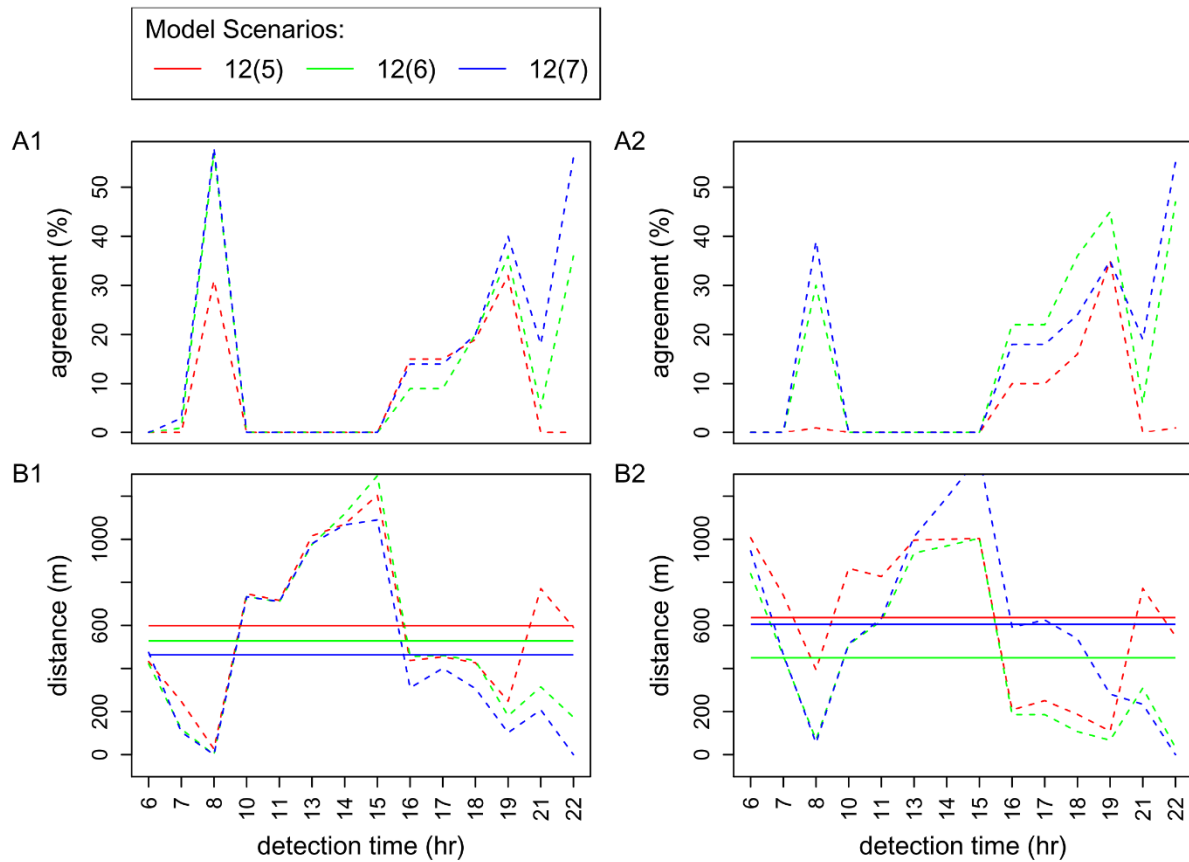


Fig 7.29 Comparison of the modelled swim scenarios of the J-1162 jellyfish model in terms of (A) percentage agreement and (B) centroid distance shown by the particles released at (1) surface and (2) mid-depth water.

Fig 7.30 shows snapshots of particle locations at two times of interest based on the observed movement of J-1162 across travel instances. As shown in Fig 7.27(A), J-1162 was detected in zone S6 at 15 hrs and then moved east to be detected within S5 at 16 hrs. Later, it was still within S5 at 19 hrs, but by 21 hrs, it had moved back westward to S6. For the 15-16 hr period, Fig 7.30(A) shows that the particles modelled by Scenario-12(7) did not follow the observed transport, with most of the particles being located east of S5. In contrast to this, at the later 19-21 hr period, Fig 7.30(B) shows that the swim mechanism used in scenario-12(7) was able to transport the particles in a similar fashion to the observations with the particles moving westward from S5 towards S6.

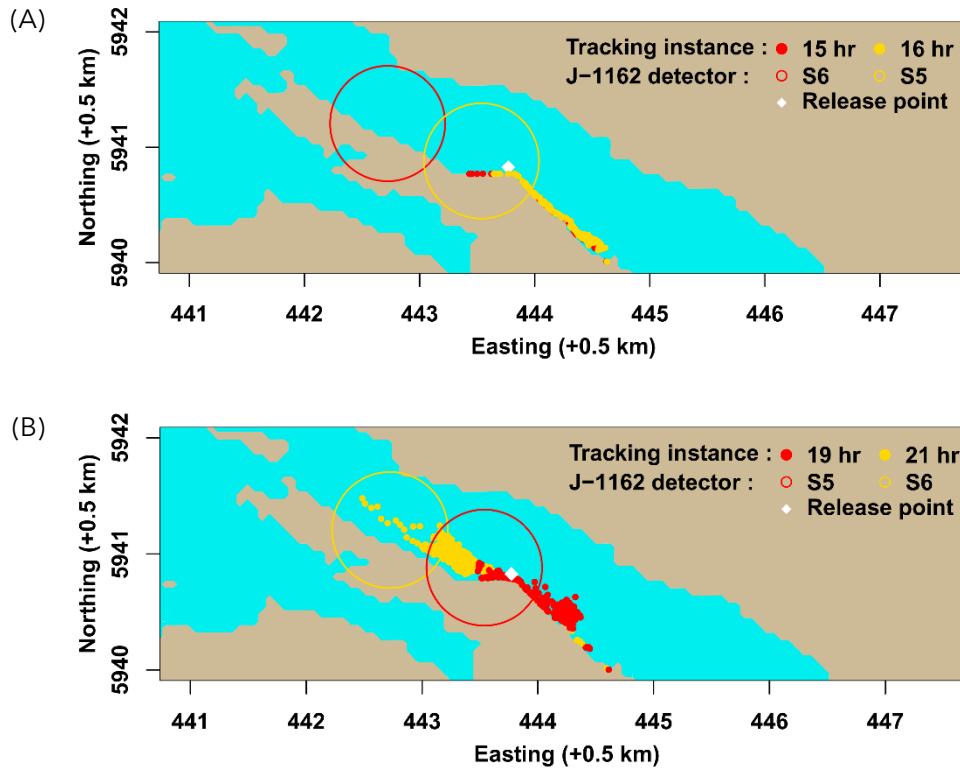


Fig 7.30 Snapshot of particle locations (A) 15-16 hr and (B) 19-21 hr after their release in all depths in Scenario-12(7).

7.3.5.2. J-18500 Swim Scenarios

Swim scenario 12(4) was also used to model the transport of J-18500, which was also released in the S5 detection zone but at a different time from J-1162. The spatiotemporal distributions and detections are presented in Fig 7.31, along with the recorded detections, which were available up to 53 hours after the release. Looking at the observed detections, the jellyfish initially travelled from S5, west to S6 and back again to S5; it then continued east to S4, where it remained for most of the rest of the detection period. The figure shows that the model was able to reproduce the transport relatively well, with the particles initially remaining around S5 and then moving eastward toward S4. This indicates that the speed and direction of the swim specified in the model were suited to reproducing the jellyfish movements.

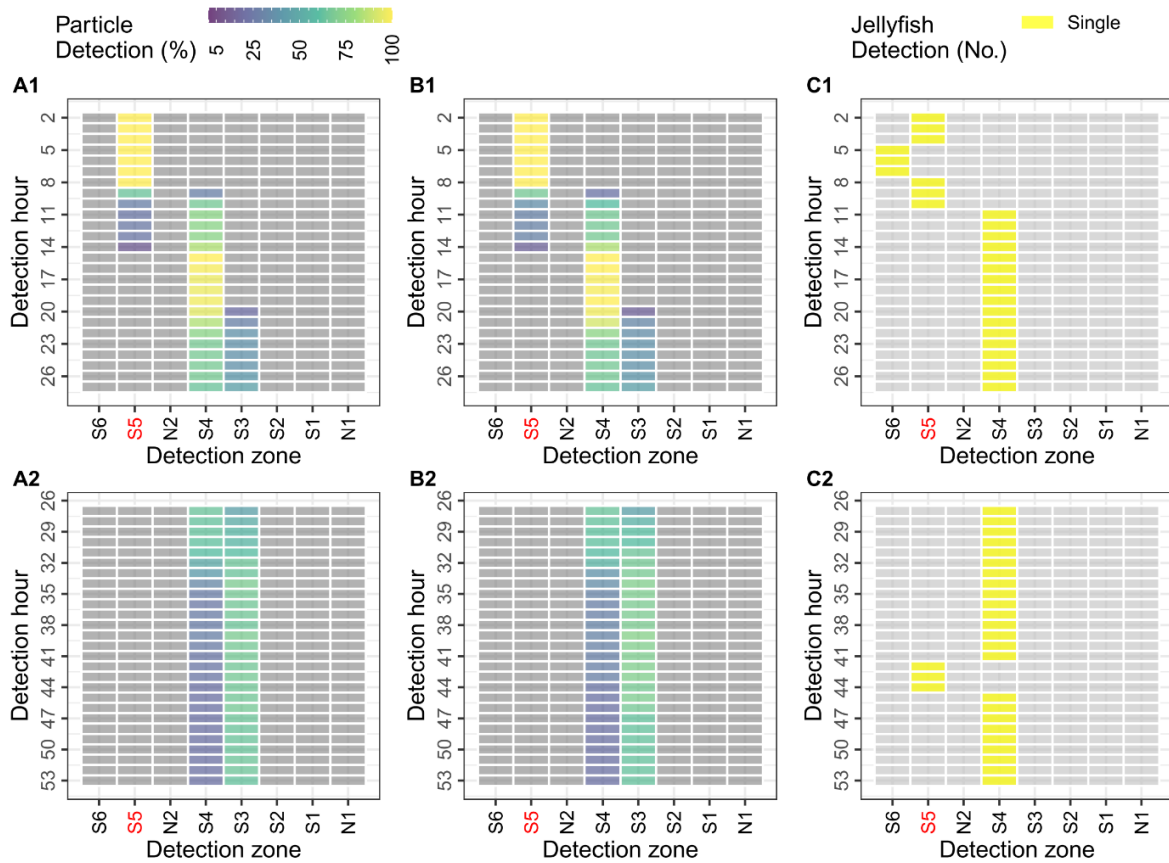


Fig 7.31 Modelled and observed spatiotemporal detections of the J-18500 jellyfish model [(A) surface and (B) mid-depth releasing particles and (C) observation].

The transport agreements of the modelled particles are presented in Table 7.6. Once again, the particle retention was 100 % in all scenarios due to the short simulation period. The modelled transport agreed in most of the detection instances except when the jellyfish travelled to the west at hr 3. Particles released at the surface and mid-depth did not generate any remarkable variation in transport. Except at a few limited instances of time where there was no agreement (0 %), the swim scenario achieved between 22-100 % agreement in most detection instances over the transport period. The highest agreement (100 %) was achieved at the instances immediately to the release of the particles; these dropped over time yet were still at 22 % at the end of the transport simulation.

Chapter 7: Swim Modelling

Table 7.6 Quantitative transport agreement of surface and mid-depth releasing particles (as per J-18500) in Scenario-12(4).

Model: Swim Scenario 12(4)															
First half (detections within 2~27 hr period)								Last half (detections within 28~53 hr period)							
Detector	Detection time (hr)	Particle releasing depth						Detector	Detection time (hr)	Particle releasing depth					
		Surface			Mid-depth					Surface			Mid-depth		
		1	2	3	1	2	3			1	2	3	1	2	3
S5	2	100	100	0	100	100	0	S4	28	100	63	0	100	63	0
S5	3	100	100	0	100	100	0	S4	29	100	63	0	100	62	0
S5	4	100	100	0	100	100	0	S4	30	100	62	0	100	62	0
S6	5	100	0	400	100	0	384	S4	31	100	60	0	100	59	0
S6	6	100	0	439	100	0	420	S4	32	100	49	10	100	55	0
S6	7	100	0	600	100	0	581	S4	33	100	41	63	100	38	40
S5	8	100	100	0	100	100	0	S4	34	100	33	181	100	35	133
S5	9	100	64	0	100	67	0	S4	35	100	28	242	100	31	174
S5	10	100	29	25	100	36	17	S4	36	100	26	269	100	29	199
S4	11	100	74	0	100	67	0	S4	37	100	27	262	100	29	192
S4	12	100	74	0	100	67	0	S4	38	100	28	240	100	31	170
S4	13	100	74	0	100	68	0	S4	39	100	29	222	100	31	169
S4	14	100	84	0	100	84	0	S4	40	100	27	246	100	30	205
S4	15	100	100	0	100	100	0	S4	41	100	25	307	100	29	234
S4	16	100	98	0	100	100	0	S5	42	100	0	1314	100	0	1242
S4	17	100	96	0	100	98	0	S5	43	100	0	1317	100	0	1246
S4	18	100	96	0	100	98	0	S5	44	100	0	1331	100	0	1270
S4	19	100	97	0	100	100	0	S4	45	100	22	392	100	23	361
S4	20	100	94	0	100	97	0	S4	46	100	22	479	100	22	412
S4	21	100	84	0	100	91	0	S4	47	100	22	508	100	22	474
S4	22	100	74	0	100	75	0	S4	48	100	22	553	100	22	514
S4	23	100	68	0	100	67	0	S4	49	100	22	563	100	22	523
S4	24	100	68	0	100	66	0	S4	50	100	22	549	100	22	513
S4	25	100	68	0	100	67	0	S4	51	100	22	538	100	22	513
S4	26	100	68	0	100	67	0	S4	52	100	22	520	100	22	510
S4	27	100	64	0	100	64	0	S4	53	100	22	524	100	22	524
Column headings: [1] Number of particles available in the domain, [2] Percentage of available particles agreed to the reference jellyfish (calculated with respect to the column of the block marked by 1), [3] Centroid distance (m) from the periphery of the respective detector															

The percentage agreements and centroid distances shown in Table 7.6 are plotted against time in Fig 7.32, along with the corresponding results from two other swim

scenarios to allow comparison across different swim rules. Scenario-12(4) was compared with Scenario-12(1), which used a lower swim speed combination, and Scenario-4, which used against-tide ebb-swimming at 100% of the current speed. In the figure, the dashed lines indicate the recorded agreement and centroid distance values, and the solid lines indicate the time-averaged values of the metrics. The figure shows that Scenario 12(4) produced higher agreement levels and lower centroid distances than the other two scenarios. Thus, Scenario-12(4) outperforms them over the tracking period. This agrees with the findings for the J-18495 jellyfish model and, furthermore, suggests the need to use a time-varying swim behaviour in jellyfish transportation modelling again.

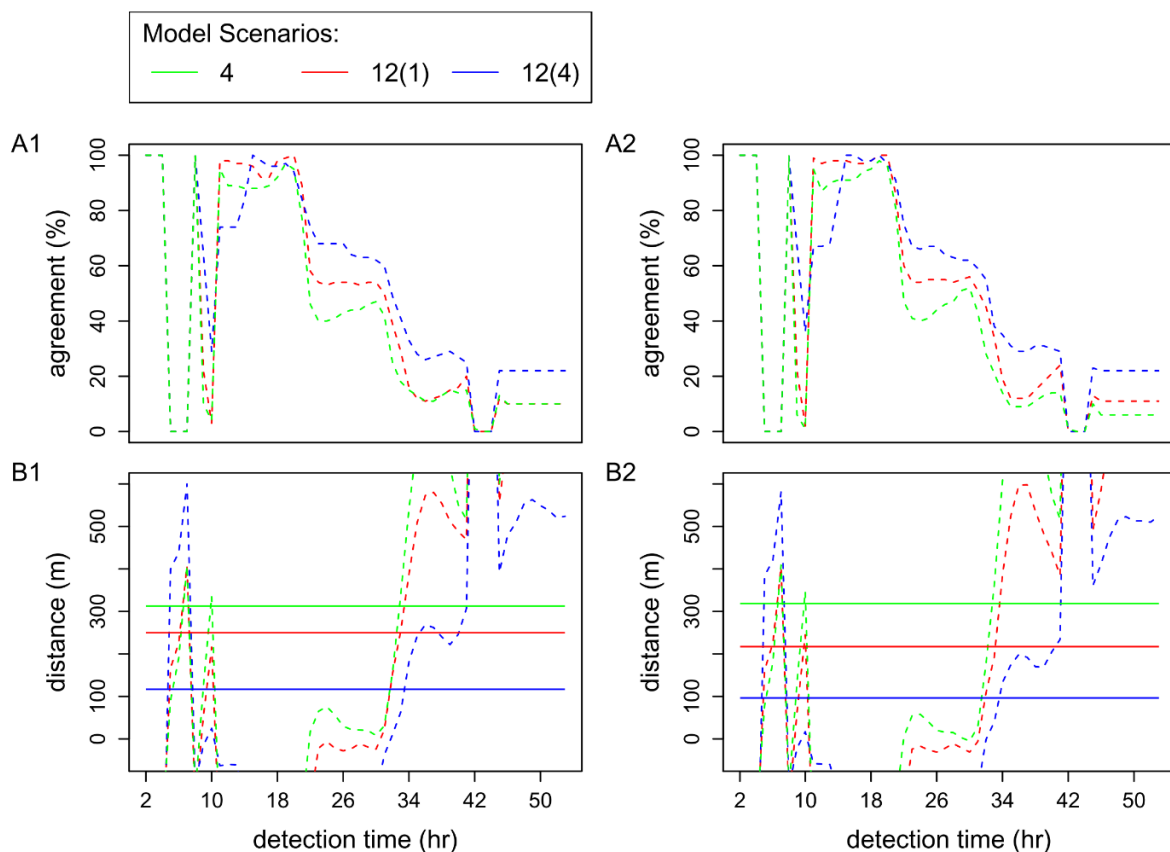


Fig 7.32 Comparison of the modelled swim scenarios of the J-18500 jellyfish model in terms of (A) percentage agreement and (B) centroid distance shown by the particles released at (1) surface and (2) mid-depth water.

Fig 7.33 shows a snapshot of modelled particle locations from Scenario-12(4) at 15 and 52 hrs after the release. In these instances, the jellyfish was detected within the

same detector zone, S4, even though the times were separated by 37 hrs. The jellyfish had to have held itself within S4 by actively preventing or limiting its drift on the flood tide currents prevailing in this period. According to Fig 7.33, all the particles were detected, like the jellyfish within S4 at the 15th hr of the travel. Later, unlike the jellyfish, the particles started leaving the detector's range and were transported eastward inside the harbour by the model. Most of the particles left S4 by the 52nd hr of the travel, yet some particles could manage to stay there by the force of the swim modelled. This suggests that J-18500 transportation involved active swimming in combination with passive drifting.

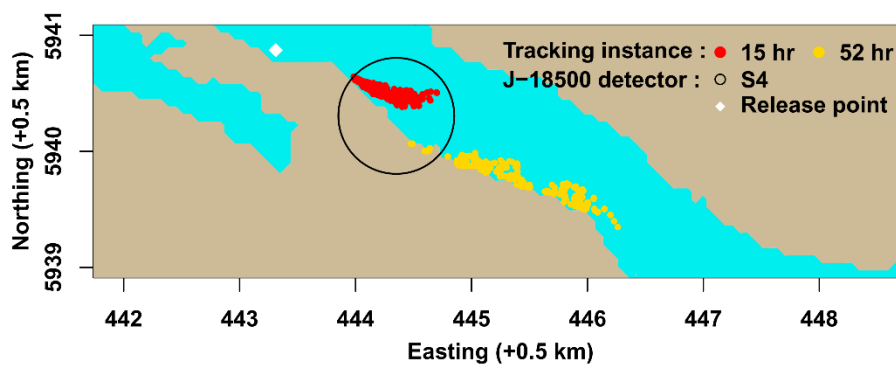


Fig 7.33 Snapshot of particle locations of the J-18500 jellyfish model at two different travel instances of (A) 15 hr and (B) 52 hr after their release in different depths as per Scenario-12(4).

7.3.6. Swimming Versus Passive Drift

Multicriteria analysis (MCA) scores for the best swim models and the passive drift models applied to the three jellyfish – J-18495, J-1162 and J-18500- are presented in Fig 7.34. The figure shows the MCA agreement scores over the respective tracking periods; instantaneous scores are displayed by the dashed lines and time averages by the solid lines. For J-18495 and J-1162, the passive drift models achieved better performance in the short term, while longer term, the swim models produced a better agreement. For J-18500, the swim model outperformed the passive drift model for the whole period of observations. In general, it can therefore be concluded that including swimming behaviour improved model performance.

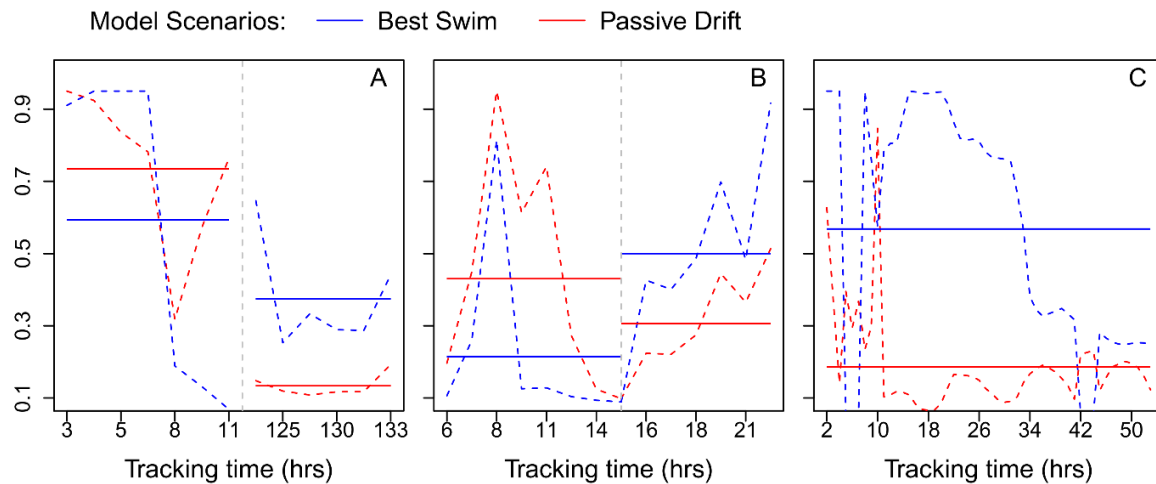


Fig 7.34 Comparing MCA scores of (A) J-18495, (B) J-1162, and (C) J-18500 jellyfish models between the best swim and passive drift scenarios at short- and long-term simulations. Real estimations are represented by the dashed lines and calculated temporal means by the solid lines.

7.4. Summary and Conclusions

There are some key conclusions described as follows.

- 9) The installation of the swim submodel within the base hydrodynamic model was successful. The model particles were able to move three-dimensionally. Their movements in the horizontal and vertical directions were the results of combined actions of active and passive motions, which was the key design of the swim model. The modelled swim was synchronous with the flow-induced passive drifts as a joint transport activity. The vertical swimming behaviour of jellyfish designed to be implemented in terms of DVM strategy and simulated along with the horizontal swimming was able to induce the transport agreement.
- 10) The swimming strategies were found to be sensitive to the depth at which particles were released, with Scenario 12 being the most sensitive.
- 11) Dependence, specificity, and orientation of tide significantly influenced the particle transport results. Ebbtide dynamics of the Killary harbour were found to be crucial for the jellyfish transport modelling in the harbour.

- 12) Swim speed and direction were found to be the most critical specifications in jellyfish transport modelling. Combined with various physical and hydrodynamic conditions, those specifications, as per Rule-12, resulted in a south-easterly net transport of the modelled particles by allowing them to move from their release point to approximately 5.5 km inside the harbour in 7 days.
- 13) Swim peaking during slack tide had the ability to create a variation in transport over an ordinary current-oriented strategy. Maintaining a minimum swim against diminishing current flows also demonstrated a likely variation. Their incorporation in the modelling may be potential on travel occasions, while jellyfish individuals exhibit such swimming behaviours due to their individual variations.
- 14) The drift-neutralization function during the anti-tide swim was found to be a potentially applicable swimming mechanism in the swim modelling from a technical perspective, which is important to ensure that a jellyfish refuses to drift and prefers to cruise in the opposite direction.
- 15) A coordinated swim implemented upon a complex correlation of speed, depth, DVM, and tidal direction created a higher differential force than tidal drift, which worked in the resultant direction. The net directional effect overpowered the short-term mobilizations, which were more vivid in the long term. The resultant effect of the swim based on the subsurface current speeds had a better clustering and higher inward navigating tendency than the stronger surface currents.
- 16) Jellyfish might demonstrate adaptive swim behaviour skills. The observed jellyfish in Killary might have processed the swim in two ways: (1) they might swing onto variable swim speed levels, whereas the model could only support swimming at a flow-constant speed level, and (2) they might swing onto variable swim strategies while travelling whereas the model supports were limited only to a constant strategy over the period. Therefore, specifying a flow-independent fixed speed for a swim in the modelling was later considered an overconfident and imprudent approach.
- 17) The time-constant swim model could not sufficiently ensure a greater

agreement at each detection instance, which reveals the potentiality of a time-varying swim model in modelling jellyfish transportation.

- 18) Swim in the modelling induced variable levels of transport agreement to the observation being higher mostly immediately to the release of the particles and lower mostly in the longer period, yet higher than the drift-only modelling results. The swim strategy devised upon analysing the observed transport of jellyfish (i.e., Rule-12) was found to be more logical and realistic from a modelling perspective and produced higher transport agreements to the observation. Scenario-12(4) demonstrated a maximum long-term agreement at 55 % at 120 hr in J-18495 jellyfish modelling.
- 19) The agreements are neither constantly better nor constantly worse in a particular scenario. Scenario ranking carried out through MCA for all the jellyfish models results in a higher score of 0.375~0.568 in the swim-coupled and a lower score of 0.134~0.306 in the drift-only transport simulations. Additionally, this provided learning elements and insights to understand transports on the behavioural swim.
- 20) Particles getting varied mechanical drives from different flows at the start of their transport might potentially cause transport variations on the go. Besides adaptation and adjustment, the depth at the source and its associated vertical migrations were also important influential factors in jellyfish transport modelling.
- 21) The variations in the observed jellyfish transport might have been linked to their individual variations (e.g., size). This was demonstrated in the model jellyfish transport performance also. J-18495 model jellyfish might use a swim that helped it to limit the flow-induced westerly drift and move eastward inside the harbour. J-1162 were mostly active on drift-dominated westerly transports. J-18500 transportation was tide-restricted rather than drift-oriented.
- 22) With-flood and anti-ebb swimming strategies transporting the jellyfish inside the harbour might have the potential to cause swarm formation there. Particles having a higher clustering and limited spreading tendency might indicate a likelihood of a potential jellyfish bloom.

CHAPTER 8: SUMMARY, CONCLUSIONS, AND RECOMMENDATIONS

8.1. Summary of the Research

The focus of this research was the investigation of jellyfish transport in an Irish fjord (Killary Harbour) using a numerical modelling approach. In recent times, jellyfish have gained notable negative public attention due to beach closures and mass kills of marine-farmed fish arising from the sudden occurrence of jellyfish swarms or 'blooms'. These occurrences will likely become more frequent as studies have shown that jellyfish numbers have been increasing in recent years.

Computer models that are able to simulate the movements of jellyfish can play an essential role in understanding how we can prevent them from adversely affecting human activities. While jellyfish are primarily thought to drift passively in ocean currents, studies have shown that they also have the ability to swim independently of the currents, i.e. they possess horizontal and vertical motility. However, there is limited understanding of jellyfish motility and its cues. This research therefore aimed to develop a model that could simulate the transport of jellyfish in coastal waters and use the model to investigate the effects of different transport mechanisms including passive drifting and various swimming behaviours. An existing oceanographic modelling tool (EFDC), which can simulate coastal water movements, was used to develop the model so that it could simulate the movement and behaviours of jellyfish on local tidal flows.

The model developed in the research has been tested by application to Killary Harbour, an Irish fjord where both fish farms and jellyfish are present. The spatial scale of this modelling effort focused exclusively on the estuary or fjord level, restricting the investigation of the transport and distribution of the virtual jellyfish (particles) solely within this geographic context. Regarding the temporal scale, the simulations conducted using this model were constrained to a period corresponding to a complete tidal cycle, encompassing both spring and neap tides, or at least a portion thereof. The research could, and should, be extended to study

Chapter 8 - Conclusions

the jellyfish transport a longer timescales and larger regional spatial scales. Hydrodynamic model performance was assessed by comparison with measured water velocities. The Killary hydrodynamics sourced from previous ADCP records were used for this comparative analyses. Similarly model predictions of jellyfish transport were assessed by comparison with observations of jellyfish transport in the harbour. The jellyfish activity within the harbour was recorded in a previous study by researchers from University College Cork and involved tagging jellyfish with electronic chips, which tracked their movements. These records were analysed and used for the comparative analyses and for evidence of jellyfish motility. The developed models were used to investigate the sensitivity of jellyfish movements to the different controlling physical and biological processes.

With the primary aim of this research to develop a coastal hydrodynamic model to simulate the transport and fate of jellyfish and use this to investigate their transport mechanisms, a literature on jellyfish transport mechanisms and modelling was first conducted. This provided an understanding of the known transport mechanisms and any numerical modelling strategies that have been used to study these. Gaps in the previous studies were identified, some of which were addressed in the present research.

The three-dimensional EFDC hydrodynamic model developed to simulate the Killary circulations was used as the base model for the study. EFDC contains a Lagrangian particle tracking submodel which is dynamically linked with the hydrodynamic model and was used as the basis of the jellyfish transport model. The LPT submodel code was modified to develop three different jellyfish transport models: (1) a passive-drift model, (2) a diel vertical migration (DVM) model, and (3) a swim model. The passive-drift model includes passive advective transport by tidal currents as the only mode of transport. The diel migration model includes both passive drifting and diel migration behaviour and the swim model includes passive drifting, and both diel migration and horizontal swimming behaviours. The synchronized modelling of these behavioural processes resulted in improved agreement between the simulated results and the transport observations. Model assessment and evaluation, transport scenario simulations, and model sensitivity

analyses carried out in this research have resulted in insights into jellyfish transportation. The comparative transport agreements across the models developed and tested have helped investigate the performances of the different modelling strategies, and thus has contributed new knowledge in the science and art of jellyfish transport modelling.

8.2. Key Conclusions of the Research

The key conclusions from the research based on (1) the hydrodynamic modelling of Killary fjord, (2) the passive drift jellyfish transport model, (3) the diel migration transport model and (4) the swim model are now summarized.

8.2.1. Hydrodynamic Modelling of Killary Harbour

Using the EFDC model, a hydrodynamic model was developed to simulate hydrodynamic circulation within Killary Harbour. In addition to driving the jellyfish transport models, it was also used to examine the impacts of relevant processes on the tidal currents. Based on the investigation, several important conclusions were drawn, which are highlighted below:

- 1) The model analysis provides a comprehensive characterisation of the Killary Harbour water structure. It can be classified as stratified or partially mixed with a stronger stratification seen at the spring tide inside the harbour increasing with distance upstream and characterised by low-haline colder surface water with significant haloclines and thermoclines.
- 2) The estuarine baroclinity influenced the flow dynamics of the harbour. The stratification induced eddies or hydrodynamic turbulence within the harbour by generating variable density flows, which jointly with the advective currents enhanced the harbour circulations.
- 3) The model appeared relatively insensitive to the marine boundary conditions for salinity and temperature for the short time periods simulated. However, they are more likely to influence longer term simulations as monthly and seasonal variations would be more significant.

4) The wind shows influence over the salinity and temperature structures, and by extension the hydrodynamic currents of the harbour. The time-varying wind showed higher mixing and stronger surface currents than the south-westerly time-constant wind at 8 m/s speed, mainly inside the harbour where most aquacultural activities are usually located.

5) The freshwater discharge from the rivers had the most significant influence on the stratification and the current flows. The influences are seen for both time-constant and time-varying river discharge scenarios. As would be expected, higher discharge scenarios induced stronger influences, which were most noticeable for the surface currents.

8.2.2. Passive-drift Modelling of Jellyfish

The Lagrangian passive drift transport model that was coupled with the hydrodynamic model was used to simulate the passive transport of jellyfish in the harbour to investigate jellyfish transport mechanisms. Particle transport in this model was based on advection and diffusion. Based on the analyses, several important conclusions were drawn, which are highlighted below:

1) Observed transport of jellyfish in Killary was partially tidal. The tidal transport (passive-drift) modelling of jellyfish partially agreed with the observations but differences between them indicated there may be non-tidal independent behavioural motility involved.

2) The model diffusivity parameter that could control the swarm or dispersion of the modelled particles (i.e. virtual jellyfish) can be used for calibrating their transportation in the modelling.

3) The depth of the particles varied by their release and subsequent vertical movements influenced their net transportation indicating its significance in the modelling.

4) The surface wind increased the dispersion of particles, whereas the river discharge influenced their net longitudinal transport.

8.2.3. DVM Modelling of Jellyfish

The DVM model was developed to simulate the light-induced vertical movement behaviour of jellyfish. The execution of this movement was governed in the model by a suite of four movement strategies including twenty conditions, which were tested by simulating different scenarios. The strategies ensure that jellyfish stayed above a user-specified threshold depth during nighttime and below the threshold depth during daytime. The vertical swimming speed of the jellyfish was also user-specified. The DVM results were compared with those from the basic passive drift model and the observed movements to determine the influence of vertical migration on the jellyfish transport and on model performance. In their transport agreements with the observation. The investigation draws several important conclusions, which are highlighted below:

- 1) The DVM model was able to reproduce the idealised diel migratory behaviour of jellyfish.
- 2) The modelled transport was not sensitive to the vertical motility rate in shallow coastal waters; however, it was sensitive to the migration-limiting threshold depth.
- 3) The influences of the DVM on the particle transport was variable for the different jellyfish modelled and resulted in mixed transport agreements suggesting the possible effect of individual variations in jellyfish migratory behaviour. Although the DVM Scenario 4 model transport specific to J-18495 agreed better with the observations than the corresponding passive drift only model, overall, it could not be concluded that the DVM model produced better agreement with the observed jellyfish transports than the passive drift.
- 4) The DVM reduced spreading and induced clustering of the particles suggesting the potential for contributing to bloom formation.
- 5) As some results did show better transport agreement using the DVM, it can potentially be worth including this jellyfish behaviour in their transport modelling but better understanding of the behaviour is needed from study of jellyfish in the field. In particular, knowledge of vertical swimming rates, cues for vertical migration, depths at which time is spent and the time spent at different depths is crucial.

8.2.4. Swim Modelling of Jellyfish

The swim model was developed to simulate the three-dimensional swimming behaviour of jellyfish. The model incorporated a total of 19 rules and sub-rules to govern jellyfish swimming, which was coupled synchronously with passive drifting to simulate joint transport. Additionally, the vertical swimming behaviour of jellyfish was incorporated by implementing a DVM strategy, which was simulated along with horizontal swimming. To test the model, simulations were conducted using various swim scenarios. To evaluate the model's performance, its results were compared with those obtained from the earlier transport models and the observed transports. The investigation draws several important conclusions, which are highlighted below:

- 1) The swimming strategies that were developed and tested in this study were found to be sensitive to several factors, including the depth at which particles were released into the water, the dependence on tidal patterns, as well as the swim speed, swim direction, and specific orientation of the tide used to drive particle movement.
- 2) Swim modelling could generate higher transport agreements than DVM-only or drift-only models for jellyfish in Killary. The agreements are neither constantly better nor constantly worse in a particular swim scenario. Of the swim rules tested, Rule 12(4) produced the highest agreement with the observed jellyfish transport. It was found here that the dynamics of the ebb tide in Killary Harbour are crucial for modelling jellyfish transport in the harbour.
- 3) By incorporating certain swim rules into the model, such as peak swimming or minimal swimming, it is possible to simulate specific travel scenarios in which jellyfish exhibit the appropriate swimming behaviour based on their individual observed variations.
- 4) The drift-neutralization function used during anti-tide swimming could be a useful mechanism in swim modelling, particularly in situations where a jellyfish is trying to resist drifting and prefers to swim in the opposite direction.

5) The analysis of jellyfish models showed variable results when using the same swim rule, which suggests that jellyfish may exhibit adaptive swimming behaviours that are different from the constant speed and time strategies used in the swim modelling.

6) The with-flood and anti-ebb swimming, which transport jellyfish into the harbour, may potentially cause swarm formation there. The presence of particles that tend to cluster together and have limited spreading may indicate a higher likelihood of a potential jellyfish bloom.

8.3. Recommendations for future work

The following are some suggestions for future extensions to the research.

Particle transport modelling typically involves determining the random walk movements of particles using a diffusivity parameter that is simulated within the model based on flow dynamics. However, it may be worthwhile to investigate the possibility of incorporating behavioural diffusivity into the diffusion process. To better understand jellyfish transport behaviour, we can explore potential correlations between their diffusion and other behavioural factors and integrate this information into our modelling. This approach can provide more accurate predictions of the likelihood of jellyfish bloom formation.

While the research strongly benefitted from having observational records of jellyfish transport to use for comparison with the modelled transports; these data had some significant limitations. The data were only available for a small number of jellyfish and for relatively short periods of time which made it difficult to fully ascertain the accuracy of the various transport models. In addition, the receivers only determined that jellyfish were inside their radius of detection rather than giving their actual positions. This added further uncertainty to the comparison of modelled and measured datasets. It is therefore recommended that more detailed studies of jellyfish transport are carried out using GPS trackers that give three-dimensional positions of the jellyfish. These data will enable determination of swimming

Chapter 8 - Conclusions

behaviours to inform transport models and provide much richer datasets for comparison with transport model predictions.

The current DVM model for jellyfish uses a spatiotemporally constant threshold depth to instruct vertical migration. While this simplifies the modelling process, it may compromise the accurate replication of the real jellyfish behaviour and its extent of vertical movement. To improve the model's accuracy, a dynamic threshold depth concept could be introduced based on a combined correlation of cloud cover, water turbidity or transparency, and luminosity, which are the key factors that determine the light penetration into the water, the basis for DVM.

To simplify the implementation of the DVM and the swimming rules developed in this study, the Lagrangian particle tracking was solved using the first-order Euler method. However, the transport rules could be integrated into the model to be solved using the fourth-order Runge-Kutta scheme, which is considered to have higher precision, and the resulting transport simulations can be assessed as to whether they can improve jellyfish transport prediction.

Further developments/refinements of the jellyfish transport models could be made as follows. As the swim model using constant swimming speeds did not provide good agreement it may be that implementation of time-varying swim speeds may improve model predictions. In reality, it is more likely that any swimming by jellyfish would be done at variable swimming speeds. The transport models developed here did not dynamically incorporate individual physio-biological variations of the jellyfish, dynamically in the model, e.g. through incorporation of life cycle modelling. It is recommended that dynamic life cycle variables such as strobilation, growth, metamorphosis, mortality, size, shape be incorporated into future model iterations to determine their relative influences on transport. The model did not incorporate any behavioural movements based upon food and prey availability; again, these could also be explored in future models.

REFERENCES

- Ai, H., Zhang, W., Hu, X., He, Q., & Liu, Y. (2014). The Research and Application Progress of Environmental Fluid Dynamics Code. *Journal of Water Resources Research*, 3, 247-256. https://pdf.hanspub.org/JWRR20140300000_37902537.pdf
- AQUAFACT. (2013). *Technical Advisors Report: Killary Mussel Licence Renewal Appeal (Site T9/317)* (pp. 1-41). AQUAFACT International Services Ltd. www.aquafact.ie
- ARAKAWA, A., & LAMB, V. R. (1977). *Computational Design of the Basic Dynamical Processes of the UCLA General Circulation Model*. 17, 173-265. <https://doi.org/10.1016/B978-0-12-460817-7.50009-4>
- Baliarsingh, S. K., Lotliker, A. A., Srichandan, S., Samanta, A., Kumar, N., & Balakrishnan Nair, T. M. (2020). A review of jellyfish aggregations, focusing on India's coastal waters. *Ecological Processes*, 9, 1-9. <https://doi.org/10.1186/s13717-020-00268-z>
- Bandara, K., Varpe, Ø., Wijewardene, L., Tverberg, V., & Eiane, K. (2021). Two hundred years of zooplankton vertical migration research. *Biological Reviews*, 96(4), 1547-1589. <https://doi.org/10.1111/BRV.12715>
- Baxter, E. J., Rodger, H. D., McAllen, R., & Doyle, T. K. (2011). Gill disorders in marine-farmed salmon: Investigating the role of hydrozoan jellyfish. *Aquaculture Environment Interactions*, 1(3), 245-257. <https://doi.org/10.3354/aei00024>
- Baxter, E. J., Sturt, M. M., Ruane, N. M., Doyle, T. K., McAllen, R., Harman, L., & Rodger, H. D. (2011). Gill damage to Atlantic Salmon (*Salmo salar*) caused by the common jellyfish (*Aurelia aurita*) under experimental challenge. *PLoS ONE*, 6(4), 4-9. <https://doi.org/10.1371/journal.pone.0018529>
- Berline, L., Zakardjian, B., Molcard, A., Ourmières, Y., & Guihou, K. (2013). Modeling jellyfish *Pelagia noctiluca* transport and stranding in the Ligurian Sea. *Marine Pollution Bulletin*, 70(1-2), 90-99.

<https://doi.org/10.1016/j.marpolbul.2013.02.016>

Bernsen, E., Dijkstra, H. A., & Wubs, F. W. (2008). A method to reduce the spin-up time of ocean models. *Ocean Modelling*, 20(4), 380-392. <https://doi.org/10.1016/J.OCEMOD.2007.10.008>

Blumberg, A.F., & Mellor, G. L. (1987). *A Description of a Three-Dimensional Coastal Ocean Circulation Model* (N. S. Heaps (ed.); Vol. 4). Coastal and Estuarine Sciences, American Geophysical Union. <https://agupubs.onlinelibrary.wiley.com/doi/10.1029/CO004p0001>

Blumberg, Alan F., Galperin, B., & O'Connor, D. J. (1992). Modeling Vertical Structure of Open-Channel Flows. *Journal of Hydraulic Engineering*, 118(8), 1119-1134. [https://doi.org/10.1061/\(ASCE\)0733-9429\(1992\)118:8\(1119\)](https://doi.org/10.1061/(ASCE)0733-9429(1992)118:8(1119))

Boero, F. (2013). REVIEW OF JELLYFISH BLOOMS IN THE MEDITERRANEAN AND BLACK SEA. *STUDIES AND REVIEWS: GENERAL FISHERIES COMMISSION FOR THE MEDITERRANEAN (FAO)*, 92.

Bosch-Belmar, M., Azzurro, E., Pulis, K., Milisenda, G., Fuentes, V., Kéfi-Daly Yahia, O., Micallef, A., Deidun, A., & Piraino, S. (2017). Jellyfish blooms perception in Mediterranean finfish aquaculture. *Marine Policy*, 76(November 2016), 1-7. <https://doi.org/10.1016/j.marpol.2016.11.005>

Bosch-Belmar, M., M'Rabet, C., Dhaouadi, R., Chalghaf, M., Yahia, M. N. D., Fuentes, V., Piraino, S., & Yahia, O. K. D. (2016). Jellyfish stings trigger gill disorders and increased mortality in farmed sparus aurata (linnaeus, 1758) in the mediterranean sea. *PLoS ONE*, 11(4), 1-11. <https://doi.org/10.1371/journal.pone.0154239>

Brian, A., Venables, B., Bates, D. M., Firth, D., & Ripley, M. B. (2022). *Package 'MASS'*.

Brotz, L., Cheung, W. W. L., Kleisner, K., Pakhomov, E., & Pauly, D. (2012). Increasing jellyfish populations: Trends in Large Marine Ecosystems. *Hydrobiologia*, 690(1), 3-20. <https://doi.org/10.1007/s10750-012-1039-7>

Chapman, J. W., Klaassen, R. H. G., Drake, V. A., Fossette, S., Hays, G. C., Metcalfe,

- J. D., Reynolds, A. M., Reynolds, D. R., & Alerstam, T. (2011). Animal orientation strategies for movement in flows. In *Current Biology* (Vol. 21, Issue 20). <https://doi.org/10.1016/j.cub.2011.08.014>
- Cheng, J., Li, S., Ding, F., & Yan, L. (2004). Primary analysis on the jellyfish bloom and its cause in the East China Sea and the Yellow Sea. *Modern Fish Inf*, 19, 10-12. https://www.jstage.jst.go.jp/article/pbr/3/Supplement/3_Supplement_125
- Christie, D., & Neill, S. P. (2022). Measuring and Observing the Ocean Renewable Energy Resource. *Comprehensive Renewable Energy*, 149-175. <https://doi.org/10.1016/B978-0-12-819727-1.00083-2>
- Chung, D. H., & Craig, P. M. (2009). Implementation of a Lagrangian particle tracking sub-model for the Environmental Fluid Dynamics Code. *Dynamic Solutions-International, LLC Knoxville, TN and Hanoi Vietnam*, 1-21. WWW.DS-INTL.BIZ
- Condon, R. H., Duarte, C. M., Pitt, K. A., Robinson, K. L., Lucas, C. H., Sutherland, K. R., Mianzan, H. W., Bogeberg, M., Purcell, J. E., Decker, M. B., Uye, S. I., Madin, L. P., Brodeur, R. D., Haddock, S. H. D., Malej, A., Parry, G. D., Eriksen, E., Quinones, J., Acha, M., ... Graham, W. M. (2013). Recurrent jellyfish blooms are a consequence of global oscillations. *Proceedings of the National Academy of Sciences of the United States of America*, 110(3), 1000-1005. <https://doi.org/10.1073/pnas.1210920110>
- Condon, R. H., Graham, W. M., Duarte, C. M., Pitt, K. A., Lucas, C. H., Haddock, S. H. D., Sutherland, K. R., Robinson, K. L., Dawson, M. N., Decker, M. B., Mills, C. E., Purcell, J. E., Malej, A., Mianzan, H., Uye, S. I., Gelcich, S., & Madin, L. P. (2012). Questioning the rise of gelatinous Zooplankton in the world's oceans. *BioScience*, 62(2), 160-169. <https://doi.org/10.1525/bio.2012.62.2.9>
- Courant, R., Friedrichs, K., & Lewy, H. (1928). Über die partiellen Differenzengleichungen der mathematischen Physik [On the partial difference equations of mathematical physics]. *Mathematische Annalen* 1928 100:1, 100(1), 32-74. <https://doi.org/10.1007/BF01448839>
- Cowen, R. K., Lwiza, K. M. M., Sponaugle, S., Paris, C. B., & Olson, D. B. (2000).

- Connectivity of marine populations: Open or closed? *Science*, 287(5454), 857–859. <https://doi.org/10.1126/science.287.5454.857>
- David, C., Vaz, S., Loots, C., Antajan, E., van der Molen, J., & Travers-Trolet, M. (2015). Understanding winter distribution and transport pathways of the invasive ctenophore *Mnemiopsis leidyi* in the North Sea: coupling habitat and dispersal modelling approaches. *Biological Invasions*, 17(9), 2605–2619. <https://doi.org/10.1007/s10530-015-0899-y>
- Dawson, M. N., Gupta, A. Sen, & England, M. H. (2005). Coupled biophysical global ocean model and molecular genetic analyses identify multiple introductions of cryptogenic species. *Proceedings of the National Academy of Sciences of the United States of America*, 102(34), 11968–11973. <https://doi.org/10.1073/pnas.0503811102>
- Depra, D. (2015). *New Study Finds Jellyfish Swim Actively Against Current, Possess Advanced Orientation Abilities*. Tech Times. <https://www.techtimes.com/articles/28519/20150124/new-study-finds-jellyfish-swims-actively-against-current-possess-advanced-orientation-abilities.htm>
- Doyle, T K, Hays, G. C., Harrod, C., & Houghton, J. D. R. (2014). Ecological and Societal Benefits of Jellyfish. In *Jellyfish Blooms* (Vol. 9789400770, Issue June, pp. 105–127). <https://doi.org/10.1007/978-94-007-7015-7>
- Doyle, Thomas K., De Haas, H., Cotton, D., Dorschel, B., Cummins, V., Houghton, J. D. R., Davenport, J., & Hays, G. C. (2008). Widespread occurrence of the jellyfish *Pelagia noctiluca* in Irish coastal and shelf waters. *Journal of Plankton Research*, 30(8), 963–968. <https://doi.org/10.1093/plankt/fbn052>
- Doyle, Thomas K., Houghton, J. D. R., Buckley, S. M., Hays, G. C., & Davenport, J. (2007). The broad-scale distribution of five jellyfish species across a temperate coastal environment. *Hydrobiologia*, 579(1), 29–39. <https://doi.org/10.1007/s10750-006-0362-2>
- Dunsbergen, D. W., & Stalling, G. S. (1993). *The combination of a random walk method and a hydrodynamic model for the simulation of dispersion of dissolved*

matter in water. www.witpress.com,

- Dupont, N., Klevjer, T. A., Kaartvedt, S., & Aksnes, D. L. (2009). Diel vertical migration of the deep-water jellyfish *Periphylla periphylla* simulated as individual responses to absolute light intensity. *Limnology and Oceanography*, 54(5), 1765-1775. <https://doi.org/10.4319/lo.2009.54.5.1765>
- EPA. (2022). *Environmental Fluid Dynamics Code (EFDC)*. United States Environmental Protection Agency. <https://www.epa.gov/ceam/environmental-fluid-dynamics-code-efdc>
- ESRI. (2018). ArcGIS [GIS software]. Version 10. In Redlands, CA: *Environmental Systems Research Institute*. Redlands, CA: Environmental Systems Research Institute.
- Fossette, S., Gleiss, A. C., Chalumeau, J., Bastian, T., Armstrong, C. D., Vandenabeele, S., Karpytchev, M., & Hays, G. C. (2015). Current-oriented swimming by jellyfish and its role in bloom maintenance. *Current Biology*, 25(3), 342-347. <https://doi.org/10.1016/j.cub.2014.11.050>
- Freer, J. J., & Hobbs, L. (2020). DVM: The World's Biggest Game of Hide-and-Seek. *Frontiers for Young Minds*, 8. <https://doi.org/10.3389/FRYM.2020.00044>
- Galperin, B., Kantha, L. H., Hassid, S., & A. Rosati, A. (1988). A Quasi-Equilibrium Turbulent Energy Model for Geophysical Flows. *Journal of the Atmospheric Sciences*, 45(1), 55-62.
- Garm, A., & Ekström, P. (2010). Evidence for multiple photosystems in jellyfish. *International Review of Cell and Molecular Biology*, 280(C), 41-78. [https://doi.org/10.1016/S1937-6448\(10\)80002-4](https://doi.org/10.1016/S1937-6448(10)80002-4)
- Gemmell, B. J., Costello, J. H., Colin, S. P., Stewart, C. J., Dabiri, J. O., Tafti, D., & Priya, S. (2013). Passive energy recapture in jellyfish contributes to propulsive advantage over other metazoans. *Proceedings of the National Academy of Sciences of the United States of America*, 110(44), 17904-17909. <https://doi.org/10.1073/pnas.1306983110>
- Gill, V. (2015). Jellyfish "can sense ocean currents" - BBC News. BBC News - Science

- & Environment. <https://www.bbc.com/news/science-environment-30936192>
- Gjelsvik Tiller, R., Mork, J., Richards, R., Eisenhauer, L., Liu, Y., Nakken, J. F., & Borgersen, Å. L. (2014). Something fishy: Assessing stakeholder resilience to increasing jellyfish (*Periphylla periphylla*) in Trondheimsfjord, Norway. *Marine Policy*, 46, 72-83. <https://doi.org/10.1016/J.MARPOL.2013.12.006>
- Gómez, A. R., & Gutiérrez-Hernández, O. (2020). Impact of Jellyfish and Other Gelatinous Organisms on the Andalusian Coast: Implications for Sun and Beach Tourism. *Estudios Geográficos*, 81(288), 38. <https://doi.org/10.3989/ESTGEOGR.202053.033>
- Goy, J., Morand, P., & Etienne, M. (1989). Long-term fluctuations of *Pelagia noctiluca* (Cnidaria, Scyphomedusa) in the western Mediterranean Sea. Prediction by climatic variables. *Deep Sea Research Part A. Oceanographic Research Papers*, 36(2), 269-279. [https://doi.org/10.1016/0198-0149\(89\)90138-6](https://doi.org/10.1016/0198-0149(89)90138-6)
- Graham, W. M., Martin, D. L., Felder, D. L., Asper, V. L., & Perry, H. M. (2003). Ecological and economic implications of a tropical jellyfish invader in the Gulf of Mexico. *Biological Invasions*, 5(1-2), 53-69. <https://doi.org/10.1023/A:1024046707234/METRICS>
- Graham, W. M., Pagès, F., & Hamner, W. M. (2001). A physical context for gelatinous zooplankton aggregations: A review. *Hydrobiologia*, 451, 199-212. <https://doi.org/10.1023/A:1011876004427>
- Guo, X. (2002). A Triply Nested Ocean Model for Simulating the Kuroshio-Roles of Horizontal Resolution on JEBAR. *JOURNAL OF PHYSICAL OCEANOGRAPHY*.
- Halsband, C., Majaneva, S., Hosia, A., Emaus, P. A., Gaardsted, F., Zhou, Q., Nøst, O. A., & Renaud, P. E. (2018). Jellyfish summer distribution, diversity and impact on fish farms in a Nordic fjord. *Marine Ecology Progress Series*, 591(October), 267-279. <https://doi.org/10.3354/meps12274>
- Hamrick, J. M. (2007). The Environmental Fluid Dynamics Code User Manual US EPA Version 1.01. In *Tetra Tech, Inc., 10306 Eaton Place, Suite 340, Fairfax, VA 22030*. Tetra Tech, Inc., 10306 Eaton Place, Suite 340, Fairfax, VA 22030.

https://www.epa.gov/sites/default/files/2016-01/documents/efdc_user_manual_epa_ver-101.pdf

Hamrick, J.M. (2007). The Environmental Fluid Dynamics Code Theory and Computation Volume 1: Hydrodynamics and Mass Transport. In *Tetra Tech, Inc., 10306 Eaton Place, Suite 340, Fairfax, VA 22030*. Tetra Tech, Inc., 10306 Eaton Place, Suite 340, Fairfax, VA 22030.

Hamrick, John M. (1992). A Three-Dimensional Environmental Fluid Dynamics Computer Code: Theoretical and Computational Aspects. In *Special report in applied marine science and ocean engineering ; no. 317.. Virginia Institute of Marine Science, College of William and Mary*. (Issue 317). <https://doi.org/10.21220/V5TT6C>

Hamrick, John M. (1996). User's manual for the Environmental Fluid Dynamics Computer Code. In *Special Reports in Applied Marine Science and Ocean Engineering (SRAMSOE) No. 331. Virginia Institute of Marine Science, College of William and Mary*. (Issue 331). <https://doi.org/https://doi.org/10.21220/V5M74W>

Hays, G. C., Doyle, T. K., Houghton, J. D. R., Lilley, M. K. S., Metcalfe, J. D., & Righton, D. (2008). Diving behaviour of jellyfish equipped with electronic tags. *Journal of Plankton Research*, 30(3), 325–331. <https://doi.org/10.1093/plankt/fbn003>

Hayter, E. J. (2014). Literature Review of EFDC Applications Demonstrating Capability for Use in the Jacksonville Harbor Feasibility Study. In *U.S. Army Corps of Engineers, Engineer Research and Development Center*. U.S. Army Corps of Engineers, Engineer Research and Development Center.

Heer, T., Wells, M. G., Jackson, P. R., & Mandrak, N. E. (2020). Modelling grass carp egg transport using a 3-D hydrodynamic river model: The role of egg retention in dead zones on spawning success. *Canadian Journal of Fisheries and Aquatic Sciences*, 77(8), 1379–1392. https://doi.org/10.1139/CJFAS-2019-0344/SUPPL_FILE/CJFAS-2019-0344SUPPLB.AVI

Heger, T., & Trepl, L. (2003). Predicting biological invasions. *Biological Invasions*, 5(4), 313–321. <https://doi.org/10.1023/b:binv.00000005568.44154.12>

- Hodson, T. O. (2022). Root-mean-square error (RMSE) or mean absolute error (MAE): when to use them or not. *Geoscientific Model Development*, 15(14), 5481-5487. <https://doi.org/10.5194/GMD-15-5481-2022>
- Hogan, T. (2012). *Deadly jellyfish with 50m tentacles land on beaches | Independent.ie*. Irish Independent. <https://www.independent.ie/news/deadly-jellyfish-with-50m-tentacles-land-on-beaches/26892805.html>
- Holt, J. T., & James, I. D. (2001). An s coordinate density evolving model of the northwest European continental shelf: 1. Model description and density structure. *Journal of Geophysical Research: Oceans*, 106(C7), 14015-14034. <https://doi.org/10.1029/2000JC000304>
- Hur, Y.-T., & Park, J.-H. (2009). Assessment of EFDC Model for Hydrodynamic Analysis in the Nakdong River. *Journal of Korea Water Resources Association*, 42(4), 309-317. <https://doi.org/10.3741/JKWRA.2009.42.4.309>
- Jackson, J. B. C., Kirby, M. X., Berger, W. H., Bjorndal, K. A., Botsford, L. W., Bourque, B. J., Bradbury, R. H., Cooke, R., Erlandson, J., Estes, J. A., Hughes, T. P., Kidwell, S., Lange, C. B., Lenihan, H. S., Pandolfi, J. M., Peterson, C. H., Steneck, R. S., Tegner, M. J., & Warner, R. R. (2001). Historical Overfishing and the Recent Collapse of Coastal Ecosystems. *Science*, 293(5530), 629-637. <https://doi.org/10.1126/SCIENCE.1059199>
- James, S. C., O'Donncha, F., & Plew D. R. (2016). Calibration of a 3D hydrodynamic aquaculture model. *OCEANS 2016 MTS/IEEE Monterey*, 1-7. <https://doi.org/10.1109/OCEANS.2016.7761411>
- James, Scott C., Jones, C. A., Grace, M. D., & Roberts, J. D. (2010). Advances in sediment transport modelling. [Http://Dx.Doi.Org/10.1080/00221686.2010.515653](http://Dx.Doi.Org/10.1080/00221686.2010.515653), 48(6), 754-763. <https://doi.org/10.1080/00221686.2010.515653>
- James, Scott C., Lefantzi, S., Barco, J., Johnson, E., & Roberts, J. D. (2011). Verifying marine-hydro-kinetic energy generation simulations using SNL-EFDC. *OCEANS'11 MTS/IEEE KONA*, 1-9. <https://doi.org/10.23919/OCEANS.2011.6106918>

- Jaspers, C., Huwer, B., Antajan, E., Hosia, A., Hinrichsen, H. H., Biastoch, A., Angel, D., Asmus, R., Augustin, C., Bagheri, S., Beggs, S. E., Balsby, T. J. S., Boersma, M., Bonnet, D., Christensen, J. T., Dänhardt, A., Delpy, F., Falkenhaus, T., Finenko, G., ... Woźniczka, A. (2018). Ocean current connectivity propelling the secondary spread of a marine invasive comb jelly across western Eurasia. *Global Ecology and Biogeography*, 27(7), 814-827. <https://doi.org/10.1111/geb.12742>
- Ji, Z. G., Morton, M. R., & Hamrick, J. M. (2001). Wetting and Drying Simulation of Estuarine Processes. *Estuarine, Coastal and Shelf Science*, 53(5), 683-700. <https://doi.org/10.1006/ECSS.2001.0818>
- Ji, Zhen Gang. (2017). Hydrodynamics and Water Quality: Modeling Rivers, Lakes, and Estuaries. In *Hydrodynamics and Water Quality: Modeling Rivers, Lakes, and Estuaries* (2nd ed.). John Wiley & Sons, Inc. <https://doi.org/10.1002/9781119371946>
- Johnson, D R, & Perry, H. M. (1999). Blue Crab Larval Dispersion and Retention in the Mississippi Bight. *Bulletin of Marine Science*, 65(1), 129-149. https://aquila.usm.edu/fac_pubsAvailableat:https://aquila.usm.edu/fac_pubs/4666
- Johnson, Donald R., Perry, H. M., & Burke, W. D. (2001). Developing jellyfish strategy hypotheses using circulation models. *Hydrobiologia*, 451, 213-221. <https://doi.org/10.1023/A:1011880121265>
- Johnson, Donald R., Perry, H. M., & Graham, W. M. (2005). Using nowcast model currents to explore transport of non-indigenous jellyfish into the Gulf of Mexico. *Marine Ecology Progress Series*, 305, 139-146. <https://doi.org/10.3354/meps305139>
- Kaartvedt, S., Klevjer, T. A., Torgersen, T., Sørnes, T. A., & Røstad, A. (2007). Diel vertical migration of individual jellyfish (*Periphylla periphylla*). *Limnology and Oceanography*, 52(3), 975-983. <https://doi.org/10.4319/lo.2007.52.3.0975>
- Kawahara, M., Uye, S. I., Ohtsu, K., & Iizumi, H. (2006). Unusual population explosion of the giant jellyfish *Nemopilema nomurai* (Scyphozoa: Rhizostomeae) in East

- Asian waters. *Marine Ecology Progress Series*, 307, 161-173.
<https://doi.org/10.3354/MEPS307161>
- Keegan, B. F., & Mercer, J. P. (1986). An Oceanographical Survey of Killary Harbour on the West Coast of Ireland. *Proceedings of the Royal Irish Academy. Section B: Biological, Geological, and Chemical Science*, 86B, 1-70.
<http://www.jstor.org/stable/20494455>
- Kideys, A. E. (2002). Ecology: Fall and rise of the Black Sea ecosystem. *Science*, 297(5586), 1482-1484. <https://doi.org/10.1126/science.1073002>
- Kim, C. K., Park, K., Powers, S. P., Graham, W. M., & Bayha, K. M. (2010). Oyster larval transport in coastal Alabama: Dominance of physical transport over biological behavior in a shallow estuary. *Journal of Geophysical Research: Oceans*, 115(C10), 10019. <https://doi.org/10.1029/2010JC006115>
- Kim, D. H., Seo, J. N., Yoon, W. D., & Suh, Y. S. (2012). Estimating the economic damage caused by jellyfish to fisheries in Korea. *Fisheries Science*, 78(5), 1147-1152. <https://doi.org/10.1007/S12562-012-0533-1/METRICS>
- Kimmerer, W. J., Gross, E. S., & MacWilliams, M. L. (2014). Tidal migration and retention of estuarine zooplankton investigated using a particle-tracking model. *Limnology and Oceanography*, 59(3), 901-916.
<https://doi.org/10.4319/LO.2014.59.3.0901>
- King, T. L., Bentley, R. J., Thornton, L. E., & Kavanagh, A. M. (2016). Using kernel density estimation to understand the influence of neighbourhood destinations on BMI. *BMJ Open*, 6(2). <https://doi.org/10.1136/bmjopen-2015-008878>
- King, T. L., Thornton, L. E., Bentley, R. J., & Kavanagh, A. M. (2015). The Use of Kernel Density Estimation to Examine Associations between Neighborhood Destination Intensity and Walking and Physical Activity. *PLOS ONE*, 10(9), e0137402. <https://doi.org/10.1371/JOURNAL.PONE.0137402>
- Kloog, I., Haim, A., & Portnov, B. A. (2009). Using kernel density function as an urban analysis tool: Investigating the association between nightlight exposure and the incidence of breast cancer in Haifa, Israel. *Computers, Environment and Urban*

<https://doi.org/10.1016/J.COMPENVURBSYS.2008.09.006>

- Kumar, B. S., Mohanty, A. K., Das, N. P. I., Satpathy, K. K., & Sarkar, S. K. (2017). Impingement of marine organisms in a tropical atomic power plant cooling water system. *Marine Pollution Bulletin*, 124(1), 555-562. <https://doi.org/10.1016/J.MARPOLBUL.2017.07.067>
- Large, W. G., McWilliams, J. C., & Doney, S. C. (1994). Oceanic vertical mixing: A review and a model with a nonlocal boundary-layer parameterization. *Reviews of Geophysics*, 32(4), 363-403. <https://doi.org/10.1029/94RG01872>
- Lee, P. L. M., Dawson, M. N., Neill, S. P., Robins, P. E., Houghton, J. D. R., Doyle, T. K., & Hays, G. C. (2013). Identification of genetically and oceanographically distinct blooms of jellyfish. *Journal of the Royal Society Interface*, 10(80). <https://doi.org/10.1098/rsif.2012.0920>
- Li, X., WANG, Y., & ZHANG, S. (2009). Numerical simulation of water quality in Yangtze Estuary. *Water Science and Engineering*, 2(4), 40-51. <https://doi.org/10.3882/j.issn.1674-2370.2009.04.004>
- Li, Z., Gross, T. F., Brown, C. W., Wang, H. V., & Hood, R. R. (2002). A near real time simulation of salinity, temperature and Sea Nettles (*Chrysaora quinquecirrha*) in Chesapeake Bay. *Proceedings of the Seventh International Conference on Estuarine and Coastal Modeling, St. Petersburg, Florida, United States, 2001*, 467-478. [https://doi.org/10.1061/40628\(268\)29](https://doi.org/10.1061/40628(268)29)
- Liu, Z., Hashim, N. B., Kingery, W. L., & Huddleston, D. H. (2007). Hydrodynamic modeling of St Louis Bay estuary and watershed using EFDC and HSPF. *9th International Symposium on Fluid Control Measurement and Visualization 2007, FLUCOME 2007*, 3, 1540-1551. <https://doi.org/10.2112/1551-5036-52.sp1.107>
- Longhurst, A. R., Bedo, A. W., Harrison, W. G., Head, E. J. H., & Sameoto, D. D. (1990). Vertical flux of respiratory carbon by oceanic diel migrant biota. *Deep Sea Research Part A. Oceanographic Research Papers*, 37(4), 685-694. [https://doi.org/10.1016/0198-0149\(90\)90098-G](https://doi.org/10.1016/0198-0149(90)90098-G)

- Luo, X., & Li, X. (2018). Using the EFDC model to evaluate the risks of eutrophication in an urban constructed pond from different water supply strategies. *Ecological Modelling*, 372, 1-11. <https://doi.org/10.1016/J.ECOLMODEL.2018.01.020>
- Lynam, C. P., Gibbons, M. J., Axelsen, B. E., Sparks, C. A. J., Coetzee, J., Heywood, B. G., & Brierley, A. S. (2006). Jellyfish overtake fish in a heavily fished ecosystem. *Current Biology: CB*, 16(13). <https://doi.org/10.1016/J.CUB.2006.06.018>
- Mackie, G. O., Larson, R. J., Larson, K. S., & Passano, L. M. (1981). Swimming and vertical migration of *Aurelia aurita* (L) in a deep tank . *Marine Behaviour and Physiology*, 7(4), 321-329. <https://doi.org/10.1080/10236248109386993>
- Maguire, S. (2017). *Warning issued after potent jellyfish washed up on Donegal beach* - *Donegal Daily*. Donegal Daily. <https://www.donegaldaily.com/2017/07/10/warning-issued-after-potent-jellyfish-washed-up-on-donegal-beach/>
- Manning, A., & Dawkins, M. S. (2012). *An introduction to animal behaviour*. Cambridge University Press.
- Marcos-López, M., Mitchell, S. O., & Rodger, H. D. (2016). Pathology and mortality associated with the mauve stinger jellyfish *Pelagia noctiluca* in farmed Atlantic salmon *Salmo salar* L. *Journal of Fish Diseases*, 39(1), 111-115. <https://doi.org/10.1111/jfd.12267>
- Martin, V. J. (2002). Photoreceptors of cnidarians. *Canadian Journal of Zoology*, 80(10), 1703-1722. <https://doi.org/10.1139/z02-136>
- Masilamoni, G., Jesudoss, K. S., Nandakumar, K., Satpathy, K. K., Nair, K. V. K., & Azaariah, J. . (2000). Jellyfish ingress: A threat to the smooth operation of coastal power plants. *Current Science*, 79(5), 567-569.
- Matanoski, J. C., & Hood, R. R. (2006). An individual-based numerical model of medusa swimming behavior. *Marine Biology*, 149(3), 595-608. <https://doi.org/10.1007/s00227-006-0244-1>
- McLaughlin, R. (2021). *Beachgoers "blown away" by strange species* - *Donegal Daily*.

- Donegal Daily. <https://www.donegaldaily.com/2021/09/29/beachgoers-blown-away-by-strange-species/>
- McSorley, A. (2016). *Warning issued as swarm of deadly Portuguese man-o'-war jellyfish wash up on beaches in SIX counties - Irish Mirror Online*. Irish Mirror. <https://www.irishmirror.ie/news/irish-news/warning-issued-swarm-deadly-portuguese-8940191>
- Mellor, G. L., & Yamada, T. (1982). Development of a Turbulence Closure Model for Geophysical Fluid Problems. *Reviews of Geophysics*, 20(4), 851-875.
- Mellor, George L. (2004). USERS GUIDE FOR A THREE-DIMENSIONAL, PRIMITIVE EQUATION, NUMERICAL OCEAN MODEL. *POM User Manual*. <http://www.aos.princeton.edu/WWWPUBLIC/htdocs.pom/>
- Mills, C. E. (2001). Jellyfish blooms: Are populations increasing globally in response to changing ocean conditions? *Hydrobiologia*, 451(1), 55-68. <https://doi.org/10.1023/A:1011888006302>
- Mitchell, S. O., Bresnihan, S., & Scholz, F. (2021). Mortality and skin pathology of farmed Atlantic salmon (*Salmo salar*) caused by exposure to the jellyfish *Physalia physalis* in Ireland. *Journal of Fish Diseases*, 44(11), 1861-1864. <https://doi.org/10.1111/JFD.13499>
- Molnar, J. L., Gamboa, R. L., Revenga, C., & Spalding, M. D. (2008). Assessing the global threat of invasive species to marine biodiversity. *Frontiers in Ecology and the Environment*, 6(9), 485-492. <https://doi.org/10.1890/070064>
- Moon, J. H., Pang, I. C., Yang, J. Y., & Yoon, W. D. (2010). Behavior of the giant jellyfish *Nemopilema nomurai* in the East China Sea and East/Japan Sea during the summer of 2005: A numerical model approach using a particle-tracking experiment. *Journal of Marine Systems*, 80(1-2), 101-114. <https://doi.org/10.1016/j.jmarsys.2009.10.015>
- Moriarty, P. E., Andrews, K. S., Harvey, C. J., & Kawase, M. (2012). Vertical and horizontal movement patterns of scyphozoan jellyfish in a fjord-like estuary. *Marine Ecology Progress Series*, 455, 1-12.

<https://doi.org/10.3354/meps09783>

- Moustafa, M. Z., & Hamrick, J. M. (1994). Modeling circulation and salinity transport in the Indian River Lagoon. In M. L. Spaulding (Ed.), *Proceedings of the 3rd International Conference on Estuarine and Coastal Modeling* (pp. 381–395). American Society of Civil Engineers.
- Nagata, R. M., Haddad, M. A., & Nogueira, M. (2009). The nuisance of medusae (Cnidaria, Medusozoa) to shrimp trawls in central part of southern Brazilian Bight, from the perspective of artisanal fishermen. *Journal of Aquatic Sciences*, 4, 312–325.
- Neil, T. R., & Askew, G. N. (2018). Jet-paddling jellies: Swimming performance in the Rhizostomeae jellyfish *Catostylus mosaicus*. *Journal of Experimental Biology*, 221(24). <https://doi.org/10.1242/jeb.191148>
- Nilsson, D. E., Gislén, L., Coates, M. M., Skogh, C., & Garm, A. (2005). Advanced optics in a jellyfish eye. *Nature*, 435(7039), 201–205. <https://doi.org/10.1038/nature03484>
- Nunes, J. P., Ferreira, J. G., Bricker, S. B., O’Loan, B., Dabrowski, T., Dallaghan, B., Hawkins, A. J. S., O’Connor, B., & O’Carroll, T. (2011). Towards an ecosystem approach to aquaculture: Assessment of sustainable shellfish cultivation at different scales of space, time and complexity. *Aquaculture*, 315(3–4), 369–383. <https://doi.org/10.1016/j.aquaculture.2011.02.048>
- O’Donncha, F. (2012). Physical and numerical modelling of impeded tidal flows: Effects of aquaculture structures on hydrodynamics and material transport. [Doctoral Dissertation, National University of Ireland, Galway]. Access to Research at NUIG (ARAN) Repository. <https://aran.library.nuigalway.ie/handle/10379/3066?show=full>
- O’Donncha, Fearghal, James, S. C., & Ragnoli, E. (2017). Modelling study of the effects of suspended aquaculture installations on tidal stream generation in Cobscook Bay. *Renewable Energy*, 102, 65–76. <https://doi.org/10.1016/j.renene.2016.10.024>

- O'Donncha, Fearghal, Ragnoli, E., & Suits, F. (2014). Parallelisation study of a three-dimensional environmental flow model. *Computers and Geosciences*, 64, 96–103. <https://doi.org/10.1016/j.cageo.2013.12.006>
- O'Sullivan, K. (2017). *Stinger jellyfish swarms wipe out farmed salmon in west of Ireland - Local Environmental Observer (LEO) Network*. The Irish Times. <https://www.leonetwork.org/en/posts/show/343A1FB5-E067-4E1D-BB99-CAB8DD248886>
- Pak, G., Kim, Y., Yoon, J., Mallari, K. J. B., Baek, J., Jung, M., & Kim, D. (2016). Modelling of suspended sediment in a weir reach using EFDC model. *Water Science and Technology*, 73(7), 1583–1590. <https://doi.org/10.2166/WST.2015.574>
- Park, I., Seo, I. W., Kim, Y. Do, & Han, E. J. (2017). Turbulent Mixing of Floating Pollutants at the Surface of the River. *Journal of Hydraulic Engineering*, 143(8). [https://doi.org/10.1061/\(asce\)hy.1943-7900.0001319](https://doi.org/10.1061/(asce)hy.1943-7900.0001319)
- Parzen, E. (1962). On Estimation of a Probability Density Function and Mode. <https://doi.org/10.1214/Aoms/1177704472>, 33(3), 1065–1076. <https://doi.org/10.1214/AOMS/1177704472>
- Pawlowicz, R., Beardsley, B., & Lentz, S. (2002). Classical tidal harmonic analysis including error estimates in MATLAB using T_TIDE. *Computers & Geosciences*, 28(8), 929–937. [https://doi.org/10.1016/S0098-3004\(02\)00013-4](https://doi.org/10.1016/S0098-3004(02)00013-4)
- Phillips, N. A. (1957). A Coordinate System Having Some Special Advantages for Numerical Forecasting. *Journal of Meteorology*, 14(2), 184–185. [https://doi.org/10.1175/1520-0469\(1957\)014<0184:acshss>2.0.co;2](https://doi.org/10.1175/1520-0469(1957)014<0184:acshss>2.0.co;2)
- Pitt, K. A., & Lucas, C. H. (2014). Jellyfish blooms. In *Jellyfish Blooms* (Vol. 9789400770). Springer Netherlands. <https://doi.org/10.1007/978-94-007-7015-7/COVER>
- Purcell, J. E., Baxter, E. J., & Fuentes, V. L. (2013). Jellyfish as products and problems of aquaculture. *Advances in Aquaculture Hatchery Technology*, March 2016, 404–430. <https://doi.org/10.1533/9780857097460.2.404>

- Purcell, J. E., Uye, S. I., & Lo, W. T. (2007). Anthropogenic causes of jellyfish blooms and their direct consequences for humans: A review. *Marine Ecology Progress Series*, 350, 153-174. <https://doi.org/10.3354/meps07093>
- Qiu, Z. F., Doglioli, A. M., Hu, Z. Y., Marsaleix, P., & Carlotti, F. (2010). The influence of hydrodynamic processes on zooplankton transport and distributions in the North Western Mediterranean: Estimates from a Lagrangian model. *Ecological Modelling*, 221(23), 2816-2827. <https://doi.org/10.1016/J.ECOLMODEL.2010.07.025>
- Qu, C. F., Song, J. M., Li, N., Li, X. G., Yuan, H. M., Duan, L. Q., & Ma, Q. X. (2015). Jellyfish (*Cyanea nozakii*) decomposition and its potential influence on marine environments studied via simulation experiments. *Marine Pollution Bulletin*, 97(1-2), 199-208. <https://doi.org/10.1016/J.MARPOLBUL.2015.06.016>
- Rahi, J. El, Weeber, M. P., & Serafy, G. El. (2020). Modelling the effect of behavior on the distribution of the jellyfish Mauve stinger (*Pelagia noctiluca*) in the Balearic Sea using an individual-based model. *Ecological Modelling*, 433(July), 109230. <https://doi.org/10.1016/j.ecolmodel.2020.109230>
- Rakow, K. C., & Graham, W. M. (2006). Orientation and swimming mechanics by the scyphomedusa *Aurelia* sp. in shear flow. *Limnology and Oceanography*, 51(2), 1097-1106. <https://doi.org/10.4319/LO.2006.51.2.1097>
- Rathi, A. (2014). *Jellyfish are the most energy efficient swimmers, new metric confirms*. The Conversation - Science & Technology. <https://theconversation.com/jellyfish-are-the-most-energy-efficient-swimmers-new-metric-confirms-26729>
- Richardson, A. J., Bakun, A., Hays, G. C., & Gibbons, M. J. (2009). The jellyfish joyride: causes, consequences and management responses to a more gelatinous future. *Trends in Ecology and Evolution*, 24(6), 312-322. <https://doi.org/10.1016/j.tree.2009.01.010>
- Roden, C. M., Rodhouse, P. G., Hensey, M. P., McMahon, T., Ryan, T. H., & Mercer, J. P. (1987). Hydrography and the distribution of phytoplankton in Killary Harbour: a fjord in western Ireland. *Journal of the Marine Biological Association*

- of the United Kingdom, 67(2), 359-371.
<https://doi.org/10.1017/S0025315400026667>
- Rodger, H. D., Henry, L., & Mitchell, S. O. (2011). Non-infectious gill disorders of marine salmonid fish. *Reviews in Fish Biology and Fisheries*, 21(3), 423-440.
<https://doi.org/10.1007/s11160-010-9182-6>
- Rosenblatt, M. (1956). Remarks on Some Nonparametric Estimates of a Density Function. *https://Doi.Org/10.1214/Aoms/1177728190*, 27(3), 832-837.
<https://doi.org/10.1214/AOMS/1177728190>
- Ruiz-Frau, A. (2022). Impacts of jellyfish presence on tourists' holiday destination choices and their willingness to pay for mitigation measures. *Journal of Environmental Planning and Management*.
<https://doi.org/10.1080/09640568.2022.2061926>
- Rutkowski, T., Schroeder, R., & Resgalla, C. (2018). Occurrences of Jellyfish in the Industrial Fishing Activity of the Southeastern and Southern Regions of Brazil. *Marine and Coastal Fisheries*, 10(2), 144-151.
<https://doi.org/10.1002/mcf2.10017>
- Seebens, H., Schwartz, N., Schupp, P. J., & Blasius, B. (2016). Predicting the spread of marine species introduced by global shipping. *Proceedings of the National Academy of Sciences of the United States of America*, 113(20), 5646-5651.
https://doi.org/10.1073/PNAS.1524427113/SUPPL_FILE/PNAS.201524427SI.PDF
- Seo, H. (2021). The ups and downs of a great vertical migration. *Knowable Magazine*. <https://doi.org/10.1146/KNOWABLE-110421-1>
- Shen, H. H. (2002). *Environmental fluid mechanics : theories and applications*. 467.
- Shephard, S., & Gargan, P. (2017). Quantifying the contribution of sea lice from aquaculture to declining annual returns in a wild Atlantic salmon population. *Aquaculture Environment Interactions*, 9(May), 181-192.
<https://doi.org/10.3354/aei00223>
- Simberloff, D. (2000). Introduced Species: The Threat to Biodiversity & What Can Be

- Done. *American Institute of Biological Sciences*.
<http://www.actionbioscience.org/biodiversity/simberloff.html#primer>
- Simons, R. D., Siegel, D. A., Brown, K. S., Simons, R. D., Siegel, D. A., & Brown, K. S. (2013). Model sensitivity and robustness in the estimation of larval transport: A study of particle tracking parameters. *JMS*, 119, 19-29.
<https://doi.org/10.1016/J.JMARSYS.2013.03.004>
- Småge, S. B., Brevik, Ø. J., Frisch, K., Watanabe, K., Duesund, H., & Nylund, A. (2017). Concurrent jellyfish blooms and tenacibaculosis outbreaks in Northern Norwegian Atlantic salmon (*Salmo salar*) farms. *PLoS ONE*, 12(11).
<https://doi.org/10.1371/journal.pone.0187476>
- Smagorinsky, J. (1963). General Circulation Experiments with the Primitive Equations. *Monthly Weather Review*, 91(3), 99. [https://doi.org/10.1175/1520-0493\(1963\)091](https://doi.org/10.1175/1520-0493(1963)091)
- Spall, M. A., & Holland, W. R. (1991). A Nested Equation Model for Oceanic Applications. *American Meteorological Society*.
- Steinberg, D. K., & Landry, M. R. (2017). Zooplankton and the Ocean Carbon Cycle. *Annual Review of Marine Science*, 9(1), 413-444.
<https://doi.org/10.1146/ANNUREV-MARINE-010814-015924>
- Stephens, C., Antonov, J. I., Boyer, T. P., Conkright, M. E., Locarnini, R. A., O'brien, T. D., Garcia, H. E., Levitus, S., Withee, G. W., Administrator, A., Stephens, C., Antonov, J. I., Boyer, T. P., Conkright, M. E., Locarnini, R. A., O'brien, T. D., & Garcia, H. E. (2002). *World ocean atlas 2001. Volume 1, Temperature* (Vol. 1, p. pp). <https://repository.library.noaa.gov/view/noaa/1105>
- Surve, A. (2018). *Huge increase in number of potentially deadly jellyfish on Irish beaches - Irish Mirror Online*. Irish Mirror. <https://www.irishmirror.ie/news/irish-news/lions-mane-jellyfish-sightings-ireland-13162737>
- The Fish Site. (2012). Rope Mussel Producers Organise Pier Clean Up in Killary Harbour | The Fish Site. *The Fish Site*. <https://thefishsite.com/articles/rope-mussel-producers-organise-pier-clean-up-in-killary-harbour-1>

- Torres-Bejarano, F., García-Gallego, J., & Salcedo-Salgado, J. (2023). Numerical modeling of nutrient transport to assess the agricultural impact on the trophic state of reservoirs. *International Soil and Water Conservation Research*, 11(1), 197-212. <https://doi.org/10.1016/J.ISWCR.2022.06.002>
- Towers, L. (2014). *Jellyfish and Aquaculture Interactions: Last Years Irish Experience*. The Fish Site. <https://thefishsite.com/articles/jellyfish-and-aquaculture-interactions-last-years-irish-experience>
- Turchin, P. (1998). Quantitative analysis of movement: measuring and modeling population redistribution in animals and plants. *Sinauer Associates, Sunderland*.
- Tyrrell, H. J. V. (1964). The Origin and Present Status of Fick's Diffusion Law. *Journal of Chemical Education*, 41(7), 397-400. <https://pubs.acs.org/sharingguidelines>
- UISCE. (2010). Understanding Irish Shellfish Culture Environments Project Report for DAFF on Killary Harbour. In *Aquaculture Technical Section, BIM*.
- Venables, W. N., & Ripley, B. D. (2002). *Modern Applied Statistics with S*. Springer, New York. <https://doi.org/10.1007/978-0-387-21706-2>
- Watson, S. (2006). *How Jellyfish Work*. HowStuffWorks.Com. <https://animals.howstuffworks.com/marine-life/jellyfish.htm>
- Węglarczyk, S. (2018). Kernel density estimation and its application. *ITM Web of Conferences*, 23, 00037. <https://doi.org/10.1051/itmconf/20182300037>
- Wei, H., Deng, L., Wang, Y., Zhao, L., Li, X., & Zhang, F. (2015). Giant jellyfish *Nemopilema nomurai* gathering in the Yellow Sea - a numerical study. *Journal of Marine Systems*, 144, 107-116. <https://doi.org/10.1016/j.jmarsys.2014.12.001>
- Whitaker, J. D., King, R., & Knott, D. (2014). Jellyfish. *Sea Science - An Information/Education Series from the Marine Resources Division*. <http://dnr.sc.gov/marine/pub/seascience/pdf/Jellyfish.pdf>
- Wool, T. A., Davie, S. R., & Rodriguez, H. N. (2003). Development of Three-Dimensional Hydrodynamic and Water Quality Models to Support Total

- Maximum Daily Load Decision Process for the Neuse River Estuary, North Carolina. *Journal of Water Resources Planning and Management*, 129(4), 295–306. [https://doi.org/10.1061/\(asce\)0733-9496\(2003\)129:4\(295\)](https://doi.org/10.1061/(asce)0733-9496(2003)129:4(295))
- Wu, G., & Xu, Z. (2011). Prediction of algal blooming using EFDC model: Case study in the Daoxiang Lake. *Ecological Modelling*, 222(6), 1245–1252. <https://doi.org/10.1016/j.ecolmodel.2010.12.021>
- Xian, W., Kang, B., & Liu, R. (2005). Jellyfish Blooms in the Yangtze Estuary. *Science*, 307(5706), 41. <https://doi.org/10.1126/science.307.5706.41c>
- Yin, L., Shan, X., Zhao, C., Jin, X., Wang, G., & Qiao, F. (2019). A model for the transportation and distribution of jellyfish *Rhopilema esculentum* for stock enhancement in the Liaodong Bay, China. *Acta Oceanologica Sinica*, 38(1), 90–101. <https://doi.org/10.1007/s13131-019-1374-x>
- Ai, H., Zhang, W., Hu, X., He, Q., & Liu, Y. (2014). The Research and Application Progress of Environmental Fluid Dynamics Code. *Journal of Water Resources Research*, 3, 247–256. https://pdf.hanspub.org/JWRR20140300000_37902537.pdf
- AQUAFAC. (2013). *Technical Advisors Report: Killary Mussel Licence Renewal Appeal (Site T9/317)* (pp. 1–41). AQUAFAC International Services Ltd. www.aquafact.ie
- ARAKAWA, A., & LAMB, V. R. (1977). *Computational Design of the Basic Dynamical Processes of the UCLA General Circulation Model*. 17, 173–265. <https://doi.org/10.1016/B978-0-12-460817-7.50009-4>
- Baliarsingh, S. K., Lotliker, A. A., Srichandan, S., Samanta, A., Kumar, N., & Balakrishnan Nair, T. M. (2020). A review of jellyfish aggregations, focusing on India's coastal waters. *Ecological Processes*, 9, 1–9. <https://doi.org/10.1186/s13717-020-00268-z>
- Bandara, K., Varpe, Ø., Wijewardene, L., Tverberg, V., & Eiane, K. (2021). Two hundred years of zooplankton vertical migration research. *Biological Reviews*, 96(4), 1547–1589. <https://doi.org/10.1111/BRV.12715>

- Baxter, E. J., Rodger, H. D., McAllen, R., & Doyle, T. K. (2011). Gill disorders in marine-farmed salmon: Investigating the role of hydrozoan jellyfish. *Aquaculture Environment Interactions*, 1(3), 245-257. <https://doi.org/10.3354/aei00024>
- Baxter, E. J., Sturt, M. M., Ruane, N. M., Doyle, T. K., McAllen, R., Harman, L., & Rodger, H. D. (2011). Gill damage to Atlantic Salmon (*Salmo salar*) caused by the common jellyfish (*Aurelia aurita*) under experimental challenge. *PLoS ONE*, 6(4), 4-9. <https://doi.org/10.1371/journal.pone.0018529>
- Berline, L., Zakardjian, B., Molcard, A., Ourmières, Y., & Guihou, K. (2013). Modeling jellyfish *Pelagia noctiluca* transport and stranding in the Ligurian Sea. *Marine Pollution Bulletin*, 70(1-2), 90-99. <https://doi.org/10.1016/j.marpolbul.2013.02.016>
- Bernsen, E., Dijkstra, H. A., & Wubs, F. W. (2008). A method to reduce the spin-up time of ocean models. *Ocean Modelling*, 20(4), 380-392. <https://doi.org/10.1016/J.OCEMOD.2007.10.008>
- Blumberg, A.F., & Mellor, G. L. (1987). *A Description of a Three-Dimensional Coastal Ocean Circulation Model* (N. S. Heaps (ed.); Vol. 4). Coastal and Estuarine Sciences, American Geophysical Union. <https://agupubs.onlinelibrary.wiley.com/doi/10.1029/CO004p0001>
- Blumberg, Alan F., Galperin, B., & O'Connor, D. J. (1992). Modeling Vertical Structure of Open-Channel Flows. *Journal of Hydraulic Engineering*, 118(8), 1119-1134. [https://doi.org/10.1061/\(ASCE\)0733-9429\(1992\)118:8\(1119\)](https://doi.org/10.1061/(ASCE)0733-9429(1992)118:8(1119))
- Boero, F. (2013). REVIEW OF JELLYFISH BLOOMS IN THE MEDITERRANEAN AND BLACK SEA. *STUDIES AND REVIEWS: GENERAL FISHERIES COMMISSION FOR THE MEDITERRANEAN (FAO)*, 92.
- Bosch-Belmar, M., Azzurro, E., Pulis, K., Milisenda, G., Fuentes, V., Kéfi-Daly Yahia, O., Micallef, A., Deidun, A., & Piraino, S. (2017). Jellyfish blooms perception in Mediterranean finfish aquaculture. *Marine Policy*, 76(November 2016), 1-7. <https://doi.org/10.1016/j.marpol.2016.11.005>

- Bosch-Belmar, M., M'Rabet, C., Dhaouadi, R., Chalghaf, M., Yahia, M. N. D., Fuentes, V., Piraino, S., & Yahia, O. K. D. (2016). Jellyfish stings trigger gill disorders and increased mortality in farmed *sparus aurata* (linnaeus, 1758) in the mediterranean sea. *PLoS ONE*, 11(4), 1-11. <https://doi.org/10.1371/journal.pone.0154239>
- Brian, A., Venables, B., Bates, D. M., Firth, D., & Ripley, M. B. (2022). *Package 'MASS'*.
- Brotz, L., Cheung, W. W. L., Kleisner, K., Pakhomov, E., & Pauly, D. (2012). Increasing jellyfish populations: Trends in Large Marine Ecosystems. *Hydrobiologia*, 690(1), 3-20. <https://doi.org/10.1007/s10750-012-1039-7>
- Chapman, J. W., Klaassen, R. H. G., Drake, V. A., Fossette, S., Hays, G. C., Metcalfe, J. D., Reynolds, A. M., Reynolds, D. R., & Alerstam, T. (2011). Animal orientation strategies for movement in flows. In *Current Biology* (Vol. 21, Issue 20). <https://doi.org/10.1016/j.cub.2011.08.014>
- Cheng, J., Li, S., Ding, F., & Yan, L. (2004). Primary analysis on the jellyfish bloom and its cause in the East China Sea and the Yellow Sea. *Modern Fish Inf*, 19, 10-12. https://www.jstage.jst.go.jp/article/pbr/3/Supplement/3_Supplement_125/_pdf
- Christie, D., & Neill, S. P. (2022). Measuring and Observing the Ocean Renewable Energy Resource. *Comprehensive Renewable Energy*, 149-175. <https://doi.org/10.1016/B978-0-12-819727-1.00083-2>
- Chung, D. H., & Craig, P. M. (2009). Implementation of a Lagrangian particle tracking sub-model for the Environmental Fluid Dynamics Code. *Dynamic Solutions-International, LLC Knoxville, TN and Hanoi Vietnam*, 1-21. WWW.DS-INTL.BIZ
- Condon, R. H., Duarte, C. M., Pitt, K. A., Robinson, K. L., Lucas, C. H., Sutherland, K. R., Mianzan, H. W., Bogeberg, M., Purcell, J. E., Decker, M. B., Uye, S. I., Madin, L. P., Brodeur, R. D., Haddock, S. H. D., Malej, A., Parry, G. D., Eriksen, E., Quinones, J., Acha, M., ... Graham, W. M. (2013). Recurrent jellyfish blooms are

- a consequence of global oscillations. *Proceedings of the National Academy of Sciences of the United States of America*, 110(3), 1000-1005. <https://doi.org/10.1073/pnas.1210920110>
- Condon, R. H., Graham, W. M., Duarte, C. M., Pitt, K. A., Lucas, C. H., Haddock, S. H. D., Sutherland, K. R., Robinson, K. L., Dawson, M. N., Decker, M. B., Mills, C. E., Purcell, J. E., Malej, A., Mianzan, H., Uye, S. I., Gelcich, S., & Madin, L. P. (2012). Questioning the rise of gelatinous Zooplankton in the world's oceans. *BioScience*, 62(2), 160-169. <https://doi.org/10.1525/bio.2012.62.2.9>
- Courant, R., Friedrichs, K., & Lewy, H. (1928). Über die partiellen Differenzengleichungen der mathematischen Physik [On the partial difference equations of mathematical physics]. *Mathematische Annalen* 1928 100:1, 100(1), 32-74. <https://doi.org/10.1007/BF01448839>
- Cowen, R. K., Lwiza, K. M. M., Sponaugle, S., Paris, C. B., & Olson, D. B. (2000). Connectivity of marine populations: Open or closed? *Science*, 287(5454), 857-859. <https://doi.org/10.1126/science.287.5454.857>
- David, C., Vaz, S., Loots, C., Antajan, E., van der Molen, J., & Travers-Trolet, M. (2015). Understanding winter distribution and transport pathways of the invasive ctenophore *Mnemiopsis leidyi* in the North Sea: coupling habitat and dispersal modelling approaches. *Biological Invasions*, 17(9), 2605-2619. <https://doi.org/10.1007/s10530-015-0899-y>
- Dawson, M. N., Gupta, A. Sen, & England, M. H. (2005). Coupled biophysical global ocean model and molecular genetic analyses identify multiple introductions of cryptogenic species. *Proceedings of the National Academy of Sciences of the United States of America*, 102(34), 11968-11973. <https://doi.org/10.1073/pnas.0503811102>
- Depra, D. (2015). *New Study Finds Jellyfish Swim Actively Against Current, Possess Advanced Orientation Abilities.* Tech Times. <https://www.techtimes.com/articles/28519/20150124/new-study-finds-jellyfish-swims-actively-against-current-possess-advanced-orientation-abilities.htm>

- Doyle, T K, Hays, G. C., Harrod, C., & Houghton, J. D. R. (2014). Ecological and Societal Benefits of Jellyfish. In *Jellyfish Blooms* (Vol. 9789400770, Issue June, pp. 105-127). <https://doi.org/10.1007/978-94-007-7015-7>
- Doyle, Thomas K., De Haas, H., Cotton, D., Dorschel, B., Cummins, V., Houghton, J. D. R., Davenport, J., & Hays, G. C. (2008). Widespread occurrence of the jellyfish *Pelagia noctiluca* in Irish coastal and shelf waters. *Journal of Plankton Research*, 30(8), 963-968. <https://doi.org/10.1093/plankt/fbn052>
- Doyle, Thomas K., Houghton, J. D. R., Buckley, S. M., Hays, G. C., & Davenport, J. (2007). The broad-scale distribution of five jellyfish species across a temperate coastal environment. *Hydrobiologia*, 579(1), 29-39. <https://doi.org/10.1007/s10750-006-0362-2>
- Dunsbergen, D. W., & Stalling, G. S. (1993). *The combination of a random walk method and a hydrodynamic model for the simulation of dispersion of dissolved matter in water*. www.witpress.com,
- Dupont, N., Klevjer, T. A., Kaartvedt, S., & Aksnes, D. L. (2009). Diel vertical migration of the deep-water jellyfish *Periphylla periphylla* simulated as individual responses to absolute light intensity. *Limnology and Oceanography*, 54(5), 1765-1775. <https://doi.org/10.4319/lo.2009.54.5.1765>
- EPA. (2022). *Environmental Fluid Dynamics Code (EFDC)*. United States Environmental Protection Agency. <https://www.epa.gov/ceam/environmental-fluid-dynamics-code-efdc>
- ESRI. (2018). ArcGIS [GIS software]. Version 10. In *Redlands, CA: Environmental Systems Research Institute*. Redlands, CA: Environmental Systems Research Institute.
- Fossette, S., Gleiss, A. C., Chalumeau, J., Bastian, T., Armstrong, C. D., Vandenabeele, S., Karpytchev, M., & Hays, G. C. (2015). Current-oriented swimming by jellyfish and its role in bloom maintenance. *Current Biology*, 25(3), 342-347. <https://doi.org/10.1016/j.cub.2014.11.050>
- Freer, J. J., & Hobbs, L. (2020). DVM: The World's Biggest Game of Hide-and-Seek.

- Frontiers for Young Minds*, 8. <https://doi.org/10.3389/FRYM.2020.00044>
- Galperin, B., Kantha, L. H., Hassid, S., & A. Rosati, A. (1988). A Quasi-Equilibrium Turbulent Energy Model for Geophysical Flows. *Journal of the Atmospheric Sciences*, 45(1), 55-62.
- Garm, A., & Ekström, P. (2010). Evidence for multiple photosystems in jellyfish. *International Review of Cell and Molecular Biology*, 280(C), 41-78. [https://doi.org/10.1016/S1937-6448\(10\)80002-4](https://doi.org/10.1016/S1937-6448(10)80002-4)
- Gemmell, B. J., Costello, J. H., Colin, S. P., Stewart, C. J., Dabiri, J. O., Tafti, D., & Priya, S. (2013). Passive energy recapture in jellyfish contributes to propulsive advantage over other metazoans. *Proceedings of the National Academy of Sciences of the United States of America*, 110(44), 17904-17909. <https://doi.org/10.1073/pnas.1306983110>
- Gill, V. (2015). *Jellyfish "can sense ocean currents"* - BBC News. BBC News - Science & Environment. <https://www.bbc.com/news/science-environment-30936192>
- Gjelsvik Tiller, R., Mork, J., Richards, R., Eisenhauer, L., Liu, Y., Nakken, J. F., & Borgersen, Å. L. (2014). Something fishy: Assessing stakeholder resilience to increasing jellyfish (*Periphylla periphylla*) in Trondheimsfjord, Norway. *Marine Policy*, 46, 72-83. <https://doi.org/10.1016/J.MARPOL.2013.12.006>
- Gómez, A. R., & Gutiérrez-Hernández, O. (2020). Impact of Jellyfish and Other Gelatinous Organisms on the Andalusian Coast: Implications for Sun and Beach Tourism. *Estudios Geográficos*, 81(288), 38. <https://doi.org/10.3989/ESTGEOGR.202053.033>
- Goy, J., Morand, P., & Etienne, M. (1989). Long-term fluctuations of *Pelagia noctiluca* (Cnidaria, Scyphomedusa) in the western Mediterranean Sea. Prediction by climatic variables. *Deep Sea Research Part A. Oceanographic Research Papers*, 36(2), 269-279. [https://doi.org/10.1016/0198-0149\(89\)90138-6](https://doi.org/10.1016/0198-0149(89)90138-6)
- Graham, W. M., Martin, D. L., Felder, D. L., Asper, V. L., & Perry, H. M. (2003). Ecological and economic implications of a tropical jellyfish invader in the Gulf of Mexico. *Biological Invasions*, 5(1-2), 53-69.

<https://doi.org/10.1023/A:1024046707234/METRICS>

Graham, W. M., Pagès, F., & Hamner, W. M. (2001). A physical context for gelatinous zooplankton aggregations: A review. *Hydrobiologia*, 451, 199-212. <https://doi.org/10.1023/A:1011876004427>

Guo, X. (2002). A Triply Nested Ocean Model for Simulating the Kuroshio-Roles of Horizontal Resolution on JEBAR. *JOURNAL OF PHYSICAL OCEANOGRAPHY*.

Halsband, C., Majaneva, S., Hosia, A., Emaus, P. A., Gaardsted, F., Zhou, Q., Nøst, O. A., & Renaud, P. E. (2018). Jellyfish summer distribution, diversity and impact on fish farms in a Nordic fjord. *Marine Ecology Progress Series*, 591(October), 267-279. <https://doi.org/10.3354/meps12274>

Hamrick, J. M. (2007). The Environmental Fluid Dynamics Code User Manual US EPA Version 1.01. In *Tetra Tech, Inc., 10306 Eaton Place, Suite 340, Fairfax, VA 22030*. Tetra Tech, Inc., 10306 Eaton Place, Suite 340, Fairfax, VA 22030. https://www.epa.gov/sites/default/files/2016-01/documents/efdc_user_manual_epa_ver-101.pdf

Hamrick, J.M. (2007). The Environmental Fluid Dynamics Code Theory and Computation Volume 1: Hydrodynamics and Mass Transport. In *Tetra Tech, Inc., 10306 Eaton Place, Suite 340, Fairfax, VA 22030*. Tetra Tech, Inc., 10306 Eaton Place, Suite 340, Fairfax, VA 22030.

Hamrick, John M. (1992). A Three-Dimensional Environmental Fluid Dynamics Computer Code: Theoretical and Computational Aspects. In *Special report in applied marine science and ocean engineering ; no. 317.. Virginia Institute of Marine Science, College of William and Mary*. (Issue 317). <https://doi.org/10.21220/V5TT6C>

Hamrick, John M. (1996). User's manual for the Environmental Fluid Dynamics Computer Code. In *Special Reports in Applied Marine Science and Ocean Engineering (SRAMSOE) No. 331. Virginia Institute of Marine Science, College of William and Mary*. (Issue 331). <https://doi.org/https://doi.org/10.21220/V5M74W>

- Hays, G. C., Doyle, T. K., Houghton, J. D. R., Lilley, M. K. S., Metcalfe, J. D., & Righton, D. (2008). Diving behaviour of jellyfish equipped with electronic tags. *Journal of Plankton Research*, 30(3), 325–331. <https://doi.org/10.1093/plankt/fbn003>
- Hayter, E. J. (2014). Literature Review of EFDC Applications Demonstrating Capability for Use in the Jacksonville Harbor Feasibility Study. In *U.S. Army Corps of Engineers, Engineer Research and Development Center*. U.S. Army Corps of Engineers, Engineer Research and Development Center.
- Heer, T., Wells, M. G., Jackson, P. R., & Mandrak, N. E. (2020). Modelling grass carp egg transport using a 3-D hydrodynamic river model: The role of egg retention in dead zones on spawning success. *Canadian Journal of Fisheries and Aquatic Sciences*, 77(8), 1379–1392. https://doi.org/10.1139/CJFAS-2019-0344/SUPPL_FILE/CJFAS-2019-0344SUPPLB.AVI
- Heger, T., & Trepl, L. (2003). Predicting biological invasions. *Biological Invasions*, 5(4), 313–321. <https://doi.org/10.1023/b:binv.00000005568.44154.12>
- Hodson, T. O. (2022). Root-mean-square error (RMSE) or mean absolute error (MAE): when to use them or not. *Geoscientific Model Development*, 15(14), 5481–5487. <https://doi.org/10.5194/GMD-15-5481-2022>
- Hogan, T. (2012). *Deadly jellyfish with 50m tentacles land on beaches | Independent.ie*. Irish Independent. <https://www.independent.ie/news/deadly-jellyfish-with-50m-tentacles-land-on-beaches/26892805.html>
- Holt, J. T., & James, I. D. (2001). An s coordinate density evolving model of the northwest European continental shelf: 1. Model description and density structure. *Journal of Geophysical Research: Oceans*, 106(C7), 14015–14034. <https://doi.org/10.1029/2000JC000304>
- Hur, Y.-T., & Park, J.-H. (2009). Assessment of EFDC Model for Hydrodynamic Analysis in the Nakdong River. *Journal of Korea Water Resources Association*, 42(4), 309–317. <https://doi.org/10.3741/JKWRA.2009.42.4.309>
- Jackson, J. B. C., Kirby, M. X., Berger, W. H., Bjorndal, K. A., Botsford, L. W., Bourque, B. J., Bradbury, R. H., Cooke, R., Erlandson, J., Estes, J. A., Hughes, T. P., Kidwell,

- S., Lange, C. B., Lenihan, H. S., Pandolfi, J. M., Peterson, C. H., Steneck, R. S., Tegner, M. J., & Warner, R. R. (2001). Historical Overfishing and the Recent Collapse of Coastal Ecosystems. *Science*, 293(5530), 629-637. <https://doi.org/10.1126/SCIENCE.1059199>
- James, S. C., O'Donncha, F., & Plew D. R. (2016). Calibration of a 3D hydrodynamic aquaculture model. *OCEANS 2016 MTS/IEEE Monterey*, 1-7. <https://doi.org/10.1109/OCEANS.2016.7761411>
- James, Scott C., Jones, C. A., Grace, M. D., & Roberts, J. D. (2010). Advances in sediment transport modelling. *Http://Dx.Doi.Org/10.1080/00221686.2010.515653*, 48(6), 754-763. <https://doi.org/10.1080/00221686.2010.515653>
- James, Scott C., Lefantzi, S., Barco, J., Johnson, E., & Roberts, J. D. (2011). Verifying marine-hydro-kinetic energy generation simulations using SNL-EFDC. *OCEANS'11 MTS/IEEE KONA*, 1-9. <https://doi.org/10.23919/OCEANS.2011.6106918>
- Jaspers, C., Huwer, B., Antajan, E., Hosia, A., Hinrichsen, H. H., Biastoch, A., Angel, D., Asmus, R., Augustin, C., Bagheri, S., Beggs, S. E., Balsby, T. J. S., Boersma, M., Bonnet, D., Christensen, J. T., Dänhardt, A., Delpy, F., Falkenhaus, T., Finenko, G., ... Woźniczka, A. (2018). Ocean current connectivity propelling the secondary spread of a marine invasive comb jelly across western Eurasia. *Global Ecology and Biogeography*, 27(7), 814-827. <https://doi.org/10.1111/geb.12742>
- Ji, Z. G., Morton, M. R., & Hamrick, J. M. (2001). Wetting and Drying Simulation of Estuarine Processes. *Estuarine, Coastal and Shelf Science*, 53(5), 683-700. <https://doi.org/10.1006/ECSS.2001.0818>
- Ji, Zhen Gang. (2017). Hydrodynamics and Water Quality: Modeling Rivers, Lakes, and Estuaries. In *Hydrodynamics and Water Quality: Modeling Rivers, Lakes, and Estuaries* (2nd ed.). John Wiley & Sons, Inc. <https://doi.org/10.1002/9781119371946>
- Johnson, D R, & Perry, H. M. (1999). Blue Crab Larval Dispersion and Retention in

- the Mississippi Bight. *Bulletin of Marine Science*, 65(1), 129-149.
https://aquila.usm.edu/fac_pubsAvailable at: https://aquila.usm.edu/fac_pubs/4666
- Johnson, Donald R., Perry, H. M., & Burke, W. D. (2001). Developing jellyfish strategy hypotheses using circulation models. *Hydrobiologia*, 451, 213-221.
<https://doi.org/10.1023/A:1011880121265>
- Johnson, Donald R., Perry, H. M., & Graham, W. M. (2005). Using nowcast model currents to explore transport of non-indigenous jellyfish into the Gulf of Mexico. *Marine Ecology Progress Series*, 305, 139-146.
<https://doi.org/10.3354/meps305139>
- Kaartvedt, S., Klevjer, T. A., Torgersen, T., Sørnes, T. A., & Røstad, A. (2007). Diel vertical migration of individual jellyfish (*Periphylla periphylla*). *Limnology and Oceanography*, 52(3), 975-983. <https://doi.org/10.4319/lo.2007.52.3.0975>
- Kawahara, M., Uye, S. I., Ohtsu, K., & Iizumi, H. (2006). Unusual population explosion of the giant jellyfish *Nemopilema nomurai* (Scyphozoa: Rhizostomeae) in East Asian waters. *Marine Ecology Progress Series*, 307, 161-173.
<https://doi.org/10.3354/MEPS307161>
- Keegan, B. F., & Mercer, J. P. (1986). An Oceanographical Survey of Killary Harbour on the West Coast of Ireland. *Proceedings of the Royal Irish Academy. Section B: Biological, Geological, and Chemical Science*, 86B, 1-70.
<http://www.jstor.org/stable/20494455>
- Kideys, A. E. (2002). Ecology: Fall and rise of the Black Sea ecosystem. *Science*, 297(5586), 1482-1484. <https://doi.org/10.1126/science.1073002>
- Kim, C. K., Park, K., Powers, S. P., Graham, W. M., & Bayha, K. M. (2010). Oyster larval transport in coastal Alabama: Dominance of physical transport over biological behavior in a shallow estuary. *Journal of Geophysical Research: Oceans*, 115(C10), 10019. <https://doi.org/10.1029/2010JC006115>
- Kim, D. H., Seo, J. N., Yoon, W. D., & Suh, Y. S. (2012). Estimating the economic damage caused by jellyfish to fisheries in Korea. *Fisheries Science*, 78(5), 1147-

1152. <https://doi.org/10.1007/S12562-012-0533-1/METRICS>
- Kimmerer, W. J., Gross, E. S., & MacWilliams, M. L. (2014). Tidal migration and retention of estuarine zooplankton investigated using a particle-tracking model. *Limnology and Oceanography*, 59(3), 901-916. <https://doi.org/10.4319/LO.2014.59.3.0901>
- King, T. L., Bentley, R. J., Thornton, L. E., & Kavanagh, A. M. (2016). Using kernel density estimation to understand the influence of neighbourhood destinations on BMI. *BMJ Open*, 6(2). <https://doi.org/10.1136/bmjopen-2015-008878>
- King, T. L., Thornton, L. E., Bentley, R. J., & Kavanagh, A. M. (2015). The Use of Kernel Density Estimation to Examine Associations between Neighborhood Destination Intensity and Walking and Physical Activity. *PLOS ONE*, 10(9), e0137402. <https://doi.org/10.1371/JOURNAL.PONE.0137402>
- Kloog, I., Haim, A., & Portnov, B. A. (2009). Using kernel density function as an urban analysis tool: Investigating the association between nightlight exposure and the incidence of breast cancer in Haifa, Israel. *Computers, Environment and Urban Systems*, 1(33), 55-63. <https://doi.org/10.1016/J.COMPENVURBSYS.2008.09.006>
- Kumar, B. S., Mohanty, A. K., Das, N. P. I., Satpathy, K. K., & Sarkar, S. K. (2017). Impingement of marine organisms in a tropical atomic power plant cooling water system. *Marine Pollution Bulletin*, 124(1), 555-562. <https://doi.org/10.1016/J.MARPOLBUL.2017.07.067>
- Large, W. G., McWilliams, J. C., & Doney, S. C. (1994). Oceanic vertical mixing: A review and a model with a nonlocal boundary-layer parameterization. *Reviews of Geophysics*, 32(4), 363-403. <https://doi.org/10.1029/94RG01872>
- Lee, P. L. M., Dawson, M. N., Neill, S. P., Robins, P. E., Houghton, J. D. R., Doyle, T. K., & Hays, G. C. (2013). Identification of genetically and oceanographically distinct blooms of jellyfish. *Journal of the Royal Society Interface*, 10(80). <https://doi.org/10.1098/rsif.2012.0920>
- Li, X., WANG, Y., & ZHANG, S. (2009). Numerical simulation of water quality in

- Yangtze Estuary. *Water Science and Engineering*, 2(4), 40-51.
<https://doi.org/10.3882/j.issn.1674-2370.2009.04.004>
- Li, Z., Gross, T. F., Brown, C. W., Wang, H. V., & Hood, R. R. (2002). A near real time simulation of salinity, temperature and Sea Nettles (*Chrysaora quinquecirrha*) in Chesapeake Bay. *Proceedings of the Seventh International Conference on Estuarine and Coastal Modeling, St. Petersburg, Florida, United States, 2001*, 467-478. [https://doi.org/10.1061/40628\(268\)29](https://doi.org/10.1061/40628(268)29)
- Liu, Z., Hashim, N. B., Kingery, W. L., & Huddleston, D. H. (2007). Hydrodynamic modeling of St Louis Bay estuary and watershed using EFDC and HSPF. *9th International Symposium on Fluid Control Measurement and Visualization 2007, FLUCOME 2007*, 3, 1540-1551. <https://doi.org/10.2112/1551-5036-52.sp1.107>
- Longhurst, A. R., Bedo, A. W., Harrison, W. G., Head, E. J. H., & Sameoto, D. D. (1990). Vertical flux of respiratory carbon by oceanic diel migrant biota. *Deep Sea Research Part A. Oceanographic Research Papers*, 37(4), 685-694. [https://doi.org/10.1016/0198-0149\(90\)90098-G](https://doi.org/10.1016/0198-0149(90)90098-G)
- Luo, X., & Li, X. (2018). Using the EFDC model to evaluate the risks of eutrophication in an urban constructed pond from different water supply strategies. *Ecological Modelling*, 372, 1-11. <https://doi.org/10.1016/J.ECOLMODEL.2018.01.020>
- Lynam, C. P., Gibbons, M. J., Axelsen, B. E., Sparks, C. A. J., Coetzee, J., Heywood, B. G., & Brierley, A. S. (2006). Jellyfish overtake fish in a heavily fished ecosystem. *Current Biology: CB*, 16(13). <https://doi.org/10.1016/J.CUB.2006.06.018>
- Mackie, G. O., Larson, R. J., Larson, K. S., & Passano, L. M. (1981). Swimming and vertical migration of *Aurelia aurita* (L) in a deep tank . *Marine Behaviour and Physiology*, 7(4), 321-329. <https://doi.org/10.1080/10236248109386993>
- Maguire, S. (2017). *Warning issued after potent jellyfish washed up on Donegal beach - Donegal Daily*. Donegal Daily. <https://www.donegaldaily.com/2017/07/10/warning-issued-after-potent-jellyfish-washed-up-on-donegal-beach/>

- Manning, A., & Dawkins, M. S. (2012). *An introduction to animal behaviour*. Cambridge University Press.
- Marcos-López, M., Mitchell, S. O., & Rodger, H. D. (2016). Pathology and mortality associated with the mauve stinger jellyfish *Pelagia noctiluca* in farmed Atlantic salmon *Salmo salar* L. *Journal of Fish Diseases*, 39(1), 111-115. <https://doi.org/10.1111/jfd.12267>
- Martin, V. J. (2002). Photoreceptors of cnidarians. *Canadian Journal of Zoology*, 80(10), 1703-1722. <https://doi.org/10.1139/z02-136>
- Masilamoni, G., Jesudoss, K. S., Nandakumar, K., Satpathy, K. K., Nair, K. V. K., & Azaariah, J. . (2000). Jellyfish ingress: A threat to the smooth operation of coastal power plants. *Current Science*, 79(5), 567-569.
- Matanoski, J. C., & Hood, R. R. (2006). An individual-based numerical model of medusa swimming behavior. *Marine Biology*, 149(3), 595-608. <https://doi.org/10.1007/s00227-006-0244-1>
- McLaughlin, R. (2021). *Beachgoers “blown away” by strange species - Donegal Daily*. Donegal Daily. <https://www.donegaldaily.com/2021/09/29/beachgoers-blown-away-by-strange-species/>
- McSorley, A. (2016). *Warning issued as swarm of deadly Portuguese man-o'-war jellyfish wash up on beaches in SIX counties - Irish Mirror Online*. Irish Mirror. <https://www.irishmirror.ie/news/irish-news/warning-issued-swarm-deadly-portuguese-8940191>
- Mellor, G. L., & Yamada, T. (1982). Development of a Turbulence Closure Model for Geophysical Fluid Problems. *Reviews of Geophysics*, 20(4), 851-875.
- Mellor, George L. (2004). USERS GUIDE FOR A THREE-DIMENSIONAL, PRIMITIVE EQUATION, NUMERICAL OCEAN MODEL. *POM User Manual*. <http://www.aos.princeton.edu/WWWPUBLIC/htdocs.pom/>
- Mills, C. E. (2001). Jellyfish blooms: Are populations increasing globally in response to changing ocean conditions? *Hydrobiologia*, 451(1), 55-68. <https://doi.org/10.1023/A:1011888006302>

- Mitchell, S. O., Bresnihan, S., & Scholz, F. (2021). Mortality and skin pathology of farmed Atlantic salmon (*Salmo salar*) caused by exposure to the jellyfish *Physalia physalis* in Ireland. *Journal of Fish Diseases*, 44(11), 1861-1864. <https://doi.org/10.1111/JFD.13499>
- Molnar, J. L., Gamboa, R. L., Revenga, C., & Spalding, M. D. (2008). Assessing the global threat of invasive species to marine biodiversity. *Frontiers in Ecology and the Environment*, 6(9), 485-492. <https://doi.org/10.1890/070064>
- Moon, J. H., Pang, I. C., Yang, J. Y., & Yoon, W. D. (2010). Behavior of the giant jellyfish *Nemopilema nomurai* in the East China Sea and East/Japan Sea during the summer of 2005: A numerical model approach using a particle-tracking experiment. *Journal of Marine Systems*, 80(1-2), 101-114. <https://doi.org/10.1016/j.jmarsys.2009.10.015>
- Moriarty, P. E., Andrews, K. S., Harvey, C. J., & Kawase, M. (2012). Vertical and horizontal movement patterns of scyphozoan jellyfish in a fjord-like estuary. *Marine Ecology Progress Series*, 455, 1-12. <https://doi.org/10.3354/meps09783>
- Moustafa, M. Z., & Hamrick, J. M. (1994). Modeling circulation and salinity transport in the Indian River Lagoon. In M. L. Spaulding (Ed.), *Proceedings of the 3rd International Conference on Estuarine and Coastal Modeling* (pp. 381-395). American Society of Civil Engineers.
- Nagata, R. M., Haddad, M. A., & Nogueira, M. (2009). The nuisance of medusae (Cnidaria, Medusozoa) to shrimp trawls in central part of southern Brazilian Bight, from the perspective of artisanal fishermen. *Journal of Aquatic Sciences*, 4, 312-325.
- Neil, T. R., & Askew, G. N. (2018). Jet-paddling jellies: Swimming performance in the Rhizostomeae jellyfish *Catostylus mosaicus*. *Journal of Experimental Biology*, 221(24). <https://doi.org/10.1242/jeb.191148>
- Nilsson, D. E., Gislén, L., Coates, M. M., Skogh, C., & Garm, A. (2005). Advanced optics in a jellyfish eye. *Nature*, 435(7039), 201-205. <https://doi.org/10.1038/nature03484>

- Nunes, J. P., Ferreira, J. G., Bricker, S. B., O'Loan, B., Dabrowski, T., Dallaghan, B., Hawkins, A. J. S., O'Connor, B., & O'Carroll, T. (2011). Towards an ecosystem approach to aquaculture: Assessment of sustainable shellfish cultivation at different scales of space, time and complexity. *Aquaculture*, 315(3-4), 369-383. <https://doi.org/10.1016/j.aquaculture.2011.02.048>
- O'Donncha, F. (2012). Physical and numerical modelling of impeded tidal flows: Effects of aquaculture structures on hydrodynamics and material transport. [Doctoral Dissertation, National University of Ireland, Galway]. Access to Research at NUIG (ARAN) Repository. <https://aran.library.nuigalway.ie/handle/10379/3066?show=full>
- O'Donncha, Fearghal, James, S. C., & Ragnoli, E. (2017). Modelling study of the effects of suspended aquaculture installations on tidal stream generation in Cobscook Bay. *Renewable Energy*, 102, 65-76. <https://doi.org/10.1016/j.renene.2016.10.024>
- O'Donncha, Fearghal, Ragnoli, E., & Suits, F. (2014). Parallelisation study of a three-dimensional environmental flow model. *Computers and Geosciences*, 64, 96-103. <https://doi.org/10.1016/j.cageo.2013.12.006>
- O'Sullivan, K. (2017). *Stinger jellyfish swarms wipe out farmed salmon in west of Ireland - Local Environmental Observer (LEO) Network*. The Irish Times. <https://www.leonetwork.org/en/posts/show/343A1FB5-E067-4E1D-BB99-CAB8DD248886>
- Pak, G., Kim, Y., Yoon, J., Mallari, K. J. B., Baek, J., Jung, M., & Kim, D. (2016). Modelling of suspended sediment in a weir reach using EFDC model. *Water Science and Technology*, 73(7), 1583-1590. <https://doi.org/10.2166/WST.2015.574>
- Park, I., Seo, I. W., Kim, Y. Do, & Han, E. J. (2017). Turbulent Mixing of Floating Pollutants at the Surface of the River. *Journal of Hydraulic Engineering*, 143(8). [https://doi.org/10.1061/\(asce\)hy.1943-7900.0001319](https://doi.org/10.1061/(asce)hy.1943-7900.0001319)
- Parzen, E. (1962). On Estimation of a Probability Density Function and Mode. <https://doi.org/10.1214/Aoms/1177704472>, 33(3), 1065-1076.

<https://doi.org/10.1214/AOMS/1177704472>

- Pawlowicz, R., Beardsley, B., & Lentz, S. (2002). Classical tidal harmonic analysis including error estimates in MATLAB using T_TIDE. *Computers & Geosciences*, 28(8), 929-937. [https://doi.org/10.1016/S0098-3004\(02\)00013-4](https://doi.org/10.1016/S0098-3004(02)00013-4)
- Phillips, N. A. (1957). A Coordinate System Having Some Special Advantages for Numerical Forecasting. *Journal of Meteorology*, 14(2), 184-185. [https://doi.org/10.1175/1520-0469\(1957\)014<0184:acshss>2.0.co;2](https://doi.org/10.1175/1520-0469(1957)014<0184:acshss>2.0.co;2)
- Pitt, K. A., & Lucas, C. H. (2014). Jellyfish blooms. In *Jellyfish Blooms* (Vol. 9789400770). Springer Netherlands. <https://doi.org/10.1007/978-94-007-7015-7/COVER>
- Purcell, J. E., Baxter, E. J., & Fuentes, V. L. (2013). Jellyfish as products and problems of aquaculture. *Advances in Aquaculture Hatchery Technology*, March 2016, 404-430. <https://doi.org/10.1533/9780857097460.2.404>
- Purcell, J. E., Uye, S. I., & Lo, W. T. (2007). Anthropogenic causes of jellyfish blooms and their direct consequences for humans: A review. *Marine Ecology Progress Series*, 350, 153-174. <https://doi.org/10.3354/meps07093>
- Qiu, Z. F., Doglioli, A. M., Hu, Z. Y., Marsaleix, P., & Carlotti, F. (2010). The influence of hydrodynamic processes on zooplankton transport and distributions in the North Western Mediterranean: Estimates from a Lagrangian model. *Ecological Modelling*, 221(23), 2816-2827. <https://doi.org/10.1016/J.ECOLMODEL.2010.07.025>
- Qu, C. F., Song, J. M., Li, N., Li, X. G., Yuan, H. M., Duan, L. Q., & Ma, Q. X. (2015). Jellyfish (*Cyanea nozakii*) decomposition and its potential influence on marine environments studied via simulation experiments. *Marine Pollution Bulletin*, 97(1-2), 199-208. <https://doi.org/10.1016/J.MARPOLBUL.2015.06.016>
- Rahi, J. El, Weeber, M. P., & Serafy, G. El. (2020). Modelling the effect of behavior on the distribution of the jellyfish Mauve stinger (*Pelagianoctiluca*) in the Balearic Sea using an individual-based model. *Ecological Modelling*, 433(July), 109230. <https://doi.org/10.1016/j.ecolmodel.2020.109230>

- Rakow, K. C., & Graham, W. M. (2006). Orientation and swimming mechanics by the scyphomedusa *Aurelia* sp. in shear flow. *Limnology and Oceanography*, 51(2), 1097-1106. <https://doi.org/10.4319/LO.2006.51.2.1097>
- Rathi, A. (2014). *Jellyfish are the most energy efficient swimmers, new metric confirms*. The Conversation - Science & Technology. <https://theconversation.com/jellyfish-are-the-most-energy-efficient-swimmers-new-metric-confirms-26729>
- Richardson, A. J., Bakun, A., Hays, G. C., & Gibbons, M. J. (2009). The jellyfish joyride: causes, consequences and management responses to a more gelatinous future. *Trends in Ecology and Evolution*, 24(6), 312-322. <https://doi.org/10.1016/j.tree.2009.01.010>
- Roden, C. M., Rodhouse, P. G., Hensey, M. P., McMahon, T., Ryan, T. H., & Mercer, J. P. (1987). Hydrography and the distribution of phytoplankton in Killary Harbour: a fjord in western Ireland. *Journal of the Marine Biological Association of the United Kingdom*, 67(2), 359-371. <https://doi.org/10.1017/S0025315400026667>
- Rodger, H. D., Henry, L., & Mitchell, S. O. (2011). Non-infectious gill disorders of marine salmonid fish. *Reviews in Fish Biology and Fisheries*, 21(3), 423-440. <https://doi.org/10.1007/s11160-010-9182-6>
- Rosenblatt, M. (1956). Remarks on Some Nonparametric Estimates of a Density Function. <https://doi.org/10.1214/Aoms/1177728190>, 27(3), 832-837. <https://doi.org/10.1214/AOMS/1177728190>
- Ruiz-Frau, A. (2022). Impacts of jellyfish presence on tourists' holiday destination choices and their willingness to pay for mitigation measures. *Journal of Environmental Planning and Management*. <https://doi.org/10.1080/09640568.2022.2061926>
- Rutkowski, T., Schroeder, R., & Resgalla, C. (2018). Occurrences of Jellyfish in the Industrial Fishing Activity of the Southeastern and Southern Regions of Brazil. *Marine and Coastal Fisheries*, 10(2), 144-151. <https://doi.org/10.1002/mcf2.10017>

- Seebens, H., Schwartz, N., Schupp, P. J., & Blasius, B. (2016). Predicting the spread of marine species introduced by global shipping. *Proceedings of the National Academy of Sciences of the United States of America*, 113(20), 5646-5651. https://doi.org/10.1073/PNAS.1524427113/SUPPL_FILE/PNAS.201524427SI.PDF
- Seo, H. (2021). The ups and downs of a great vertical migration. *Knowable Magazine*. <https://doi.org/10.1146/KNOWABLE-110421-1>
- Shen, H. H. (2002). *Environmental fluid mechanics : theories and applications*. 467.
- Shephard, S., & Gargan, P. (2017). Quantifying the contribution of sea lice from aquaculture to declining annual returns in a wild Atlantic salmon population. *Aquaculture Environment Interactions*, 9(May), 181-192. <https://doi.org/10.3354/aei00223>
- Simberloff, D. (2000). Introduced Species: The Threat to Biodiversity & What Can Be Done. *American Institute of Biological Sciences*. <http://www.actionbioscience.org/biodiversity/simberloff.html#primer>
- Simons, R. D., Siegel, D. A., Brown, K. S., Simons, R. D., Siegel, D. A., & Brown, K. S. (2013). Model sensitivity and robustness in the estimation of larval transport: A study of particle tracking parameters. *JMS*, 119, 19-29. <https://doi.org/10.1016/J.JMARSYS.2013.03.004>
- Småge, S. B., Brevik, Ø. J., Frisch, K., Watanabe, K., Duesund, H., & Nylund, A. (2017). Concurrent jellyfish blooms and tenacibaculosis outbreaks in Northern Norwegian Atlantic salmon (*Salmo salar*) farms. *PLoS ONE*, 12(11). <https://doi.org/10.1371/journal.pone.0187476>
- Smagorinsky, J. (1963). General Circulation Experiments with the Primitive Equations. *Monthly Weather Review*, 91(3), 99. [https://doi.org/10.1175/1520-0493\(1963\)091](https://doi.org/10.1175/1520-0493(1963)091)
- Spall, M. A., & Holland, W. R. (1991). A Nested Equation Model for Oceanic Applications. *American Meteorological Society*.
- Steinberg, D. K., & Landry, M. R. (2017). Zooplankton and the Ocean Carbon Cycle.

- Annual Review of Marine Science*, 9(1), 413-444.
<https://doi.org/10.1146/ANNUREV-MARINE-010814-015924>
- Stephens, C., Antonov, J. I., Boyer, T. P., Conkright, M. E., Locarnini, R. A., O'Brien, T. D., Garcia, H. E., Levitus, S., Withee, G. W., Administrator, A., Stephens, C., Antonov, J. I., Boyer, T. P., Conkright, M. E., Locarnini, R. A., O'Brien, T. D., & Garcia, H. E. (2002). *World ocean atlas 2001. Volume 1, Temperature* (Vol. 1, p. pp). <https://repository.library.noaa.gov/view/noaa/1105>
- Surve, A. (2018). *Huge increase in number of potentially deadly jellyfish on Irish beaches - Irish Mirror Online*. Irish Mirror. <https://www.irishmirror.ie/news/irish-news/lions-mane-jellyfish-sightings-ireland-13162737>
- The Fish Site. (2012). Rope Mussel Producers Organise Pier Clean Up in Killary Harbour | The Fish Site. *The Fish Site*. <https://thefishsite.com/articles/rope-mussel-producers-organise-pier-clean-up-in-killary-harbour-1>
- Torres-Bejarano, F., García-Gallego, J., & Salcedo-Salgado, J. (2023). Numerical modeling of nutrient transport to assess the agricultural impact on the trophic state of reservoirs. *International Soil and Water Conservation Research*, 11(1), 197-212. <https://doi.org/10.1016/J.ISWCR.2022.06.002>
- Towers, L. (2014). *Jellyfish and Aquaculture Interactions: Last Years Irish Experience*. The Fish Site. <https://thefishsite.com/articles/jellyfish-and-aquaculture-interactions-last-years-irish-experience>
- Turchin, P. (1998). Quantitative analysis of movement: measuring and modeling population redistribution in animals and plants. *Sinauer Associates, Sunderland*.
- Tyrrell, H. J. V. (1964). The Origin and Present Status of Fick's Diffusion Law. *Journal of Chemical Education*, 41(7), 397-400. <https://pubs.acs.org/sharingguidelines>
- UISCE. (2010). Understanding Irish Shellfish Culture Environments Project Report for DAFF on Killary Harbour. In *Aquaculture Technical Section, BIM*.
- Venables, W. N., & Ripley, B. D. (2002). *Modern Applied Statistics with S*. Springer, New York. <https://doi.org/10.1007/978-0-387-21706-2>

- Watson, S. (2006). *How Jellyfish Work*. HowStuffWorks.Com.
<https://animals.howstuffworks.com/marine-life/jellyfish.htm>
- Węglarczyk, S. (2018). Kernel density estimation and its application. *ITM Web of Conferences*, 23, 00037. <https://doi.org/10.1051/itmconf/20182300037>
- Wei, H., Deng, L., Wang, Y., Zhao, L., Li, X., & Zhang, F. (2015). Giant jellyfish *Nemopilema nomurai* gathering in the Yellow Sea - a numerical study. *Journal of Marine Systems*, 144, 107-116.
<https://doi.org/10.1016/j.jmarsys.2014.12.001>
- Whitaker, J. D., King, R., & Knott, D. (2014). Jellyfish. *Sea Science - An Information/Education Series from the Marine Resources Division*.
<http://dnr.sc.gov/marine/pub/seascience/pdf/Jellyfish.pdf>
- Wool, T. A., Davie, S. R., & Rodriguez, H. N. (2003). Development of Three-Dimensional Hydrodynamic and Water Quality Models to Support Total Maximum Daily Load Decision Process for the Neuse River Estuary, North Carolina. *Journal of Water Resources Planning and Management*, 129(4), 295-306. [https://doi.org/10.1061/\(asce\)0733-9496\(2003\)129:4\(295\)](https://doi.org/10.1061/(asce)0733-9496(2003)129:4(295))
- Wu, G., & Xu, Z. (2011). Prediction of algal blooming using EFDC model: Case study in the Daoxiang Lake. *Ecological Modelling*, 222(6), 1245-1252.
<https://doi.org/10.1016/j.ecolmodel.2010.12.021>
- Xian, W., Kang, B., & Liu, R. (2005). Jellyfish Blooms in the Yangtze Estuary. *Science*, 307(5706), 41. <https://doi.org/10.1126/science.307.5706.41c>
- Yin, L., Shan, X., Zhao, C., Jin, X., Wang, G., & Qiao, F. (2019). A model for the transportation and distribution of jellyfish *Rhopilema esculentum* for stock enhancement in the Liaodong Bay, China. *Acta Oceanologica Sinica*, 38(1), 90-101. <https://doi.org/10.1007/s13131-019-1374-x>